Biological and Medical Physics, Biomedical Engineering

Victor Kolikov
Philip Rutberg

Pulsed Electrical Discharges for Medicine and Biology

Techniques, Processes, Applications

Springer

Pulsed Electrical Discharges for Medicine and Biology

BIOLOGICAL AND MEDICAL PHYSICS, BIOMEDICAL ENGINEERING

The fields of biological and medical physics and biomedical engineering are broad, multidisciplinary and dynamic. They lie at the crossroads of frontier research in physics, biology, chemistry, and medicine. The Biological and Medical Physics, Biomedical Engineering Series is intended to be comprehensive, covering a broad range of topics important to the study of the physical, chemical and biological sciences. Its goal is to provide scientists and engineers with textbooks, monographs, and reference works to address the growing need for information.

Books in the series emphasize established and emergent areas of science including molecular, membrane, and mathematical biophysics; photosynthetic energy harvesting and conversion; information processing; physical principles of genetics; sensory communications; automata networks, neural networks, and cellular automata. Equally important will be coverage of applied aspects of biological and medical physics and biomedical engineering such as molecular electronic components and devices, biosensors, medicine, imaging, physical principles of renewable energy production, advanced prostheses, and environmental control and engineering.

More information about this series at http://www.springer.com/series/3740

Victor Kolikov · Philip Rutberg

Pulsed Electrical Discharges for Medicine and Biology

Techniques, Processes, Applications

Springer

Victor Kolikov
Russian Academy of Sciences
Institute for Electrophysics
and Electric Power
St. Petersburg
Russia

Philip Rutberg
Russian Academy of Sciences
Institute for Electrophysics
and Electric Power
St. Petersburg
Russia

ISSN 1618-7210 ISSN 2197-5647 (electronic)
Biological and Medical Physics, Biomedical Engineering
ISBN 978-3-319-18128-8 ISBN 978-3-319-18129-5 (eBook)
DOI 10.1007/978-3-319-18129-5

Library of Congress Control Number: 2015938735

Springer Cham Heidelberg New York Dordrecht London

Printed on acid-free paper

Springer International Publishing AG Switzerland is part of Springer Science+Business Media (www.springer.com)

Foreword

The main motivation for authors to collect the accumulated experience and experimental data in this area is the growing interest of researchers and practitioners to innovative electrophysical methods for environment pollution abatement and to application of the nanotechnologies' products to medicine, biology, and other fields.

Under the authors' direct participation and their guidance, wide investigations have been implemented. They are aimed at identifying opportunities for use of nanoparticles of metals and their oxides in medicine (surgery, dentistry, and oncology). The studies performed in vivo clearly show that such nanoparticles are not genotoxic and mutagenic. Thus, the nanoparticles formed in water by the PED water treatment may be used for both external and internal medical applications.

It was found that the PED could be used as a source of intensive shock waves to implement a novel technology for viruses soft destroying and preparing anti-virus vaccines. With the authors' participation, electric pulsed generators of high efficiency and electro discharge chambers have been developed. These apparatuses are able to decontaminate water from almost all known bacteria and spores of fungal cultures opportunistic to human beings. Moreover, such equipment can be used as the nanoparticles generator of all available metals.

The book summarizes the results of investigations published in papers and presented in conference proceedings. The book includes chapters dedicated to detailed description of both the PED in water and properties of the WND of various metals and their oxides formed by the discharge treating of water.

I am sure that this book will be useful for researchers in the mentioned fields and students of relevant specialties.

St. Petersburg — Prof. Sergey Bobashev

Preface

This book is based on the results of experimental and theoretical studies presented in articles and in conferences.

Initially, the research was focused on the processes accompanying the pulsed electric discharges in water. These processes include: shock waves, UV-irradiation, generation of nanoparticles (as a result of thermoelectric erosion of metal electrodes), photolysis which is accompanied by generation of hydrogen peroxide (H_2O_2), reactive OH radicals, and hydrated electrons. These studies were intended to justify the use of these discharges for the decontamination of mineral and sewage water, as well as an alternative to traditional methods of disinfection for potable water. It was confirmed that pulsed electrical discharges in water destroy the whole spectrum of pathogens and the spores of opportunistic to human fungi.

Particular interest evoked the phenomenon of prolonged microbial resistance of water treated by electric discharges, i.e., the ability of water to kill the bacteria for a long time. There are two groups of factors cause bactericidal action of pulsed electric discharges in water:

- UV-irradiation and shock waves (factors of current action)
- Hydrated electrons, OH radicals, H_2O_2, nanoparticles, and positive ions of metal electrodes (factors of post action).

Since the lifetime of hydrated electrons, OH radicals, and H_2O_2 is no more than several days, it is evident that only the nanoparticles and positive ions are responsible for prolonged microbial resistance of water.

Based on the obtained results, a study was performed on the impact of water dispersions of nanoparticles on bacterial medium in vivo. Local use of water dispersion of nanoparticles in treatment of purulent wounds with chronic constituent elements was used, which showed that the bacterial contamination had disappeared by the 7th day. At the same time, the signs of cellular atypia are absent.

In addition, there have been studies conducted on the antitumor effects of silver nanoparticles on Pliss lymphosarcoma. As a result, it was found that intravenous injection of the water dispersions of silver nanoparticles leads to a significant

reduction in the growth rate of Pliss lymphosarcoma. One possible antitumor mechanism is the restoration of the equilibrium of the silver concentration in the DNA of the tumor cells. Another mechanism is an impact of nanoparticles' surface electric charge on the electronic processes of cell homeostasis.

Another application of nanoparticles in medicine is used in stomatology. It was shown that during the treatment, the periodontal pocket depth had decreased by 2.5 mm, bleeding index was 1 point, and PCR-RT data appeared within normal values in 3 weeks that coincided with absence of exudates from periodontal pockets.

Particular object of the medical study was the identification of mutagenicity and genotoxicity of nanoparticles. Experiments in vivo have shown that the nanoparticles are not genotoxic or mutagenic.

The goal of the biological investigations was to determine the connection between the properties of the nanoparticles and peculiarities of their interaction with the human blood serum, as highly concentrated solutions of macromolecules. It was found that albuminous and lipoprotein structures of HBS are agglutinated on the surface of the nanoparticles, forming supramolecular complexes. Thus, the higher the concentration of nanoparticles in dispersion is, the larger complexes are formed. At early stages of the process rather small complexes of albuminous and immunoglobulins are formed, then lipoproteins are agglutinated, and finally, complexes of large (more than 2 μm) hydrodynamic radius are formed. Interactions of the nanoparticles with blood serum are of the same type and have differed only quantitatively. These distinctions are connected with the sizes of nanostructure aggregates in the dispersions. Known correlation between patients' state and blood properties allows us to suppose potential diagnostic significance of new integral characteristics of patient state, characteristic radii of nanoparticles-serum components complex formed. Obtained results, taken together with data available from the literature, lead us to the possibility of using such nanostructures for diagnosis of some conformational diseases such as Alzheimer disease.

Studying the "soft" damaging effects of intensive shock waves generated by pulse electric discharges on the shell of the virus showed that this method could be a novel one for preparing antivirus vaccines.

The statement above shows the potential use of pulsed electrical discharges and water dispersions of nanoparticles in various fields of medicine, biology, and ecology.

The book may be of interest to both undergraduate and graduate students in related disciplines, and to professionals employed in other fields of studies who would want to further explore this subject in-depth.

St. Petersburg

Victor Kolikov
Philip Rutberg

Acknowledgments

We would like to thank A. Arutjunan, Yu. Aristov, E. Bogomolova, I. Cherepkova, V. Dolgosaburov, M. Dubina, V. Egorov, V. Gusarov, E. Ignat'eva, L. Kaftyreva, M. Khalilov, O. Kiselev, D. Korotkov, S. Korotkov, V. Kurochkin, S. Landa, F. Moiseenko, A. Moshkin, L. Noskin, L. Panina, G. Shtorina, A. Sirotkin, V. Voejkov, N. Volkov, and I. Voskresenskaya for contribution in the research, discussions, and interpretations. Co-workers: A. Bogomaz, A. Bratsev, A. Leks, M. Pinchuk, V. Popov, A. Rutberg, V. Snetov, and A. Ufimtsev for their collaboration. S. Kumkov for text editing.

Contents

Abbreviations

AFM	Atomic force microscopy
CEWL	Chicken egg white lysozyme
CFU	Colony forming units
DNA	Deoxyribonucleic acid
EPR	Electron paramagnetic resonance (spectroscopy)
LCL	Luminal-dependent chemiluminescence (intensity)
LP	Plyss lymphosarcoma
LSPR	Localized surface plasmon resonance
MS-ICP	Mass spectrometry with inductively coupled plasma
NIR	Near infrared
PBS	Phosphate buffered saline
PED	Pulsed electric discharge(s)
PMRW	Prolonged microbial resistance of water
QLS	Quasi-elastic light-scattering
RSD	Reversively switching dynistor
RT-PCR	Real-time polymerase chain reaction
SEM	Scanning electron microscopy
TBC	Total bacterial count
TEM	Transmissive electronic microscopy
THP	Tamm-Horsfall protein
UDP	Ultra dispersed powder(s)
UPF	Ultraviolet protection factor
UV	Ultraviolet (irradiation)
UV-Vis	Ultraviolet-visible (spectroscopy)
WDN	Water dispersion(s) of nanoparticles

Symbols

A	Rate of generation
A_p	Protein content in mixture
$A(G)$	Nanoparticles contribution to light-scattering
a	Coefficient of thermal conductivity
$\overrightarrow{B}$	Magnetic field
B	Strength of magnetic field
B_{abs}	Energy coefficient of absorption
C_α	Volumetric concentrations of atoms
C_e	Volumetric concentrations of electrons
C_0–C_n	Coefficients for full Stark width of Ballmer lines
D	Diffusion coefficient
d	Characteristic size of cuvette
E	Optical density of sample
E_k	Kinetic energy
E_p	Potential energy
E_a	Relative activation energy
E_O, E_H	Energies of ionization
e	Charge of electron
g	Acceleration of gravity
H_β, H_χ, H_δ, H_ε	Spectral lines of hydrogen of Ballmer series
I_0	Central component of spectrum
j	Current density
k	Boltzmann constant
k_e	Molar extinction coefficient
k_s	Coefficient of sticking
L_{ts}	Lightsum of test sample
L_{cs}	Lightsum of control sample
l	Width of interelectrode gap
M_s	Scalar value of magnetic saturation
m_c	Mass concentration

N	Number of nanoparticles
N_e	Number of electrons
N_{ec}	Number of ectons
N_i, N_0	Initial concentration
N_f	Final concentration
N_n	Number of nanoparticles in cluster
$N(t)$	Discharge power
n	Concentration (charged nanoparticles)
P	Pressure (of plasma)
q	Charge of nanoparticles
R_h	Hydrodynamic radius of nanoparticles
r_{ec}	Radius of ecton
r_m	Radius of cluster
r_n	Radius of nanoparticles
S	Factor of regulating motion of spin probe
S_e	Area of electrode
T	Temperature
t	Time
t_e	Time of extinction
t_{ec}	Lifetime of ecton
U_a	Near-anode voltage drop
V	Volume
V_p	Volume of paintable sample
V_s	Volume of serum
v	Velocity
$\vec{v}_0$	Velocity field of stationary flow
α	Reaction rate constant
γ	Adiabatic index
γ_1	Coefficient of electromagnetic irradiation
Δ	Coulomb logarithm
$\Delta\lambda$	Width of line
η	Dynamic viscosity coefficient (viscosity)
ρ	Recalculated density of cluster
ρ_0	Density of pure liquid
ρ_m	Density of cluster material
ρ_n	Density of nanoparticle material
$\sigma_{e\alpha}$	Cross section of electron-atom collisions
σ_{abs}	Cross section of absorption
τ	Rotational correlation time

Chapter 1
Introduction

Abstract This book is based on papers, which present the application of the pulsed electrical discharges in water and water dispersions of metal and oxide nanoparticles in surgery, dentistry, oncology, biology, and ecology. Initially, the researches were focused on the physical processes and parameters of the pulsed discharges in water to prove their possibility for bacterial purification of water and sewage from almost all known bacteria and spores of fungi. It was founded for the first time that the so called prolonged microbial resistance of water treated by the pulsed electric discharges due to the nanoparticles and positive ions emitting by them. It has been shown that the nanoparticles are not genotoxic and mutagenic. The intensive shock waves generated by the pulsed discharges represent a novel technique of "soft" destroying of viruses' membranes and this way to prepare anti-virus vaccines. This book is useful for researchers and graduate students in the field.

Disinfecting effect of electric current in water is known for a long time and the first attempt of its usage in 1871 had been undertaken. In 1898 Bredig and then Svedberg in 1909 have applied an electric arc for the first time [1] and pulsed electric discharges (PED) [2] to produce water dispersions of metal and organic sol-gels. During last century, PED in water were applied, basically, to destruct microbes, spores, protozoa, etc., and to transform organic and inorganic compounds.

The medical investigations for the last decades have shown that the sharp rise of oncological and cardiovascular diseases is a result of a chlorine disinfection of the tap water [3, 4]. It was revealed that chlorinated potable water contains steady macroradicals, which provoke occurrence and development of various serious diseases [5].

It is well known that distinctive feature of electrophysical techniques such as electronic beams, ozonation, PED, etc. is that they do not use harmful and dangerous substances containing dioxins of chlorine and fluorine. At the same time a PED equipment is much easier and cheaper, than, for example, electronic beams one.

This determines an importance and urgency of works, which are addressed to search of alternative and safe ways of water disinfection. Moreover, studies of pulsed electric fields influence on man's cells and organic tissue (including the cancer tissue) are implementing now [6].

V. Kolikov and P. Rutberg, *Pulsed Electrical Discharges for Medicine and Biology*, Biological and Medical Physics, Biomedical Engineering,
DOI 10.1007/978-3-319-18129-5_1

There are some methods for water and air purification from microbic and other pollutions, which use the electric energy. Most effective methods are pulsed electric fields [7, 8], glow discharges [9, 10], streamer/corona discharges [11, 12], gliding discharges [13], barrier discharges [14], and PED [15–18].

The methods mentioned above are of approximately equal efficiency for destruction of microbes, because of in all of them, the acting factors are the same ones: UV-irradiation, OH radicals, H_2O_2, O_3, etc. However, the PED methods have essential advantages in comparison with others: first, intensive shock waves; second, the effect of prolonged microbial resistance of water (PMRW), i.e., the property of treated water to destroy the bacteria for a long time (several months) after treatment by the PED [19–21]. Due to this property, water treated by the PED is the bactericidal agent.

When the absence of negative action of the electric methods on human beings has been confirmed, their application in medicine, pharmaceutics, food industry, and other areas is widely expected [22, 23]. Nowadays, the electric methods for disinfecting the drains of hospitals and industrial enterprises can be used.

Last years, the powerful PED were applied for water purification from chemical pollutions, including salts of heavy metals [24–29].

Besides this area of researches of the PED in water, it is necessary to mention the WDN, which have now found wide applications in medicine and biology.

The progress in contemporary studies in experimental and clinical oncology is largely determined by intensive introduction of achievements of fundamental physics and chemistry [30, 31]. Nanoparticles, nanotubes, nanocapsules, dendrimers, and nanoconductors comprise incomplete list of high-tech developments used for studying targeted delivery of anticancer drugs and radioactive labels to cancer cells as well as for designing new methods of precise detection of transformed cells, proteins, DNA, and individual genes [32, 33].

In particular, promising nanotechnological approaches in oncological studies are based on the use of nanoparticles those exhibit new physicochemical and biological properties [34]. It is known that silver nanoparticles and ions possess an intrinsic cytotoxic activity [35, 36] and have a prolonged antimicrobial effect when applied to silicon structures [37].

Results of microbiological studies indicate that the interaction of silver ions with molecules of extracellular lipoprotein matrix increases permeability of the plasma membrane of microbial cells and eventually causes their death [38]. The result of our study demonstrated that the WDN of silver nanoparticles exhibit antitumor properties in vivo. The observed cytostatic effect was confirmed by significant growth suppression, cytodystrophic changes, and fibrosis of transplanted the Pliss lymphosarcoma in the rats that received regular intravenous injections of the silver WDN. Impact of silver atoms on stabilization of molecular structure of the DNA, inhibition of tumor growth and/or reversion of the malignant phenotype requires further study on tissue, cellular, and molecular levers. Further studies of mechanisms of the discovered biological effect may become the basis for development of nanoparticles based preparations for treating malignant neoplasms in clinical practice [39].

Bactericidal properties of the silver WDN can use in surgery for treatment of upper purulent wounds with a chronic component [19, 40, 41]. The patients with such wounds are of large number and differ on etiology of diseases but the common feature of these diseases is long treatment without marked positive changes [42]. Therefore, long application of antibiotics leads to abnormality of immune processes and antibacterial resistance to microbial flora [43]. Moreover, local antiseptics are frequently toxic and one can oppress processes of repairing the wounds [44]. However, under usage of water dispersions of silver nanostructures, there were no cellular atypia and preternatural exhibitions of inflammatory reactions. It is possible to assume that, in prospect, this method will allow one to correct the practice of outpatient therapy of chronic and slow pyoinflammatory diseases.

Other area of application of the WDN is stomatology. Generalized periodontitis is systemic disease with progressive destruction of periodontal tissues and first symptoms presentation in young age. The incidence of periodontitis in 35–44 years old population is 98 %. The WDN of silver for clinical research had been used. As our researches have shown, periodontal pocket depth is decreased in average on 2.2 mm, bleeding index was of 1 point, and the RT-PCR data appeared within normal values in 3 weeks that coincided with absence exudates from periodontal pockets.

Distinctive property of magnetic nanoparticles (that explains interest to them) is their mobility under action of a magnetic field, which can be used for their directed transportation, sedimentation and concentration in the required area. Our researches have shown that nanoparticles, consisting of iron oxides, can be used as magneto-active agents for transformation of cells of microorganisms into microaggregates for their directed transport or concentration under action of a magnetic field [45].

We investigated connection between the properties of the metal oxide nanostructures produced by the PED in water and peculiarities of their interaction with the human blood serum, lysozyme, and albumin solutions under various conditions.

By means of dynamic light scattering technique, atomic force, and transmissive electronic microscopes, it was found that the albumins and lipoproteins of blood serum are aggregated on the surface of the nanostructures and form the supramolecular complexes.

In single protein system, it was shown that aggregation ability strongly depends on folding state of lysozyme and loading state of albumin. Since the nanostructures have specific effect and different absorptive abilities to the biological objects, possibility appears for developing new tools for diagnosis of some conformational diseases. Potential diagnostic is proposed estimation of new integral characteristics of patient state and characteristic radii of nanostructures-serum components complex [46–48].

Thus, the PED applications are prospective to water purification from microbic and chemical pollutions and producing (by the PED) water dispersions of metal and oxide nanoparticles. It is promising in ecological, biological, and medical problems.

The investigations were carried out for more than 20 years at the Institute for Electrophysics and Electric Power of the Russian Academy of Sciences (IEE RAS) in collaboration with the following institutes and universities:

- A.F. Ioffe Physical-Technical Institute of the Russian Academy of Science, St.-Petersburg, Russia (developing of pulsed electric high-voltage generators)
- Pasteur Institute, St.-Petersburg, Russia (bactericidity of WDN)
- Institute for Toxicology, St.-Petersburg, Russia (impact of the WDN on laboratory animals)
- A.A. Uhtomsky Physiology Research Institute of St.-Petersburg State University, St.-Petersburg, Russia (fungicide activity of the WDN)
- Institute of Analytical Instruments of the Russian Academy of Sciences,
- St.-Petersburg, Russia (chemical and physical properties of the WDN)
- N.N. Petrov Institute for Oncology, St.-Petersburg, Russia (impact of the silver WDN on tumor growth in vivo)
- Institute for Nuclear Physics of the Russian Academy of Sciences, Gatchina, Russia (interaction of the WDN and biological objects)
- Institute for Influenza of the Russian Academy of Medicine Sciences,
- St.-Petersburg, Russia (impact of electric pulses and shock wives on viruses)
- Oryol State University, Medical Institute, Oryol, Russia (treatment of pyoinflammatory diseases with a chronic component by means of the WDN)
- Dental Center "PetroDent", Russia (treatment of periodontal diseases by means of the WDN)
- St.-Petersburg State Technological Institute, St.-Petersburg, Russia (chemical properties of the WDN)
- Moscow State University, Moscow, Russia (chemical properties of the WDN)

References

1. G. Bredig, Z.F. Electrochemie **4**, 514 (1899)
2. Svedberg, *Die Methoden zur Herstellung kolloider Losungen anorganisher Stoiie* (Dresden, 1909)
3. J.M. Price, *Coronaries, Cholesterols, Chlorine* (Pyramid Publications Ltd., Llanidloes, 1984)
4. M.S. Gottlieb, J.K. Carr, D.T. Morris, Int. J. Epidem. **10**, 117 (1981)
5. V.L. Voejkov, R.R. Asfaramov, V.M. Rozental, 3rd International Conference Ecopolis 2000: Ecology and Steady Development of City (Moscow, 2000) (in Russian)
6. S.J. Beebe, P.M. Fox, L.J. Rec, K. Sommers, R.H. Stark, K.H. Schoenbach, The 28th International Conference on Plasma Science and 13th IEEE International Pulsed Power Conference (Las Vegas, 2001)
7. L.A. Kulskij, O.S. Savluk, E.G. Dejnega, *Influence of an Electric Field on Processes of Disinfecting of Water* (Naukova Dumka, Kiev, 1980) (in Russian)
8. K.H. Schoenbach, F.E. Peterkin, R.W. Kldew, S.J. Beebe, J. IEEE Trans. Plasma Sci. **2**, 25 (1997)
9. N.M. Efremov, B.Yu. Adamiak, V.I. Blochin, S.Je. Dadeshev, K.I. Dmitriev, K.N. Semjonov, V.F. Levachov, V.F. Jusbashev, J. IEEE Trans. Plasma Sci. **1**, 28 (2000)
10. T.C. Montie, K. Kelly-Winterberg, J.R. Roth, J. IEEE Trans. Plasma Sci. **1**, 28 (2000)
11. I.V. Lisitsyn, H. Nomiyama, S. Katsuki, H. Akiyama, in *12th IEEE International Pulsed Power Conference,* Monterey, 1999
12. A. Abou-Ghazala, S. Katsuki, K.H. Schoenbach, F.C. Dobbs, K.R. Moreira, J. IEEE Trans. Plasma Sci. **4**, 30 (2002)

13. J. Yan, C. Du, X. Li, X. Sun, M. Ni, K. Cen, B. Cheron, J. Plasma Source Sci. Technol. **14**, 637 (2001)
14. X. Lei, Z. Rui, L. Peng, D. Li-Li, Z. Ru-Juan, J. Chin. Phys. **6**, 13 (2004)
15. L. Edebo, I. Selin, J. Gen. Microbiol. **50**, 261 (1968)
16. V.L. Gorjachev, Ph.G. Rutberg, V.N. Fedjukovich, Rus. J. Fuel Power Heat Syst. **2**, 36 (1998)
17. V.L. Gorjachev, A.N. Bratsev, V.N. Fedjukovich, Ph.G. Rutberg, H.W. Greene, P.E. Chism, USA Pat. 5464513 (1995)
18. F.G. Rutberg, V.A. Kolikov, V.E. Kurochkin, L.K. Panina, Rus. Pat. 2286951 (2006) (in Russian)
19. Ph.G. Rutberg, V.A. Kolikov, V.E. Kurochkin, L.K. Panina, A.Ph. Rutberg, J. IEEE Trans. Plasma Sci. **4**, 35 (2007)
20. N.T. Muzirthuck, J. Hygiene Sanit. **1**, (1990) (in Russian)
21. V.A. Kolikov, V.E. Kurochkin, L.K. Panina, Ph.G. Rutberg, Doklady Biol. Sci. **403**, 279 (2005)
22. B. Roodenburg, J. Morren, S.W.H. de Haan, P.C. Wouters, G. de Jong, I.E. Pol, Y.L.M. Creygthon, European Pulsed Power Symposium, 2002)
23. A.H. El-Hag, S.H. Jayaram, M.W. Griffiths, J. IEEE Trans. Plasma Sci. **4**(part 2), 34, (2006)
24. A.M. Sizikov, L.T. Bugaenko, O.A. Golovina. in *2nd International Symposium on Theoretical and Applied Plasma Chemistry*, Riga, 1991
25. A.M. Sizikov, E.G. Volf, T.A. Kalinina, V.Ju. Ufimtcev. in *2nd International Symposium on Theoretical and Applied Plasma Chemistry*, Riga, 1991
26. V.F. Levchenko, *Electric Discharge in Liquids and Its Application in Industry* (Nikolaev, 1988)
27. V.F. Levchenko, Z.P. Giil, *Electric Discharge in Liquids and Its Application in Industry* (Nikolaev, 1988)
28. V.F. Levchenko, V.P. Sergeenkov, M.S. Tjutujnik, *Electric Discharge in Liquids and its Application in Industry* (Nikolaev, 1988)
29. A.N. Malinin, V.E. Sabinin, A.N. Sidorov, Lett. in JTP **1**, 20 (1994)
30. M.C. Roco, S. Williams, P. Alivisatos, (World Technology Division, Loyola College, 1999)
31. D. Hanahan, R.A. Weinberg, Cell **1**, 100 (2000)
32. K.Y. Kim, Nanomed. **2**, 3 (2007)
33. A.G. Cuenca, H. Jiang, S.N. Hochwald, M. Delano, W.G. Cance, S.R. Grobmyer, Cancer **3**, 107 (2006)
34. M. Ferrari, Nat. Rev. Cancer **3**, 5 (2005)
35. J.S. Kim, E. Kuk, K.N. Yu, J.H. Kim, S.J. Park, H.J. Lee, S.H. Kim, Y.K. Park, Y.H. Park, C. Y. Hwang, Y.K. Kim, Y.S. Lee, D.H. Jeong, M.H. Cho, Nanomed. **1**, 3 (2007)
36. C. Baker, A. Pradhan, L. Pakstis, D.J. Pochan, S.I. Shah, J. Nanosci. Nanotech. **2**, 5 (2005)
37. F. Furno, K.S. Morley, B. Wong, B.L. Sharp, P.L. Arnold, S.M. Howdle, R. Bayston, P.D. Brown, P.D. Winship, H.J. Reid, J. Antimicrob. Chemother. **6**, 54 (2004)
38. I. Sondi, B. Salopek-Sondi, J. Colloid Interface Sci. **1**, 275 (2004)
39. Ph.G. Rutberg, M.V. Dubina, V.A. Kolikov, F.V. Moiseenko, E.V. Ignat'eva, N.M. Volkov, V.N. Snetov, A.Yu. Stogov, Doklady Biochem. Biophys. **421**, 191 (2008)
40. Ph. Rutberg, V. Kolikov, V. Snetov, A. Stogov, A. Moshkin, M. Khalilov, J. Phys. Conf. Ser. **1**, 275 (2011)
41. Ph. Rutberg, V. Kolikov, A. Moshkin, V. Snetov, A. Stogov, M. Khalilov, J. Phys.: Conf. Ser. **1**, 291 (2011)
42. D.N. Fedorov, A.N. Ivashkin, V.V. Shinin, A.V. Vasiljev, A.A. Ivanov, Arch. Pathol. **1**, 64 (2002)
43. A.V. Volenko, A.A. Men'shikov, G.P. Titova, S.V. Kuprikov, J. Surg. **10**, 808 (2004)
44. A.N. Ljapunov, B.M. Datsenko, N.A. Mohert, *The Problem of Medicinal Therapy* (Kiev, 1995) (in Russian)
45. F.G. Rutberg, V.A. Kolikov, V.N. Snetov, A.Yu. Stogov, E.G. Abramov, E.V. Bogomolova, L.K. Panina, J. Tech. Phys. **12**, 57 (2012)

46. Ph. Rutberg, V. Kolikov, V. Snetov, A. Stogov, L. Noskin, S. Landa, A. Arutjunan, O. Kiselev, V. Egorov, A. International Conference Bio & Food Electrotechnologies (BFE2009), Compiègne, 2009
47. Ph. Rutberg, V. Kolikov, V. Snetov, A. Stogov, L. Noskin, S. Landa, A. Arutjuman, V. Egorov, A. Sirotkin, J. High Temp. Mater. Proc. **3**, 13 (2009)
48. Ph. Rutberg, V. Kolikov, V. Snetov, A. Stogov, L. Noskin, S. Landa, A. Arutjunan, V. Egorov, A. Sirotkin, Proceedings of the 10th European plasma conference on high temperature plasma processes, Patras, 2008

Chapter 2
Experimental Facility

Abstract Several experimental installations have been developed at the IEE RAS for investigation of the PED parameters in water and the WDN electrophysical and chemical properties. Installations for electrodischarge treatment of water are various both in characteristics of electric pulses and in their productivity (maximal productivity of such installations is 50 l/min). Each installation includes generator of high-voltage pulses, electrodischarge chamber, and some of them has control system. Control system ensures the smooth operation of the installation for the time due to the presence of the consumable electrode material (wire). These installations are bases for the experimental test bench arranged with the diagnostic devices and necessary ancillaries both for investigation of the PED and for study of properties of the WDN of various metals and their oxides. During the research were developed several high-voltage pulse generators for electrodischarge treatment of liquids with various specific electrical resistivity ranging from distillated water to weak water solutions of salts (2–55 μS/cm). Electric discharge chambers are usually monoblocks of polycarbonate (Lexan) with openings for water inlet and outlet and a pair of electrodes located coaxially. Axis of the electrodes is perpendicular to the flow of water.

2.1 Test Bench of Electrodischarge Installations

The experimental test bench includes the units:

- Diagnostic devices for measuring the electric parameters of discharge (current, voltage drop on electric arc, distribution of electric potential on length of arc) and of pulsed pressure in volume of the discharge chamber
- High-speed cameras register shock waves and evolution of arc channel during electric discharge

The electrodischarge installations can function under two modes:

- Monopulsed mode that, as a rule, is used in wide scale diagnostics of discharge by all available diagnostic means

V. Kolikov and P. Rutberg, *Pulsed Electrical Discharges for Medicine and Biology*, Biological and Medical Physics, Biomedical Engineering,
DOI 10.1007/978-3-319-18129-5_2

- Multipulsed mode is used for producing of water dispersions of metal and oxide nanoparticles and at investigation of dependence of multipulse effect on biological and other objects

Under all modes, input energy of a single pulse is 0.3–1.0 J. Electrodischarge chambers are of two types: flowing and cuvette. Volume of chambers is 2–50 cm^3. In some cases to achieve required effect on objects under investigation, number of pulses can reach several thousands.

2.2 Types of Pulsed High-Voltage Generators

This chapter presents the design principles of electrical circuits of high-voltage pulsed generators for powerful electrodischarge installations, which can be used for antibacterial water treatment, production of water dispersions of nanoparticles, and other purposes.

It is known that liquids (and water, in particular), which are intended for electrodischarge treatment, have various specific resistance. The aim of the work was to design power supplies for electrodischarge installations with maximal wide operating range on this parameter. Several schematics solutions of power supplies are presented in this chapter.

The power supplies for the electrodischarge installations are generators of high-voltage pulses of various types.

Figure 2.1 shows schematic diagram of the generator for treatment of water or water solutions, which specific conductivity is 2–80 μS/cm.

Voltage of ~220 V and frequency of 50 Hz through autotransformer *Tr1* and step-up transformer *Tr2* is delivered onto the rectifier *D1–D4*. The filter capacitor *C1* smoothes over pulsations of rectified voltage. Reactor *L1* limits current picks in the circuit at the switching-on of the generator. It is chosen $C1 \gg C2$, therefore, at switching-on of the thyristor *T1*, the capacitor *C2* is charged up to the double voltage of the filter capacitor *C1*.

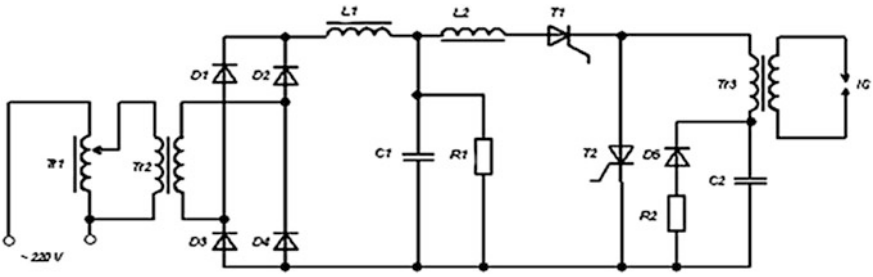

Fig. 2.1 High-voltage pulsed generator of output impedance 500 Ω

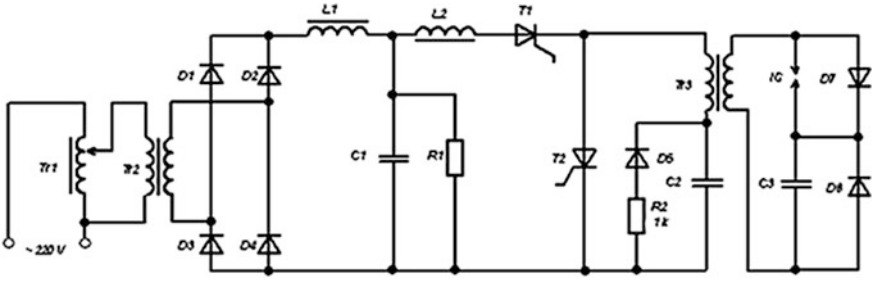

Fig. 2.2 High-voltage pulsed generator for treatment of low resistance water solutions (variant 1)

After that, the capacitor *C2* is switched over to the thyristor *T2*. There is discharge of *C2* on a primary winding of the high-voltage pulsed transformer *Tr3*. From its secondary winding, the high-voltage pulse is delivered to water interelectrode gap *IG*. The thyristor keys *T1* and *T2* operate serially. The circuit *R2–D5* eliminates voltage on *C2* in the case of the opposite recharging. The output voltage of the generator is controlled by autotransformer *Tr1*.

Output impedance of the generator is $\sim$500 Ω, therefore, at operation under high specific conductivity, the output voltage cannot achieve nominal value. Thus, breakdown of the interelectrode gap is prevented in liquids with such conductivity.

Possible decision of this problem is in reducing the output resistance of the generator. However, it can lead to excessive increase of capacitor *C2* and, as consequence, to significant loading on key *D6* and to essential increase of power. Under usage of thyristor key, loadings can exceed maximal value.

Other possible solution of this problem is in changing the high-voltage part of the generator (variant 1) (Fig. 2.2).

After switching-on of the thyristor *T2*, the capacitor *C3* charges through diode *D7* or under its absence (it is possible at operation with solutions with low specific resistance) through the interelectrode gap *IG*. After charge of the capacitor *C3* and magnetic saturation of transformer core of *Tr3*, the voltage on capacitor *C3* is applied to interelectrode gap *IG*. In this circuit, the following condition is satisfied:

$C2/C3 = W_2/W_1$, where *W1*, *W2* are numbers of coils in primary and secondary windings of the transformer *Tr3*.

Figure 2.3 shows diagram of variant 2 of high-voltage generator. In this variant of high-voltage generator after switching-on of the thyristor *T2*, the capacitor *C3* charges through the diode *D6* is charged. Then, after saturation of transformer core of *Tr4*, the voltage is applied to the interelectrode gap *IG*.

The diode *D6* prevents recharge of the condenser *C3*. The secondary winding of transformer *Tr4* serves for magnetic reversal of the core. Various tapes of generators (Figs. 2.2 and 2.3) are functionally similar.

The transformer *Tr3* in Fig. 2.4 performs two functions: charging transformer, and reactor of saturation.

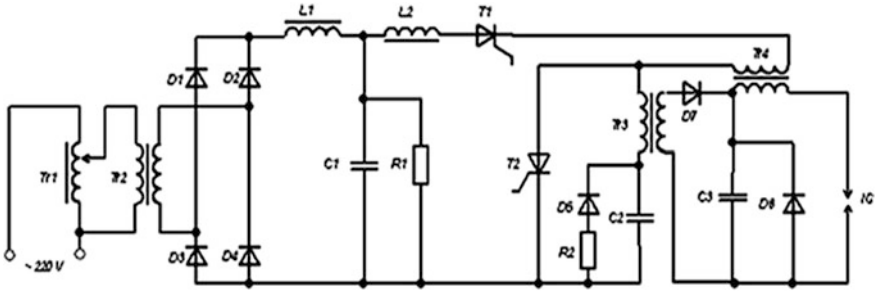

Fig. 2.3 High-voltage pulsed generator for low resistance water solutions treatment (variant 2)

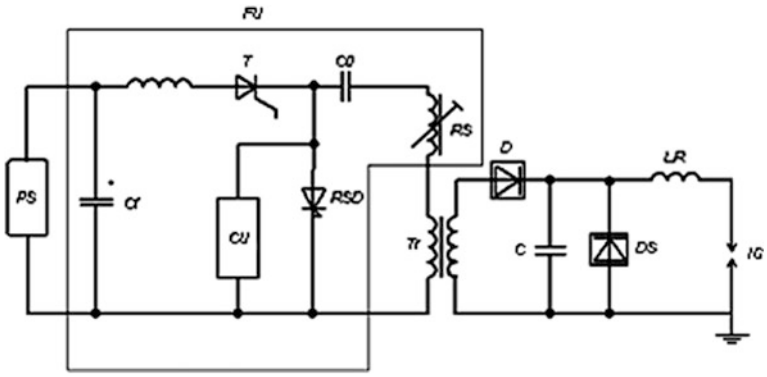

Fig. 2.4 Basic circuit of the generator [2]

In Fig. 2.3, the transformer *T4* is a magnetic key, which switches out inter-electrode gap from *C3* for the time of the capacitor charging.

In Fig. 2.3 duration of discharge pulse is longer than in Fig. 2.2 because of the greater inductance of dispersion of the transformer *Tr4* in comparison with *Tr3* one.

2.3 High Efficiency Two-Channel Generator

The developed two-channel generator has a high reproducibility of the electrodischarge processes, provides effective water treatment, and produces water dispersions of oxide and metal nanoparticles with the required physical and chemical properties.

Generator was developed for stable forming (in two electrodischarge chambers or, later, in more ones) the pulses of voltage ~40 kV, pulsed current 30–40 A, current rise rate 10^7 A/s, and of frequency 100 Hz [2]. The main problems were in

fulfilling the requirements to provide steady breakdown of two interelectrode gaps under unstable breakdown voltage and prebreakdown stage. Also, it was necessary to ensure high efficiency of operation under fast transfer of energy into the discharge and large ratio of high initial resistance of interelectrode gap before its breakdown and low resistance after the breakdown.

The basic circuit of the generator includes: power supply *PS*, filter capacitor *Cf*, pulse forming block *FU*, inductor *L0*, thyristor *T*, control unit *CU*, reversively switching dynistor *RSD* as a switcher, low-voltage capacitor *C0*, reactor of saturation *RS*, pulsed transformer *Tr*, diodes *D*, high-voltage capacitor *C*, limiting reactor *LR*, shunting diodes *DS*, and interelectrode gap *IG* (Fig. 2.4).

The *RSD* differs from classic thyristors by high reverse se, absence of control electrode, and its switching-on by short reverse blocked voltage.

Low losses of energy in the *RSD* are not limited by the short powerful pulses from the capacitor *C0* in a primary winding of the transformer *Tr*. High amplitude of the pulses allows one to use a pulsed transformer *Tr* with the big turn ratio. Thus, the high output voltage of the generator for electric breakdown of the interelectrode gap *IG* is formed at low voltage on the capacitor *C0* and low number of coils in the primary winding of the transformer *Tr*.

Low charging voltage of the capacitor *C0* stipulates small size and high reliability of elements of the charging circuit. Short duration and low amplitude of pulses of voltage in the primary winding of the transformer provide its rather small size, simple design, and high reliability.

In the basic circuit (Fig. 2.4), the energy of the capacitor *C0* is accumulated after switching-on of the thyristor T. Thus, resonant charging of *C0* is carried out from the capacitor *Cf* (here, $Cf >> C0$) that is feeding from the low voltage power supply *PS*. The charging current flows through the reactor of saturation *RS* and one turn of the primary winding of the transformer *Tr*. Thus, magnetization reversal of their cores up to initial status is provided.

The capacitor *C* is the load of the transformer *Tr*. At switching-on of the *RSD*, the high voltage capacitor *C* is charged and the voltage is applied to the interelectrode gap *IG*. The diodes *D* prevent the discharging of the capacitor *C* through the secondary winding of the transformer *Tr* during prebreakdown stage. After breakdown, the capacitor *C* is discharged through the interelectrode gap *IG*. After forming the arc channel, the resistance of the interelectrode gap *IG* is decreased by 10^3–10^5 times. Thus, the reactor *LR* limits the discharge current of the capacitor *C*.

After the peak, the discharge current is switched-on through *DS*, thus, the voltage on the capacitor *C* is close to zero and all energy is dissipated in the circuit *L–IG*.

The basic shortcoming of the circuit is that it does not allow one to provide simultaneous feeding the two interelectrode gaps because of sparseness between the moments of their breakdown. In this case, if one of the gaps had been breakdowned, then the voltage on the second one decreases down to the voltage on the first gap. As a consequence, the voltage on the second gap becomes not enough to breakdown it.

In the circuit of the two-channel generator (Fig. 2.5), this shortcoming is absent.

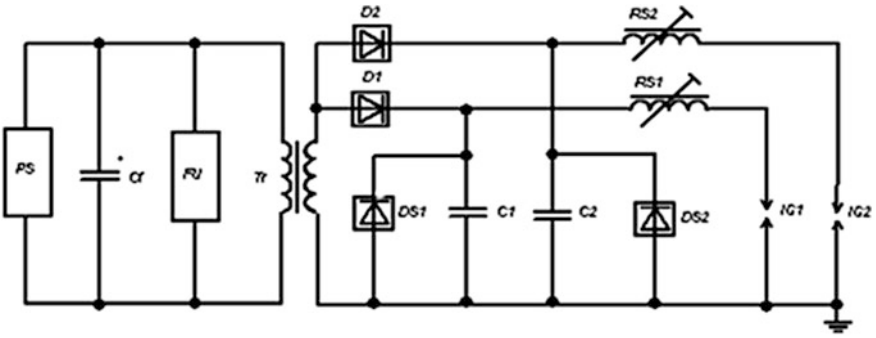

Fig. 2.5 Circuit of the two-channel generator [2]

Here, the secondary winding of transformer *Tr* is loaded on two parallel circuits containing the high-voltage capacitors *C1*, *C2* and reactors of saturation *RS1*, *RS2*. The reactors *RS1*, *RS2* in their initial status have very high inductance and, thus, block charging of capacitors *C1*, *C2*. During the charge of the capacitors *C1*, *C2* and up to the maximal voltage the saturation of cores of the reactors *RS1*, *RS2* is occurred. Thus, their inductance sharply decreases and the voltage on interelectrode gaps *IG1*, *IG2* increases sharply.

Blocks of diodes *D1*, *D2* prevent the discharge of the capacitors *C1* and *C2* through the secondary winding of the transformer *Tr*, and block the reactors *RS1* and *RS2* that prevents recharging the capacitors *C1* and *C2*.

As a result, independently on the time of delays of the interelectrode gaps *IG1* and *IG2* breakdown, the capacitors *C1* and *C2* are charged up to the maximal voltage, and after breakdown of the interelectrode gaps all energy stored in *C1* and *C2* is inputted into the interelectrode gaps *IG1* and *IG2*.

A model sample of the pulsed two-channel high-voltage generator accordingly to the circuit shown in Fig. 2.5 has been developed. In the generator, the power supply *PS* with the two-half-period diode rectifier provides charging the filter capacitor *Cf* up to 300 V from an electrical system of 220 V, 50 Hz.

Investigation of a generator with two electrodischarge chambers with copper electrodes of 1 mm in diameter and interelectrode gap 3–5 mm in distilled water was performed.

Low resistance of the discharge circuit after breakdown stipulates long duration of the discharge pulse. Thus, the current is decreased with the time constant L_{RS1}/R, where L_{RS1} is inductance of the reactor *RS1* after saturation of the core; *R* is the total resistance of discharge channel, winding of reactor *RS1*, and the diode block *DS1*. The discharge duration essentially exceeds the necessary duration for producing the water dispersions with the optimal sizes of nanoparticles.

For reducing the discharge pulse duration, the circuit of recuperation *Tr1–D1* and *Tr2–D2* has been added to the generator circuit (Fig. 2.6). Generator consists of power supply *PS*, filter capacitor *Cf*, forming unit *FU* (Fig. 2.4), pulsed transformer *Tr*, blocks of diodes *D1*, *D2*, blocks of shunting diodes *DS1*, *DS2*, block of

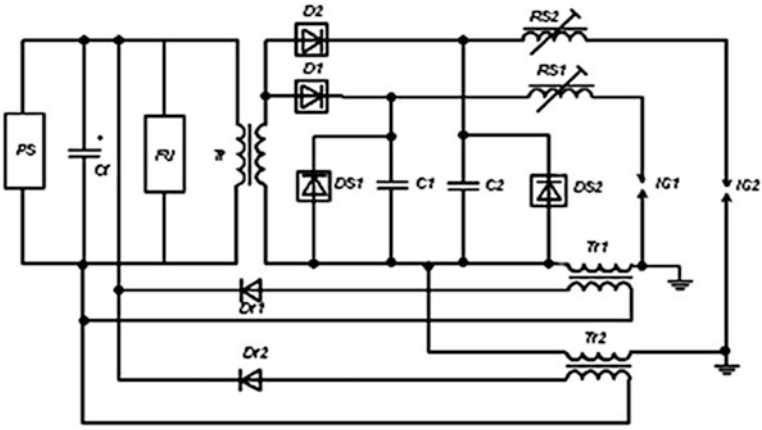

Fig. 2.6 Generator with the circuit of energy recuperation [2]

charging high-voltage capacitors *C1*, *C2*, reactors of saturation *RS1*, *RS2*, circuits of recuperation *Tr1* and *Dr1*, *Tr2* and *Dr2*, and interelectrode gaps *IG1*, *IG2*. These circuits provide reduction of duration discharge current by transfer of part of energy in the capacitor of filter *Cf*.

In Fig. 2.6, the discharge current proceeds through the primary winding of the transformers *Tr1* and *Tr2*. Thus, the voltage on the secondary winding appears that exceeds the charging one on the capacitor *Cf*. As a result, the current through the diodes *D1* and *D2* returns the energy from the output circuits *C1–RS1–IG1* and *C2–RS2–IG2* into the filter capacitor *Cf*. Because of high wave resistance of the output circuits, the discharge current does not practically vary. Since the significant part of energy after the maximum of the current is transferred into the filter capacitor *Cf*, the duration of the discharge is reduced essentially.

Figure 2.7 shows the typical oscillograms of the voltage drop (*U* is 10 kV/div) on the interelectrode gaps *IG1* and *IG2*, and the discharge current (*I* is 10 A/div) (Time is 10 μs/div) at pulse repetition rate of 100 Hz.

Amplitude of voltage on the interelectrode gap is 39 kV, amplitude of current is 35 A, front of current is 5 μs, duration of a pulse of a current is 40 μs.

2.4 Portable Generator

Besides the stationary powerful generators, a portable generator of moderate power has been developed. This apparatus is intended for use in places where there is no electric supply, for example, in expeditions.

Figure 2.8 shows the block diagram of the portable apparatus for electrodischarge treatment of water.

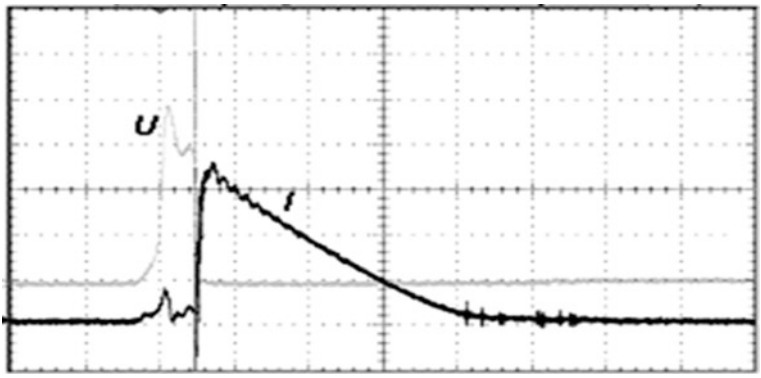

Fig. 2.7 Oscillograms of the discharge current and voltage drop [2]

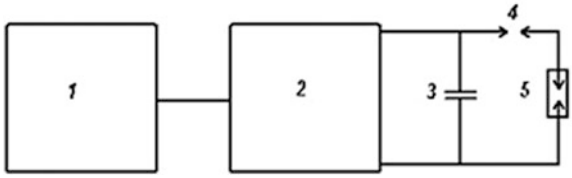

Fig. 2.8 Block diagram of the portable apparatus

Operation mode of the apparatus is the following: after power supply (*1*) switching-on, during 0.1 s the capacitor (*3*) by means of the voltage converter (*2*) is charged up to voltage of breakdown of switch (*4*). The gap between electrodes of air switch is varied from 4 to 8 mm that corresponds to the breakdown voltage of 25–50 kV. Then after breakdown of the switch (*4*), the energy stored in the capacitor (*3*) is applied to the interelectrode gap (*5*) where the arc channel in water is formed.

Figures 2.9 and 2.10 show oscillograms of the voltage drop across the interelectrode gap and discharge current in the output circuit.

Tests of the device have shown its high efficiency and suitability of its circuit solutions for development of a serial sample.

2.5 Electrodischarge Chambers

Other main element of apparatus for electrodischarge treatment of water is the electrodischarge chamber. The design and material of the chamber are to correspond to the requirements:

- High dielectric durability
- Tightness
- Long resource of operation under impact of the intensive shock waves causing cracks and splits

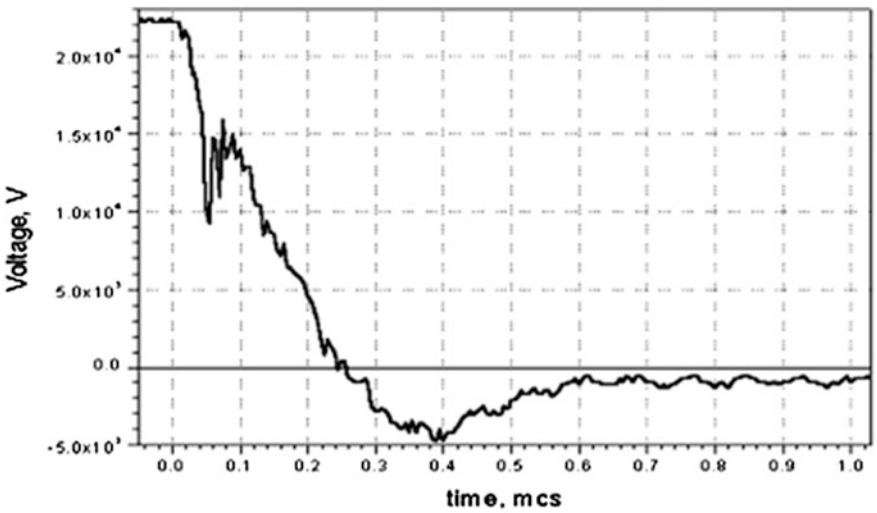

Fig. 2.9 Oscillogram of the voltage drop across the interelectrode gap

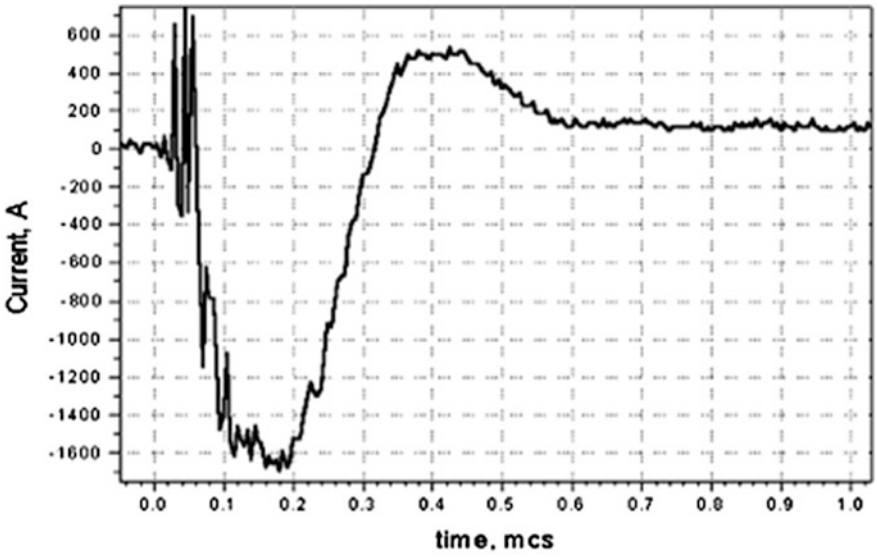

Fig. 2.10 Oscillogram of the discharge current

The polycarbonate eminently corresponds to all requirements mentioned above. However, it does not exclude use of metals, for example, steel that, however, results in complication of the discharge chamber design.

Developing the discharge chamber, it is necessary to take into account for what purposes it is intended. For example, for a laboratory installation, its optical characteristics (optical windows of material with a wide range of transmitting frequencies) are the main ones, while its high mechanical stability to shock waves is not so important.

On the contrary, for the industrial apparatus, this last requirement is determining while requirements to its optical properties are not important. Moreover, for the industrial apparatus, the long, continuous, and self-contained operation is essential. This requirement results from the electrothermal erosion of the electrode metal. Erosion "eats" metal of electrodes. This is why the interelectrode gap comes wider that demands supply of electrodes into the discharge chamber.

To increase the operating time of the electrodischarge chamber, the automatic system of electrodes control has been developed. The system includes the control unit and feeder of the electrodes into the discharge chamber.

The electrodischarge chamber comprises the case with the water-passing channel and two electrodes.

There are two main types of the electrode systems: "wire to plate" and "wire to wire".

In the first type, one of the electrodes is flat, but the other one is sharp-pointed. In the second type, both of electrodes are sharp-pointed, i.e., are wires.

Electrodes of various metals were used: steel, copper, silver, titan, some alloys, etc. Optimal diameter of the wire is 1–2 mm. Electrodes are supplied into the discharge chamber by means of a feeder, which, in its turn, is moved by the control unit.

The control unit generates driving signal to the feeder after the third missed discharge pulse.

Operation of the control unit is based on comparison of number of signals from two electric gauges: one in the primary and other in the secondary windings of the output transformer.

Figure 2.11 shows the experimental electrodischarge chamber with feeder.

Some other experimental electrodischarge chambers are shown in Fig. 2.12 and Fig. 2.13.

2.6 Pilot Industrial Electrodischarge Apparatus

A large number of tests with various electrodischarge chambers and pulsed generators were implemented. Volume investigations were performed of the electrodes shapes, electrode metals erosion, and of properties of water nanoparticles dispersions. The results show that the apparatus is suitable for industrial manufacturing and its practical application has been developed. However, investigations of all these aspects are now continuing.

The apparatus is intended for two main purposes:

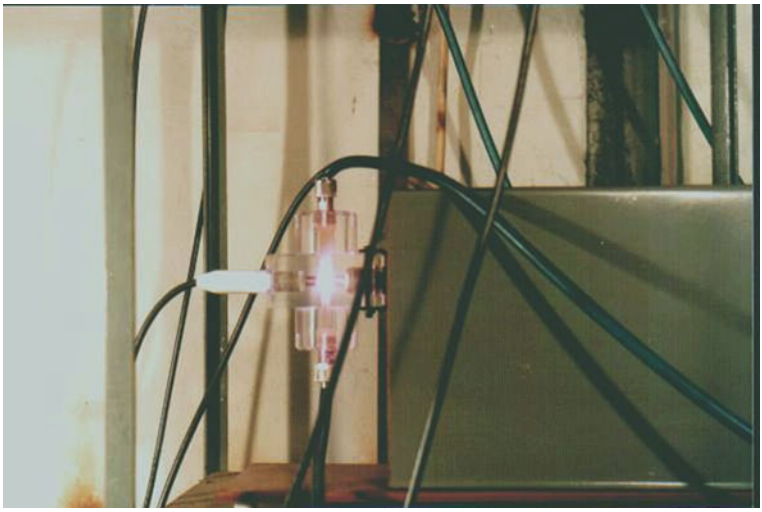

Fig. 2.11 Electrodischarge chamber (*left*), generator, and feeder (*right*)

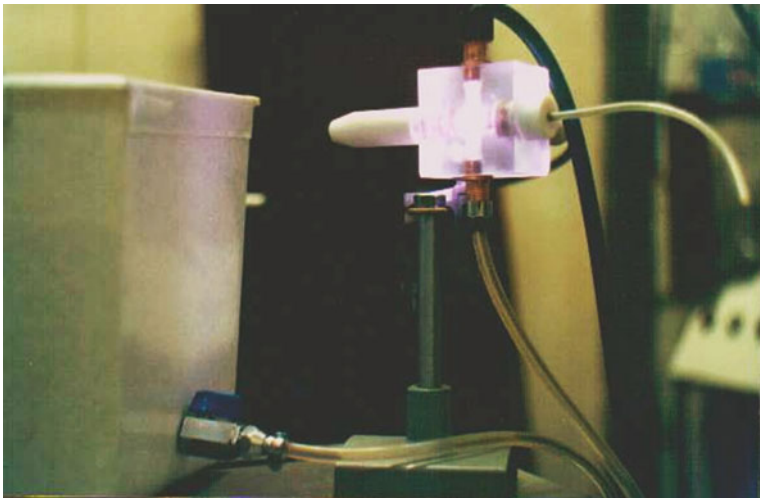

Fig. 2.12 Electrodischarge chamber "wire to plate"

- Purification of a sewage water of medical institutions, industrial plants, etc. from microbic pollutions
- Preparation of metal and oxide nanoparticles water dispersions, which can be used in medicine, biology, and pharmacology

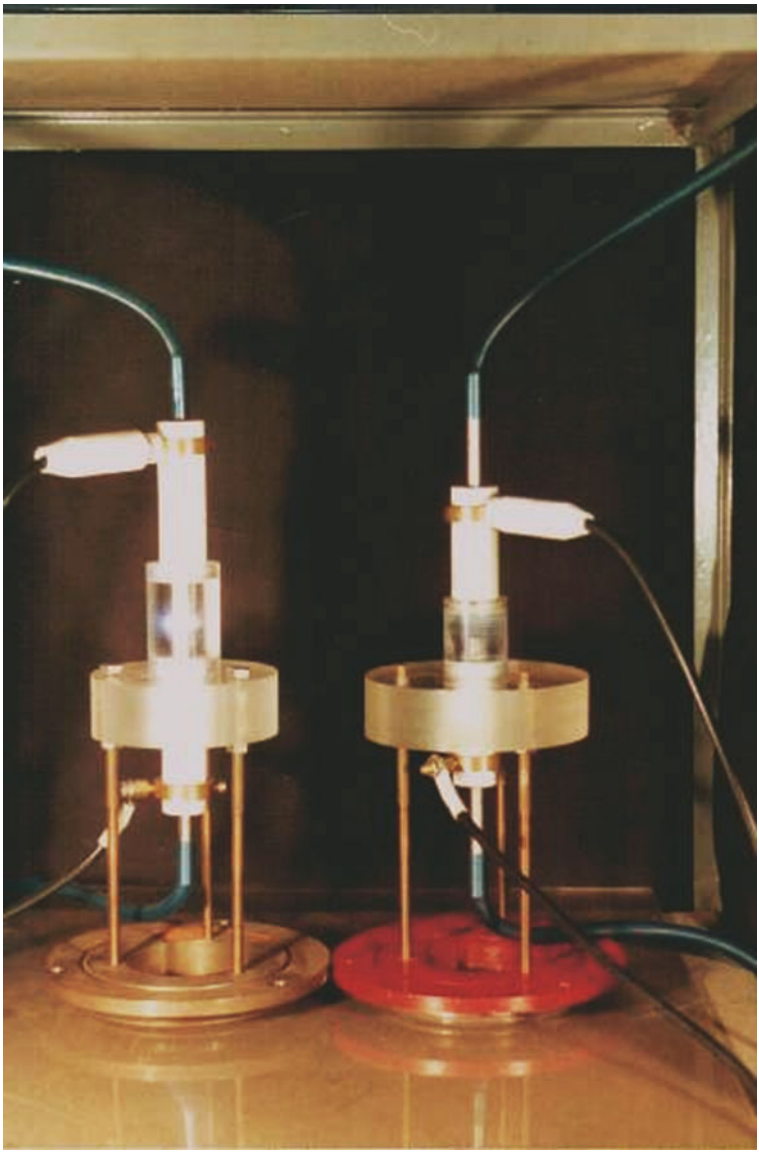

Fig. 2.13 Electrodischarge chambers "wire to tube"

The following factors affect the purification of water from pathogenic microbes:

- UV-irradiation
- Shock waves
- Nanoparticles, ions, OH–radicals, H_2O_2, O_3, O, etc.

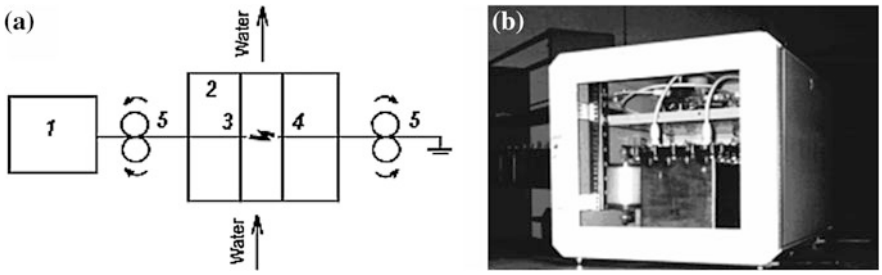

Fig. 2.14 Diagram (**a**) and image of the apparatus (**b**) [1]

Sum of all these factors leads to the so-called synergetic effect when simultaneous impact of two or several factors is more effective than impact of each factor separately.

Investigation of dependence of the water nanoparticles dispersions properties on parameters of electric discharges has shown that the low energy discharges are the most appropriate in various applications. Here, duration of the discharges is of 1–20 μs, open–circuit voltage for stable operating mode is 40–60 kV. The most suitable electrode system is "wire to wire" with the interelectrode gap ~10 mm, and diameter of electrodes 1–2 mm.

Figure 2.14 shows the block diagram (a) and image (b) of the apparatus, where (1) is generator; (2) is electrodischarge chamber; (3 and 4) are wire electrodes; (5) are feeders.

Figure 2.15 shows the basic element of the apparatus, namely, the unit of electrodischarge water treatment.

The unit comprises a case *3*, high-voltage generator (*1*), and electrodischarge chamber with feeder (*2*) (Fig. 2.16). These elements are located on two levels, and the electrodischarge chamber (for convenience of service) is mounted on a sliding shelf (*4*).

Main characteristics of the apparatus:

Open-circuit voltage	60 kV
Peak current	40 A
Duration of a pulse	20 μs
Pulse repetition rate	50; 100 Hz
Energy for deep water purification	10 J/ml
Maximal productivity	50 l/min
Power consumption	200 W
Width	60 cm
Height	60 cm
Depth	80 cm

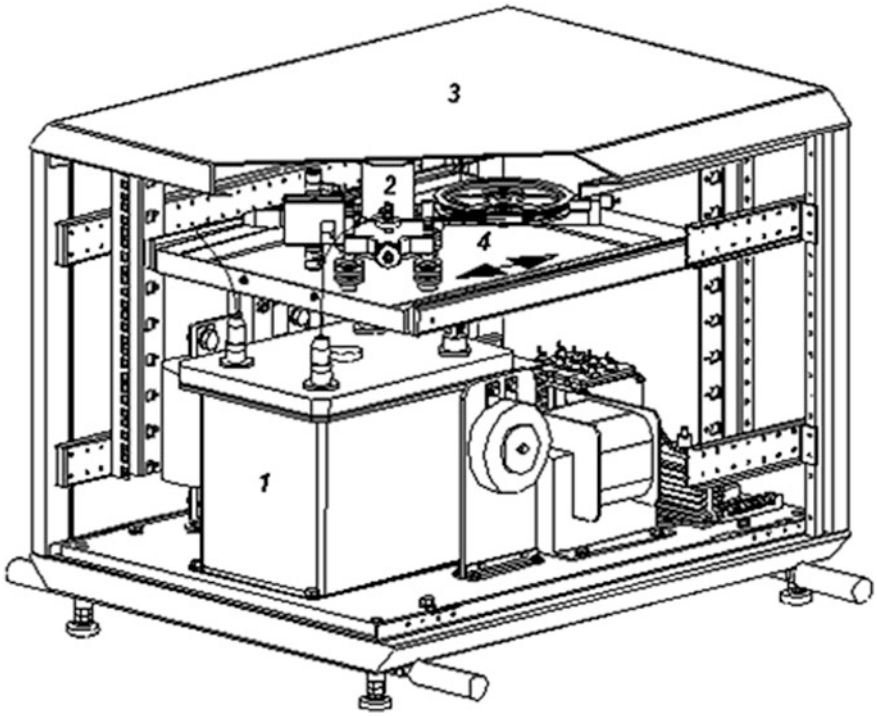

Fig. 2.15 Unit of the electrodischarge water treatment

Figure 2.16 shows schematic diagram (a), and elements of the high-voltage generator (b).

An output circuit of the high-voltage generator includes the capacitors *C6* and *C7*, and the control switch (thyristor *VS1*) for discharging the capacitors onto the primary winding of the output transformer *TV2* (Fig. 2.16a). For convenience of adjustment and replacement of elements of the generator: output transformer (*1*), thyristor (*2*), generator of driving pulses (*3*), store capacitors (*4*), reactor (*5*), transformer of charge control (*6*), capacitors (*7*), reactor (*8*), diodes (9), switch (*10*), and basic plate (*11*) it was designed as a system of the blocks and all elements of the generator are located on a single basic plate (*11*) (Fig. 2.16b).

The design provides both partial access to the elements of the generator and its full convenient dismantles. The electrodischarge chamber and feeder are incorporated into one unit (Fig. 2.17).

The basic element of the unit is the holder (*2*). The following elements are located on the holder:

– Electrodischarge chamber (*1*)
– Massive electrode (*6*)

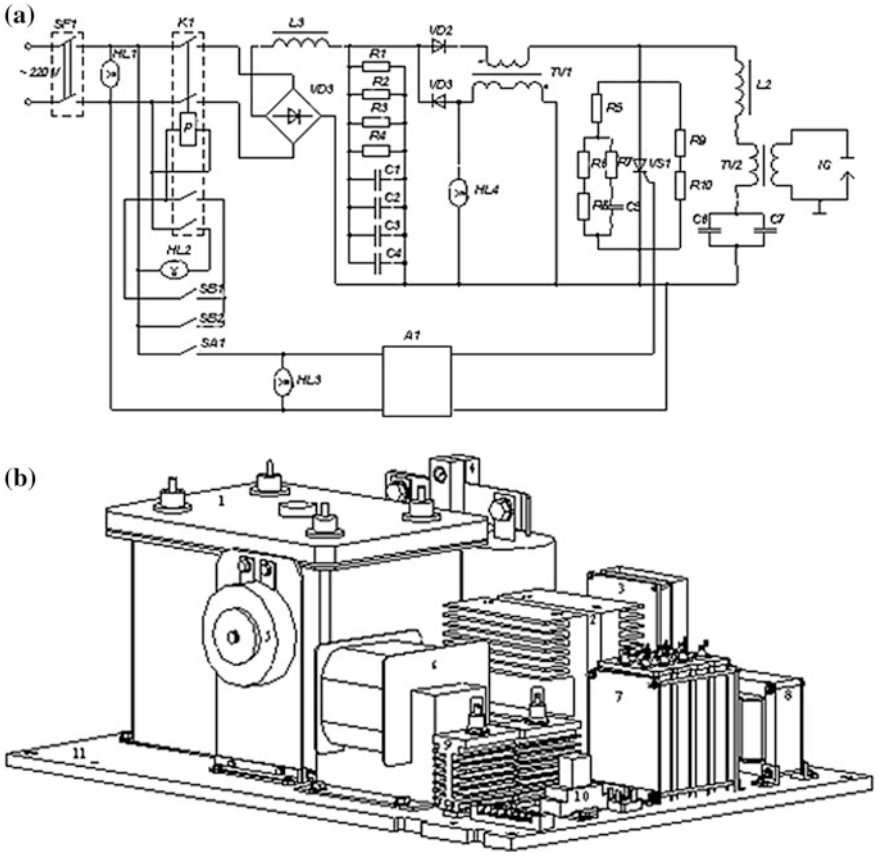

Fig. 2.16 High-voltage generator of pulses

– Reel (*11*) of wire electrode (*7*)
– Feeder (*3*, *8*, *9*, *10*)

By means of the insulators (*4*), the unit of electrodischarge chamber is installed on the pallet (*5*) that prevents possible leaking of water onto high-voltage elements of the generator. The water passes into the electrodischarge chamber is passed through the lead-in (*12*), and is removed through the lead-out (*13*). The negative potential of voltage is connected to the massive electrode (cathode) (*6*), and the positive one is connected to the wire (anode) (*7*) through the clamping roller (*9*) and drive roller (*8*).

The control system manages the feeder and the work of the apparatus in the whole. The control system is located in a separate block that includes a number of electronic circuits and is connected to the unit of electrodischarge water treatment. On the control board of the block the buttons of switching-on and switching-out and indicators of apparatus operating mode are located.

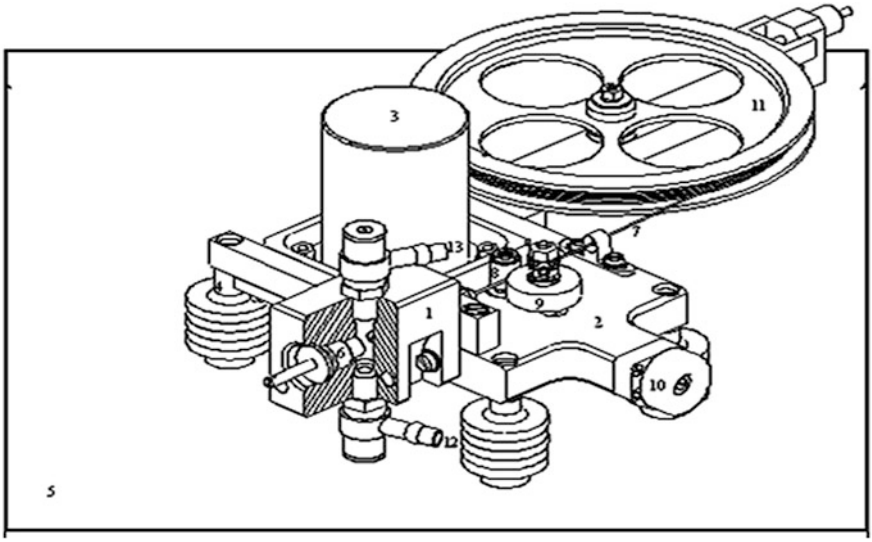

Fig. 2.17 Unit of the electrodischarge chamber and feederFeeder

Power supply of the apparatus is switched on by the switch *SF1* (Fig. 2.16a). The pecking motor operates at idle. After pressing the button *SB1* the electromagnet of the contractor *K1* is energized, its contacts are closed, the basic elements of the apparatus are energized, and the indicator *HL2* lights up. By pressing of the button *SA1*, the power supply is intended on the generator *A1*, operating by the thyristor *VS1*. After that, the voltage is delivered onto the interelectrode gap of the electrodischarge chamber through the step up transformer *TV2*. During the apparatus operation, the electrodes wear out, and the interelectrode gap is increased. As a result, this leads to missed discharges. The dropouts of the discharges are fixed by the gauges located in the primary and secondary windings of the output transformer *TV2*. The signals of the dropouts of the discharges are processed by the control system and at their number of three; the driving signal is given out onto the pecking motor.

References

1. Ph.G. Rutberg, V.A. Kolikov, V.E. Kurochkin, L.K. Panina, AP.h. Rutberg, J. IEEE. Trans. Plasma. Sci. **4**, 35 (2007)
2. Yu.V. Aristov, V.A. Kolikov, S.V. Korotkov, D.A. Korotkov, V.N. Snetov, A.Yu. Stogov, J. Electrotech. Resource Saving **4**, (2012)

Chapter 3
Diagnostic Techniques

Abstract By types of measured values, the measuring techniques can be divided into electrotechnical (Rogovsky coils, current shunts, and high-voltage dividers), optical (digital high-speed cameras, digital imaging spectrograph), physical (mass spectrometer with inductively coupled plasma (MS-ICP), transmissive electronic microscope (TEM), electron paramagnetic resonance spectroscope (EPR), ultraviolet-visible spectroscope (UV-Vis), atomic force microscope (AFM), scanning electron microscope (SEM), laser correlation spectrometer of dynamic quasi-elastic light scattering (LCS-03)), chemical (high-performance liquid chromatograph), and biological (real-time polymerase chain reaction analyzer (RT-PCR)). Complex of measurements is aimed to determination of both parameters and characteristics of physical processes taking place during the PED in water and to determination of physical and parameters of the WDN formed by means of the PED in water. Moreover, the special kind of measurements (or precisely saying, researches) are implemented in the form of biological and medical tests which allow one to determine the effect of nanoparticles of various metals on biological objects and alive organisms.

3.1 Electrical Measurements

For estimation of efficiency and power balance of an electrophysical apparatus, it is necessary to know its electric characteristics. In our case, these are discharge current, voltage drop on the interelectrode gap, and input power of the apparatus.

Measuring process of these parameters is hampered by their special characteristics. First, short duration of process; second, high ratio of voltage drop on the gap to the prebreakdown level. The solution of this task is in application of some hard wire in measuring circuits, which limits the prebreakdown voltage at registration. Thus, measurement of the input power is a routine electrotechnical procedure.

The main electrical parameters such as discharge current and voltage drop are measured by the Rogovsky coil and potentiometer-type voltage dividers.

V. Kolikov and P. Rutberg, *Pulsed Electrical Discharges for Medicine and Biology*, Biological and Medical Physics, Biomedical Engineering,
DOI 10.1007/978-3-319-18129-5_3

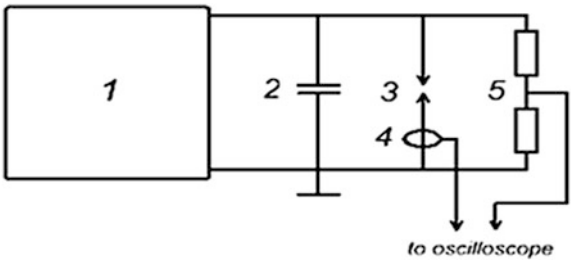

Fig. 3.1 Output discharge circuit with the Rogovsky coil and voltage divider

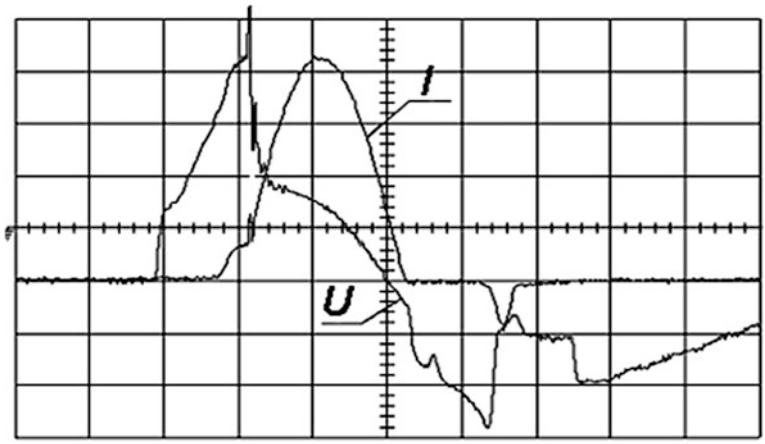

Fig. 3.2 Oscillograms of the discharge current (*I*) and voltage drop (*U*) [1]

Figures 3.1 shows the output discharge circuit of the electrodischarge apparatus with the Rogovsky coil (*4*) and voltage divider (*5*), power supply (*1*), high-voltage capacitor (*2*), and interelectrode gap (*3*).

Figure 3.2 shows the typical oscillograms of discharge current and voltage drop. (*I*) is current (10 A/div), (*U*) is voltage (400 V/div), and time is 10 μs/div.

3.2 Optical Registration

Optical registrations of pulsed electric discharges and wave phenomena in water were carried out by the high-speed cameras and imaging spectrograph. The optical devices have the following characteristics:

- Digital camera K-011 allows registering 9 frames with an exposition up to 0.1 μs and time between frames up to 0.1 μs (Fig. 3.3a)

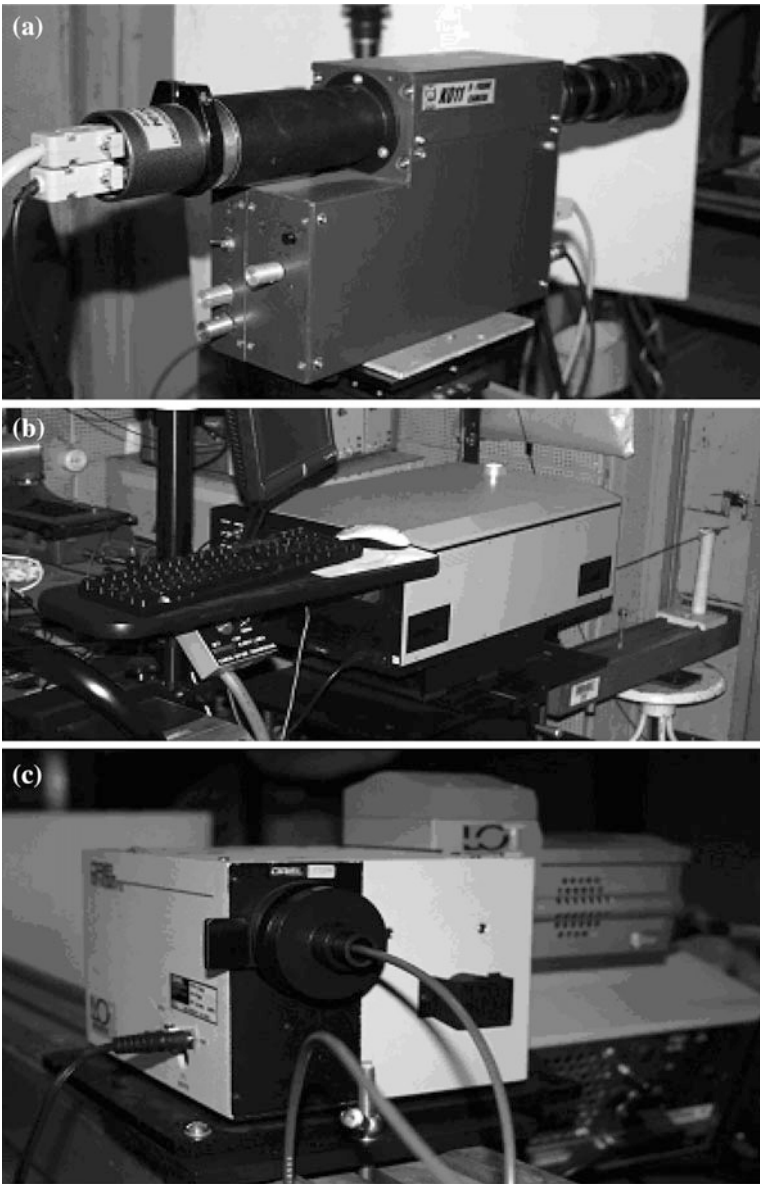

Fig. 3.3 Units of the experimental test bench [3]

- 16-frames digital high-speed camera Cordin-222-16 has exposition time less than 5 ns (Fig. 3.3b)
- Time resolution of digital imaging spectrograph MS 127i is 5 ns (Fig. 3.3c)

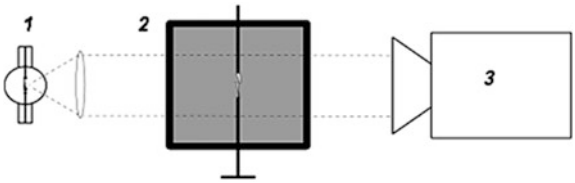

Fig. 3.4 Scheme of the optical diagnostic installation [3]

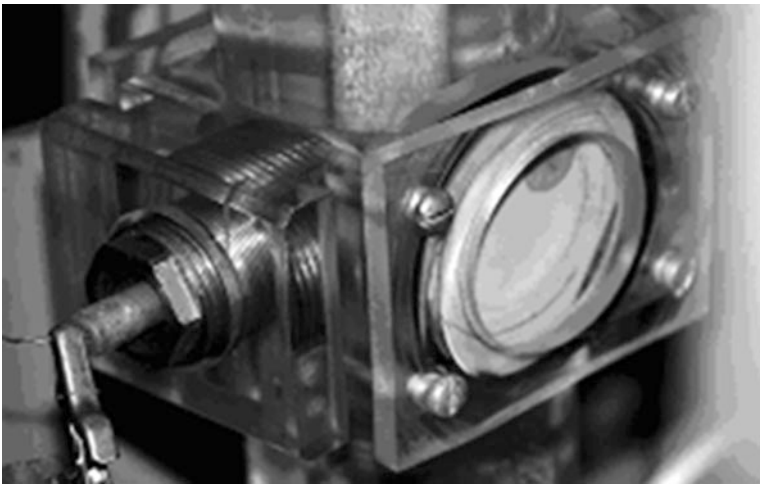

Fig. 3.5 Electrodischarge chamber with quartz windows

For hydrodynamic structure of the shock waves studying, the optical diagnostic installation using direct shadow method with a time resolution of 5 ns and a spatial resolution of 0.1 mm was developed (Fig. 3.4) Xenon lamp (*1*) was used as a backlight source for illumination of the discharge gap (*2*). The registration of process was carried out by the high-speed digital camera Cordin-222-16 (*3*).

Diagnostic system was controlled by the synchronizing pulse from a digital comparator responding to reduction of voltage on the interelectrode gap. The delay between the image exposition start and the synchronizing pulse was ≤50 ns. So, the system allowed one to record series of images for subsequent independent discharges just from the breakdowns beginning.

Electric discharges under investigation were initiated in polycarbonate discharge chamber (Fig. 3.5) with volume of 8 cm^3. The discharge chamber was powered from an electric pulsed generator. Conditions of experiments: water consumption 0–2 l/min, duration of electric pulses 0.1–20.0 μs, energy ≤ 1 J/pulse, repetition rate 1–150 Hz, electrode system is “wire to wire”, diameter of axisymmetric electrodes

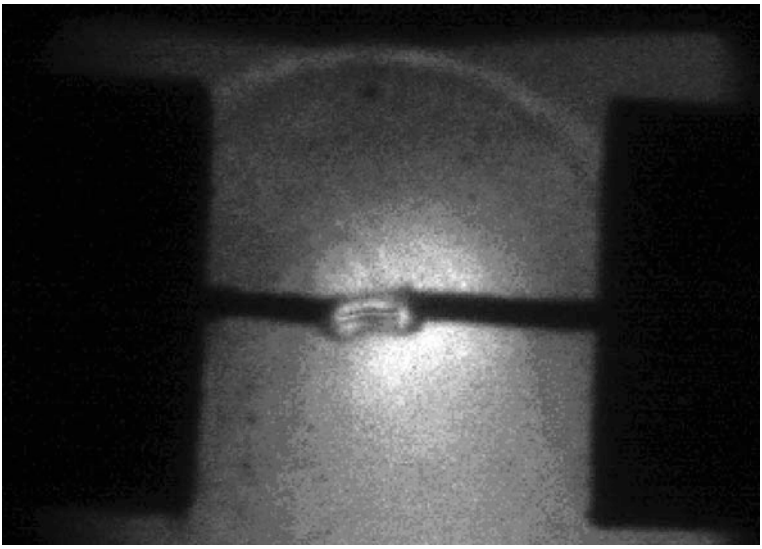

Fig. 3.6 Image of visible "merge" of two shock waves

0.5 mm, and interelectrode gap 1–10 mm. For precise optical diagnostic in the chamber, quartz windows were installed.

Figure 3.6 shows two spherical shock waves formed near the ends of the closely set electrodes. The waves visibly "merge" in one wave till 3.5 μs.

3.3 Physical and Chemical Measurements

The physical and chemical properties of metal and oxide nanoparticles, their water dispersions (produced by means of treatment of water by electric discharges), and effects of nanoparticles on biological objects were studied. The following main diagnostic techniques and devices were used.

Mass spectrometry with inductively coupled plasma (MS-ICP) was used to confirm that the electrodes' erosion produces nanoparticles of metal in water. The MS-ICP is a type of mass spectrometry, which is able to detect metals and several non-metals of concentrations as low as $1–10^{12}$ cm^{-3}. This is achieved by ionizing the sample with inductively coupled plasma and then using a mass spectrometer to separate and quantify those ions.

Transmissive electronic microscopy (*TEM*) was applied to obtain images of the nanoparticles and aggregates that are formed both of particles itself (Fig. 3.7) and of particles with biological objects. The following operations are implemented in measuring. A drop-sample of the nanostructures dispersion is placed onto carbon-coated copper grids for 30 s. The excess of liquid is removed by the filter paper from the grids. The grids are dried at a room temperature, and then are examined by

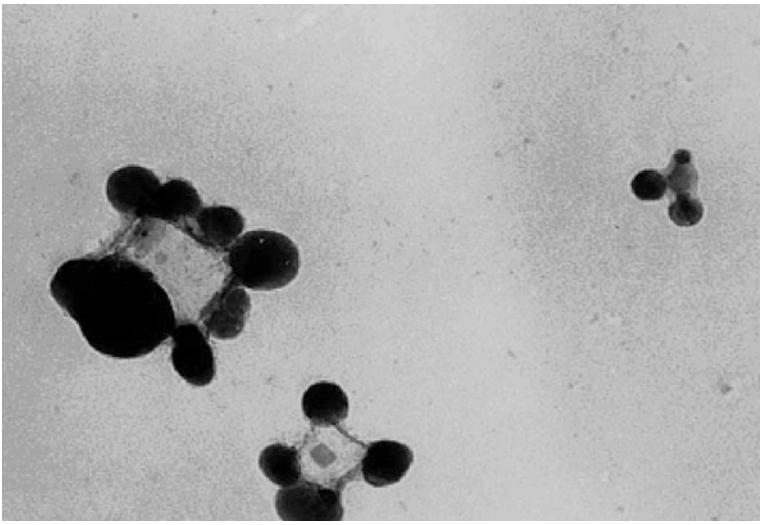

Fig. 3.7 Transmissive electronic microscopy image of the silver nanoparticles' aggregates (×200,000) [1]

a transmission electron microscope. For negative staining, 1.5 % solution of sodium phosphomolybdate is used.

High-performance liquid chromatography is a chromatographic technique used to separate a mixture of compounds in analytical chemistry and biochemistry with the purpose of identifying, quantifying, or purifying individual components of the mixture.

Electron paramagnetic resonance spectroscopy (*EPR*) is a technique for studying materials with unpaired electrons. The basic concepts of EPR are analogous to those of nuclear magnetic resonance (NMR), but these are electron spins that are excited instead of spins of atomic nuclei. Since the most stable molecules have all their electrons paired, the EPR technique is less widely used than NMR.

Ultraviolet-visible spectroscopy (*UV-Vis*) was used to determine the phase state of nanoparticles matter. The UV-Vis refers to absorption spectroscopy or reflectance spectroscopy in the ultraviolet-visible spectral region. This means it uses light in the visible and adjacent (near UV and near infrared (NIR)) ranges. The absorption or reflectance in the visible range directly effects on the perceived color of the chemicals involved. In this region of the electromagnetic spectrum, molecules undergo electronic transitions. This technique is complementary to fluorescence spectroscopy. But the fluorescence is stipulated by transitions from the excited state to the ground state, while the absorption measures transitions from the ground state to the excited one.

Capillary electrophoresis was applied to measure surface electric charge of nanoparticles. It is also known that the capillary zone electrophoresis can be used to separate ionic species by their charge, frictional forces, and hydrodynamic radius.

In traditional electrophoresis, electrically charged analytes move in a conductive liquid medium under the influence of an electric field. The technique of capillary electrophoresis was designed to separate species and is based on their size to charge ratio in the interior of a small capillary filled with an electrolyte.

X-ray analysis is a method used for determining the atomic and molecular structure of a crystal, in which the crystalline atoms cause the X-rays beam to diffract into many specific directions. By measuring the angles and intensities of these diffracted beams, a crystallographer can produce a three-dimensional picture of the electrons density within the crystal. From picture of the electrons density, the mean positions of atoms in the crystal can be determined, as well as, their chemical bonds, their disorder, and various other information.

Spectrum analysis measures the magnitude of the input signal versus frequency within the full frequency range of the instrument. The primary application is to measure the power of the spectrum of known and unknown signals. The input signal (measured by the spectrum analyzer) is electrical. But spectral compositions of other signals, such as acoustic pressure waves and optical light waves, can be determined by using appropriate transducers.

Scanning electron microscope (*SEM*) is a type of electron microscope that produces images of a sample by scanning it with a focused beam of electrons. The electrons interact with atoms in the sample and produce various signals that can be detected. In the turn, they contain information about the sample's surface topography and composition. The electron beam is generally scanned in a raster scan pattern, and the beam's position is combined with the detected signal to produce the image. SEM can achieve resolution better than 1 nm. Specimens can be observed in high vacuum, low vacuum, and in environmental. The SEM specimens can be observed in wet conditions. In our investigations, the SEM was used to research the qualitative structure of nanoparticles.

Atomic force microscopy (*AFM*) was used for determination of forms and sizes of nanoparticles (Fig. 3.8). A drop-sample of the nanostructures dispersion is put on surface of hydrogel-coated slide and dried for 1 h at a room temperature. The samples were examined with Solver Bio Scanning Probe Microscope in semi-contact mode using cantilever.

Laser correlation spectrometry of quasi-elastic light-scattering (*QLS*) was applied to measuring the nanoparticles sizes and their surface electric charge. Measurements of nanostructures size and their distribution in size are obtained by means of laser correlation spectrometer with quasi-elastic light-scattering. The quasi-elastic light-scattering method is based on interaction of a monochromatic coherent light with the particles in a liquid. Information about particles size is contained in a spectrum of fluctuations of light-scattered on particles. Nanoparticles sizes are estimated most precisely when their lorentzian is determined not less than by five points on the lorentzian half-width and when a range of measurement is not less than ten half-widths of the lorentzian [4]. Measuring the every sample is repeated in each point no less than five times, and then the data of measurements are averaged.

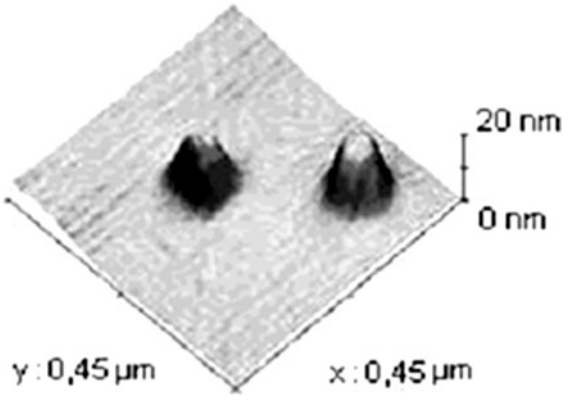

Fig. 3.8 3D atomic force microscopy image of the silver nanoparticles [2]

Real-time polymerase chain reaction (*RT-PCR*) is a laboratory technique based on the polymerase chain reaction, which is used to amplify and simultaneously quantify a targeted DNA molecule. For one or more specific sequences in a DNA sample, the RT-PCR enables both detection and quantification. The quantity can be either an absolute number of copies or a relative amount when normalized to the DNA input or additional normalizing genes.

3.4 Biological and Medical Tests

To research bactericidity of water nanoparticles dispersions, the melanin containing fungi *Ulocladium chartarum*, *U. consortiale*, *Phaeococcomyces* sp. have been chosen. These fungi are known as high tolerant ones against various kinds of external effects. Results of tests were estimated morphologically for revealing: possible infringements of their normal development and germination of spores after treatment by the water dispersion.

Cultivation of treated spores was made in Petri cups on oaten agar at temperature 23 °C, and in alveolus of microcidal tablets in a liquid nutrient medium and in water. Registration of the fungi growth in wells was performed on 96-channel photometer in a discriminate mode.

Duration of an exposition in water dispersion and the subsequent duration of cultivation of fungi were varied in dependence of test conditions. The antimicrobial activity of water nanoparticles dispersions has also been examined on *E-coli*, *Klebsiella pneumonia*, *Staphylococcus aureus*, *Pseudomonas aeruginosa*, *Salmonella typhimurium*, *Serratia marcescens*, *Citrobacter freundii*, *Bacillus subtilis*, and *Candida albicans*.

Clinical researches of method for curing the purulent wounds with a chronic component treatment were performed. The curing was carried out by water dispersions of nanoparticles. The water dispersions have been chosen with maximal

share of "small" nanostructures and maximal surface electric charge. The clinical research was implemented on 133 rats of both sexes of line "VISTAR" with weight of 170 ± 30 g. The animals were divided in three groups: one control group of 31 animals, and two test groups of 51 animals each. For treatment of wounds, the water dispersions of the silver nanoparticles were used. Purulent wounds with initial area of 150 ± 50 mm^2 were made by means of sewing (into the inter shoulder-blade areas) the gauze napkin impregnated by a solution of low viral strain of *Staphylococcus aureus*.

Lancing and surgical sanitation of the abscess were carried out on the 7th day after infecting. Treatment procedures were performed by using the water dispersions of 4.5 mg/l and solution of sodium hypochlorite of 600 mg/l in test groups of animals once-per-day during 14 days. For a comprehensive estimation of wound healing process, the methods of planimetric, bacteriological, histological examination of the wounds were used. The estimations were carried out at the 3rd, 5th, 7th, 10th, and 14th days.

The study of effect of water silver nanoparticles dispersion on periodontal microflora was performed on 21 patients of the age from 30 to 40 years. The patients were chosen with the diagnosis of moderate generalized periodontitis, with periodontal pocket depth of 5–6 mm, and alveolar bone resorption of 1/2 of the root length. The diagnosis was estimated by measuring the periodontal pocket depth by the periodontal probe.

The samples of the periodontal bacteria of all patients were taken from the periodontal pockets by sterile paper points. Further, the samples were placed into the sterile test Eppendorf tubes with preservative agent. This allowed us to estimate quantification of the periodontal bacteria.

Separately, we took the oral swab into other test tubes with a nutrient medium for revealing the oral bacteria. Examination was carried out at the date of the first survey and after 3 weeks of the patients' treatment.

The antitumor effect of water dispersions of the silver nanoparticles was studied on 19 male inbred albino rats weighing 250–300 g. The rats were divided into two groups: experimental and control ones. The Pliss lymphosarcoma cells were transplanted to animals under aseptic conditions by injecting the tumor tissue suspension into the subcutaneous tissue of the right hind limb. The silver WND were injected through a plastic catheter of 0.7 mm in diameter. The catheter was transplanted into the jugular vein and subcutaneously fixed in the occipital region of the head. Immediately after the tumor transplantation, the experimental rats daily (and twice a day) received injections of water dispersions of the silver nanoparticles in 1 ml of saline. The control animals were administered with saline. The tumors sizes were estimated as the mean value of two transverse diameters of a tumor node. All died animals were subjected to necropsy and subsequent histological study. The results were statistically processes using the unpaired Student's *t*-test by the standard method. The growth of the Pliss lymphosarcoma was observed in all animals starting the third day after the tumor transplantation.

References

1. Ph.G. Rutberg, V.A. Kolikov, V.E. Kurochkin, L.K. Panina, A.Ph. Rutberg, J. IEEE. Trans. Plasma. Sci. **4**, 35 (2007)
2. Ph. Rutberg, V. Kolikov, V. Snetov, A. Stogov, L. Noskin, S. Landa, A. Arutjuman, V. Egorov, A. Sirotkin, J. High Temp. Material Proc. **3**, 13 (2009)
3. V.A. Kolikov, M.E. Pinchuk, A.G. Leks, Ph.G. Rutberg, Proc. SPIE Paper **192**, 6279 (2007)
4. A. Lebedev, J. Levchuk, A. Lomakin, V. Noskin, *Laser Correlation Spectroscopy in Biology* (Naukova Dumka, Kiev, 1987). (in Russian)

Chapter 4
Electrophysical Processes in Water

Abstract In this chapter, the results of experimental and theoretical researches of the PED in water with energy lower of 1 J/pulse are presented. Erosion of electrodes made of various metals was studied on discharge chambers with flowing water. The basic data on the main characteristics of the PED have been obtained by studying the spectral characteristics of discharge plasma. Temperature of discharge column, which was estimated by comparison of relative intensities of radiation in the lines is $\sim 10^4$ K. At that temperature, the discharge column is a source of the UV-irradiation in wide wave range, in particular, 200–400 nm. Depending on inputted energy and discharge power, the widening of the discharge channel results in shock waves of various intensities. Behind the front of shock wave the cavitation bubbles are formed. At most cases, the shock waves are formed near the ends of electrodes and have similar velocities. Shock waves in water have high gradient of pressure, so at the size of a bacterium, the difference of pressure is enough to damage bacterial membrane and to destroy it. It was confirmed by the mass spectrometry with inductively connected plasma (MS-ICP) that the electrodes erosion produces nanoparticles of metals and their oxides in water. Size of the area of the most intensive impact of the UV-irradiation, electron hydrated electrons, and active radicals is 10–30 mm. Shares of the below factors in total bactericidity of PED are distributed as follows: UV-irradiation 70–90 %; shock waves 20–40 %; other factors 10–20 % Gorjachev et al. (J. Fuel Power Heat Syst. 2:36, 1998). PED are used for purification of wastewater containing various organic compounds, urea resin, trichlorfon, saturated, unsaturated and aromatic hydrocarbons, salts of strontium and cobalt.

4.1 Parameters and Properties of Electric Discharges

The following main PED properties and parameters of its plasma were the aims of investigations: spectral characteristics, temperature, pressure, concentration of the charged particles, etc. Registration of spectra by means of diffraction spectrograph and imaging spectrograph was implemented under conditions [1]:

V. Kolikov and P. Rutberg, *Pulsed Electrical Discharges for Medicine and Biology*, Biological and Medical Physics, Biomedical Engineering,
DOI 10.1007/978-3-319-18129-5_4

Amplitude of the discharge current	30–50 A
Average voltage drop on an arc	700–900 V
Duration of a pulse	1–20 μs
Pulse repetition rate	0.5 Hz
Interelectrode gap	3–5 mm
Electrodes	Steel and copper
Exposition	200 pulses

The discharge radiation spectra with various couples of electrodes were received based on multiple expositions. Each spectrum has the form of a continuum with a failure in the range 500–600 nm and a strong maximum at ~650 nm, onto which the line spectrum of relatively low intensity is imposed (Fig. 4.1). A bright line is H_α of atomic hydrogen 656.28 nm, a continuum in range 390–490 nm are widened lines H_β, H_χ, H_δ, H_ε, are lines of metal atoms (Cu, Fe, and Ti).

The continuum has been identified as the Stark splitted lines of the Ballmer series of the hydrogen line spectrum with additional lines of the electrodes metals. Such character of a spectrum with obvious absence of reabsorption in a continuum (under optically transparent plasma) has allowed estimating concentration of electrons in the discharge plasma by the Stark splitting of lines of the atomic hydrogen.

Estimation was made by the spectra H_α and H_β lines, which have been registered by various numbers of expositions (from 50 up to 300). Concentration of electrons was calculated by the formula

$$n_e = 10^{13}(\Delta\lambda)^{3/2}\left[C_0(T) + \sum_{n=1}^{m} C_n(T)(\ln\Delta\lambda)^n\right] \text{ cm}^{-3} \tag{4.1}$$

where $\Delta\lambda$ is the width of a line, T is the temperature, C_0–C_n are the coefficients for full Stark width of the Ballmer lines (Table 4.1).

Lengths of waves of spectral lines of hydrogen of the Ballmer series: H_α is 656.3 nm; H_β is 486.1 nm; H_χ is 434.1 nm; H_δ is 410.2 nm; H_ε is 397.0 nm.

Estimation was implemented under the assumption that the plasma temperature was about $T = 10^4$ K. This assumption does not affect the estimation of n_e as of weak dependence of n_e on the temperature (Fig. 4.2).

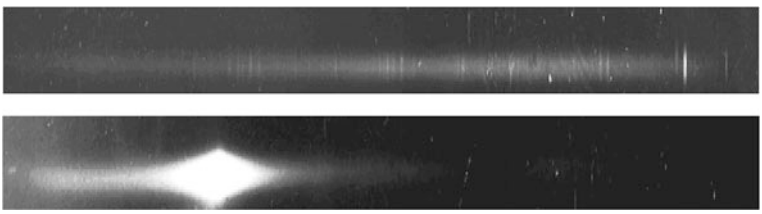

Fig. 4.1 Spectrum of the discharge radiation

Table 4.1 Coefficients for full Stark width of the Ballmer lines

	n_e (cm^{-3})	T (K)	C_0	C_1	C_2	C_3
H_α	10^{16}–10^{18}	10,000	671.4	−227.5	44.72	−2.325
		20,000	759.5	−252	43.51	−2.723
		40,000	2076.7	−1320	338.5	−30.657
H_β	10^{14}–10^{17}	10,000	36.56	−1.45	−0.109	0.005
		20,000	36.18	−1.41	−0.325	0.07
		40000	35.96	−1.48	0.366	−0.124

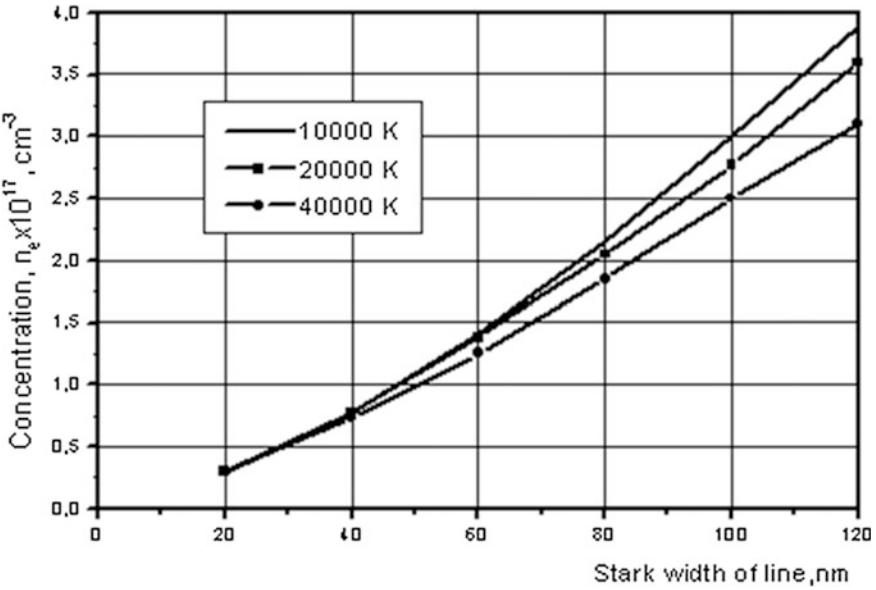

Fig. 4.2 Concentration of electrons versus full Stark width of line H_α under various temperatures of plasma

At $T = (1–4) \times 10^4$ K the accuracy of electrons concentration definition is within the limits of an error of measurement of the line half width. The value of the n_e, calculated by the line H_α is $(2.0 \pm 0.5) \times 10^{17}$ cm^{-3}, and by the line H_β is $(4.5 \pm 1.0) \times 10^{17}$ cm^{-3}.

On the basis of the relative intensity of lines of the copper and hydrogen lines (given by the Stark splitting), the relative concentration of atoms of copper (N_{Cu}/N_H) has been calculated by formula

$$\frac{J_{Cu}}{J_H} = \left(\frac{g_1 f_{12}}{g_0 \lambda^3}\right)_{Cu} \left(\frac{g_0 \lambda^3}{g_1 f_{12}}\right)_H \frac{N_0^{Cu}}{N_0^H} \exp\left(\frac{E_2^H - E_2^{Cu}}{T}\right). \tag{4.2}$$

For calculation of concentration, the hydrogen line H_β 486.1 nm and the copper 465.1 nm line were used. By exposition of ~200 pulses, the value of $N_{Cu}/N_H = (2 \pm 1) \times 10^{-4}$ was obtained.

For measuring the integral luminosity in the range of 220–260 nm, a photocell was used. The photocell absolute calibration and calibration of the path measurement of radiation were performed by the plasma brightness standard ISP-1 (Pulse-5).

To determine the temperature of the discharge plasma, registration of the discharge spectra was carried out by imaging spectrograph.

Figure 4.3 shows the relative intensity distribution of the discharge column radiation on electrodes about 70 % of the silver and 30 % of the copper alloy.

The temperature of discharge column, which was estimated by comparison of relative intensities of radiation in the lines, is $\sim 10^4$ K. At such a temperature, the discharge column is a source of the UV-irradiation in wide wave range, particularly, 200–400 nm [2, 3]. Being effectively absorbed by water, the UV-irradiation, produces H_2O_2, O_3, O, and OH radicals [4, 5], which destroy microbes and some organic compounds.

The average specific electric conductivity is $\sim 10^3$ $(\Omega\ m)^{-1}$. It was estimated for the following parameters of the discharge column: diameter of ~1 mm, length of 10–13 mm, and resistance of 15–20 Ω.

Figure 4.4 shows the plasma electric conductivity as a function of its temperature and pressure, which were calculated under assumption of the thermodynamic equilibrium of the column structure.

Thus, from Fig. 4.4 it is seen that under pressure of 0.5–6 MPa (pulsed pressure measured on the wall of the discharge chamber), the temperature of the discharge column is $(0.9–1.1) \times 10^4$ K. This is in a good accordance with the data above.

Figure 4.5 shows images of the evolution of structure of the discharge column, registered by high-speed camera under length of the discharge channel is 13.5 mm.

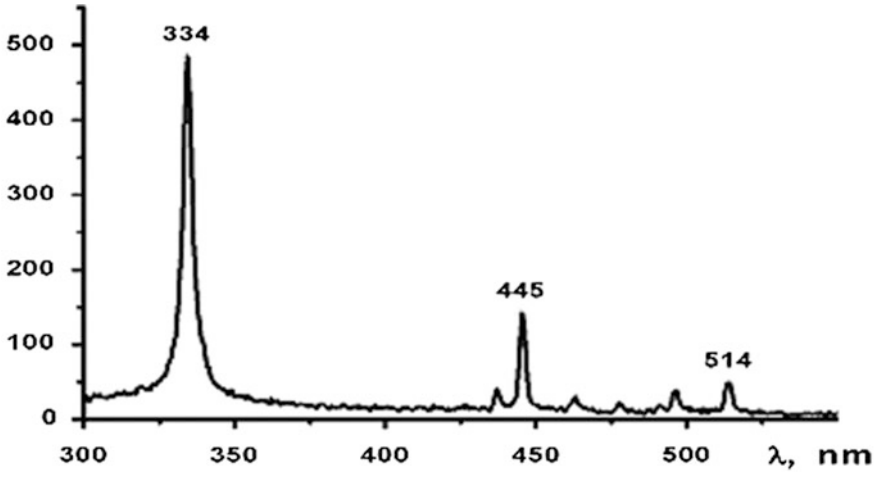

Fig. 4.3 Spectrum of the discharge radiation (intensity in relative units) [6]

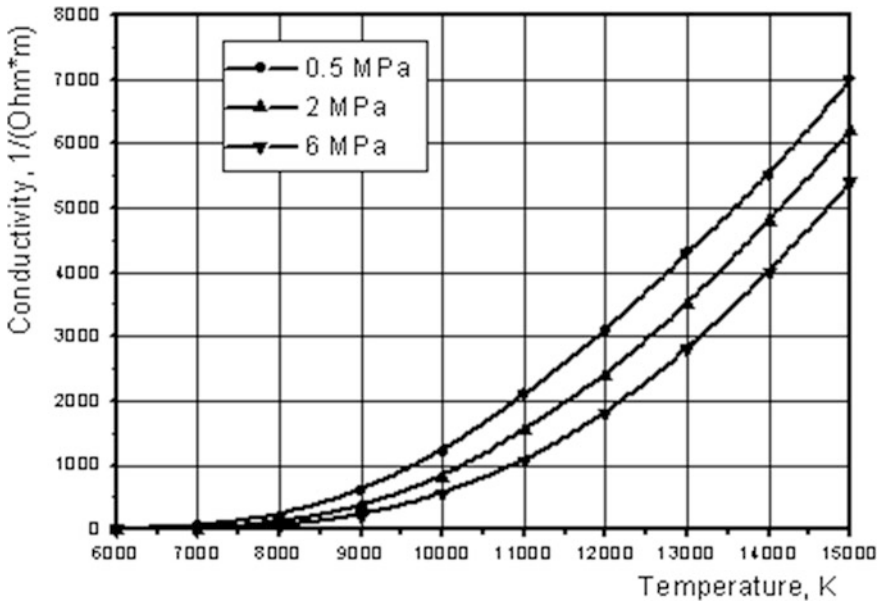

Fig. 4.4 Specific electric conductivity of plasma versus temperature and pressure [6]

Using the images of the discharge channel and the data of volt-ampere characteristics, the values of electric conductivity of the discharge plasma at the instants near to maximum of the current were calculated.

Values of electric conductivity obtained from experiments were compared with calculated ones, in which the temperature and pressure were varied. These data have allowed us to estimate the plasma thermodynamic temperature as (0.9–1.1) × 10^4 K in the discharge channel. Brightness temperature was determined based on the radiation intensity is some lower of (7.5–8.8) × 10^3 K. It means that the discharge plasma channel with diameter of ~1 mm is not an absolutely black body in spite of the high density of plasma.

Temperature obtained by calculation of physical characteristics of the discharge is also higher than the brightness one.

For estimation of parameters of plasma in a column of the discharge, the task of properties of plasma has been solved. For calculation of key parameters of the plasma column, the model presented by the following system of equations was used:

$$\begin{aligned} &\frac{\gamma}{\gamma-1}P\frac{dS}{dt}+\frac{1}{\gamma-1}S\frac{dP}{dt}=\frac{N(t)}{l} \\ &P=\frac{\rho}{2\pi}\frac{d^2S}{dt^2}\ln\left(\frac{\sqrt{\pi}l_k}{\sqrt{S}}\right)-\frac{\rho}{8\pi S}\left(\frac{dS}{dt}\right)^2 \end{aligned} \tag{4.3}$$

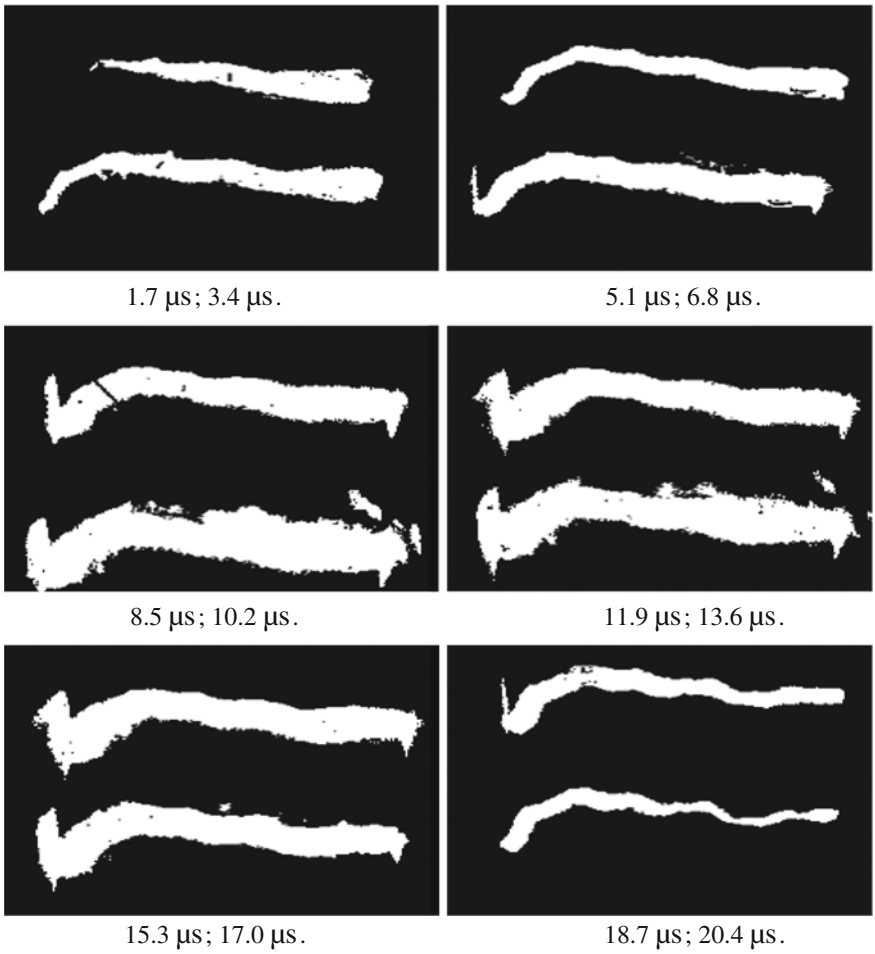

Fig. 4.5 Evolution of the discharge column

here the first equation gives a balance of energy of a plasma column of area $S = \pi \cdot r^2$, and of length l, where P is pressure of plasma, γ is adiabatic exponent, $N(t) = J(t)\ U(t)$ is electric power of the discharge (determined experimentally). The second is Riley equation, where ρ is density of water.

Experiments showed that at low energy of a pulse (about 0.5 J), the temperature in a column of the oxygen-hydrogen plasma is (1.0–1.5) × 10^4 K. Calculation results on specific electric conductivity of plasma for thermodynamical equilibrium depending on temperature and pressure are presented in Fig. 4.4.

The plots show that the gas state is well described by equation of an ideal gas without taking into account the ionization. Therefore, it is possible to add equation of condition of an ideal gas to the basic system of equations. To choose the initial

conditions for numerical integration, the following assumption was made: after passage of the leader (i.e., the instant of breakdown of the interelectrode gap), a cylindrical channel filled by water steam (at $T = 400$ K) is formed. The radius of the channel varies in the range 0.1–0.2 mm. Using these data, the value of electric conductivity of the discharge plasma has been calculated.

Calculation of electric conductivity of the water plasma was carried out by the Frost's formula

$$\sigma = \frac{4}{3\sqrt{\pi}} \frac{C_e e^2}{\sqrt{2 m_e k T}} \int_0^\infty \frac{x^{0.5} e^{-x} dx}{\sum\limits_\alpha C_\alpha \sigma_{e\alpha}}, \tag{4.4}$$

where $x = \frac{m_e V_e^2}{2kT_e}$, $\sigma_{e\alpha}$ is cross-section of electron—atom collisions; C_e, C_α are volumetric concentrations of atoms and electrons.

Values of the cross-sections of collisions of a neutral particle with atom are referenced ones. Values of the cross-sections of collisions electron with electron, electron with ion were calculated by the formulas

$$\begin{aligned} \sigma_{ee} &= 16\pi \left(\frac{e^2}{8\pi \cdot \varepsilon_0 x} \right)^2 \Delta \\ \sigma_{ei} &= 4\pi \left(\frac{e^2}{8\pi \cdot \varepsilon_0 x} \right)^2 \Delta \end{aligned} \tag{4.5}$$

where Δ is Coulomb logarithm.

Here, the integral was calculation by the Simpson's formula in a range of (0–12) eV.

Concentration of components was calculated by an iterative method from the system of the equations

Condition of regulation

$$C_e + C_+ + C_H + C_O = 1.$$

In this calculation, only the single ionization was taken into account under full dissociation

$$\begin{aligned} &C_e = C_+ = C_{H+} + C_{O+} \\ &(C_H + C_{H+})/(C_O + C_{O+}) = 2 \\ &C_e C_{H+} C_H^{-1} = K_H \\ &C_e C_{O+} C_O^{-1} = K_O. \end{aligned}$$

Constants of balance were calculated by the formulas:

$$K_H = kTp^{-1}\left(\frac{2\pi \cdot m_e kT}{h^2}\right)\exp\left(\frac{-E_H}{kT}\right)$$
$$K_O = \frac{8}{5 \cdot 1.77}kTp^{-1}\left(\frac{2\pi \cdot m_e kT}{h^2}\right)\exp\left(\frac{-E_O}{kT}\right) \quad (4.6)$$

where E_O, E_H are energies of ionization.

Further, the data of electric conductivity were used for estimation of temperature inside the discharge column. These estimations confirm results of analysis of the plasma spectral characteristics. The plasma is optically transparent since the equilibrium thermodynamic temperature is much more than the temperature determined by the value of radiation.

Along with a monopulse operating mode of the generator, the oscillatory mode was organized and techniques of measuring the current, voltage, and pressure on walls of the electrodischarge chamber were advanced.

Comparison of the pulsed pressure under the same energy in pulse was carried out for two electric discharges (Figs. 4.6 and 4.7): "slow" of 20 μs duration and

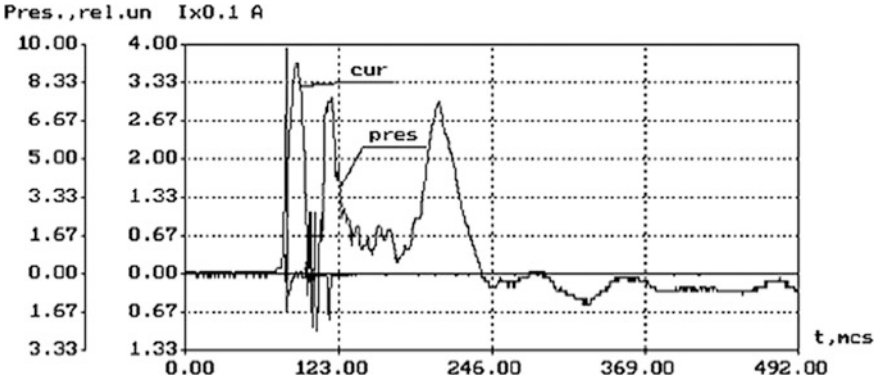

Fig. 4.6 Current and pressure under monopulse "slow" mode [6]

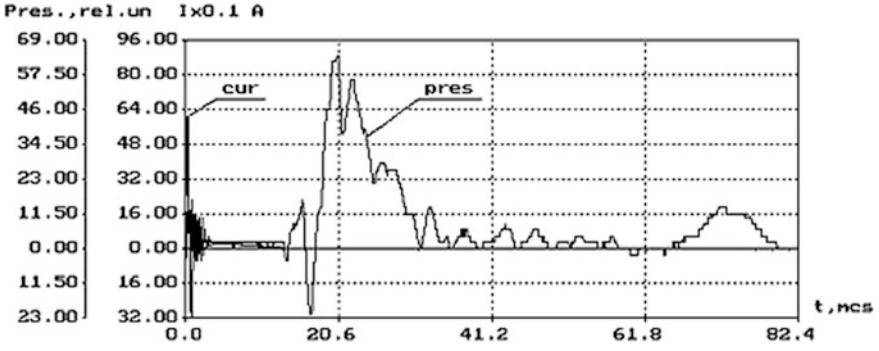

Fig. 4.7 Current and pressure under oscillatory "fast" mode [6]

current rise rate dI/dt of 5×10^6 A/s; and "fast" of 1 μs duration and current rise rate of 2×10^9 A/s. The discharge power increasing results in the proportional increase of the pulse pressure. Therefore, for the "slow" discharges, the amplitude of the shock wave measured at the wall of the discharge chamber is ~0.5 MPa (~7 rel. units) and for the "fast" ones the pressure is ~4 MPa (~60 rel. units).

4.2 Main Characteristics of Pulsed Electric Discharges in Water

Until now, properties and characteristics of the PED in water were mainly studied for the solution of two technical problems: the first is usage of water as a high-voltage insulator, and the second one is application of electric explosion for development of various hydro-pulsed technologies. Only in recent decades, these investigations are also addressed to ecology, biology and medicine.

The main results of researches of the breakdown in water and the PED have been presented in papers [7–10]. These investigations are necessary to develop facilities using the PED in water for the mentioned purposes. In these papers, the effect of various factors onto mechanism of the breakdown and onto breakdown voltage was determined. The following factors were studied: γ-quanta, electron beams, variation of water temperature, initial conductivity, geometry and material of electrodes.

Figure 4.8 shows the qualitative current-voltage characteristic of the electric breakdown in water for the homogeneous field with flat electrodes. This characteristic was defined based on the generalized results of these investigations.

Here:

- Area I is similar to dependent conductivity in gases and corresponds to the ion conductivity caused by dissociation and ionization stipulated by the radiation and conductivity of the hydrated electrons
- Area II usually takes place due to impurities in the water
- Area III corresponds to the electrical breakdown of water in a homogeneous field

In all cases, the streamers appear up to the instant of the breakdown except for very short pulses. Remind that streamers are branched structures consisting of the conducting and filiform channels. Along the streamers, the leaders are moved from the origin points (as a rule, these are some irregularities on the surface of the electrode) to the opposite electrode. The leaders connect electrodes across the interelectrode gap and initiate the discharge that is similar to the electric arc in gases.

The hypothesis was propounded that explains the leader appearance due to impact ionization of the water molecules by electrons or ions emitted from the electrodes surface and accelerated by the electric field [7].

But this hypothesis is not valid for the following reasons:

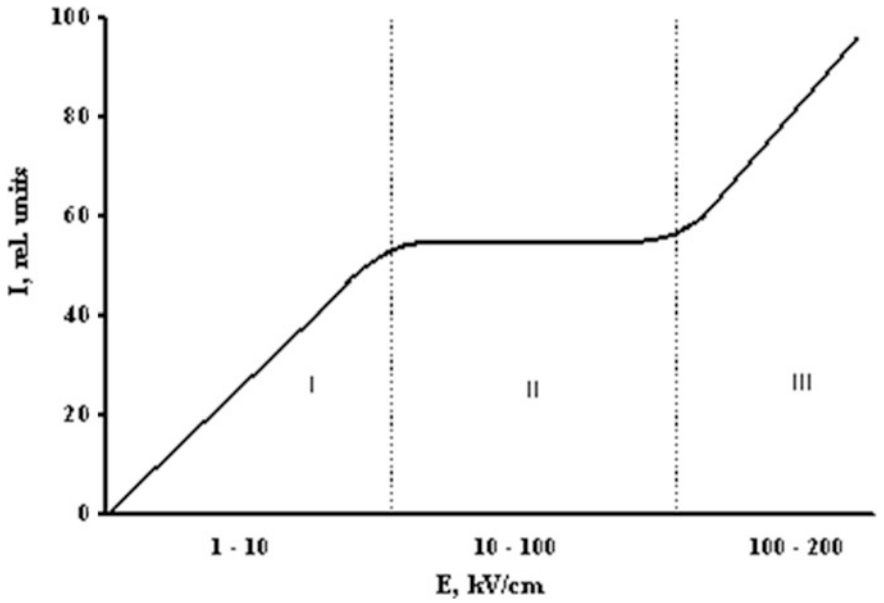

Fig. 4.8 Qualitative current-voltage characteristic of electric breakdown [1]

- It was established that the electrons are slow-moving in a liquid (hydrated) $\mu = 10^{-6}$ m^2/(V s) up to the field strength of 2×10^9 V/m
- External radiation does not effect on the breakdown voltage
- Sharp change of the phase state of the liquid precedes to occurrence of the leader; by optical methods, it was found that in dependence on the field strength and pulse duration, the "breach" of fluid (electrostriction) or forming of the gas bubble appears [11]
- Occurrence and motion of the leader are accompanied by strong hydrodynamic perturbations among them, namely, by generation of the shock waves [12]

Thus, it can be assumed that the electrical breakdown of the microsecond range is occurred when the energy of the electric field produces gas microcavity. The gas in the cavity is ionized and forms the plasma, which has a significant electric space charge in the "head" of the leader [12]. Depending on duration of the pulse, voltage, and state of the electrodes surface, the following reasons of the "gap" of the fluid are possible [10, 13–15]:

- Under the effect of the electric field, the gas is "pulled" from the pores of the electrode
- Separation of the liquid from the electrode surface
- Due to the electrostriction pressure

These phenomena may arise at voltages of 200–500 kV under short pulses of $\sim$1–10 ns, or at a local overheating of the liquid up to the boiling point [10].

The overheating is caused by current flow near the electrode tip under the pulse duration of 10–1000 ms and voltage of 10–40 kV. Formation of a gas cavity in fluid at the breakdown requires a certain time. The following formula presents the dependency obtained experimentally for quasi–uniform field and flat or cylindrical electrodes [10, 13]

$$E = k/t^{1/3} S_e^{1/10} \tag{4.7}$$

where $k \sim 1$ is depended on the type of liquid, t is time; S_e is area of electrode.

Let us consider in details the breakdown process that has occurred in the "wire to plate" electrode system at pulse durations of 10–100 μs, as this type of PED are of the greatest interest for technological applications [12, 15]. The breakdown is occurred due to the forming of the leader near the tip of the electrode, and the breakdown voltage is less if the tip electrode is anode (Fig. 4.9).

Before occurrence of the leader near the tip electrode, the spherical glowing area of 50–150 μm in diameter is formed. Then for 0.5 μs, numerous small torches occur that results in forming the leader. The latter moves spasmodically to the plate electrode with the average velocity of 10^4 m/s.

During its motion, the leader creates plasma channel expanding with the velocity of (1–6) × 10^3 m/s. Father ionization of the gas in the bubble occurs due to auto-ionization in the electric field of the space charge. The electron concentration achieves 10^{17}–10^{18} cm^{-3}.

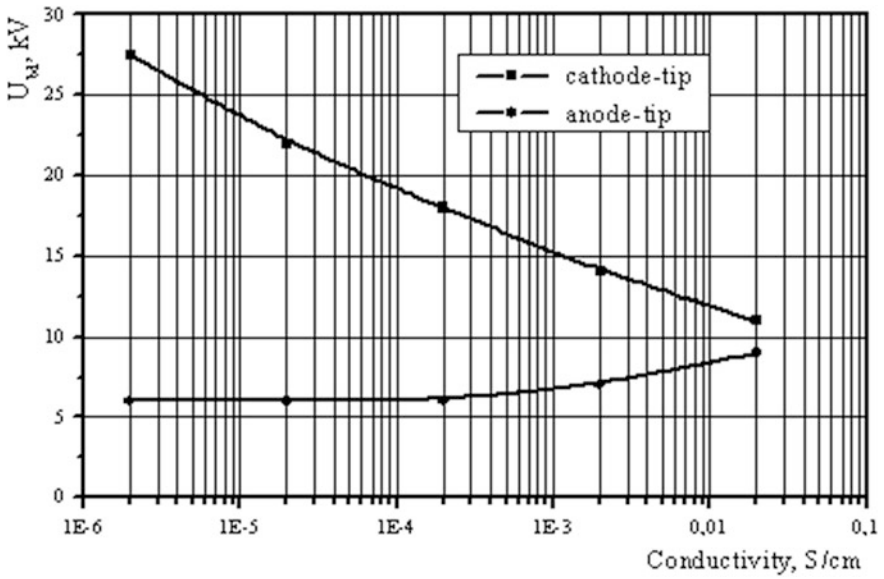

Fig. 4.9 Breakdown voltage versus electrode shape and conductivity of water

When the leader reaches the surface of the opposite plate electrode, the electric arc occurs in the gas cavity created by the moving leader. The voltage and current of the discharge depend on parameters of the power supply and size of the inter-electrode gap. The current-voltage characteristic has a falling character due to increase of the electric conductivity, expansion of the arc channel, and the gas cavity.

At this stage, the main input of the discharge energy takes place. Under this, the main share of the electric energy (of 200 J/cm^3) is transformed to the mechanical work for the gas cavity expansion [12, 16–18].

Since of the bubble expansion during 10^{-6}–10^{-5} s, the shock waves in water are generated. Their intensity is increased when the energy input into the discharge increases [12, 17]. Convergent shock waves can also be formed around the tip electrode under collapse of the discharge bubble.

Intensive shock waves generated during the gas cavity expansion under large pulse energy (significantly larger than 1 J) make high mechanical stresses in the walls of the discharge chamber.

In the unit, the stresses are especially appearing on the tip electrode and in the electrode itself, whereby it is destroyed rapidly. Thus, under these conditions, the shock waves make it difficult to develop reliable discharge chambers. These drawbacks can be eliminated by the PED impact (with energy lower than 1 J) on the water flow in the channel [19].

During the study of the PED, electrodischarge chambers of various designs were used: cylindrical, rectangular of flow-through, and cuvette types. In the most of experiments, the electrode systems “wire to wire” or “wire to plate” with the tip electrodes of 1–2 mm diameter were used. The following electrode materials were applied: silver, copper, stainless steel, tungsten, and their alloys.

A series of experiments with thick electrodes of the cylindrical shape was carried out including ones with the axial hole, through which the air was blown down. The bubbles formed around the electrode surface initiated the electric breakdown of the interelectrode gap at lower voltage. The purpose of these experiments was to reduce the mechanical stress on the electrode and to decrease its erosion. However, the discharge chamber complexity is not offset by the achieved results.

Investigation of the shock waves was carried out; they were generated by the PED in the special cylindrical chamber of 5–6 cm diameter and height of 1.5 cm. The pressure was measured by piezoelectric transducers placed on the sidewall of the discharge chamber. The measurement results were compared with calculations, in which the discharge channel is considered to be cylindrical. Change of the pressure in the channel of the discharge is described by the energy equation [14].

$$\frac{d}{dt}\left(\frac{PV}{\gamma - 1}\right) + P\frac{dV}{dt} = N(t) \tag{4.8}$$

where V is volume; P is pressure; $\gamma = c_p/c_v$ is adiabatic index, $N(t)$ is discharge power. Equation of the state water (equation Theta)

$$(P + B)/(P_0 + B) = (\rho/\rho_0)^k \tag{4.9}$$

where B = 304.5 MPa, k = 7.15.

System of (4.8) and (4.9) is closed by equation of the wave's motion in water. Remind that this motion is produced by motion of the boundary "water-wall of the discharge channel". From numerical solution of the equation system, the pressure changes (in the water surrounding the discharge channel) are obtained in space and time.

The main results of the calculation are the following: the PED in water at low pulse energy generates the shock wave; the pressure amplitude on front of the shock wave depends on the energy and power of the discharge, and it decreases with distance from the discharge channel by the law l/r, where l is the width of the interelectrode gap.

In experiments with moveless water, the relative distribution of the hydrated electrons concentration in the space between electrodes was measured [20]. The hydrated electron is bounded by polar water molecules [21]. They are extremely active in the chemical and biological processes. The lifetime of the hydrated electrons in water is $\sim$450 μs.

The relative distribution of the hydrated electron in the discharge area was determined from the absorption of the laser radiation with a wavelength of 632.8 nm. Here, ability of the hydrated electrons rapidly to absorb radiation over the wide spectral band with λ_{max} = 715 nm was used.

Size of area of the most intensive impact of the UV-irradiation, electron hydrated electrons, and active radicals is 10–30 mm. Thus, conventional cross-section diameter of the culvert channel of the discharge chamber must match this value to provide the maximum effect on chemical and bacterial contaminations.

Note that the PED with low (≤1 J) energy in a pulse does not generate very intensive shock waves in the electric discharge chamber. It results in consumption of additional energy to mechanical work. In the turn, efficiency of chemical and bactericidal effects of such PED is higher than of the high-energy (≥1 kJ) discharges. This feature of the low energy PED allows one to design electrodischarge chambers with resource of operation up to 10^3–10^4 h.

4.3 Shock Waves, Cavitation, and UV-Irradiation

Nowadays the low energy PED have wide prospects in various applications such as materials processing, plasma-chemical technologies, medicine, and biology [22–26]. One of such important practice is usage of the PED for water purification from pathogenic microbes [19]. In each case, advantages of the PED are caused by many physical, technical, and economical factors. Successful applications in medicine and biology are connected with prolonged microbial resistance of water (PMRW) [6, 27], and with high efficiency of purification from organic and other substances [28–34].

The UV-irradiation and shock waves play the main role among the factors of disinfection of water by the PED [16]. To destroy bacteria by the shock waves, it is necessary to break the bacteria membrane. In this case, thickness of the shock wave front must be comparable with size of microorganisms, and the amplitude of pressure in the front of shock wave must be ≥2 MPa [35].

So far, the process of energy transfer from the discharge channel to the shock wave is not studied completely. Simple increasing of energy input into the discharge does not lead to proportional increasing of the pressure steepness and amplitude pressure of the shock wave [18, 36]. Since the electro acoustic coefficient of energy transfer from discharges to water is low, the energy released in the channel of the leader is small because of high ballast resistance of water [37].

The following characteristics of the PED are most optimal on effectiveness and most suitable for technical implementation: duration of 1–20 μs, energy of 0.2–1.0 J/pulse, current rise rate of 10^5–10^9 A/s, and pulse repetition rate of 50–100 Hz. The optimal electrode system is "wire to wire" or "wire to plate" for the interelectrode gap about 10 mm and the wire electrode diameter of 1 mm. The most effective action of the UV-irradiation and shock waves onto pathogenic microbes takes place under the pipe culvert diameter of 10 mm [38].

The researches of the shock waves and the UV-irradiations were performed in the electrodischarge chamber with copper and steel electrodes that is modeling the unit meant for practical usage, and several high voltage generators for various modes of the PED functioning.

The measurement schemes of laboratory installations are presented in Fig. 4.10. Here *1* is electrodischarge chamber, *2* is converging lens, *3* is fiber-optic cable, *4* is imaging spectrograph, and *5* is 9-frames high-speed digital camera.

Typical oscillograms of the discharge current and voltage drop on the interelectrode gap are presented in Fig. 4.11, where *I* is current 10 A/div., *U* is voltage 400 V/div., and time 10 μs/div.

Till the instance of the interelectrode gap breakdown, the prebreakdown stage proceeds. During this stage for ∼5 μs, the current increases up to 7 A and voltage increases up to 35 kV (the voltage oscillogram has restriction on 1700 V). Since the breakdown and forming the discharge channel, the current increases up to maximal

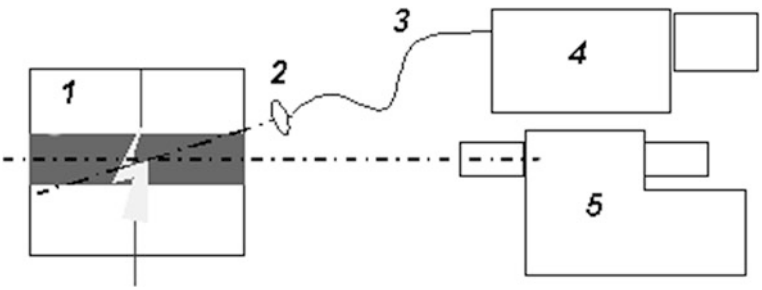

Fig. 4.10 Scheme of the diagnostic techniques [39]

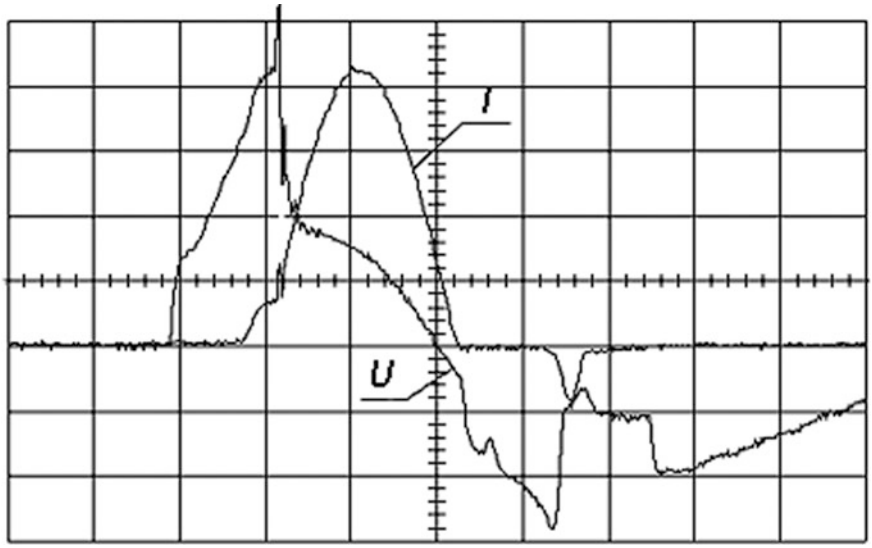

Fig. 4.11 Oscillograms of the current and voltage drop across interelectrode gap [39]

value of 43 A for 8 μs. Thus, the current shape is close to a sine wave, the voltage drop on the gap monotonically decreases from 1 kV to zero.

The mean value of the voltage drop on the gap is ~700 V. The pulse duration is 20 μs. The input electrical energy during the pulse is ~0.4 J. Depending on the inputted energy and discharge power, the widening of the discharge channel results in shock waves of various intensities.

Images of evolution of the discharge channel under various powers of discharge, unipolar and oscillate modes, and with interelectrode gap of 10 mm were registered by the high-speed camera. Processes are presented in Fig. 4.12, where sequence of images from left to right and top downward. In oscillograms the current pulse above, pulses from high-speed camera below.

One hundred experiments were performed near the current maximum of the first half-period by the high-speed camera NanoGate-1 under exposition of 10 ns. Analysis of images shows that in 10 % of cases there are more than one channel of the discharge simultaneously: six discharges with two channels, and four discharges with three channels (Fig. 4.13).

Configurations of the discharges with several channels are steady, i.e. the discharge channels exist for all time of the current pulse half-period. In the second half-period, the point of the breakdown and the form of the channel do not correspond to the point and form of the previous discharge channel.

Figure 4.14 shows the images of the streamer in 100 ns and stages of the leader head motion along the streamer channel from the cathode to anode across the 16 mm interelectrode gap in 200 and 300 ns after its breakdown. Thus, the leader

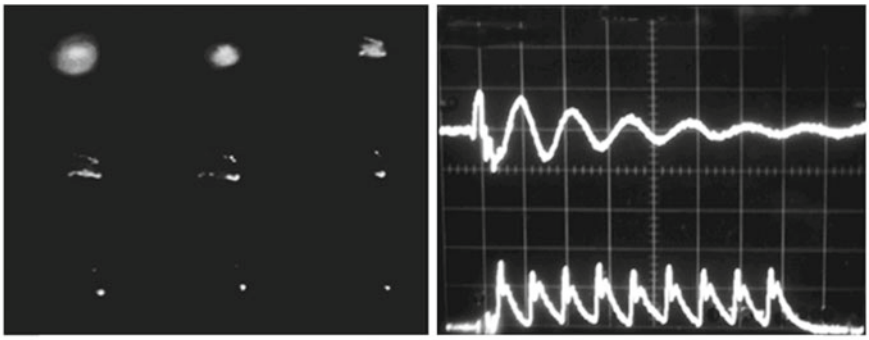

Current 40 A/div. Current rise rate ~ 4×10^8 A/s. Time 0.25 μs/div.

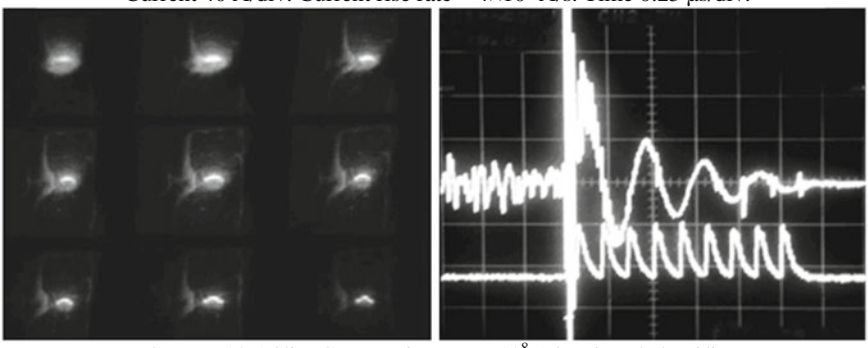

Current 10 A/div. Current rise rate ~ 10^8 A/s. Time 0.5 μs/div.

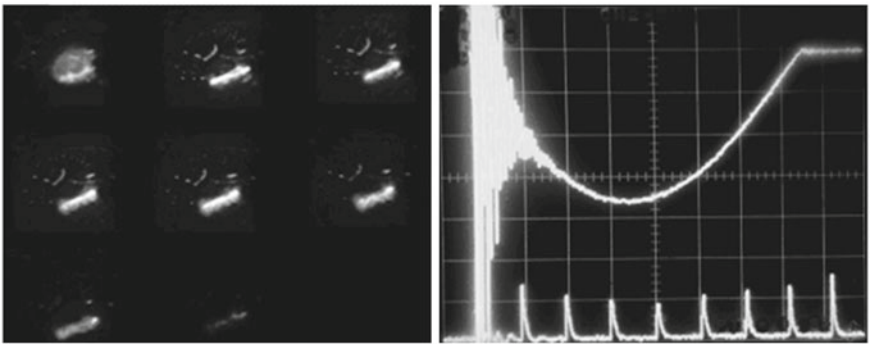

Current 10 A/div. Current rise rate ~ 5×10^6 A/s. Time 2 μs/div.

Fig. 4.12 Evolution of the discharge channel (*left*) and oscillograms of discharge current (*right*) [39]

head velocity is more than 1.6×10^5 m/s that agrees rather well with the experimental data obtained in [40].

It is known that the widening of the discharge channel during the earliest stage of the discharge results in generation of the shock wave [41–44], and than (through

Fig. 4.13 Forms of the discharge channel [39]

$\sim$350 μs) cavitation bubble is formed [18]. In later stage, the bubble is collapsed with generation of second shock wave (Fig. 4.15).

Shock wave velocities were measured under various discharge powers, energy inputs, and interelectrode gaps. The shock wave velocity was calculated by the shock wave coordinates measured from frame-to-frame (Fig. 4.16) and by difference of time between the frames. The shock waves in water have high gradient of pressure at their fronts, so, for the size of a bacterium, the difference of pressure is enough to damage bacterial membrane and to destroy it [39].

The amplitude pressure in the shock wave front measured at the distance $\sim$10 mm from discharge column. The pressure in this point was ranged from 0.5 to 4 MPa.

Figure 4.16 shows two spherical shock waves forming near the ends of the electrodes. In the very early stage, their velocity is $\sim 10^4$ m/s.

Essentially lower (<1,500 m/s) measured velocity of the shock wave propagation were obtained in [40, 41]. This fact is explained by the high shock wave velocity decrement at large (more than 1 μs) time of the shock wave propagation [40], and large (more than 10 mm) distance of the pressure transducer from the plasma channel [41].

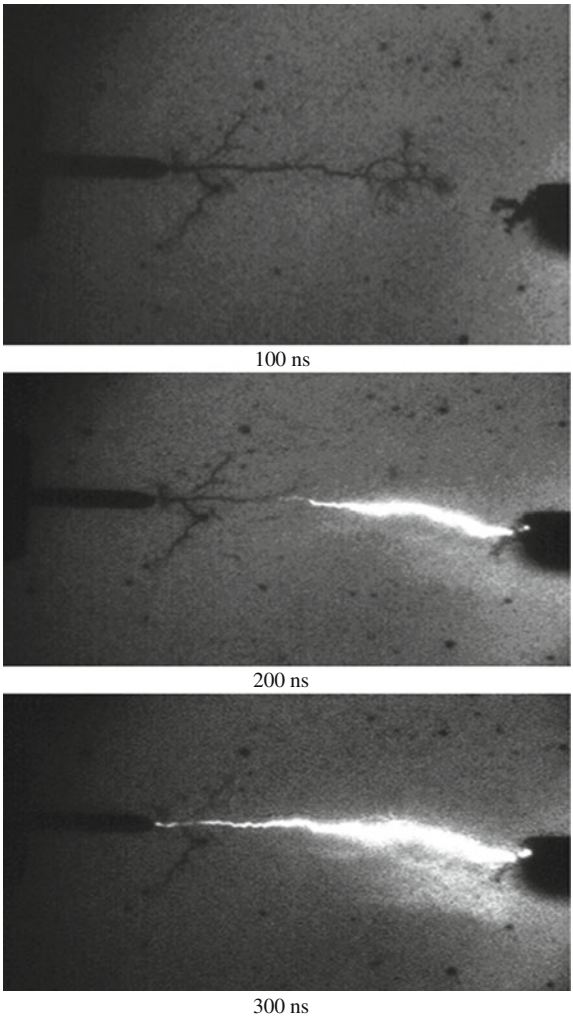

Fig. 4.14 Shadow images of the streamer and discharge channel forming [39]

The initial stage of the shock wave formation is characterized by local extreme parameters of substance. Pressure in the shock wave front under velocity of $\sim 10^4$ m/s, according to [45] is 1.2×10^{11} Pa.

After $\sim$500 ns in the far Fraunhofer zone both waves merged visually in one quasispherical wave with velocity of $\sim 1.5 \times 10^3$ m/s.

Dependencies of the shock wave velocity on time are presented in Fig. 4.17. In Fig. 4.17a the energy in pulse is 0.35 J under interelectrode gap of 1.7 mm is (Δ), and 7 mm is (□).

In Fig. 4.17b, the interelectrode gap is 7 mm under the energy in pulse of 0.15 J (Δ), and 0.35 J (□).

The rising of the interelectrode breakdown voltage stipulates the increasing of number of streamers, value of inputted energy in main discharge channel, and shock

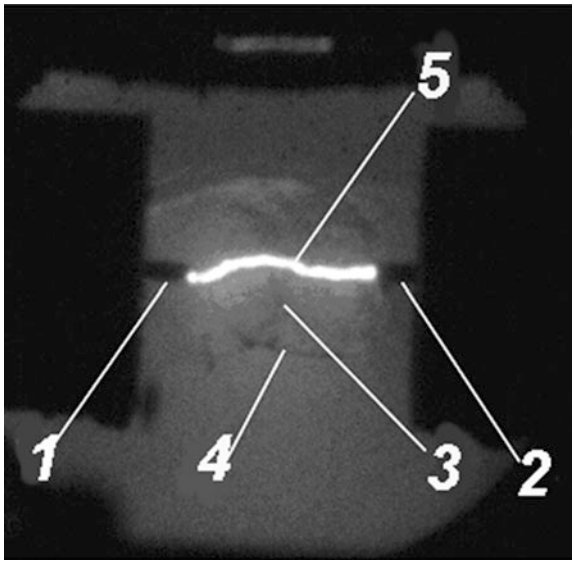

Fig. 4.15 Shadow image of the discharge

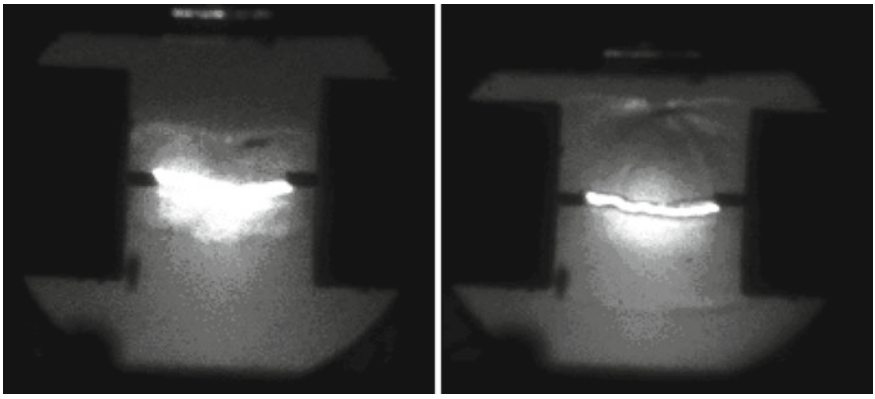

Fig. 4.16 Forming and propagation of the shock waves

wave' intensity too. The increasing of the discharge power under the same energy leads to growing of pressure in the shock wave front [18].

Figure 4.17b shows that the velocity of the shock wave under the low energy almost the same as under the high energy. The shock wave velocity is increased at increasing of interelectrode gap (Fig. 4.17a).

Image of the shock waves for oscillated pulsed discharge (Fig. 4.18) shows that up to first microsecond from the beginning of the discharge the shock waves

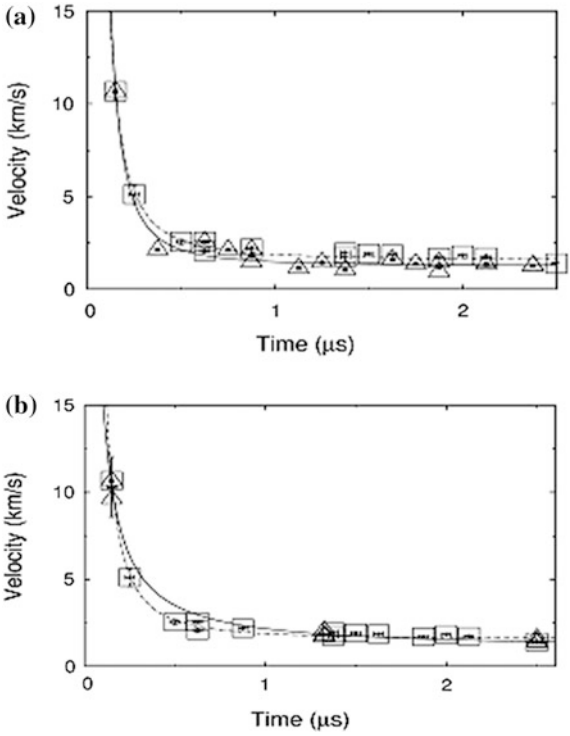

Fig. 4.17 Shock wave velocity versus time after breakdown

sequence is formed. Thus, time coordinates of the shock waves fronts are corresponded to maxima of the current. Average for the process velocity of the first shock wave propagation is 2,000 m/s.

Figure 4.19 shows the process of the formation, expansion and contraction of the bubble. Typically, the bubble has a hemispherical shape when the radius of the maximum. Its initial form depends on the form of the breakdown channel. Lifetime and radius of the bubble are determined by the energy inputted in the discharge channel.

Figure 4.20 shows the dependencies of bubble radius on time. Here the interelectrode gap is 7 mm, energy in pulse is 0.35 J (Δ), and 0.15 J (□).

After expansion, the bubble is contracted and disappeared near electrodes' end (a) or between them (b) with the shock wave generation (c) (Fig. 4.21).

Channel discharge stage is occurred in the water vapor of the expanding bubble at short interelectrode gaps. At early stage of discharge, the pressure value is of hundreds of atmospheres. Pressure in bubble is decreased to 1 MPa by the end of discharge current. So the processes at the stage are similar to discharge in gas of high pressure.

Calculated heat flux on electrode tips shows that liquid phase appeared on electrodes surface after several microseconds.

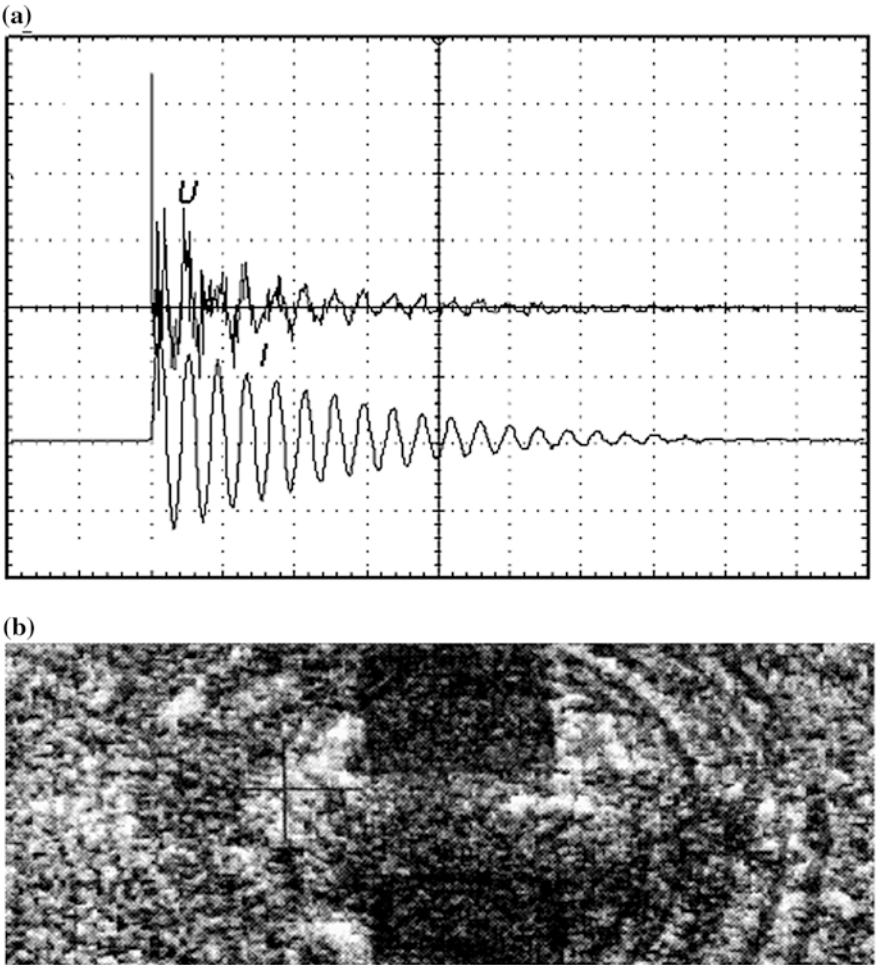

Fig. 4.18 Oscillograms of the voltage (U) and current (I) (**a**), and the shock waves sequence formed to 1st μs under oscillate mode (**b**)

Specific erosion of the electrode is higher at short interelectrode gap then that at long one and has similar values under various electric charge/energy. Specific electrode erosion under gap of ~ 2 mm and energy of 0.35 J/pulse for anode is of 2.2×10^{-4} g/C and for cathode of 2.2×10^{-4} g/C correspondingly.

Temperature of the discharge column estimated by various methods is $\sim 10^4$ K. Under this temperature, the discharge column is a source of the UV-irradiation ranged, particularly, in the range of 200–400 nm. This UV-irradiation, absorbed by water, produces H_2O_2, O_3, O, and OH radicals, which destroy microbes and some chemical compounds.

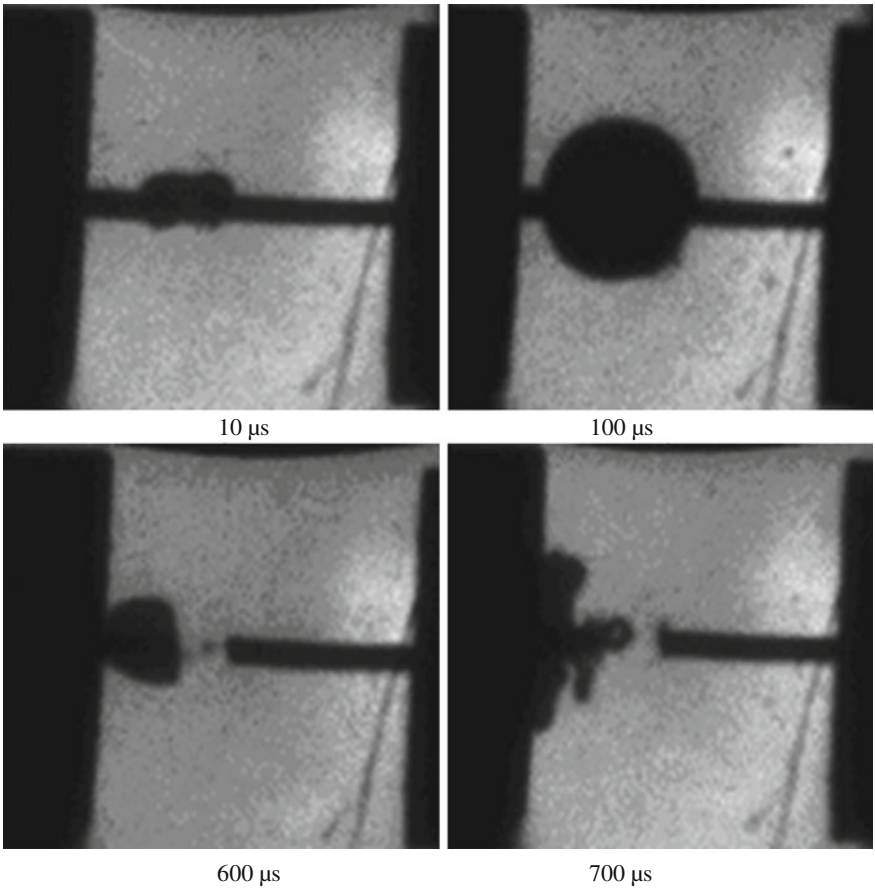

Fig. 4.19 Cavitation bubble evolution

Fig. 4.20 Bubble radius versus time

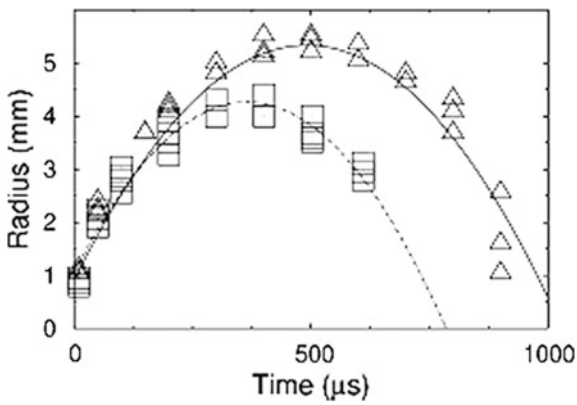

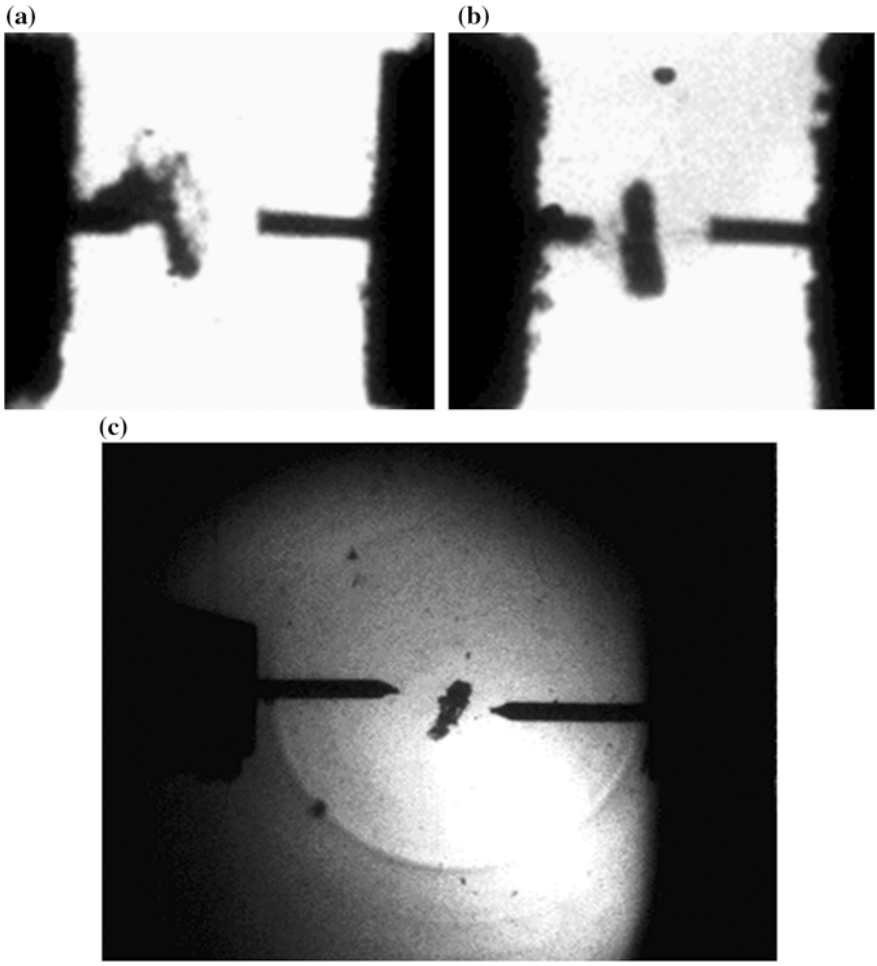

Fig. 4.21 Bubble collapse and shock waves' generation

4.4 Impacts of the PED on Water Media

Increasing pollution of the natural water makes the problem of cleaning and disinfection to be more urgent. Cleaning must be performed down to safe levels of contaminants that are in form of particles or solutions. Disinfection involves complete destruction of pathogenic microorganisms.

The same oxidizing agents and physical impacts can be used for both cleaning and disinfection of water. However, problem of the tap water disinfection deserves special attention. This is stipulated by the fact that the widespread application of contemporary disinfection reagents leads itself to appearance of revealed toxic,

carcinogenic, other adverse aftereffects, and of by-products of the disinfection reactions.

For the last decades, medical investigations have shown that a sharp rise of oncological and cardiovascular diseases is a result of the chlorine disinfection of water [46, 47]. It was revealed that chlorinated tap water contains steady macro-radicals, which provoke occurrence and development of mentioned and other serious diseases [48].

Methods of water treatment are divided into reagent: chemical, chemical-free, and combined ones.

Chemical methods of water disinfection. Among the chemical methods and agents for water disinfection are chlorination, ozonation, and processing by hydrogen peroxide, silver, copper, iodine agents, etc.

Chlorination is the most common way of disinfection. Chlorine is characterized by the wide antimicrobial activity. However, chlorine and its compounds are toxic ones. Despite this, for guaranteed bactericidal effect, they are commonly used with excessive doses of chlorine that leads to denaturizing of water. Furthermore, action of the chlorine depends on type of the microorganisms and chemical composition of the water. Various anthropogenic contaminants can significantly effect on the efficiency of disinfection, since the chlorine forms the halogen compounds in water. Accumulation of them is dangerous due to their negative biological activity (as mentioned above). In spite of usage of the chlorine is reduced continuously, total rejection of the chlorination is not yet possible. Therefore, this method should be combined with other less dangerous methods of disinfection.

Ozonation is an alternative to chlorination. Ozone is of 15–20 times stronger oxidant than chlorine. It destroys not only bacteria, but also removes metal impurities, odors, taste, facilitates the subsequent coagulation and filtration of the waste. However, application of ozone does not preclude formation of toxic products: bromates, aldehydes, carboxylic acids, etc. But now, the effect of ozone on human health is not studied enough. Note also that high dose of ozone ~ 12 mg/l is needed for the desired degree of water purification. The main disadvantage of ozonation is the high cost and power consumption of equipment: consumption of the electrical energy to produce 1 kg of ozone is 30–40 kW h.

Application of the hydrogen peroxide provides destruction of organic compounds without formation of the toxic products. Hydrogen peroxide is stable in water, and its use does not require sophisticated equipment. However, to achieve the desired degree of decontamination, much of the disinfectant is necessary. For example, to reduce concentration of the *E.coli* by three orders, it requires 260 mg/l of the disinfectant and 90 min of exposition. This limits application of this method.

Silver has broad antimicrobial action and bactericidal aftereffect (property of treated water to keep its bactericidity for a long time). But silver is an expensive metal. In addition, effectiveness of its action depends on the physical-chemical properties of water. Therefore, the disinfection by means of silver is possible in the case of a small volume of water.

Copper is the alternative to silver. Copper ions as silver ones have an inactivating effect on viruses and bacteria, but their concentration must thus be some

higher, because of its lower toxicity. Except silver and copper for antimicrobial treatment of water, the iodine compounds can be used.

Physical methods of water disinfection are the UV-irradiation, ionizing radiation, ultrasound, and heating.

UV-irradiation is the most widely used method. Application of the UV-irradiation is justified when the water meets to all indicators except the microbiological one. Over the last 10–15 years, the USA, Canada, and Western Europe states developed over 150 facilities of the UV-irradiation with performance of 10–350 m^3 per day. The minimal effective energy dose for treatment is ranged from 16 to 40 mJ/cm^2. The main advantages of this method compared to ozonation are the following:

- Energy consumption is lower by 4 times (compared with chlorination—(0.02–0.05) kW h/m^3)
- Degree of disinfection under the radiation dose increasing grows exponentially, and in the case of overdose the adverse effects are absent

Negative aspects of this method are the dependence of bactericidity on turbidity and chromaticity of the water, type of microbes and their concentration. Additionally, this method does not provide the bactericidal aftereffect.

Γ-irradiation. For the total water disinfection by means of the γ-irradiation, the dose of $\sim 10^5$ R is needed. This dose of radiation cleans completely water from all kinds of microorganisms and viruses, but the high safety of application is required.

Ultrasonic disinfection. Advantage of the ultrasonic disinfection of water is its bactericidal effect that is independent of the physical-chemical parameters of water. The disadvantage is the same as that of the V-irradiation, i.e., absence of the aftereffect. Water disinfection by the ultrasound is of 2–4 times more expensive than treatment with the UV-irradiation.

Thermal disinfection. For thermal disinfection of tap water, the flame, high-temperature plasma, hot air, superheated steam, and boiling are used. The advantages of boiling is the high efficiency of the bactericidity regardless the properties of water. Disadvantage is in low productivity and high-energy consumption. There exist reports about possibility of application of other physical factors to water disinfection such as the electromagnetic fields, laser radiation, degassing, etc.

Combined methods of disinfection. Traditional methods of disinfection are not always effective. Furthermore, each separate cleaning method has certain disadvantages and limitations. Therefore, in recent years, investigators search for new methods of decontamination and develop techniques based on the combined effect of multiple factors. Since simultaneous usage of chlorine and hydrogen peroxide, chlorine and ozone, silver and copper ions make it possible to reduce concentration of the reagents and processing time and raise the bactericidity. However, all these methods have not the aftereffect and are difficult in control of the purification degree. Thus, the methods of disinfection of tap water used currently do not meet fully contemporary hygiene requirements in a number of significant indicators.

Bactericidal effect of the PED. The total bactericidal effect of the PED and associated with them factors is in the following. Various biological objects, such as

bacteria, phages, viruses, and fungal spores containing in the water are destroyed or killed partially or entirely under the action of the PED in dependence on the inputted energy. This effect is rather stable, however, in many articles, various energies correspond to the same bactericidal action. From our point of view, this difference is explained by the fact that in these studies different metal electrodes were used.

It is known that one of the factors of disinfection is metal or oxide nanoparticles of the electrodes, which are dissociated in water and emit the toxic ions. The ions of various metals differ in toxicity and are ordered as follows: Ag > Cu > Cd, Zn, Pb > Mn, Fe > Mg, Ca [49].

Among the numerous theories explaining the mechanism of effect of the ions on the microorganisms, the most common is the adsorption theory. According to this theory, the cell loses its viability because of interaction of the electrostatic forces between the cells inside the bacteria. Note that the bacteria have a negative charge but the charge of metal ions is positive. So, the mentioned electrostatic forces are generated due to adsorption of the ions by the bacterial cell.

The mechanism of bactericidal effect of the ions on microorganisms and viruses is the following. The ions react with the cell membrane, it is a structure consisting of specific proteins (peptidoglycans) connected by aminoacids to provide mechanical strength and stability.

Further, the ions interact with external peptidoglycans and block their ability to transfer oxygen inside the cells of the bacteria. As a result, this causes "suffocation" of the microorganism and its death.

The main experimental data on disinfection of water by electric discharges were obtained in 70–80s of the last century [50–53]. There, the impact mainly by the PED of high (0.2–1.0 kJ) energy per pulse on motionless water was carried out. Such discharges produced the electric explosion or electrohydraulic shock.

The level of the PED effect was controlled by varying the pulsed energy and pulse number. Based on the data, one can evaluate effectiveness of the bactericidal action of the electric explosion or electrohydraulic shock [50].

The specific energy, which reduces concentration of the *E.coli* bacteria by 3–4 orders, is from 1 to 20 J/ml. According to other studies, the specific energy may be in the wider interval is from 1 to 100 J/ml.

Reliable and numerous data on the bactericidal effect of the PED were obtained in our Institute for the energy lower than 1 J/pulse [19].

The experiments in the cuvette and discharge flow chamber were conducted. In the second case, the level of effect by water consumption, pulse repetition rate, and the energy of a single pulse were varied.

It should be noted that the effect does not essentially depend on the properties of the water. This holds in the saline solution and in natural, tap, or distilled water.

The advantage of the bactericidal action of the PED over the ozonation and UV-irradiation is in its long-term aftereffect. The water treated by the PED keeps its bactericidity up to one year [27].

The paper [54] presents the data of two series of tests using the electrohydraulic shock treatment of water. In the first series, the sterile tap water after infection by

the *E.coli* (strain 149) was treated by the PED. Then it was divided into two parts: one was stored at 16–18 °C and the second one at 37 °C.

From each sample, the 0.1 ml seedlings on the Endo and Eijkman media were taken at the same time. Results of the tests are presented in Table 4.2.

In the second series, the degree of bactericidity of the treated water was determined. For this one, the tap autoclaved and treated by the PED water into sterile glass flasks was placed.

After 2–3 h, 5, 10, 20 days, and 3, 4, 5 months, from the flask were selected 50 ml probes of treated water to the tubes and than infected by *E.coli* to concentrations of 10^2, 10^3, and 10^4 ml^{-1}.

In the control series, 50 ml probes of the sterile untreated water were taken from the flask and then infected as in the test series. The results are presented in Tables 4.3 and 4.4.

The similar results were obtained in [55]. There in contrast to data obtained in [54], the experiments were carried out with the well water and steel electrodes, when in [54] the copper and silver electrodes were used. All experiments were performed with the initial concentration of bacteria (0.1–7.5) × 10^3 ml^{-1} and the energy of 80–200 J/pulse.

At the initial stage of the research with water treated by the PED, the effect of exposure time on bacteria and their survival was studied [38]. The obtained data under the PED of 0.5 J/pulse are presented in Table 4.5.

Table 4.2 Results of the tests on survival after exposure

Energy (J/ml)	Temperature (°C)	Survival after exposure %				
		Hours		Days		
		0.5	3	1	2	5
0.31	18	11	9.8	2.6	0.9	0
0.31	37	–	2,6	0	0	0
0.63	18	1.8	0.5	0	0	0
0.63	37	–	0	0	0	0
Check	18	100	110	150	190	190
Check	37	–	78	Total growth		

Notes The initial concentration of the bacteria is 10^4 ml^{-1}. *Dash* No measurements were made

Table 4.3 Degree of bactericidity of the treated water

Energy (J/ml)	Growth on Endo medium			Growth on Eijkman medium	
	Time of seeding after infection				
	0.2 h	2 h	24 h	48 h	72 h
Check	1,000	670	7,600	Growth	Growth
0.3	980	630	5	–	Growth
1.6	870	95	0	–	Growth
2.2	1,100	30	0	No growth	–
2.6	1,100	10	0	No growth	–
3.1	1,000	0	0	No growth	–

Table 4.4 Degree of bactericidity of the treated water

Time storage of water after treatment	Number of probes	Initial number of cells in 1 ml	Death of bacteria at exposure %				
			3 h	24 h	48 h	72 h	95 h
2–3 h	4	1.2×10^3	60.9	99.8	100	–	–
15 days	4	1.4×10^3	45.9	83.8	91.6	100	99.9
1 month	4	1.3×10^3	50.5	87.2	98.4	98.9	100
4 months	4	1.2×10^3	86.7	100	–	–	–

Notes Energy is 3.1 J/ml. *Dash* No measurement. Taken as 100 % the number of bacteria within 10–15 min after infection

Table 4.5 Effect of exposure time on bacteria' survival

Anode is copper	Initial concentration $N_0 = 5.12 \times 10^2$ ml^{-1}		
Energy J/ml	Concentration of bacteria after exposure l^{-1}		
	15 min	30 min	60 min
1.9	45	22	<3
2.9	3	<3	<3
5.0	<3	<3	<3
Anode is steel	Initial concentration $N_0 = 1.8 \times 10^3$ ml^{-1}		
Energy J/ml	Concentration of bacteria after exposure l^{-1}		
	15 min	15 min	15 min
1.9	674	22	<3
3.2	61	<3	<3
4.4	<3	<3	<3

To study the mechanism of bactericidal effect of the PED the authors of the works [53, 54] estimated the separate contributions of the UV-irradiation and shock waves in the total bactericidity. At the experiments, for the same PED, were determined the bactericidal effect of UV-irradiation when the shock waves were shielded (PED in air in quartz tube), and when the UV-irradiation was eliminated (PED in opaque thin rubber sheath with low acoustic impedance).

Shares of the factors in total bactericidity are distributed as follows [1]:

UV-irradiation	70–90 %
Shock waves	20–40 %
Other factors	10–20 %

We have studied the effects of electrohydraulic shocks at the same inputted energy. The shocks were initiated in two ways: the first one by means of the self-breakdown, and the second one by explosion of a metal wire. It was established that under the PED initiation by explosion of the metal wire, the shock waves had

higher rise rate of the pressure. As a result, this produces the larger bactericidal effect than in the self-breakdown mode, and, moreover, reduces the initial concentration of bacteria by six orders [19].

Based on all these results, it is possible to divide all bactericidal factors of the PED in two groups:

- Factors of the local action. They are localized near the discharge channel and plasma streamers having the characteristic size about the width of the interelectrode gap. These are hydrated electrons, ions of the electrodes metal, and the active radicals
- Factors of the non-local action. These are the mechanical and electromagnetic waves. Mechanical waves (under the applied energy and discharge power) are the shock waves. Electromagnetic waves are the light and UV-irradiations and the latter one has maximum at 250–300 nm. The UV-irradiation has both the direct destructive effect on microbes and generates the photolytic reactions resulting in formation of the active radicals OH, H_2O_2, O, O_3, etc. Since all the factors affect simultaneously, the synergetic effect takes place, namely, the combined impact of the factors is more effective than the sum of their separate effects [53, 56]

Biological effect of the PED unlike the bactericidal effect of the PED is investigated not completely [38, 57]. The paper [57] presents the description of an interesting phenomenon: the effect of PED on the cultivation of ginseng cells. The paper [57] presents results of the PED application with 0.3 J/pulse and the repetition rate of 60 and 120 Hz. The quality of sludge drying was improved under treating the wastewater by means of an electrodischarge installation. The origin of the observed effect is the following. In the biological treatment of the wastewater in special chambers, special bacteria purified the water from organic and chemical contaminants. As a result, the biological solutions of humidity 96 % were obtained. These solutions were dried by means of centrifuges and filter presses with previously adding the flocculants. The daily requirement of flocculent is 100–200 kg (cost of 4.5 $/kg) for the plants processing 35–40 m^3/h. Before adding the flocculent to sludge, the treatment of the sludge by the PED was implemented with energy of 10^{-2} J/g. As a result, in dependence on the type of waste water and the type of the flocculent, the sludge moisture decreases by 15–30 % (in comparison with extraction without the PED); thus, saving of the flocculent achieves 20–30 %. Moreover, the weight of hard particles and bacteria in water after extraction is reduced by order. The annual savings by reducing weight of flocculent is 50,000–100,000 $ for plants processing 35–40 m^3/h.

A significant increase of organic matter in the content, mainly phosphorus, recorded by increase the biological demand of oxygen after the impact of the PED [57]. That was used to increase the amount of methane produced in anaerobic biological processing plants for waste water. Experiments have shown that the amount of methane generated is increased by 2 times. The use of the PED provided the efficient process without rigid stabilization of the medium temperature.

Chemical action of the PED. The results of studies of the chemical action of the PED are presented in papers [58–63]. In the work [58] authors have studied the

effects of microdischarge in thick area of 0.1 mm between the cathode and anode surfaces in the chemical solution. The microdischarge in the electrolytes and chemical solutions has all the properties of the electrical discharge in water: the breakdown occurs because of the gas bubble forming [64, 65]. In the quasi-stationary stage of the PED in the spectrum of its radiation except the lines corresponding to water radicals, lines of atoms of salts were detected. Some characteristics of the arc are presented in Table 4.6 [64].

Under action of the microdischarge on water solutions of the sulfuric acid, the sulfur dioxide and trioxide are formed [58]. The microdischarge was used for purification of the waste water containing various organic compounds, urea resin, chlorophos, saturated, unsaturated and aromatic hydrocarbons, salts of strontium and cobalt [66]. Degree of purification of the wastewater is following:

- 0.8–1.0 g/l urea resin is 90–95 %
- 0.1 g/l chlorophos is 95–100 %
- 0.1–4.0 g/l saturated, unsaturated and aromatic hydrocarbons is 90–95 %
- 0.2–30.0 g/l of oil 80–90 %
- 10^{-5}–l0^{-2} mol/l radioactive isotopes of cobalt and strontium 100 %

The power consumption was 10–100 J/ml and (0.3–2.0) × 10^4 J/ml in the latter case.

As a result of treatment, the cobalt and strontium ions in the solution were deposited on the electrode surfaces that makes it easy to dispose these substances.

Under purification of waste, the water has no contamination by intermediates. For example, under treatment of the water containing hydrocarbons, the major products of the process are hydrogen, oxygen, carbon monoxide, and light hydrocarbons.

The paper [67] presents results of experiments with the salt solutions of copper, cadmium, cobalt, nickel, iron, silver, zirconium, magnesium, and calcium with concentrations of 1.3–25 g/l and the inputted energy of 1.5–30 J/ml. For 2–20 h after the treatment, the sediment was precipitated in dependence on concentration of solution and discharge energy (excluding salts of chromium, magnesium, and calcium).

In works [61, 68], results of special studies are presented. Here, the electric explosions with energy of 5–25 kJ/pulse and duration of 25–100 μs were used to purify water from the toxic organic substances, chlorophenol, dichloroaniline, etc.

In these experiments, the kinetic coefficients characterizing dynamics of the substances destruction were determined. High degree of purification was obtained under 100–260 pulses and the inputted energy of 10^2–10^3 J/ml.

Table 4.6 Characteristics of the arc

Arc characteristics	Electrolyte concentration mol/l						
	0.02	0.03	0.04	0.05	0.06	0.08	0.09
Light radius mm	0.15	0.3	0.6	0.6	0.6	0.6	0.9
Discharge duration 10^{-4} s	0.7	2.2	2.5	2.6	2.3	1.9	5.0

The paper [62] describes application of the similar technology for the electro-decomposition of the TNT with simultaneous formation of ozone with concentration of 0.1 g/l. The PED enhances dissolution of ozone in water by generating the micro cavitation structures and, thereby, increasing the efficiency of decomposition. Complete decomposition of the TNT with concentration of 45 mol/l and the inputted energy 520 J/ml took place.

Peculiarity of investigations in paper [69] is that to impact on water solutions of organic compounds, the pulsed corona discharges were used; and in them, the arc channel and shock waves were absent. Such a discharge generates significant amount of the hydrated electrons, OH radicals, and hydrogen peroxide.

Concentration of the products increases as the corona discharge voltage increases. To increase discharge voltage from 40 to 100 kV, the activated carbon powder was used, which was added into the water with concentration of 1–10 g/l.

References

1. V.L. Gorjachev, P.G. Rutberg, V.N. Fedjukovich, Rus. J. Fuel, Power, and Heat Syst. **2**, 36 (1998)
2. A.M. Ampilov, E.M. Barkhudarov, Y.B. Bark, Y.V. Zadiraka, M. Christofi, Y.N. Kozlov, I.A. Kossyi, V.A. Kop'ev, V.P. Silakov, M.I. Taktakishvili, S.M. Temchin, J. Phys. D: Appl. Phys. **34**, 69–72 (2000)
3. B. Sun, S. Kunimoto, C. Igarashi, J. Phys. D: Appl. Phys. **39**, 3814–3820 (2006)
4. P.G. Rutberg, V.L. Goryachev, A.A. Ufimtsev, J. Tech. Phys. Lett. **2**, 24 (1998)
5. P. Lukes, B. Locke, J. Phys. D: Appl. Phys. **38**, 4047–4081 (2006)
6. P.G. Rutberg, V.A. Kolikov, V.E. Kurochkin, L.K. Panina, A.P. Rutberg, J.I.E.E.E. Trans, Plasma Sci. **4**, 35 (2007)
7. I.A. Adamchevsky, *Electric Conductivity of Liquid Dielectrics* (Energy, Moskow, 1972). (in Russian)
8. G.S. Kuchinsky, E.A. Morozov, J. Tech. Phys. Lett. **8**, 24 (1982). (in Russian)
9. V.F. Klimkin, A.G. Ponomarenko, J. Tech. Phys. **9**, 49 (1979). (in Russian)
10. V.G. Zhekul, G.B. Rakovsky, J. Tech. Phys. **1**, 53 (1983). (in Russian)
11. E.V. Yanshin, I.G. Ovchinnikov, YuN Vershinin, J. Tech. Phys. **10**, 43 (1973). (in Russian)
12. V.Y. Ushakov, *Pulsed Electric Breakdown of Liquids*, Tomsk, 1975 (in Russian)
13. I.T. Ovchinnikov, E.V. Yanshin, *Pulsed Discharge in Dielectrics* (Nauka, Novosibirsk, 1985). (in Russian)
14. V.Y. Ushakov, N.K. Kapshinikov, V.R. Kuhta, *Pulsed Discharge in Dielectrics* (Nauka, Novosibirsk, 1985) (in Russian)
15. S.M. Korobeynikov, K.Y. Yanshin, E.A. Yanshin, *Pulsed Discharge in Dielectrics* (Novosibirsk, Nauka, 1985) (in Russian)
16. V.L. Goryachev, P.G. Rutberg, V.N. Fedioukovitch, *Environmental Appl* (Adv. Oxidation Sci. Int. Symp, San Francisco, 1996)
17. V.V. Ivanov, P.S. Shvets, A.V. Ivanov, *Underwater Sparks* (Naukova Dumka, Kiev, 1982). (in Russian)
18. M.E. Pinchuk, V.A. Kolikov, P.G. Rutberg, A.G. Leks, R.V. Dolinovskaya, V.N. Snetov, A. Y. Stogov, J. of Phys.: Conf. Series 406 (2012)
19. A.A. Bogomaz, V.L. Goriachev, A.S. Remennui, P.G. Rutberg, Tech. Phys. Lett. **12**, 17 (1991)
20. V. Sokolov, G. Stain, J. of Chem. Phys. **5**, 44 (1966)

21. E. Hart, M. Anbar, *Hydrated Electron* (Atomizdat, Moskow, 1973). (in Russian)
22. P.G. Rutberg, V.L. Gorjachev, V.A. Kolikov, V.N. Snetov, A.Y. Stogov, J. High Temp. Material Processes **1**, 14 (2010)
23. F.G. Rutberg, V.A. Kolikov, V.N. Snetov, A.Y. Stogov, E.G. Abramov, E.V. Bogomolova, L. K. Panina, J. Tech. Phys. **12**, 57 (2012)
24. P. Rutberg, V. Kolikov, V. Snetov, A. Stogov, L. Noskin, S. Landa, A. Arutjunan, O. Kiselev, V. Egorov, A. in *International Conference Bio & Food Electrotechnologies (BFE2009)*, Compiègne, 2009
25. P. Rutberg, V. Kolikov, V. Snetov, A. Stogov, L. Noskin, S. Landa, A. Arutjuman, V. Egorov, A. Sirotkin, J. High Temp. Material Proc. **3**, 13 (2009)
26. P. Rutberg, V. Kolikov, V. Snetov, A. Stogov, L. Noskin, S. Landa, A. Arutjunan, V. Egorov, A. Sirotkin, in *Transactions of the* 10th *European Plasma Conference on High Temperature Plasma Processes*, Patras, 2008
27. V.A. Kolikov, V.E. Kurochkin, L.K. Panina, P.G. Rutberg, Dokl. Biol. Sci. **403**, 279–281 (2005)
28. A.M. Sizikov, L.T. Bugaenko, O.A. Golovina, in *IInd international Symposium on Theoretical and Applied Plasma Chemistry*, Riga, 1991
29. A.M. Sizikov, E.G. Volf, T.A. Kalinina, V. Ju, *Ufimtcev* (IInd international Symposium on Theoretical and Applied Plasma Chemistry, Riga, 1991)
30. V.F. Levchenko, in *Electric Discharge in Liquids and Its Application in Industry,* Nikolaev, 1988
31. V.F. Levchenko, Z.P. Giil, in *Electric Discharge in Liquids and Its Application in Industry*, Nikolaev, 1988
32. V.F. Levchenko, V.P. Sergeenkov, M.S. Tjutujnik, in *Electric Discharge in Liquids and Its Application in Industry*, Nikolaev, 1988
33. A.N. Malinin, V.E. Sabinin, A.N. Sidorov, Lett. in JTP **1**, 20 (1994)
34. L.A. Yutkin, *Electrohydraulic Effect and its Industrial Application* (Mashinostroenie, Leningrad, 1986). (in Russian)
35. K.V. Vilkov, A.L. Grigor'ev, Y.A. Nagel, I.V. Uvarova, J. Tech. Phys. Lett. **4**, 30 (2004)
36. R.V. Dolinovskaya, P.G. Rutberg, V.A. Kolikov, M.E. Pinchuk, A.G. Leks, V.N. Snetov, A. Y. Stogov, In *3rd International Congress on Radiation Physics and Chemistry of Condensed Matter*, Tomsk, Russia, 2012
37. K.A. Naugol'nykh, N.A. Roy, *Electrical Discharge in Water*, (Nauka, Moscow, 1971) (in Russian)
38. V.L. Goryachev, P.G. Rutberg, V.N. Fedioukovitch, J. High. Temp. **5**, 34 (1996)
39. V.A. Kolikov, M.E. Pinchuk, A.G. Leks, P.G. Rutberg, Proc. SPIE paper **192**, 6279 (2007)
40. V.S. Komel'kov, J. Tech. Phys. **8**, 31 (1989)
41. G. Touya, T. Reess, L. Pecastaing, A. Gibert, P. Domens, J. Phys, D. Appl. Phys. **24**, 39 (2006)
42. X. Lu, Y. Pan, K. Liu, M. Liu, H. Zhang, J. Appl. Phys. **1**, 91 (2002)
43. M. Mikula, J. Panak, V. Dvonka, J. Plasma Sources Sci. Tech. **2**, 6 (1997)
44. M.T. Camell, R.D. Alcock, D.C. Emmony, J. Phys. Med. Biol. **11**, 38 (1993)
45. A. Starikovskiy, Y. Yang, Y.I. Cho, A. Fridman, J. Plasma Sources Sci. Technol. **20**, (2011)
46. M.S. Gottlieb, J.K. Carr, D.T. Morris, Int. J. Epidem. **10**, (1981)
47. J.M. Price, *Coronaries, Cholesterols, Chlorine* (Pyramid Publications Ltd., Banhadlog Hall, Tyliwch, Landridloes, 1984)
48. V.L. Voejkov, R.R. Asfaramov, V.M. Rozental, in *3rd International Conference in Ecopolis 2000: Ecology and Steady Development of City*, Moscow, 2000 (in Russian)
49. H.A. Laitinen, *Chemical Analysis* (McGraw-Hill, New York, Toronto, London, 1960)
50. E.G. Zhuk, J. Microbio, Epidemio. J. Immunology **1**, 48 (1971). (in Russian)
51. R.A. Bretosh, L.A. Rudenko, A.F. Urusov, J. Electron. Proc. Mater (1971) (in Russian)
52. L.D. Zykina, V.S. Goldaev, J. Electron. Proc. Mater. (1974) (in Russian)
53. N.D. Ryazanov, E.N. Perevyazkina, J. Electron. Proc. Mater. **2**, (1984) (in Russian)
54. E.G. Zhuk, J. Microbio, J. Epidemio. Immuno. **4**, (1979) (in Russian)

55. S.N. Cherkinsky, T.P. Yakovleva, A.N. Menshikova et al., J. Hyg. Sanit. **2**, (1976) (in Russian)
56. E.G. Zhuk, J. Electron. Proc. Mater. **3**, (1978) (in Russian)
57. Summary of Dewatering Tests. *Technical Report* (Scientific Utilization Inc., USA, 1995)
58. A.M. Sizikov, L.T. Bugaenko, O.A. Golovina, in *International Symposium on Theory and Applications Plasma Chemistry*, Riga, 1991 (in Russian)
59. V.F. Levchenko, in *The Electrical Discharge in a Liquid and its Application in Industry*, Nikolaev, 1988 (in Russian)
60. A.N. Malinin, V.E. Sabinin, A.N. Sidorov, J. Tech. Phys. Lett. **1**, 20 (1994). (in Russian)
61. M.R. Hoffman, in *2nd International Symposium on Environmental Application of Advanced Oxidation Technology*, San Francisco, 1996
62. D.W. Wilberg, P.S. Lang, R.H. Hochemer, et al., in *2nd International Symposium on Environmental Application of Advanced Oxidation Technology*, San Francisco, USA, 1996
63. D. Grymonpre, W.C. Finney, B.R. Locke, in *2nd International Symposium on Environmental Application of Advanced Oxidation Technology*, San Francisco, 1996
64. H. Green, Scientific Utilization Inc., USA, 1995
65. A.M. Sizikov, L.T. Bugaenko, E.G. Volf, T.A. in *II International Symposium on Theory and Applications Plasma Chemistry*, Riga, 1991 (in Russian)
66. A.M. Sizikov, E.G. Volf, T.A. Kalinina, V.Y. Ufimtsev, in *II International Symposium on Theory and Applications Plasma Chemistry*, Riga, 1991 (in Russian)
67. N.M. Efremov, B.Y. Adamiak, V.I. Blochin, S.Je. Dadeshev, K.I. Dmitriev, K.N. Semjonov, V.F. Levachov, V.F. Jusbashev, J. IEEE Trans. Plasma Sci. **1**, 28 (2000)
68. L.T. Bugaenko, A.M. Sizikov, E.G. Volf, in *II International Symposium on the Theory and Applications Plasma Chemistry*, Riga, 1991 (in Russian)
69. P.S. Lang, in *2nd International Symposium on Environmental Application of Advanced Oxidation Technology*, San Francisco, 1996

Chapter 5
Substances Formed During Discharges

Abstract Up to date, there are two methods of producing the hydrated electrons: by means of radiolysis of water and water solutions by irradiation of γ-quanta, or electrons (Hart and Anbar, Hydrated electron 1973; Pikaev, Pulsed radiolysis of water and aqueous solutions 1965). Moreover, hydrated electrons are produced by means of the PED (Gorjachev et al, J Tech Phys Lett 11:16 1991). Since the plasma column of the PED in water has the temperature $T = (10–20) \times 10^3$ K and pressure $P = 10–10^3$ MPa (Ushakov, Pulsed electrical discharge in gases 1975), it is reasonable to assume that the column is a powerful pulsed source of the UV-irradiation. Being absorbed by water, the irradiation of this part of spectrum generates reaction of photolysis (Sokolov and Stain, J Chem Phys 5:44 1966; Sokolov and Stain, J Chem Phys 9:44 1966). Last years, researches have shown that the physical-chemical properties of nanoparticles qualitatively differ from ones of both macro-objects and micro-particles (Schmid et al., Nanoparticles: from theory to application 2004; Furstner et al, Active metals: preparation characterization and applications 1996; Lue, J Phys Chem Solids 62:1599–1612 2001). Nanoclusters behave as quantum dots, i.e., inside them, as well as, in atoms, the free electrons can occupy only certain allowed energy states (Kreibig and Vollmer, Optical properties of metal clusters 1995). There are "magic" numbers of packing of atoms in nanoclusters: 13, 55, 147, 309, and 561 (Teo and Zhang, Magic numbers in clusters 2002). Thus, successes in the nanoparticles synthesis and study of their properties have stimulated explosion of applied researches of nanotechnologies and, first of all: nano-electronics, nano-optic-electronics, nano-electric-chemistry, analytical and biomedical applications of nanoparticles (Drexler, Nanosystems: molecular machinery, manufacturing and computation 1992; Siegel, Nanophase materials: synthesis, structure and properties 1994).

V. Kolikov and P. Rutberg, *Pulsed Electrical Discharges for Medicine and Biology*, Biological and Medical Physics, Biomedical Engineering,
DOI 10.1007/978-3-319-18129-5_5

5.1 Short-Lived Substances

As mentioned above, the discharge channel is a powerful pulsed source of UV-irradiation in the wavelength range of 100–200 nm. Being absorbed by water, the UV-irradiation of this wavelength generates the photolytic reaction: $H_2O + h\nu \rightarrow H_2O_2 + H + OH + O_3 + O$. All of these produced substances are bactericide short living ones [1–13].

This study at the electrodischarge chamber of cuvette type was performed. In investigation, the average value of the inputted energy was varied by the number of pulses. The pulse repetition frequency was 0.5 Hz. The level of concentration of H_2O_2 was measured by titrimetric method. The experiments at distilled and tap water were carried out.

Figure 5.1 shows the dependence of the mass concentration of H_2O_2 on the average specific inputted energy and that the natures of the dependencies for the distilled and tap waters are the same ones. Similar dependences had been obtained for the concentration of the hydrogen, produced by means of the UV-irradiation of water [5]. There it was found that the presence of impurities in water significantly reduces the concentration of the H_2O_2; and this in good accordance with our results.

Character of the concentration dependence of H_2O_2 on the inputted energy reflects peculiarities of the photolysis generated by irradiation source, which has continuous or similar spectrum of a black body irradiation under the temperature of $(1–2) \times 10^4$ K. Under these temperatures, UV-irradiation in the range of 100–300 nm occupies a significant share of the spectrum.

Note that the UV-irradiation in the range of 100–200 nm is absorbed forming H_2O_2 [5, 6], and quanta with the wavelength of 200–300 nm are absorbed intensively by the molecules of H_2O_2 [14]. So, during generation of H_2O_2 by the UV-irradiation of water, the process of H_2O_2 decomposition takes place, as showed by the experiment dependence.

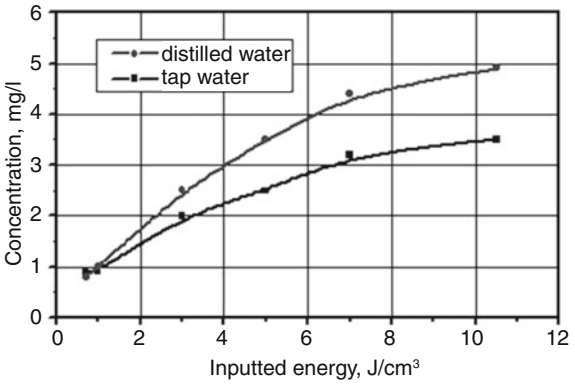

Fig. 5.1 Concentration of the hydrogen peroxide versus inputted energy

This dependence is described by the following differential equation

$$\frac{dn}{dE} = A - B_{abs} \times n \tag{5.1}$$

where n is concentration of H_2O_2 molecules; A is rate of generation of H_2O_2 at absorption of single energy of photons having highest energy yield; B_{abs} is energy coefficient of absorption of single molecule of H_2O_2.

With the first approximation for the coefficients A and B_{abs}, one can write the following equations

$$A = (\gamma_1 \Phi_1)/(h\nu_1) \tag{5.2}$$

where γ_1 is coefficient determining a share of electromagnetic irradiation in the range of $\gamma_1 + \Delta\nu$ having the greatest quantum yield of the Φ_1 for the reaction $H_2O + h\nu_1 \rightarrow H + OH$

$$B_{abs} = (\gamma_2 \Phi_2)/(h\nu_2 \sigma_{abs} d) \tag{5.3}$$

where γ_2 and Φ_2 are analogical ones to γ_1 and Φ_1 but for reaction of the return type $H_2O_2 + h\nu_2 = 2OH$ only; σ_{abs} is cross section of absorption; d is characteristic size of the cuvette, defining the absorption (in our case is the radius of the cuvette).

The quantum outputs for reactions of the photolytic generation of H_2O_2 are presented in works [5, 6, 14]. Data on the absorption cross-section for the processes of the decomposition of H_2O_2, and the quantum yield of this process are presented in [14]. These values in equations for the coefficients A and B_{abs} (3.8 and 3.9) we will use for the further estimations:

$$B_{abs} = 0.19\,\gamma_2 \Phi_2, \left(\mathrm{cm}^3/\mathrm{J}\right) \tag{5.4}$$

$$A/B_{abs}\,2.0 \times 10^2 \tag{5.5}$$

The coefficients γ_1 and γ_2 determine the overall spectral share of the irradiation energy to the energy of the PED. Thus, the coefficient γ_1 takes into account the part (100–200 nm) of the spectrum for generation of H_2O_2, and the γ_2 takes into account the part (200–300 nm) corresponding to the H_2O_2 decomposition.

Experimental determination of the irradiation energy and the determination of the blackness degree are a difficult task. But it is possible to estimate them in the first approximation. Moreover, for estimation of the ratio A/B_{abs}, one can confine by the estimation of the plasma channel temperature. So, estimation of the ratio A/B_{abs} was performed based on equations of the energy conservation. It was shown that the temperature of the plasma channel is (10–12) $\times$ 10^3 K.

This follows from comparison of the appraisal values of B_{abs} and n_∞ with experimental ones that were obtained by extrapolation of the experimental dependences by means of solution of (5.1)

$$n = n_\infty(1 - \exp(-B_{abs}\,E)) \tag{5.6}$$

where n_∞ is A/B_{abs} is the limit concentrations of H_2O_2, which can be obtained at the discharge energy: $E \gg 1/B_{abs}$.

Coefficient B_{abs} obtained experimentally is almost by order more than the calculated one.

Additional contribution into the decomposition process of H_2O_2 is stipulated by the reaction with impurities, for example, with the iron or copper ions those were formed by the electrodes erosion.

Concentration of H_2O_2 decreases fast and reaches zero value in a few days.

5.2 Nanoparticles

This group of substances includes the metal and oxide nanoparticles produced by electrothermal erosion of electrodes and metal ions under the PED.

Since much of our investigation is focused on nanoparticles and their water dispersions, it is logical to present here an overview of works related to this topic.

In recent years, there is a revival of colloid chemistry in a new form: physical chemistry of nanostructured objects. Due to demands of nanotechnology, this area is fast developing science. Many thousands of papers are published on this subject annually.

Nanoparticles are colloidal objects having size from 1 to 100 nm on at least one of their three dimensions. Recent studies have shown that physical and chemical properties of nanoparticles differ qualitatively from ones of both macro and microscopic objects [7, 9].

Unusual properties of nanoparticles are connected with the fact that, when size of the particles becomes comparable with the Bohr radius (or less it), the classic size effects transfer onto the quantum level. Under this, the kinetic energy submits to the uncertainty principle. In a metal macro-object, high density of states at the Fermi level forms a conduction band with continuous energy levels. So, the split of energy into discrete levels takes place in nanoparticles. Under this, nanoclusters behave as quantum dots, i.e., inside them, as well as, in atoms, the free electrons can occupy only certain allowed energy states [10].

With the quantum size effect, the following additional properties of metal nanoparticles appear:

- Generation of locally enhanced electromagnetic field on the surface of nanoparticles
- Changing the magnetic properties of particles from the diamagnetic to the paramagnetic and from ferromagnetic to superparamagnetic ones as their size approaches to size of the magnetic domain
- Significant reduction of melting temperature and increase of solubility
- Shift of the plasmon resonance to the blue end of spectrum band under decreasing the particle size, etc.

It should be noted that the localized surface plasmon resonance (LSPR) is the most characteristic optical property of metal nanoparticles. Resonance occurs when light of certain wavelength interacts with the surface electrons, causing their collective oscillation. Depending on the size and shape of nanoparticles, the maximum of LSPR bandwidth may be in the UV, visible, or near-infra-red (NIR) areas of spectrum.

Under decreasing the nanoparticles size, share of surface atoms is sharply increased. For example, in a nanoparticle of 5 nm diameter, 40 % of atoms are located on its surface, and in nanoparticle of 1 nm diameter, already 99 % of atoms are located there. The high surface energy of nanoparticles provides multiple interactions that form nanostructured composites of nanoparticles. This leads to increase in strength, heat resistance, and chemical stability of the nanostructured material.

Metal nanoparticles are applicable to nanofabrication that produces a variety of highly ordered nano-structures: nano-films, nano-discs, nano-crystals, nano-wires, etc. Therefore, advances in nanoparticles synthesis and study of their properties have stimulated explosion of applied research in the field of nanotechnology and, moreover, in nano-electronics, nano-optoelectronics, nano-electrochemistry, and in analytical and biomedical applications of nanoparticles [15, 16].

Methods of nanoparticles production. The classic method for colloid chemistry consists in mechanical dispersion of solids by various mills and is almost never used in contemporary nano-chemistry. It is due to high-energy consumption and, more importantly, because of high contamination of the initial product.

Contemporary methods for producing the nanoparticles can be divided into two categories:

- Producing the ultradisperced powders based on the basis of the physical processes of dispersion, evaporation, and condensation of metal
- Chemical synthesis of nanoparticles by the reduction or thermal decomposition of metal salts and organometallic compounds

In some hybrid methods, such as spray pyrolysis, the physical and chemical processes can be combined. Depending on the aggregate state of used dispersion medium, methods for nanoparticles producing are divided in gas-phase and liquid-phase ones. Here, the chemical methods are preferably applied in the liquid-phase version, but the most of physical methods are used in the gas-phase version. However, some physical methods such as the laser ablation are universal, i.e., allow one to produce dry powders and liquid colloidal dispersion of nanoparticles.

Gas-phase methods for producing the nanoparticles. They are based on the homogeneous nucleation in the vapor phase with supersaturation, condensation, and subsequent coagulation by rapid cooling of vapor. The rapid cooling is necessary to produce the ultrasmall nanoparticles and to prevent their agglomeration. In evaporative gas-phase reactors, characteristics of produced nanoparticles are determined by dynamics of formation and growth of solid phase nuclei at the initial stages of synthesis process during few milliseconds. For this time-interval, several processes take place: nucleation, surface growth of particles, collision, coalescence, sintering, etc.

Spray reactor is a kind of the gas-phase reactor, in which the metallic nanoparticles are produced from organometallic "precursors". The process has the following scheme. At the initial stage of the process, evaporation of solvent from the aerosol droplets having micron size is performed. Next, the decomposition of the organometallic "precursor" is fulfilled with excretion of the nanocluster nuclei. Further, the process is implemented in the same manner as in the evaporative gas-phase reactor. Theoretical analysis and simulation of these processes are extremely complex. So, the optimal characteristics of gas-phase and spray reactors are chosen experimentally [17–20].

The evaporation-condensation reactors differ by method of saturated vapors producing: hot-wall reactor, electric arc reactor, radio frequency heating, and flame reactor. Moreover, they differ by method of condensation: dilution cooling, condensation in inert gas, and expansion through a nozzle cooling [21–24].

In the aerosol version of evaporation-condensation method, the carbonyls and acetylacetonates of metals and organometallic compounds are used as a "precursors" [25, 26].

By means of evaporation-condensation method, nanoparticles of Cu, Fe, Ag, W, Al, In, Mg, Zn, Sn, Ga, Ti, and various oxides were prepared. This method can be easily scaled up to industrial-productive level of metallic nanopowders production, but it requires sophisticated and expensive equipment. Nanoparticles production by evaporation method gives, as a rule, logarithmically-normal distribution in size [27].

Spray pyrolysis is an aerosol method [28, 29]. In this process, solution of the "precursor" (acetate or nitrate salt of a metal or organometallic compound) is sprayed into a carrier-gas. The resulting spray is supplied into the tubular furnace, where decomposition or reduction reaction of the "precursor" is implemented with forming the metal nanoparticles.

Often, a bipolar charging device and differential flow classifier of particles mobility are installed at the output of the gas stream from the furnace. As a result, it becomes possible to produce monodisperse nanoparticles with a very narrow distribution in size [30, 31].

The main difficulty in this method is to avoid oxidation of nanoparticles. This is achieved by suitable choice of the "precursor" and by performing the process in a reducing atmosphere.

Laser ablation is new and promising physical method of metal nanoparticles preparation [32]. In this method, a powerful pulsating laser rapidly heats a thin film

or wire target of metal, generating the ionization of metal. Under further heating, the plasma is produced in the presurface layer. However, in this method, besides the atoms and ions of the target, its fragments of subnanometer/nanometer size may be rifted. So, the laser ablation cannot be regarded as a purely homogeneous nucleation process. The relative amounts of rifted atoms and particles are determined by variation of the pulse duration and inputted energy. In the laser ablation, the rate of material removal is decreased with increasing time of exposure of the target. So, one may use a rotating target. At frequency of $\sim$50 Hz, typical productivity of this method is 10–100 mg/h [33]. The laser ablation is used in the gas-phase version for preparation of dry powders, for direct deposition of nanoparticles onto a substrate, and in the liquid-phase version for preparation of aqueous or organic dispersions [34–38].

By the laser ablation method nanoparticles of Ag, Cu, Au, Pt, Pb, Cd, Bi, Ti, Si, and a number of alloys have been prepared. The undeniable advantage of this method is that it ensures the absence of reagents and ions in the nanopowder or dispersion. But low productivity is a drawback of this method.

Electric explosion of conductors. This method for plasma generation is used widely. For producing the metal nanoparticles, the process is carried out in two ways:

- Single explosion of a thin wire by passing through in the short high-current pulse
- Multiple pulsed electric discharges between two metal electrodes and causing their evaporative erosion [39]

The process is controlled by variation of voltage, value and duration of pulse current, material and size of wire, nature of medium in the discharge chamber of nanoparticles generator, and by other factors. It was found that under electric explosion of fusible highly conductive conductors (made of Al, Au, Ag, and Cu), processes of plasma forming and evaporation are dominated.

But in the case of the refractory metals (W and Mo), their spraying happen in the form of condensed droplets [40]. This new and promising method for producing the nanoparticles has been studied and now has already commercial application [41–45].

The method can be carried out in the gas-phase and liquid-phase versions. In the first case, the inert gas atmosphere is most widely used. In the most sophisticated installations, the nanopowders are formed under the jet cooling in nozzles at supersonic speeds [46]. In the second case, the electrodischarge chamber of nanoparticles generator is filled with a fluid [47, 48].

Among the advantages of the electroexplosive technology, it is possible to underline a wide range of produced nanometal and nanooxides and high performance at low cost of nanoparticles.

Chemical methods for producing the metal nanoparticles, in mainly based on the reduction reaction of salts and metal complexes [49–51]. The synthesis of nanoparticles of noble metals is presented in the reviews [52, 53]. To recover salts, variety of chemical compounds is used: borohydrides of Na, K, and Li, ascorbic

acid, hydrazine, lithium aluminum hydride, quercetin, alcohols and glycols, dimethylnaphthalides of alkali metals, citrate, and hexadetsilanilin [54–57].

Stabilization of nanoparticles. Due to the large specific surface of nanoparticles dispersion aggregately unstable. So to obtain sufficiently concentrated dispersions it is necessary to use the principles of electrostatic or steric stabilization.

Electrostatic stabilization is achieved by formation of the double electric layer around the nanoparticles. For example, on the surface of gold nanocrystals (prepared by the citrate method), the citrate anions are adsorbed, which attract the layer cations and prevent aggregation [58–60].

Steric protection method is connected with adsorption of the polymers and amphiphilic detergents. In this case, on surface of the nanoparticles, a protective layer is formed of polymer chains or ligands. The layer prevents approaching the nanoparticles to each other. It happens since during the approach, the reduction of conformational entropy of chains takes place, and such a configuration is thermodynamically unstable. In this case, the osmotic effect additionally contributes to repulsion of the nanoparticles.

For the steric stabilization of dispersions, various surfactants are used: polyvinylpyrrolidone, polyvinyl alcohol, fatty acids, and amines or thiols with long aliphatic chain [54, 61–63].

The citrate method is the oldest one for metal colloids preparation. It was designed for manufacture of the aqueous gold sols in boiling citrate solution of $HAuCl_4$. Homogeneous forming of gold nanoparticles with diameter of about 20 nm is observed after 10 min. Due to variations of the solution composition, one can change size of the nanoparticles in the range 16–150 nm. By the same method, the silver and platinum nanoparticles have been prepared [58, 64].

Sometimes, polyelectrolytes are used for synthesis of nanoparticles. The polyelectrolyte shell adsorbed on the surface of the nanoparticles has useful properties. It not only stabilizes the dispersion, but also allows a multi-layered "self-assembly" of nanoparticles. This is due to the successive layering them from the dispersions by polyelectrolytes of the opposite charge [65–67].

Recently for synthesis of metallic nanoparticles, the dendrimers are often used. The dendrimers are a new class of the monodisperse globular branched polymers. In them, all bonds that have a regular branching and internal and external functional groups to be radially focused to the central core. In the dendrimer "master" macromolecule, the internal cavities are large enough to attach the nanoscale "guests" such as metal nanoclusters [68, 69].

Synthesis of magnetic nanoparticles has its own specific features. The magnetic nanoparticles are close in size to the size of the magnetic domain. In the domain, the magnetic spins are in the same direction that makes the magnetic moment to be in one direction. By the size of magnetic domain, some classic diamagnetic, for example, Cu are became the paramagnetic and ferromagnetic, i.e. superparamagnetic.

Magnetic nanoparticles have a number of unique and promising properties in techniques such as the very high magnetoresistance. Anisotropic magnetic nanoparticles have particularly interesting properties.

Synthesis of the magnetic nanoparticles is complicated by the fact that their mutual attraction promotes aggregation. In addition, if as a magnetic material Fe or Co (i.e., easy oxidizable species) are used, then to avoid oxidation, it is necessary to avoid it just in the synthesis process and, after, to protect the output product from oxidation [70, 71].

5.3 Preliminary Results

At the initial stage of investigation, the electrodes of various metals and their alloys were used. Figure 5.2 shows the average specific erosion of some of those metals and alloys, where 1 is W + Cu; 2 is Cr_3C_2 + Cu; 3 is Ag + Cu; 4 is Fe; 5 is Mo + W + Cu; 6 is W + Ni + Fe; 7 is Cu; 8 is W + Ni + Cu.

The obtained data were used for rough estimation of the total mass concentration of the nanoparticles in water. After determination of connection between properties of the electrodes materials and bactericidal action of the treated water, further investigations were concentrated on three metals: silver, copper, and iron. The first two metals were chosen since their ions have the highest toxicity to bacteria and, as a result, are useful for practical applications. The iron was chosen for comparison with the first two metals and preparation of the magnetoactive nanoparticles.

The mass spectrometry with inductively connected plasma confirmed that the electrodes erosion produces particles of metals and their oxides in water. After that, the laser correlation spectrometer with dynamic quasi-elastic light scattering was used for determination of distributions of the particles mass fractions in size.

Figure 5.3 shows plots of average distributions in size of silver, copper, and iron nanoparticles under inputted energy of 5 and 10 J/ml. The plot shows that all particles sizes are ranged from 5 to 1,000 nm, mass of "small" particles is maximal, and mass of these nanoparticles is decreased at increase of inputted energy.

Figure 5.4 shows electronic microscopy images of silver (a) and copper (b) nanoparticles and their clusters.

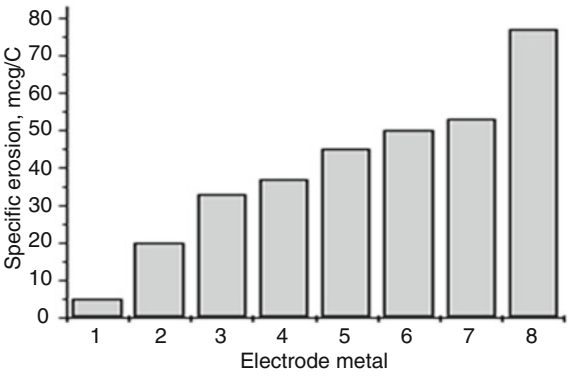

Fig. 5.2 Specific erosion of the electrodes [72]

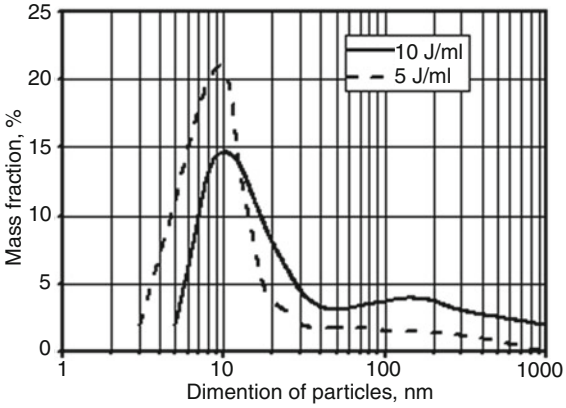

Fig. 5.3 Distributions in size of the silver, copper, and iron nanoparticles [72]

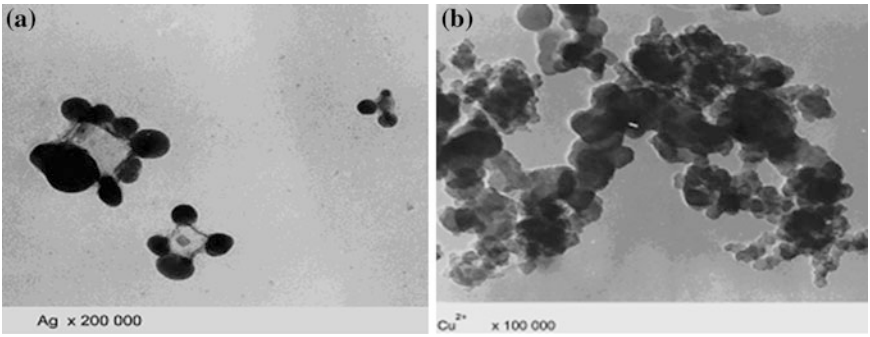

Fig. 5.4 Silver (**a**) and copper (**b**) nanoparticles [72]

Investigation of water treated with copper electrodes was implemented. We use the exclusive liquid chromatography, electronic paramagnetic resonance, spectroscopy in UV, and visible spectra. It was shown that the material of nanoparticles is not metallic but consists of the oxides Cu_2O, and CuO.

Thus, it was found that the water treated by the PED with the copper electrodes is the dispersion containing both nanoparticles of the electrodes metal and the Cu^+ and Cu^{2+} ions. These types of the nanoparticles are in the dynamic concentration equilibrium [73] and with the ratio 5:1 [74].

After from the dispersion the nanoparticles have been extracted and then put in the deionized water, about 1 h later it was detected that the ion concentration reached almost initial level, hence, the conclusion can be done that the oxide nanoparticles are sources of ions.

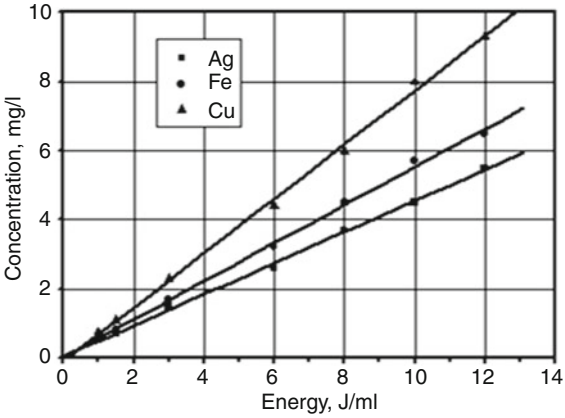

Fig. 5.5 Concentration of the silver, copper and iron nanoparticles in dispersion versus inputted energy [72]

By means of the chromatography, the mass strength of the silver, copper, and iron nanoparticles in a dispersion had been determined versus inputted energy under the complete decomposition of the nanoparticles to the ions at pH 2.5 (Fig. 5.5).

By the capillary electrophoresis, it was also found that the nanoparticles have the negative specific surface electric charge of (0.4–1.6) × 10^{-2} C/m^2 and the volume specific charge of (0.01–2.6) × 10^{-2} C/ml.

In recent years, there is a revival of colloid chemistry in a new form: physical chemistry of nanostructured objects.

Contemporary methods for producing the nanoparticles can be divided into two categories: production of the ultradisperced powders based on the physical processes of dispersion, evaporation, and condensation of metal and based on the chemical synthesis of nanoparticles by the reduction or thermal decomposition of metal salts and organometallic compounds.

The mass spectrometry with inductively connected plasma (MS-ICP) confirmed that the electrodes erosion produces nanoparticles of metals and their oxides in water.

References

1. E. Hart, M. Anbar, *Hydrated Electron* (Atomizdat, Moskow, 1973). (in Russian)
2. A.K. Pikaev, *Pulsed Radiolysis of Water and Aqueous Solutions* (Nauka, Moscow, 1965). (in Russian)
3. V.L. Gorjachev, A.S. Remennyi, N.A. Sylin, J. Tech. Phys. Lett. **11**, 16 (1991). (in Russian)
4. V.Ya. Ushakov, *Pulsed Electrical Discharge in Gases* (Tomsk, 1975) (in Russian)
5. V. Sokolov, G. Stain, J. Chem. Phys. **5**, 44 (1966)
6. V. Sokolov, G. Stain, J. Chem. Phys. **9**, 44 (1966)
7. G. Schmid et al., *Nanoparticles: From Theory to Application* (Wiley, New York, 2004)
8. A. Furstner et al., *Active Metals: Preparation* (Characterization and Applications, VCH, Weinheim, 1996)
9. J.-N. Lue, J. Phys. Chem. Solids **62**, 1599–1612 (2001)

10. U. Kreibig, M. Vollmer, *Optical Properties of Metal Clusters* (Springer, Berlin, 1995)
11. B.K. Teo, H. Zhang, *Magic Numbers in Clusters* (M. Dekker, New York, 2002)
12. K.E. Drexler, *Nanosystems: Molecular Machinery, Manufacturing and Computation* (Wiley, London, 1992)
13. R.W. Siegel, *Nanophase Materials: Synthesis, Structure and Properties* (Springer, Berlin, 1994)
14. Y. Shamb, C. Satterfield, R. Vaptwarth, *Hydride Peroxide* (Moskow, 1958)
15. G.M. Chow, K.E. Gonsalves, et al., *American Chemical Society Symposium* (Washington, 1996)
16. M.N. Rittner, (Business Communications Co, Norwalk, 2001)
17. Z.L. Wang, et al., *Handbook of Nanophase and Nanostructured Materials* vol 1, *Synthesis* (Kluwer, New York, 2002)
18. M.T. Swihart, J. Sci. **8**, 127–133 (2003)
19. A. Gutsch, M. Kramer, G. Michael, H. Muhlenweg, M. Pridohl, G. Zimmerman, KONA, **20**, 24–37 (2002)
20. Y. Singh, J.R.N. Javier, S.H. Ehrman, M.H. Magnusson, K. Deppert, J. Aerosol Sci. **33**, 1309–1325 (2002)
21. T.T. Kodas, M. Hampden-Smith, *Aerosol Processing of Materials* (Wiley-VCH, New York, 1999)
22. V. Haas, R. Birringer, H. Gleiter, S.E. Pratisinis, J. Aerosol. Sci. **28**, (1997)
23. A. Maisels, F.E. Kruis, H. Fissan, B. Rellinghaus, H. Zahres, J. Appl. Phys. Lett. **77**, (2000)
24. K. Wegner, B. Walker, S. Tsantilis, S.E. Pratsinis, J. Chem. Eng. Sci. **57**, 1753–1762 (2002)
25. M.H. Magnusson, K. Deppert, J.O. Malm, J. Mater Res. **15**, 1564–1569 (2000)
26. A.G. Nasibulin, O. Richard, E.I. Kauppinen, D.P. Brown, J.K. Jokiniemi, I.S. Altman, J. Aerosol Sci. Technol. **36**, 899 (2002)
27. H. Hahn, J. Nanostruct. Mater **9**, 3–12 (1997)
28. J.H. Kim, T.A. Germer, G.W. Mulholland, S.H. Ehrman, J. Adv. Mater. **7**, 14 (2002)
29. J.H. Kim, V.I. Babushok, T.A. Germer, G.W. Mulholland, S.H. Ehrman, J. Mater. Res. **18**, 1614 (2003)
30. D. Chen, D.Y.H. Pui, J. Nanoparticle Res. **1**, 115–126 (1999)
31. D.R. Chen, D.Y.H. Pui, D. Hummes, H. Fissan, F.R. Quant, G.J. Sem, J. Aerosol Sci. **29**, 497–509 (1998)
32. W. Marine, L. Patrone, B. Luk'yanchuk, M. Sentis, J. Appl. Surface Sci. **154**, 345–352 (2000)
33. M. Ullmann, S.K. Friedlander, A. Schmidt-Ott, J. Nanoparticle Res. **4**, 499 (2002)
34. S. Onari, M. Miura, K. Matsuishi, J. Appl. Surface Sci. **30** (2002)
35. Z. Marton, L. Landstrom, M. Boman, P. Heszler, J. Mater. Science Eng. C. **1–2**, 23 (2003)
36. Y. Kawakami, T. Seto, Y. Yoshida, E. Ozawa, J. Appl. Surface. Sci. **30**, (2002)
37. T. Tsuji, K. Iryo, N. Watanabe, M. Tsuji, J. Appl. Surface Sci. **1-2**, (2002)
38. D. Yang, D. Kim, J. Appl. Phys. A: Mater Sci. Process. (2003)
39. F. Tepper, J. Powder Metal **4**, 43 (2000)
40. P. Sen, J. Ghosh, A. Abdulla, P. Kumar, Vandana. Proc. Indian Acad. Sci. Chem. Sci. **5–6**, 115 (2003)
41. W.H. Lee, C.H. Chung, C.L. Chung, Int. J. Nanosci. **4–5**, 2 (2003)
42. Y. Fu, C. Shearwood, J. Scripta Materialia **3**, 50 (2004)
43. V.S. Giri, R. Sarathi, S.R. Chakravarthy, C. Venkataseshaiah, J. Mater. Lett. **6**, 58 (2004)
44. Yu.A. Kotov, Ch.K. Rhee, A.V. Bagazeev, I.V. Beketov, T.M. Demina, A.M. Murzakaev, O. M. Samatov, O.R. Timoshenkova, A.I. Medvedev, A.K. Shtolts, J. Metastable Nanocryst. Mater **15-16**, (2003)
45. Q. Wang, H. Yang, J. Shi, G. Zou, J. Mater. Res. Bull. **3–4**, 36 (2001)
46. Electroexploded metal particles: http://www.argonide.com
47. F.G. Rutberg, V.A. Kolikov, V.E. Kurochkin, V.G. Maltsev, Rus. Pat. 2272697 (2006) (in Russian)
48. A.F. Routberg, V.A. Kolikov, P.G. Rutberg, A.N. Bratsev, US Pat. 7374693 (2008)

49. M.A. Willard, L.K. Kurihara, E.E. Carpenter, S. Calvin, V.G. Harris, *Encyclopedia of Nanoscience and Nanotechnology* (American Scientific Publishers, USA, 2000–2004)
50. L.M. Liz-Marzan, J. Materials Today (2004)
51. C.N.R. Rao, A. Müller, A.K. Cheetham, *The Chemistry of Nanomaterials: Synthesis, Properties and Applications,* vol. 2 (Wiley, 2004)
52. I. Okura, *Encyclopedia of Nanoscience and Nanotechnology* (American Scientific Publishers, USA, 2000–2004)
53. M.C. Daniel, D. Astruc, J. Chem. Rev. **104,** 293–346(2004)
54. A. Nandi, M.D. Gupta, A.K. Banthia, J. Colloids Surfaces A **197,** 119–124 (2002)
55. Y. Liu, C.-Y. Liu, L.-bo. Chen, Z.-Y. Zhang, J. Colloid Interface Sci. **257,** 188–194 (2003)
56. C.A. Waters, A.J. Mills, K.D. Johnson, D.J. Schiffrin, J. Chem. Commun. 540–541 (2003)
57. B.L.V. Prasad, S.I. Stoeva, C.M. Sorensen, K.J. Klabunde, J. Langmuir **18,** 7515–7520 (2002)
58. I. Pastoriza-Santos, L.M. Liz-Marzan, J. Langmuir **18,** 3694–3697 (2002)
59. J. Turkevich, P.C. Stevenson, J. Hillier, J. Disc. Faraday Soc. **11,** 55–75 (1951)
60. G. Frenz, J. Nature, Phys. Sci. **241,** 20–22 (1973)
61. S. Qui, J. Dong, G. Chen, J. Colloid & Interface Sci. **216**, 257–269 (1999)
62. C.M. Liu, L. Guo, H.B. Xu, Z.Y. Wu, J. Weber, J. Microelectronic Eng. **66,** 107 (2003)
63. M.S. Hedge, D. Larcher, L. Dupont, B. Beaudoin, K. Tekaia-Elhsissen, J.M. Tarascon, J. Solid State Ionics **93**, 33 (1997)
64. G. Frenz, J. Nature, Phys. Sci. **241**, 20–22 (1973)
65. D.I. Gittins, F. Caruso, J. Phys. Chem. B **105**, 6846 (2001)
66. K.S. Mayya, B. Schoeler, F. Caruso, J. Adv. Funct. Mater **13**, 183–188 (2003)
67. D.I. Svergun, E.V. Shtykova, A.T. Dembo, L.M. Bronstein, O.A. Platonova, A.N. Yakunin, P. M. Valetsky, A.R. Khokhlov, J. Chem. Phys. **109**, 11109–11116 (1998)
68. R. Crooks, V. Chechik, B.I. Lemon III, L. Sun, L.K. Yeng, M. Zhao, *Metal Nanoparticles Synthesis, Characterization and Application* (M. Dekker, New York, 2002)
69. J.M.J. Frechet, D.A. Tomalia, *Dendrimers and Other Dendritic Polymers* (Wiley, Chichester, 2001)
70. R.H. Kodama, J. Magn. Magn. Mater. **1–3**, 200 (1999)
71. T. Hyeon, J. Chem. Commun. 927–934 (2003)
72. Ph.G. Rutberg, V.A. Kolikov, V.E. Kurochkin, L.K. Panina, A.Ph. Rutberg, J. IEEE Trans. Plasma Sci. **4**, 35 (2007)
73. H.A. Laitinen, *Chemical Analysis* (McGraw-Hill, New York, 1960)
74. V.A. Kolikov, V.E. Kurochkin, L.K. Panina, A.F. Rutberg, F.G. Rutberg, V.N. Snetov, A.Yu. Stogov, J. Tech. Phys. **2**, 52 (2007)

Chapter 6
Water Dispersions of Nanoparticles

Abstract This chapter presents data on both physical and chemical properties of the nanoparticles and their water dispersions. At present, investigations of water dispersions of nanoparticles generated by PED and their effect on biological objects need for a more detailed study of the products of erosion. This is because of one of the factors of biological activity of water are nanoparticles of several nanometers to several hundred nanometers. In order to study the electrical and chemical properties of nanoparticles in aqueous dispersions various techniques and equipment were used, including: experimental laboratory device developed on base of Doppler effect, scanning electron microscopy, spectrophotometry, infrared Fourier spectroscopy, powder X-ray diffractometry, and some other instruments and techniques. Time constant of concentration equilibration between silver nanoparticles and ions is from 3 to 7 min at changing of nanoparticles concentration from 75 to 4.75 mg/l. Time constant is increased at decrease of nanoparticles concentration in dispersion. When concentration of silver nanoparticles is changed from 6 to 160 mg/l, the average conductivity varies from 2.5 to 25 μS/cm. Electric conductivity of water dispersion of silver nanoparticles at cooling for about 10 % higher than at heating, i.e. there is thermo-conduction hysteresis. At decrease of nanoparticles concentration by diluting of initial dispersion by distillate, pH is reduced, i.e. initially alkaline reaction pH 7.4 is changed to the acid pH 6.76.

6.1 Electrothermal Erosion of Electrodes

Electrothermal erosion is the basic phenomenon under nanoparticles generation in water by the PED. As its result, the aqueous dispersions of nanoparticles; and application area of such dispersions is constantly expanded and includes biology, medicine, and ecology.

Mechanism of the electrothermal erosion. In fact, under the PED, the electrothermal erosion of the metal electrodes forms ions and nanoparticles in the water [1–3].

V. Kolikov and P. Rutberg, *Pulsed Electrical Discharges for Medicine and Biology*, Biological and Medical Physics, Biomedical Engineering,
DOI 10.1007/978-3-319-18129-5_6

It is known that mechanisms of the anode and cathode erosion differ significantly. At present, it is assumed that the main mechanism of cathode erosion consists of microscopic explosions accompanied by emission of electrons and particles of the metal in the form of individual portions or avalanches (called ectons) [4, 5]. However, a bombardment of the cathode by positive ions also is the acting factor of erosion [6].

Moreover, there is another different mechanism of erosion of the anode metal. Namely, this is melting and evaporation of the surface layer in the anode spots that is stipulated by its bombardment by electrons and negative ions [7].

Erosions of the cathode and anode differ quantitatively. Depending on the metal kind, the cathode erosion is more than the anode one by 2–5 times.

Application of water dispersions of metallic or oxide nanostructures in biology and medicine requires stability and reproducibility of physical and chemical properties of the nanoparticles, for example, of their size. Nanostructures of the Ag, Cu, Fe, Zn, and Ti were studied by laser correlation spectrometer, electronic, atomic power, tunneling, and electron microscopes.

Experimental data of the specific erosion. Specific erosion of electrode metals was determined by an installation consisting of the discharge chamber and generator of high-voltage pulses with the repetition rate of 50 Hz, current of 20 A, and current pulse duration of 20 μs. The anode electrode under studying was a cylinder of 10 mm diameter.

Measurement of erosion was carried out by weighing of the electrodes before and after tests. Tests for 8 h per day were performed during $\sim$100 h.

Results are presented in Table 6.1.

The tests show that the steady-state erosion after $\sim$50 h is fixed, and before that the specific erosion to one order, approximately, lower than its steady-state value (Table 6.1, W + Ni + Fe).

Estimated value of the specific erosion. To calculate the erosion, the model of the arc spot was used. The value of erosion is determined by the flux of atoms evaporating from the arc spot surface during the discharge. The diameter of each spot was determined by the autograph method.

The temperature of the electrode surface was determined from solutions 1–2 mm. In this case, temperature on the electrode borders was considered constant and equal to 300 K.

Inside the spot, the density of heat flux was given. This value was determined from the volt age and current waveforms. It was assumed that the value of the near-anode voltage drop is $U_a = 0.1\ U_e$.

Calculations for the copper, iron, and tungsten electrodes were made. The Table 6.2 shows the calculated and experimental values of erosion for single pulse.

In this table for comparison, the experimental data on electrode erosion of the steel and pseudo alloy Mo + W + Cu are also given. It is seen that results for the copper and tungsten coincide quite satisfactory. It is necessary to note that the experimental data are averaged for a sufficiently long time.

Table 6.1 Erosion of the electrodes

Metal	Diameter (mm)	Time (h)	Initial mass (g)	Final mass (g)	Erosion (g)	Share of initial mass (%)	Specific erosion (mg/C)
Ag	10						
Cu	10						
Fe	10	100	5.6	5.2	0.4	7.14	36
W + Cu	10	20	4.75	4.7	0.05	1	5
Cr_3C_2 + Cu	10	20	4.8	4.6	0.2	4	20
W + Ni + Cu	10	100	13.45	12.6	0.85	6.3	77
Mo + W + Cu	10	100	8.5	8	0.5	5.9	45
W + Ni + Fe	10	20	6.5	6.45	0.05	0.8	5
		100	11.6	11.05	0.55	4.74	50
		170	11.6	10.6	1	8.6	53

Table 6.2 Calculated and experimental erosion for single pulse

Calculation		Experiment	
Metal	Erosion (μg/C)	Metal	Erosion (μg/C)
Copper	5.5	Copper	10
Iron	5.0	Iron	18
Tungsten	9.4	Mo + W + Cu	20

Moreover, the data on the spot sizes used in these calculations may not match the experimental conditions, in which the discharge channel is interacted with the eroded electrode surface.

At very early stage of these works, we have defined values of the specific erosion of electrodes depending on the duration of pulse, gas bubbles, and other factors [8]. The electrodes at the PED in water are similar to phenomena of the water-cooled electrodes under stationary discharges. Under these conditions, the current flows through the surface of cathode and anode that is accompanied by emergence of an arc spot. However, due to short duration of the discharge and cavitation processes in water, quasi-explosive effects are emerged near the surface of electrodes [9].

This is evidenced by images of the electrode surfaces after long operation obtained by means of the electron microscope with various zoom (Fig. 6.1 1–8). At the steady mode, the microcaverns and microledges on the surface of electrodes are formed.

Images of the silver electrodes show that the cathode erosion occurs mainly on surfaces of their ends (Fig. 6.2a). The anodes erode also on the side surfaces. Length of the anode eroded surface is approximately equal to three its diameters (Fig. 6.2b).

Natures of erosion are different: for cathode this is forming of ectons (explosive emission) under the effect of electric field; for anode is reload of ions. Thus, specific

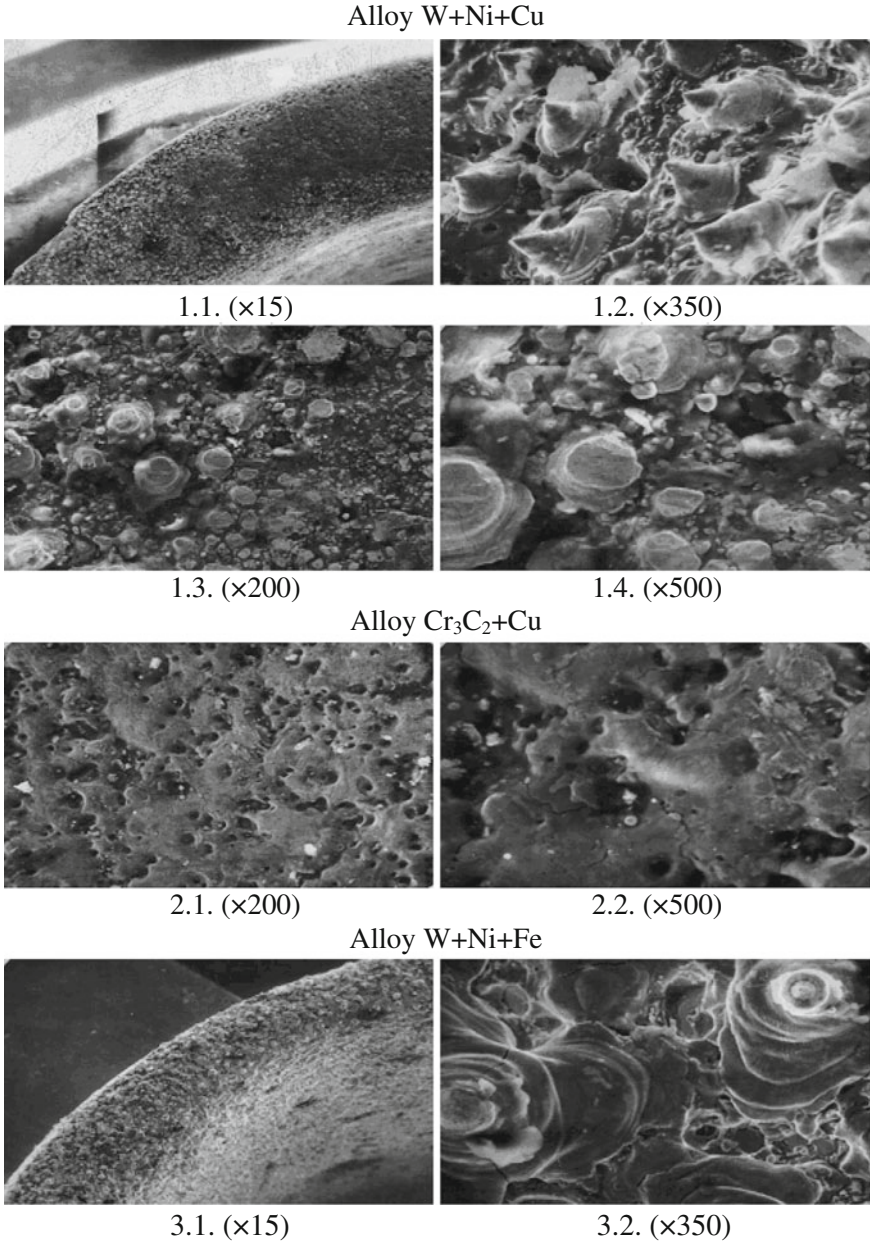

Fig. 6.1 Surfaces of the electrodes

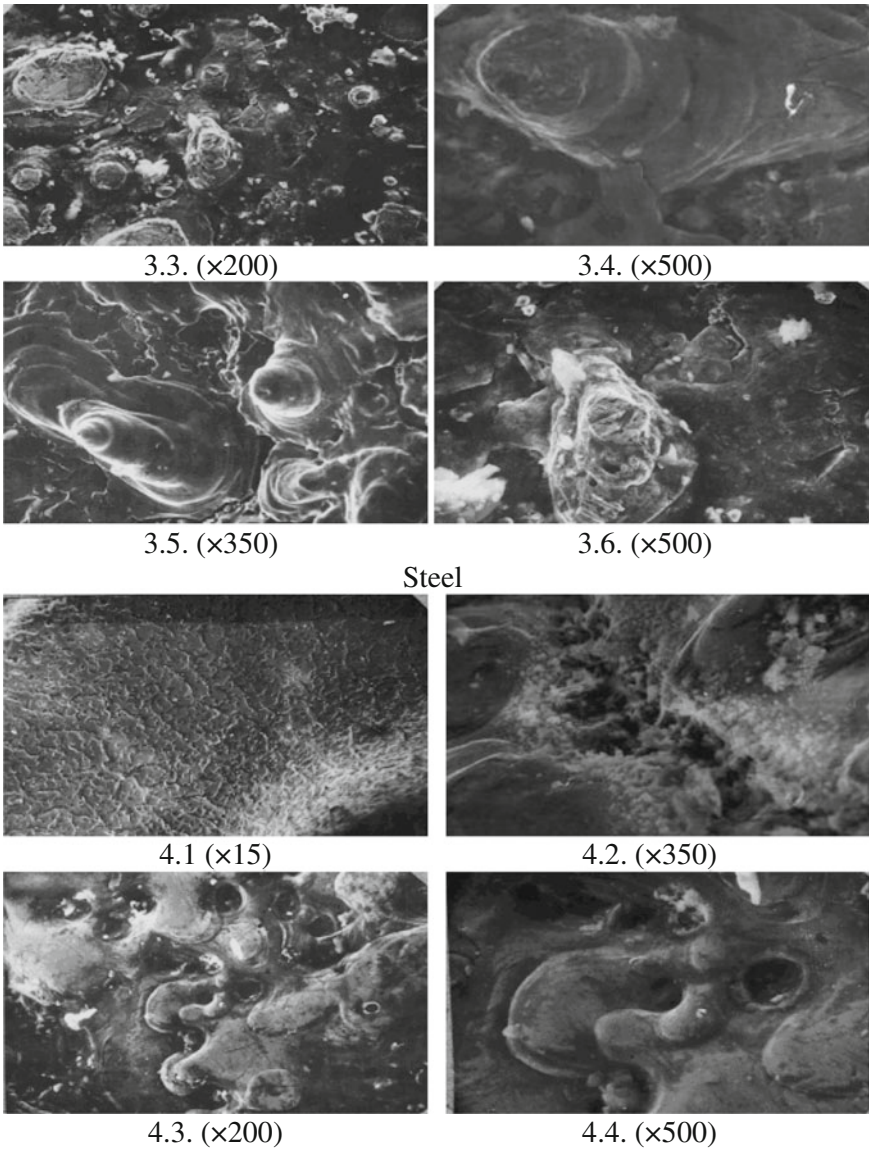

Fig. 6.1 (continued)

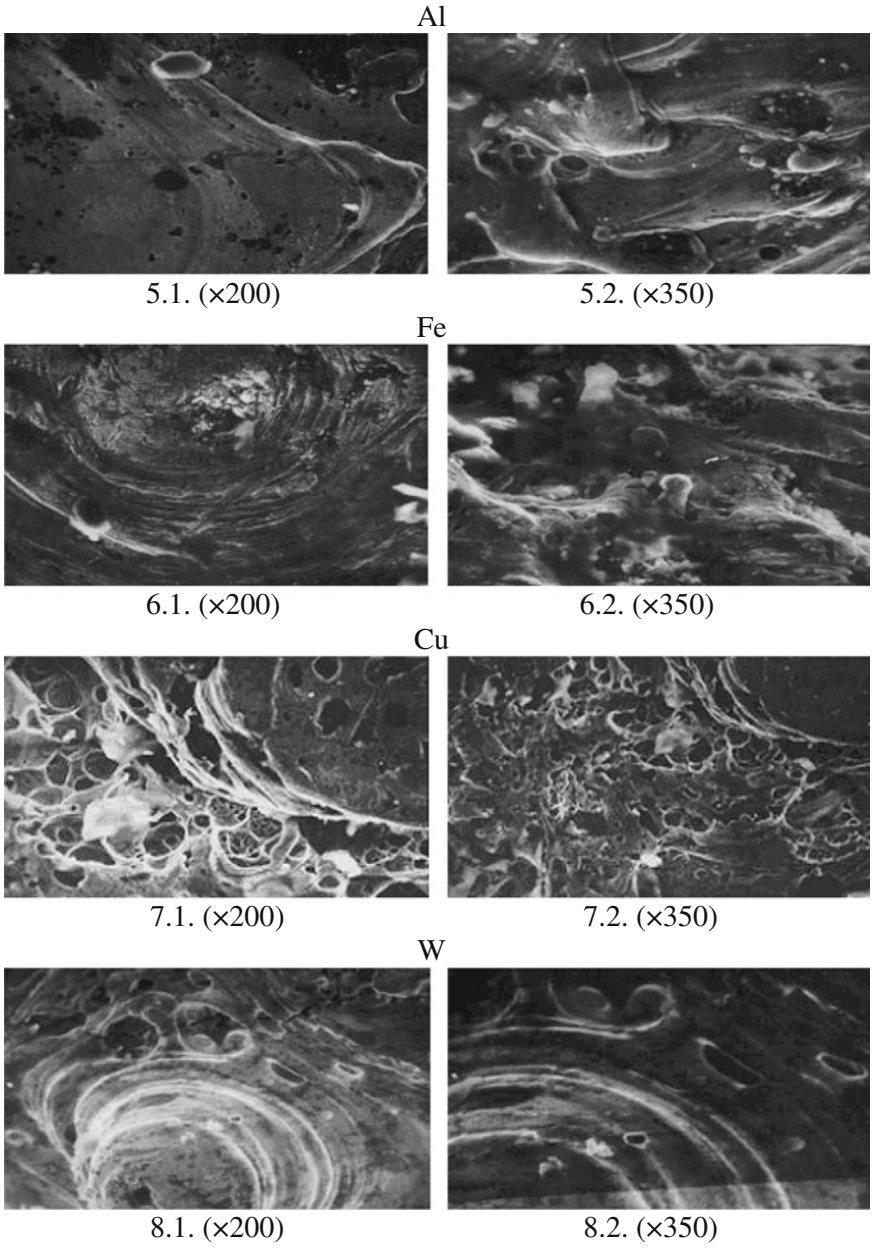

Fig. 6.1 (continued)

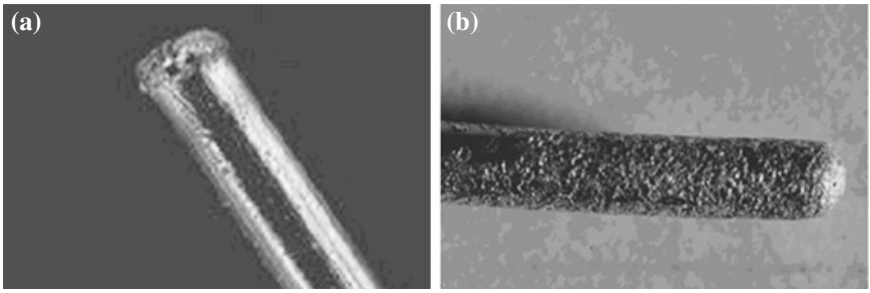

Fig. 6.2 Erosion of the electrodes (diameter 1 mm). **a** Cathode **b** Anode

values of the electrodes erosion are substantially various. The cathodes average specific erosion depends on their metal and is from 2 to 10 times more than erosion of anodes.

6.2 Parameters of Nanoparticles

At present, it is known that one of the factors of biological activity of water treated by the PED is nanoparticles of several nanometers to several hundred nanometers. So, it is necessary to implement investigations of water dispersions of nanoparticles generated by the PED. Special interest is in detailed study of the erosion products and of the dispersions effect on biological objects.

Size and form of nanoparticles. Conditions in the arc spots of the PED in water are similar to ones in electric explosion of metal wires. Currently, behavior of matter under explosion of metal wires was investigated rather well. However, the experiments and data were obtained for explosion in gases. It was found that particles formed under such explosions such explosions have size of 10–500 nm. The specific surface size of particles is 2–50 m^2/g.

Structure of particles is quite complex. They are usually formed of fragments ranged in size of 3–50 nm. These fragments are structurally organized basing on completion of the crystal lattice. Particles are not homogeneous. They have gas inclusions and pores. Also, particles have excited electronic and crystal subsystems.

Moreover, the particles have surface electric charge. The charges are formed under rapid nonequilibrium recombination, i.e., as condensation of non-ideal plasma of the explosion products under its fast cooling.

It was experimentally found that such particles are in the metastable state and have the internal energy equal to heat of fusion or even exceeding it. In such a state, the particles do not have metallic conductivity. As a result, the electric charges of particles exist for a longtime.

The following details should be noted:

- There is a share of the matter formed by electrolysis at pre-breakdown stage of discharge
- There is a share of metal determined in the arc discharge column
- The share of metal in arc column defined by the spectral method is 3×10^{-2} %;
- The share of metal due to electrolysis stipulated by Fe^{3+} is 10^{-4} %
- Peculiarity of the electrothermal erosion is that its products in water are in two phases: dissolved nanoparticles and precipitated (sediment) macroparticles

The total erosion was determined by weighing the electrodes before and after tests and by weighing the sediment after evaporation of the water.

As was mentioned above, the particles are formed by the electric explosion of metal wires [10, 11]. Formation of clusters (the smaller particles) is possible when pairs of the vapor metal are transferred into the plasma column. Clusters are formed inside the plasma column under fast cooling of the plasma as a result of its expansion [12]. Information on particles sizes can be received basing on experimental data of the wires explosion in gases and on ectons of the explosive emission.

It is evident that such an estimation of the PED in water is rather qualitative than quantitative one. To obtain quantitative information on particles, it is necessary to use optical or electron-optical methods for visualization of particles in water. Contemporary techniques for nanoparticles imaging and studying (for example, scanning electron microscopy, transmissive electronic microscopy, or laser correlation spectrometry) make it possible to obtain images of particles and their distribution in size without removal of the water.

Study of conglomerates structure was performed by atomic force microscopy. The nanoparticles of Ag, Pt, and Cu are of the most interest for us. Figure 6.3 shows image of area 20 × 20 μm obtained after drying of the silver nanoparticles dispersion.

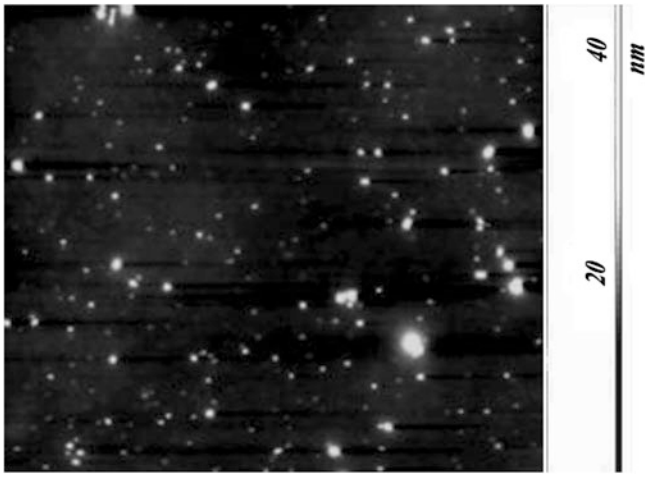

Fig. 6.3 AFM image of area 20 × 20 μm with the silver nanoparticles

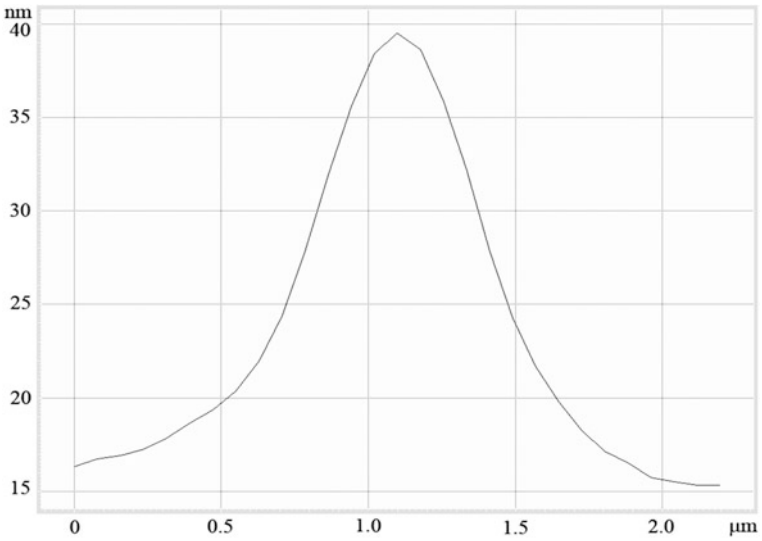

Fig. 6.4 Profile of the largest silver aggregate of X−15, Y−5

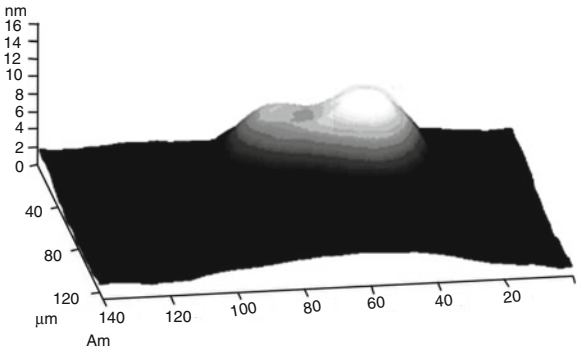

Fig. 6.5 3D surface of the silver nanoparticle of X−250, Y−250

Here, the nanoparticles of various sizes are clearly seen, and among them, the largest complex is of the size ∼1 μm (Fig. 6.4).

From detailed examination of small silver particles, it is seen that many of them are also aggregates. Figure 6.5 demonstrates the silver "tetramer" of size 50 × 20 nm and of height ∼16 nm.

Alike silver, platinum forms aggregates of various sizes; but here, the nanoparticles have stronger bonds than those of silver. We have not seen the platinum monomeric nanoparticles separately (Fig. 6.6).

Note that the height of all platinum aggregates does not exceed 10 nm. This could indicate either weak bond "monomers" in aggregate (so, under sedimentation on the substrate, it is "blurred") or aggregates are in solution in the form of flat structures (such as "flakes").

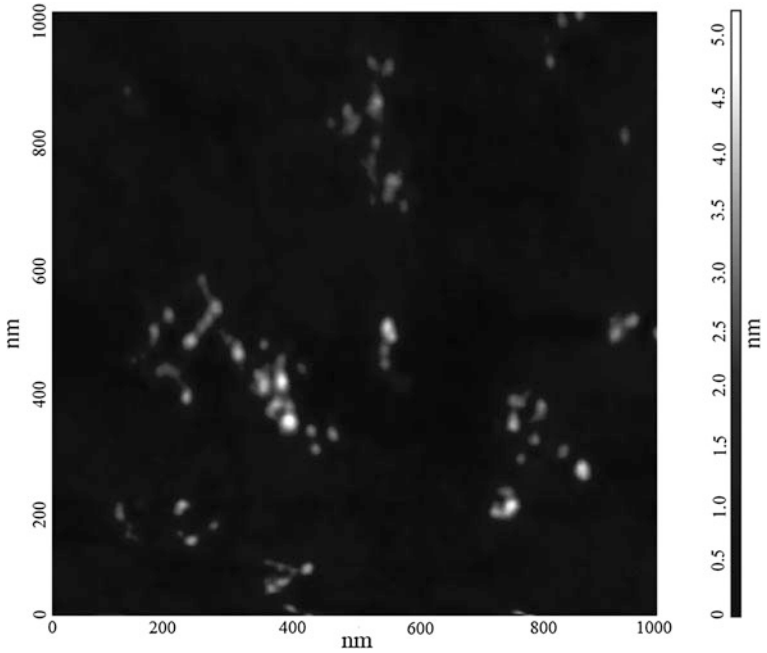

Fig. 6.6 Platinum aggregates

The largest and most stable aggregates among of investigated metals are ones of copper. Nanoparticles in these aggregates assembled as a "bunch" with the size up to 600–1,000 nm (Fig. 6.7).

Apparently, other metals Fe, Ti, and Zn have the nanoparticles sizes similar to the copper ones.

Figure 6.8 shows TEM images under various resolutions of the silver and copper nanoparticles.

In the images, one can see that "elementary" nanoparticles or monomers of copper and silver are approximately of the same size about 5–10 nm. But, at the same time, the copper nanoparticles form more complex aggregates with larger number of particles than the silver ones.

6.3 Distribution of Nanoparticles in Size

Since dimensions of the nanoparticles vary by several orders, it is necessary to know their distribution in size for various applications.

Measurements of nanoparticles distributions in size were carried out by means of the laser correlation spectrometer (LCS-03) with quasi-elastic light scattering (QLS).

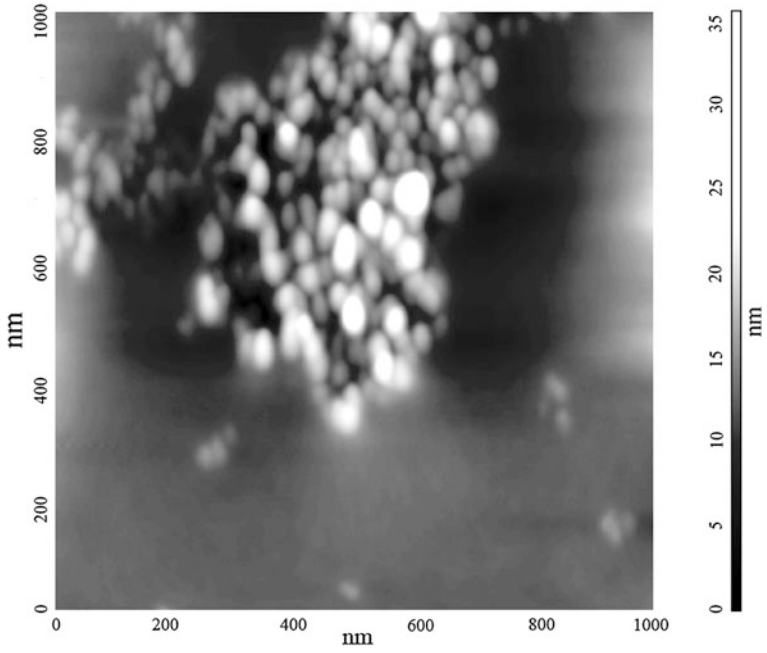

Fig. 6.7 Copper aggregate

The QLS method is based on interaction of monochromatic coherent radiation with the light scattering nanoparticles in water. Information on all dynamic processes in the water under investigation is contained in spectrum of fluctuations of the light scattering on the nanoparticles in water.

When the LCS-03 operates, the mathematical treatment is performed for calculation of spectrum of the light-scattered by the particles.

The result of this procedure is the distribution of the nanoparticles subfractions contribution to the light scattering $A(G)$ on diffusion widening (G), connected with the size of the particles hydrodynamic radius R_h by the Einstein-Stocks equation

$$G = D\,q^2 = k\,T\,q^2/6\,\pi\,\eta\,R_h \tag{6.1}$$

Further, the resulted distribution $A(G)$ is recalculated into distribution of number of particles N in sizes R_h. Hence, the intensity of light $A(G)$ (scattered by the particles) is proportional to the particles number N and the square of their form-factor $|\alpha(R_h)|^2$. So, in the case of continuous distributions

$$A(G)\,dG \sim N\,(R_h)|\alpha\,(R_h)|^2\,dR_h. \tag{6.2}$$

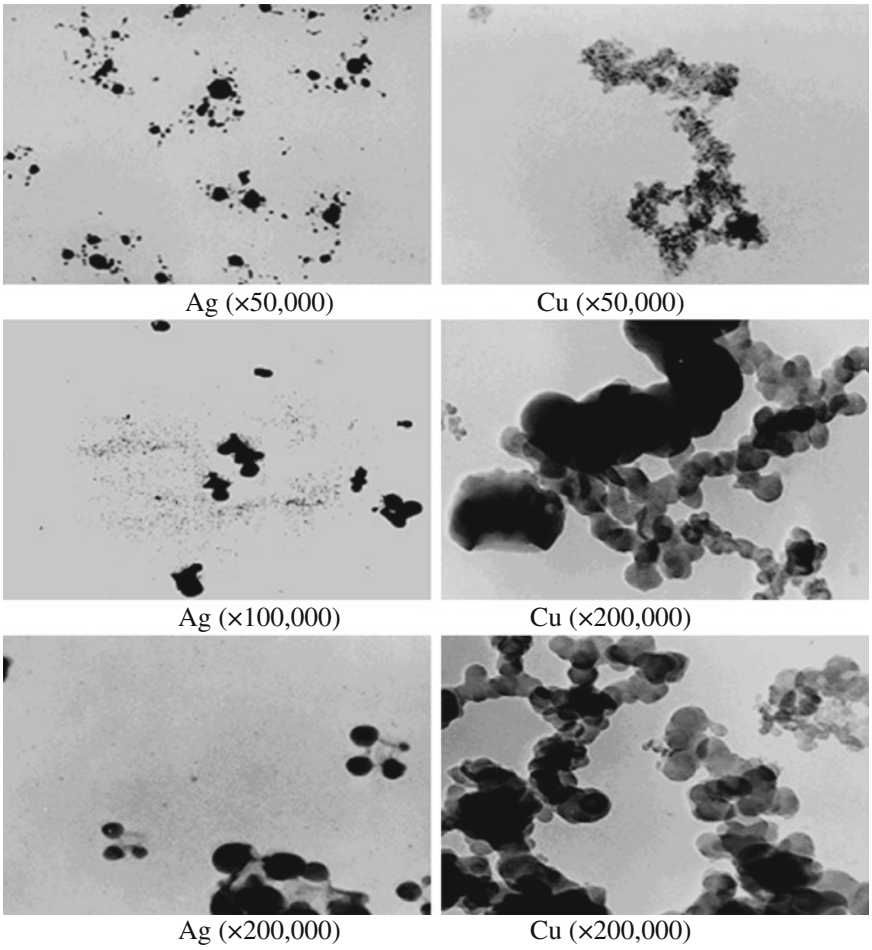

Fig. 6.8 TEM images of the silver and copper nanoparticles

Note that the particles sizes are small in comparison with q^{-1} (under the order of size, it $\lambda/2\pi$, where λ is the length of the light wave and in our case $q^{-1} = 53$ nm). We shall assume that $\alpha\,(R_h) \sim M\,(R_h)$ (i.e., the mass of the particle of radius R_h). Then $\alpha\,(R_h) \sim M\,(R_h) \sim (R_h)^n$, where $n = 3$ for solid balls, $n = 2$ for spheres both Gauss balls, and $n = 1$ for strongly extended structures (sticks). Taking into account formula (6.1)

$$N\,(R_h) = A\,(G(R_h))/(R_h)^{2n+2} \tag{6.3}$$

The mathematical treatment of the scattering spectrum makes it possible to recalculate distributions for 3 models: balls, Gauss balls, and sticks. The recalculations are performed on the basis of the exact theoretical dependence of their form-factor on dimensionless size qR (where R is the characteristic size). From the relation $A(G(R_{h1}))/A(G(R_{h2}))$ using (4.1) and (4.2), we have $N(R_{h1})/N(R_{h2})$. In particular, for a solid ball, the form-factor $\alpha(x)/\alpha(0)$

$$[(\sin x - x\cos x)\,3/x^2]^2 \tag{6.4}$$

where $x = qR$.

Spectrum of the photocurrent fluctuations from the photo detector coincides with spectrum of the scattered light and is described by the Lorenz curve (lorentzian). The lorentzian half-width is directly proportional to the diffusion factor, which, in its turn, is connected by the Einstein-Stocks formula with hydrodynamic radius R_h of nanoparticles.

For estimation of the photocurrent fluctuations of scattering nanoparticles of various sizes in polydispersity liquids, sum of the lorentzians for scattering nanoparticles with specific hydrodynamic radii is used.

Solution of the inverse problem by the regulation method makes it possible to restore the histogram of nanoparticles distribution in size from the spectrum of the photocurrent fluctuations.

There are two basic optical techniques of quasi-elastic light scattering: homodyne ("self-beatings") and heterodyne method ("beatings on the basic beam").

In the first case, the light-scattered on nanoparticles is only registered.

In the second case, the basic light interfering with light-scattered on photo detector is registered together with the light-scattered on nanoparticles.

Note that intensity of the basic beam should be in many times larger the intensity of the scattered light, and the optical waves lengths of the basic and scattered lights should not differ more than the optical coherency length of the laser.

In the homodyne method, the strong contribution is essential from deforming parasitic heterodyning in the homodyne signal stipulated by the large particles.

The same factor severely limits a range of the measured particles size in polydispersity systems such as almost all biological fluids. The heterodyne method is free of this drawback. However, it is difficult in the technical implementation and alignment.

When you have selected a mode of measuring, it is necessary to provide the most reliable recovery of the particle size. The most precise recovery of particle sizes is achieved if the lorentzian is described by at least 5 points on the half-width and the range of measurement is not less than 10 half-widths of the lorentzian.

Thus, let the particles be with hydrodynamic radius R_h from 4 to 500 nm and the half-width lorentzian of interest be of 40–2,000 Hz. So, the bandwidth of 16 kHz with resolutionof 8 Hz per channel (2,000 points of the spectrum) is the optimal one.

These conditions require the "non-smoothness" of spectrum to be less than 0.03. Since fluctuations of experimental points in the spectrum are usually accidental, it can be assumed that the "non-smoothness" value is inversely proportional to square root of the total number of the spectrum copies.

Thus, number of the accumulated copies must be at least 1,000. To eliminate influence of the unknown factors, this value is 2,000. Therefore, the number of measurements was at least five in each sample (i.e., at each point).

Under these conditions of measuring, the time taken for analysis of one sample was about 10 min. The data for all measurements were averaged.

Figure 6.9 show the distribution plots for shares of the light scattering of the silver nanoparticles fractions in size for various current pulse durations: 0.1, 1.3, 6.6, 11, 22, and 27 μs.

These figures show that distributions are polydispersity and, in dependence on a metal, they have from 3 to 5 characteristic peaks: near 10, 30–100, 100–200, 200–1000, and 1000 nm.

Figure 6.10 demonstrates plots of the size distribution of the light scattering shares for Ag, Cu, Pt, Fe, Ti, and Zn nanoparticles under the current pulse duration of 20 μs and inputted energy of 10 J/ml.

Comparison of our data with those in paper [13] gives good agreement in sizes on silver, and platinum. As noted in [14], we have also observed nanoparticles of 8–10 nm, corresponding to particles of the "hydrogen colloids", which have maximal catalytic activity.

The larger fractions of nanoparticles are formed by aggregation of "monomeric" particles of the size $\sim$10 nm. Relatively low light scattering contribution of such "monomeric" particles is increased by 10^6 times because of intensity of the light scattering on each particle under increasing of R_h by 10 times.

Therefore, one particle of 100 nm size scatters the light as 10^6 particles of 10 nm. Thus, the plots above have only illustrative character. It is so since the ratio of the mass fractions to shares of the light scattering is $\sim 1/10^3$ under increasing the size of nanoparticles by 10 times.

The general plot of the size distribution of silver nanoparticles mass fractions versus pulse duration is presented in Fig. 6.11.

Figure 6.12 shows dependence of the total mass fraction of nanoparticles with size $\leq$10 nm (black line) and $\geq$10 nm (red line) on the pulse duration. The plot shows that the maximum share of "small" nanoparticles up to 10 nm is under the pulse duration of $\sim$6 μs.

At same time, dependence of specific erosion of metals of electrodes on duration of the current pulse had been obtained (Fig. 6.13).

The plot also shows that at the current pulse duration less than 5 μs, the specific erosion is largest. Thus, based on plots in Figs. 6.12 and 6.13 it can be concluded that the optimum pulse duration is 5–10 μs.

It was found that the water treated by the PED is a disperse system consisting of ions and nanoparticles of the electrodes metal. The mass ratio of ions to

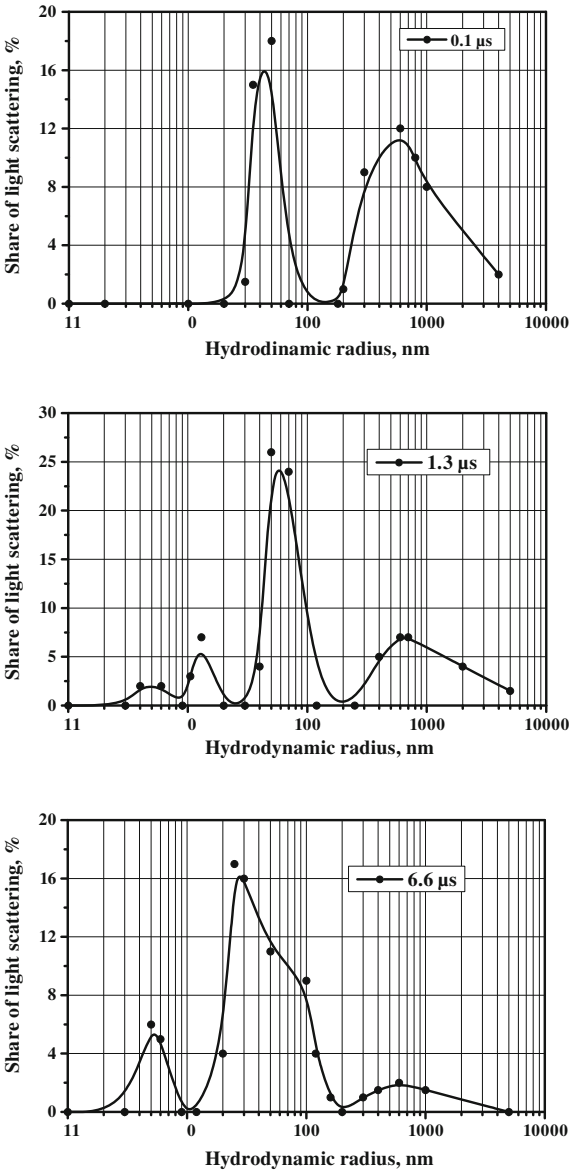

Fig. 6.9 Distributions of the light scattering shares of the silver nanoparticles fractions

Fig. 6.9 (continued)

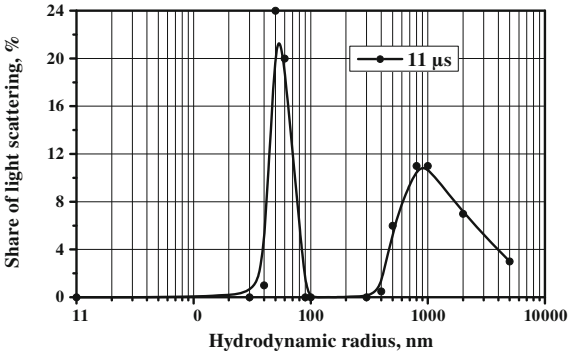

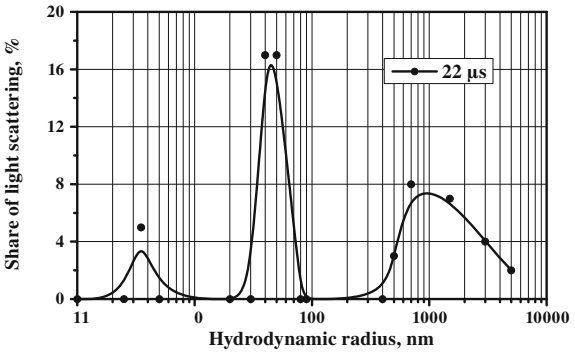

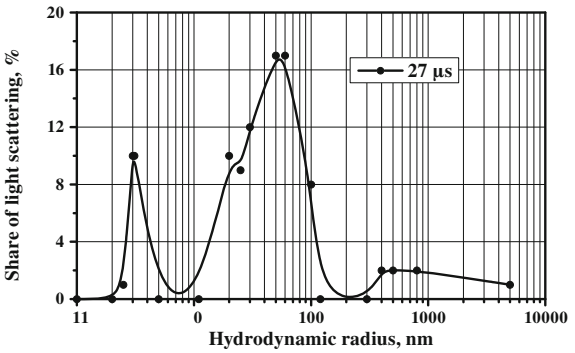

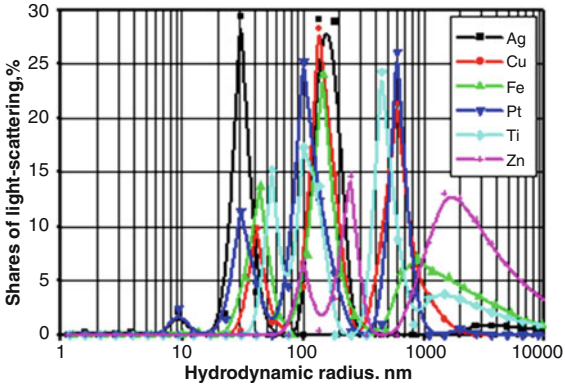

Fig. 6.10 Distribution of the light scattering shares of Ag, Cu, Fe, Pt, Ti, and Zn nanoparticles

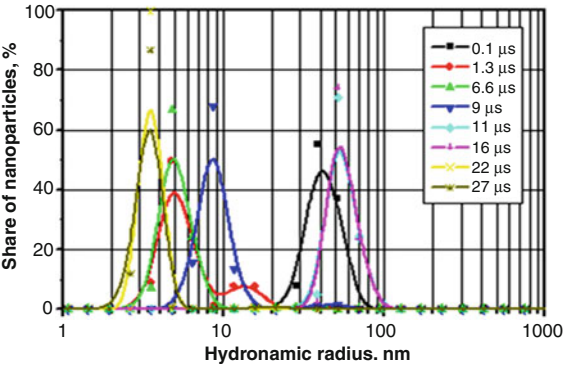

Fig. 6.11 Distributions of the mass fractions shares of the silver nanoparticles fractions in size

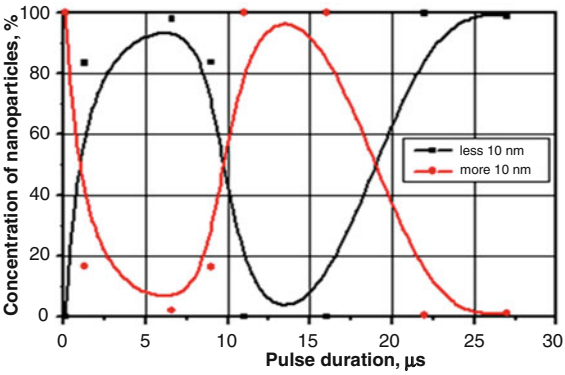

Fig. 6.12 Distribution of the mass fraction of the nanoparticles versus pulse duration

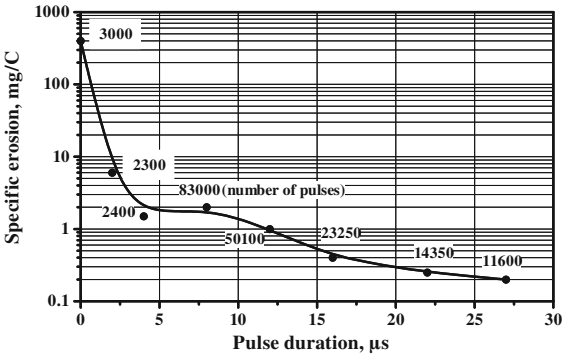

Fig. 6.13 Specific erosion of the electrodes versus pulse duration [15]

nanoparticles is 1:5 in the pre-deionized water under inputted energy of 5 J/ml, pH = 5.8–6.3 and, as mentioned above, for the copper electrodes.

Tests have shown that the "large" particles of ≥1 μm diameter settle out within several days after the water treatment.

Distributions of nanoparticles are polydispersity and, in dependence on a metal, have from 3 to 5 characteristic peaks: near 10, 30–100, 100–200, 200–1000, and 1000 nm.

6.4 Properties of Nanoparticles and the WDN

To study electrical and chemical properties of nanoparticles in the water dispersions, various techniques and equipment were used. Those are: experimental laboratory device (using the Doppler effect), scanning electron microscopy, spectrophotometry, infrared Fourier spectroscopy, powder X-ray diffractometry, and others.

Surface electric charge of nanoparticles. Electric charge on surface of nanoparticles (generated under water treatment by the PED) can be explained based on wires electric explosion in inert gases. As a result of explosions, the ultradispersed powders (UDP) having high inner energy are formed [4, 10]. The UDP energy is stipulated by increasing the melting heat that is confirmed by the following experimental facts [10]:

- Heat emission under agglomeration of the UDP
- Heat emission under burning the UDP in oxygen
- Heat emission under dissolution of the UDP in water
- Stability of the UDP against oxidation under normal temperatures and sharp increase of reactivity at exceeding the threshold temperature
- Reduction of the oxide layer thickness on the UDP particles under decreasing the particles diameter
- Separation of particles in the electrostatic filter before their contact with air

Estimated value of the UDP specific energy is ~ 10 MJ/mole.

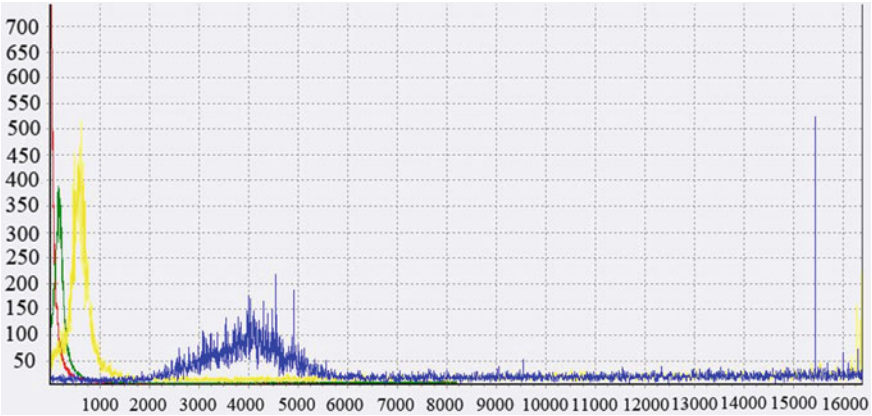

Fig. 6.14 Displacement of average lorentzians under various voltages

An experimental laboratory device (operating based on the Doppler effect) performed measuring the surface electric charge of nanoparticles. The cuvette with water dispersion of the silver nanoparticles has an optical path length of 20 mm; the interelectrode distance between the iron electrodes was 18 mm. For passage of the reference light, there were openings with a diameter of 2 mm in the electrodes.

Measurement scheme is heterodyne, and the angle between reference beam and one scattered by the particles was 90°. DC voltage applied to the electrodes was 10–250 V with current 1–60 mA. The lorentzian displacement under effect of the electric field was registered, and average value of the lorentzian displacement (proportional to velocity of nanoparticles) is increased as voltage rises (Fig. 6.14), where red line is 0 V, green is 20 V, yellow is 50 V, blue is 250 V.

Figure 6.14 shows that the voltage rise on electrodes increases not only velocity of nanoparticles, but also, the lorentzian half-width. This is so-called the diffuse peak broadening that results in increasing the measurement error. Therefore, when determining the nanoparticles surface charge, the applied voltage was limited to 20 V.

In analysis of the scattering spectrum under absence of the electric field (red line), the regularization gives two kinds of nanoparticles: of ~530 nm with contribution about 75 % and of ~180 nm with contribution about 25 %. The green line (applied field) has two split-off lines corresponding to the same nanoparticles and with the same contributions (Fig. 6.15).

Points of the split-off lines can be roughly estimated as 160 and 380 Hz. The effective uncompensated charge of the "small" nanoparticles is 1.2×10^{-16} C (800 e) and the charge of the "large" nanoparticles is 1.9×10^{-16} C (1190 e).

If we assume that the charge is only on the surface, then its surface density for the "small" nanoparticles is 3.2×10^{-4} C/m^2 or 0.002 e/nm^2 and 1.55×10^{-3} C/m^2 or 0.01 e/nm^2 for the "large" nanoparticles.

Electric charge of the "small" nanoparticles is 1.2×10^{-16} and 1.9×10^{-16} C of the large ones. Surface electric charge density of the "small" nanoparticles is 3.2×10^{-4} and 1.55×10^{-3} C/m^2 of the "large" ones.

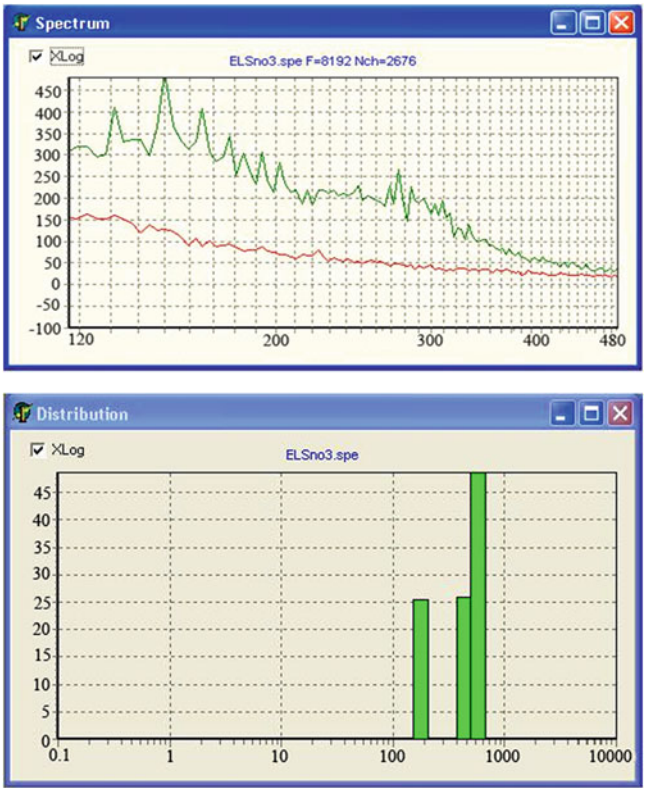

Fig. 6.15 Result of processing of scattering spectrum of the silver nanoparticles

6.5 Nanoparticles and Electric Conductivity of the WDN

It is natural to assume that the electric conductivity of water dispersions of nanoparticles should be different before and after the PED treatment. The treated water conductivity is significantly larger since of ions of the electrode metal and the charged nanoparticles that are complementary carriers of charge in the dispersion.

Estimations and experimental data. Experiments have confirmed that conductivity increases after the water treatment by the PED. Assume that nanoparticles have the electric charge $q = N_e\, e$ where: e is the charge of electron, N_e is the number of electrons.

Using the formula for mobility μ

$$\mu = N_e \frac{eD}{kT} \tag{6.5}$$

where e is charge of electron, D is diffusion coefficient, k is Boltzmann constant, T is temperature of water. We can determine conductivity associated with motion of the charged nanoparticles

$$\sigma = qn\mu \tag{6.6}$$

where n is concentration of charged nanoparticles. Diffusion coefficient for nanoparticles [16]

$$D = \frac{kT}{6\pi r\eta} \tag{6.7}$$

where r is radius of nanoparticles, η is viscosity of water.

Finally, the formula for determination of the electric conductivity produced by nanoparticles

$$\sigma = \frac{N_e^2 e^2 m_c}{8\pi^2 r^4 \rho\eta} \tag{6.8}$$

where m_c is mass concentration of metal in water, ρ is density of metal.

Formula (6.8) contains two values: the nanoparticle charge and its radius. These values had been obtained experimentally and are presented above. Size of nanoparticles suspended in the water was determined by electronic scanning and atomic-force microscopes.

However, it is necessary to make preliminary estimations of these values based on considerations of the electrode erosion at under the PED in water. We start from images of electrode surface after the multiple PED. In their quality, these images are very similar to ones (by microcraters and melts on surface of electrodes) produced by the explosive emission.

Mechanism of the explosive electron emission is described satisfactorily by the ecton model [4]. An ecton is a minimal area on the electrode surface, which appears due to concentrated heat output in the form of explosion with duration of $\sim 10^{-10}$–10^{-3} s. In solid and liquid states, the ectons localization takes place since concentration of the emission currents and occurs at the electrodes tips of various types on the electrode surface. By analogy with the explosion of metal wires, the ecton existence is estimated by integral of action h

$$h = \int_0^{t_{ec}} j^2 dt \tag{6.9}$$

where t_{ec} is lifetime of ecton, j is current density.

On the other hand, this time may be evaluated (when j is constant) by the ecton radius r_{ec}. Namely, it is a distance at which the thermal energy is distributed from the center of the ecton by means of thermal conductivity

$$r_{ec} = 2(at_{ec})^{1/2} \tag{6.10}$$

where a is coefficient of thermal conductivity.

In application to the PED in water, the model of a vacuum arc can be used as a first approximation [4]. In the case of arc discharge, each ecton is formed by drawing from the column of molten metal of size 10^2–10^3 nm and has the life-time about $t_0 = 10^{-9}$ s. So, the time between appearances of two ectons is about $\sim 2 \times 10^{-8}$ s. If we assume that during of the pulse τ = 10 μs N_{ec} ectons are generated, then their number is estimated as $N_{ec} = 10^{-5/2} \times 10^{-8} \approx 500$ ectons.

Weight of one ecton can be found by taking into account that erosion per one pulse is $\sim 10^{-8}$ g [8]. So, the weight of one ecton is 2×10^{-11} g. For copper, for example, this weight corresponds to the ecton radius $r_{ec} \approx 0.5$ μm. Since of the arc mode with duration $\sim$10–20 μs, there is a high probability of occurrence of the liquid phase in the arc spot. As a result, the small droplets can give some contribution to erosion. These are particles of sizes more than 10^{-6} m. Now let us use: the data of nanoparticles distribution in size, the data of measured water specific resistivity for copper electrodes (under inputted energy W of 8 J/cm^3), and using formula for electric conductivity. Further, giving the nanoparticles radius r, it is possible to determine their electric charges q:

$$r = 10^{-6}\,\text{m} \quad q = 10^8\,\text{e}$$
$$r = 10^{-8}\,\text{m} \quad q = 10^4\,\text{e}$$

where e is charge of electron (1.6×10^{-19} C), q is charge of nanoparticles.

To refine these estimations, we must have more detailed information about nanoparticles of 10–100 nm. It should be noted that at significant charges on nanoparticles, their "solution" in water is nonideal plasma, where parameter $\gamma = E_p/E_k \gg 1$, where $E_p = \frac{N_e^2 e^2}{4\pi r \varepsilon_0 \varepsilon}$ is potential energy of the nanoparticles interaction, $r = (n)^{-1/3}$; $E_k \approx kT$ is kinetic energy.

The nanoparticles are formed as a result of erosion. Their total mass is determined by weighing the electrodes before and after tests. In addition, this value is determined by weighing the sediment after evaporation of the treated water. Evaporation is carried out in a special box under very clean conditions. The results of measurements obtained by these methods are practically the same with accuracy of 5–10 %.

Figure 6.16 shows the experimental plot of conductivity of water dispersion of the silver nanoparticles depending on their concentration.

It was estimated that for copper electrodes under the inputted energy 8 J/cm^3, the nanoparticles electric charges are 10^8 e for their radius of 10^{-6} m, and 10^4 e for the radius 10^{-8} m. Conductivity of water dispersion of the silver nanoparticles is from 2 to 25 S/cm for their concentrations up to 180 mg/l.

6.6 Chemical Properties of Nanoparticles

Chemical state and structure of nanoparticles were determined by a complex of mutually supplementing and correcting methods [17].

In particular, we used the scanning electron microscopy, spectrophotometry, IR-Fourier spectroscopy, and powder X-ray diffractometry [18].

The morphology of nanoparticles and elemental analysis was carried out by the FEI Quanta 200 scanning electron microscope. Spectroscopic measurements were performed by the UV1700 Shimadzu spectrophotometer and FSM-1202 Fourier spectrometer.

The X-ray diffraction patterns were recorded on the XRD-7000 Shimadzu powder diffractometer and were processed using the PDW in software package with the PDF 2 powder diffractogram data base.

The SEM, IR-Fourier spectrometry, and X-ray diffractometry were performed on the nanopowders prepared by evaporation of the water from water dispersions under the temperature of 45 °C.

In the experiments, water dispersions of the silver, copper, and iron nanoparticles were used. Mass concentrations of the nanoparticles in water dispersions are given in Table 6.3.

The SEM images of sample 1 and results of its elemental analysis indicate that the agglomerates of nanoparticles are different in shape and consist mainly of the metallic silver.

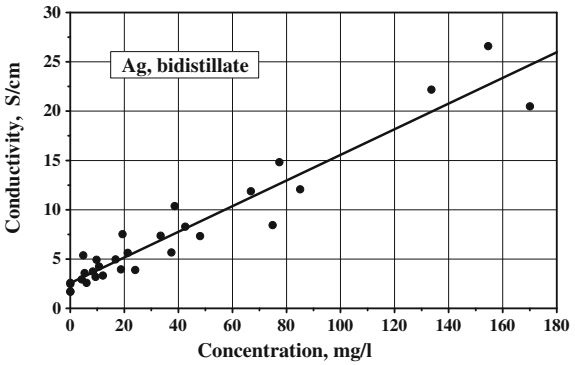

Fig. 6.16 Conductivity of water dispersion of the silver nanoparticles versus concentration

Table 6.3 Mass concentrations of the nanoparticles in water dispersions

Sample number	Metal	Concentration (mg/l)
1	Ag	35.3
2	Cu	36.7
3	Cu	50–60
4	Fe	13.1
5	Fe	50–60

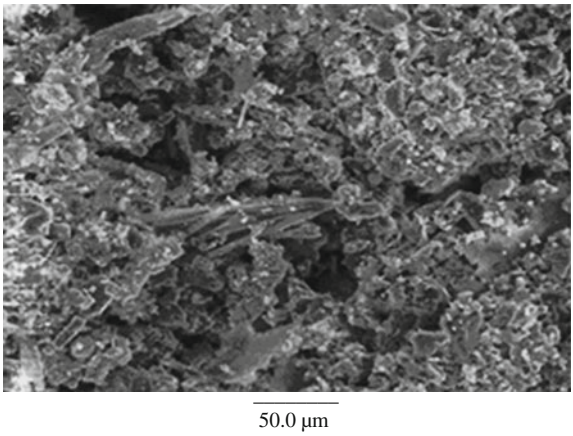

Fig. 6.17 SEM image of the iron nanoparticles (sample 4) [18]

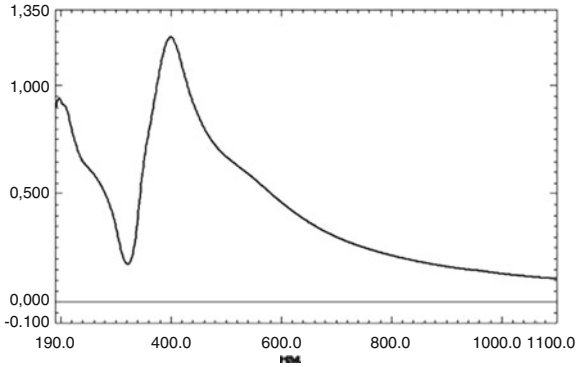

Fig. 6.18 Absorption spectrum of water dispersion of the silver nanoparticles (sample 1) in UV and visible ranges [18]

The similar analysis of the copper and iron samples 2–5 shows that these nanoparticles also contain oxygen. The SEM image of sample 4 indicates that nanoparticles of the iron oxides (as well as ones of the silver and copper) form agglomerates of various shapes (Fig. 6.17).

To determine the composition and structure of nanoparticles in water dispersions, we used spectroscopy in the UV, visible, and IR ranges, as well as the X-ray phase elemental analysis. The absorption spectrum (Fig. 6.18) of water dispersion of the silver nanoparticles in the UV and visible ranges has a characteristic peak at 380–440 nm. It coincides with the absorption peak of the silver nanoparticles obtained in works [19, 20], and with two shoulders at 230–250 and 520–560 nm. The similar spectrum is observed for nanoparticles obtained by the laser evaporation-condensation method [21].

Comparison of two absorption spectra was implemented. The first one was of the silver WDN. The second one was the UV absorption spectra calculated for Ag12-3O cluster model including the cation vacancy on Ag(111) surface using layered

silver oxide as a prototype [22]. The comparison shows that the shoulder at 230–250 nm and the broad peak at 380–440 nm can be attributed to the metallic silver.

However, the shoulder at 520–560 nm can be associated with peaks at 515 and 565 nm in spectrum calculated for clusters simulating the oxidized silver surface.

While the shoulder at 520–560 nm can be associated with peaks at 515 and 565 nm in spectrum calculated for clusters simulating the oxidized silver surface [22].

The shoulder (but not a peak) in this spectral region indicates low concentration of the silver oxide on the nanoparticles surface.

It was recorded IR spectra of water dispersions of copper and iron and their oxides (according to results of elemental analysis) nanoparticles.

Figure 6.19 shows the IR spectrum of copper nanoparticles prepared by evaporation of water (sample 3). We compared the IR spectrum of sample 3 with results obtained in [23, 24] and with the Zair data base. The comparison indicates that the broad band of frequencies 500–600 cm^{-1} is also present for the sample under investigation.

In the frequency range 1,400–1,700 cm^{-1}, a number of peaks are observed. They may correspond to shoulders at 1,400 and 1,650 cm^{-1} in CuO spectrum by the Zair data base, as well as, to deformational oscillations in a water molecule. These oscillations may be present in the sample after its incomplete evaporation.

The narrow and high peak in the IR spectrum of Cu_2O at 600 cm^{-1} and the shoulder at 1,100 cm^{-1} almost coincide with corresponding peak and shoulder in the CuO spectrum.

Diffraction patterns of the copper nanoparticles (Fig. 6.20) indicate the copper oxide I, copper oxide II, and metallic copper nanoparticles, where vertical lines is reference peak values Cu_2O (•), CuO (■) and Cu (×). Numbers in data base PDF 2: 00-003-0892, 00-002-1040, 00-004-0836, respectively.

Sizes of regions of the coherent scattering of nanoparticles of the copper oxide I, copper oxide II, and metallic copper were determined by using the Scherer formula from the data on the line widths of the X-ray diffraction patterns.

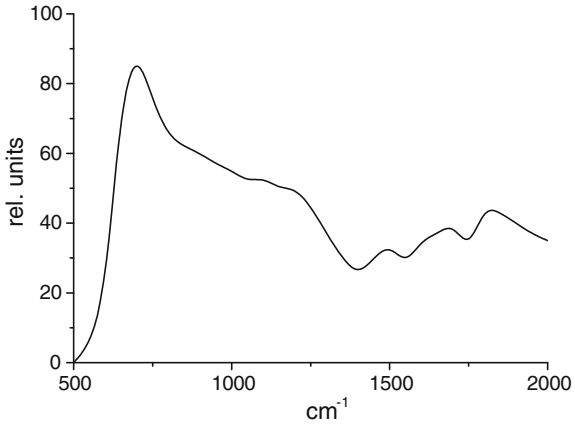

Fig. 6.19 IR transmission spectrum of the copper nanoparticles (sample 3) [18]

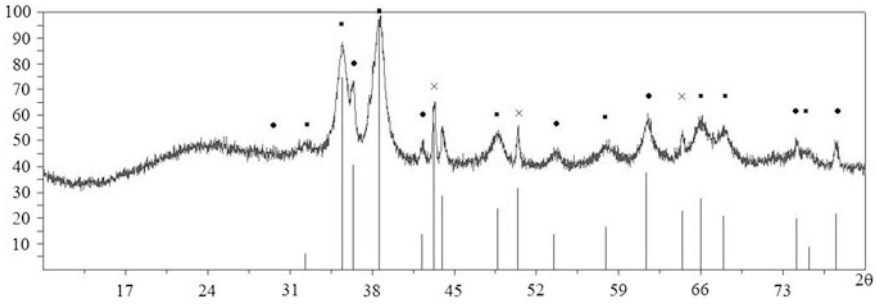

Fig. 6.20 Diffraction patterns of the copper nanoparticles (sample 3) [18]

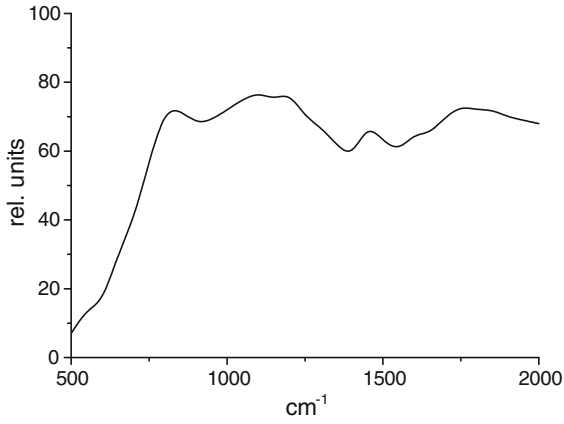

Fig. 6.21 IR transmission spectrum of the iron nanoparticles (sample 5) [18]

Figure 6.21 shows the IR spectrum of the iron nanoparticles (sample 5). We compared these results with the spectrum of the Zair data base. The comparison shows that the characteristic absorption bands in the IR spectrum of Fe_2O_3 at 500–600 and 1,000–1,100 cm^{-1} are clearly manifested in the sample under investigation.

Presence of the Fe_2O_3 nanoparticles in water dispersions is confirmed by comparison of the absorption bands in the nanoparticles IR spectra with the results presented in [25].

Absorption in the ranges of 1,400–1,700 and 3,400–3,500 cm^{-1} can be associated with the deformational and valence oscillations of O–H bond in a water molecule, which can be in the sample after its incomplete evaporation.

The X-ray diffraction patterns of the iron nanoparticles (Fig. 6.22) indicate small peaks corresponding to the magnetite (Fe_2O_4) and hematite (Fe_2O_3), and absence of the metallic iron, where vertical lines are reference values of peaks Fe_3O_4 (×), Fe_2O_3 (■). Numbers in data base PDF 2: 00-011-0614 and 00-002-0919, respectively.

For observed iron oxides, sizes of regions of the coherent scattering of the magnetite and hematite were determined by the Scherer formula.

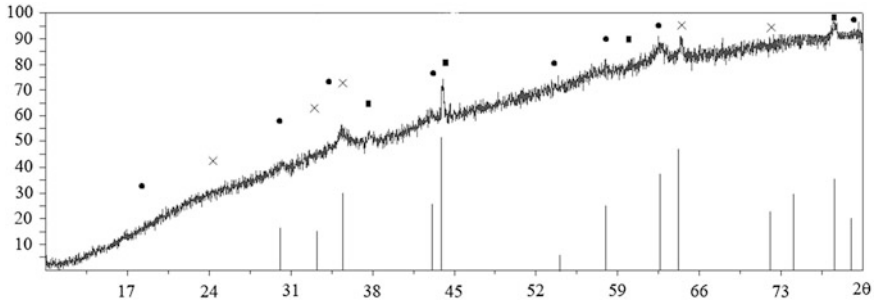

Fig. 6.22 Diffraction patterns of the iron nanoparticles (sample 5) [18]

Thus, by the UV, visible, IR spectroscopy, and X-ray diffractometry, it was established that the oxidation degree of the metallic nanoparticles (formed by the PED in water under identical conditions) increases in the following sequence: Ag, Cu, and Fe. Oxidation of the metal nanoparticles in the electric arc discharge channel can be explained by interaction of the vapors and metal particles containing O, OH, O_2, and H_2O [26].

The oxidation degree of metallic nanoparticles outside the discharge channel is determined by the electrochemical activity of metals, which is highest for the iron.

6.7 Physical Properties of the WDN

For a certain time after their preparation, water dispersions of nanoparticles have unstable physical and chemical properties. These include the electric conductivity that is determined by the ratio of the ions concentration to their sources, i.e., the nanoparticles. Note, also, the dependence of electric conductivity on temperature, which has a special feature of the temperature hysteresis.

Investigations were performed by means of the Anion 4100 device used for the pH and electric conductivity measuring.

By double repetitive dilution of the silver nanoparticles water dispersions for changing their conductivity, the time constants of concentration equilibration had been determined between nanoparticles and ions under nanoparticles dissolving in water (Fig. 6.23).

Figure 6.23 shows that the time constant of concentration equilibration is from 3 to 7 min at change of concentration of nanoparticles from 75 to 4.75 mg/l, and the time constant is increased at decrease of nanoparticles concentration in dispersion.

Figure 6.24 shows dependence of the electric conductivity of the silver nanoparticles water dispersion on the nanoparticles concentration.

When concentration of nanoparticles is changed from 6 to 160 mg/l, the average value of conductivity varies from 2.5 to 25 μS/cm.

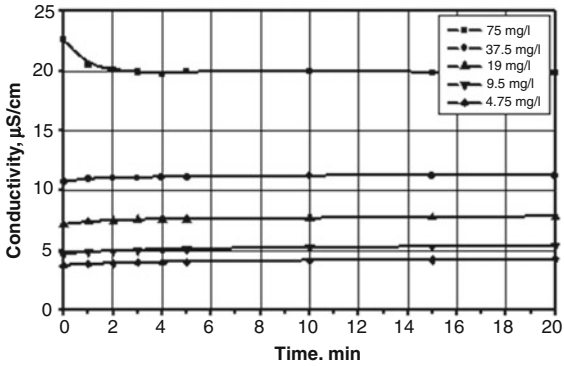

Fig. 6.23 Dynamics of concentration equilibration between nanoparticles and ions

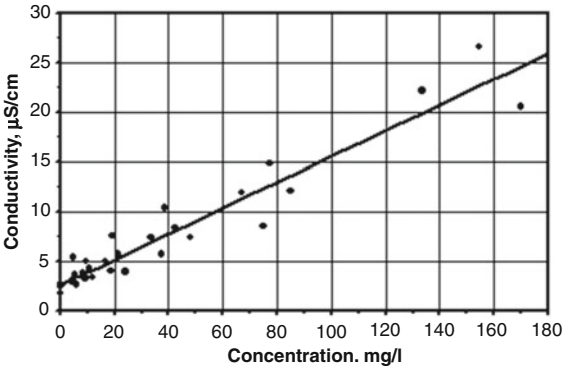

Fig. 6.24 Electric conductivity of the silver WDN versus nanoparticles concentration

Dependence of conductivity of water dispersion of the silver nanoparticles on temperature is presented in Fig. 6.25. The dependence has been built during heating and cooling the water dispersion at concentration of the silver nanoparticles 33 mg/l.

When the dispersion is heated from 30 to 90 °C, the conductivity is doubled and is 25 µS/cm.

The values of electric conductivity under cooling for about 10 % higher than corresponding values of electric conductivity at heating. So, there is some kind of the thermo-conduction hysteresis.

In our opinion, the nature of these relationships could be explained by the following facts. By increase of the ions mobility (that increases conductivity), and additional dissolution of nanoparticles, i.e., by an additional yield of ions under heating. By some excess of conductivity during cooling due to the inertia of the electron—ion recombination.

Dependence of the water dispersion excess for the Ag nanoparticles on their concentration has been determined (Fig. 6.26).

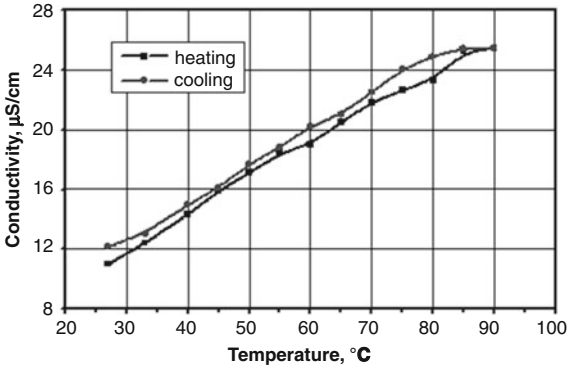

Fig. 6.25 Conductivity of the silver nanoparticles water dispersion versus temperature

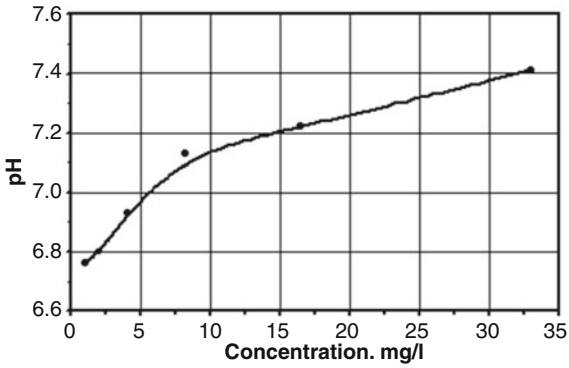

Fig. 6.26 PH of the silver WDN versus concentration of the nanoparticles

It was found that under decrease of the nanoparticles concentration by distillate diluting the initial dispersion, the pH is reduced, i.e., the initial alkaline reaction pH 7.4 is changed to the acid pH 6.76.

6.8 Study of the WDN by Physical and Chemical Methods

Study of the structure and other physical parameters of water dispersions of nanoparticles was performed by the method of electron paramagnetic resonance (EPR) and chemiluminescence.

Investigation of the WDN by the EPR method. Four samples of the WDN and one control sample (untreated by the PED) were investigated. The following parameters were measured: pH, contents of Ca^{2+}, and conductivity.

By the EPR method (EPR-probes, 5-doxyl stearic acid as a probe), the following structural properties of water were measured:

Table 6.4 Physic-chemical characteristics of the WDN

No.	Inputted energy (J/ml)	pH (24 ° C)	Ca^{2+} mg/l	R μS	S	$\tau \times 10^{-10}$ s	I_0 mm	I_0 day after
	Control	5.6	0.1	2.6	0.0476 ± 0.003	1.06 ± 0.106	100	98
1	1.0	5.88	1.0	4.05	0.0453 ± 0.0031	0.93 ± 0.09	100	105
2	5.0	5.77	0.9	4.5	0.0450 ± 0.003	0.93 ± 0.09	67	52
3	10.0	5.92	1.2	5.1	0.0405 ± 0.0028	0.53 ± 0.05	10.0	5.5
4	4.5	–	3.0	8.2	–	–	76	–

- S is factor of regulating the motion of the spin probe
- τ is rotational correlation time
- I_0 is central component of spectrum (triplet of the probe, which characterizes the signal volume)

The S-value of the regulating factor of the spin probe motion is related with the angle of oscillation of the probe molecule w.r.t. the Z-axis (the axis of nitroxyl fragment of the probe molecule).

The more freedom of axis of the spin probe oscillations, the less system is ordered, into which the probe is injected, i.e., the less is the factor of order.

The τ is the rotational correlation time characterizing the microviscosity of the medium, in which the probe is rotated. The value of τ is calculated by formula for the rapidly rotating radical.

Physic-chemical characteristics of the WDN in Table 6.4. The table shows that the pH, content of Ca^{2+}, and conductivity for all samples are approximately the same. A minor exception is sample 4 apparently due to the glass bottle: other samples were bottled in polyethylene ones.

Experiments with the EPR-probes showed that under the PED, the structure of the water is changed depending on the inputted energy. Under increasing the inputted energy, values of S and τ are reduced. The structure of the WDN is disordered and the microviscosity is reduced (for sample 3 in two times).

In column of Table 6.4 the values of I_0 are intensity of the central component of the 5-dioxilstearic acid spectrum, which characterizes the signal value of probe. The signal is decreased from sample 1 to 3, i.e., the inputted energy higher, the probe signal is lower. Apparently, an unknown active structure is created, which restores a probe. The sample 3 contains this active structure in the most degree. In the samples taken on the second day (column 8), the signal probe continued to decrease, while in the control one, the signal did not change.

Structure of the WDN based on data obtained by means of the EPR-probe is changed in comparison with the control one: it is disordered and its microviscosity is reduced (the values of S and τ are reduced).

The intensity of the EPR-probe signal is decreased in the WDN. The stronger intensity, the higher is the inputted energy that indicates to unidentified structure

forming that, in the turn, restores the probe. In the check sample, this effect was not observed for 2 days.

Investigation of the WDN by chemiluminescence. During the performed chemiluminescent analysis of the WDN, it was found that all samples:

- Differ in terms of treatment and are also significantly different in parameters of chemiluminescence
- Samples' properties change on time significantly; the most intensive chemiluminescence was observed in sample 5, but in samples 1 and 6, the chemiluminescence is practically absent

Previously, it was found that the tap water has its own chemiluminescence, which significantly (sometimes by tens or hundreds times) increases after injection of the luminol.

It is known that the chemiluminescence is a result of free radicals reactions, which are characterized by extremely high power outputs.

Products of the radicals' recombination reactions are formed in the electronic-excited state. So, under specific conditions, the electronic excitation energy can leave the reaction system in the form of visible or even UV-light. To register chemiluminescence, highly sensitive counters of single photons or luminometers are used.

If the reaction system is in contact with air, then the oxygen can be involved in the reaction processes. In this system, there are the following active oxygen forms: singlet oxygen, superoxide radical, peroxyl radicals, hydrogen peroxide, and hydroperoxides.

Presence of the active oxygen forms can be detected by introducing the special reagents (fluorescent probes) into the probe; for example, such as luminol, which increases the radiation intensity by tens times.

Thus, weak but appreciable radiation of the tap water increases sharply under injection of the luminol (distilled water has not such properties). This indicates to reactions with the active oxygen forms. The last fact indicates to free radicals presence in the system, which are capable to activate the oxygen.

Presence of the long-lived free radicals in the initial tap water is a result of its chlorination of the natural water containing organic impurities. It has recently been found that the macroradicals are formed (with sufficiently high probability) since of the chlorine interaction with complex polymeric organic molecules.

Unlike most of previously studied free radical particles, such ones are long-lived ones.

It was also found that under settling the water tap in air, there is a gradual decrease of the luminol-dependent chemiluminescence intensity (LCI). Usually, the LCI intensity reduces to the background levels after 3 days of settling. This shows almost a complete cessation of the radical reactions in the water.

It is interesting to note the following fact. It is known that use of a fresh tap water for aquariums or watering plants adversely effects on living organisms; and the water toxicity is lost only after about 3-days settling. Thus, any methods to

expedite removal of the radical particles from the water improve its quality for consumer.

As was recently identified, one of these methods is the gas purging of the water by: air, nitrogen, and argon. After passing through the water of gas bubbles, the chemiluminescence intensity, especially in presence of the luminol is increased sharply.

The following fact was unexpected. Namely, the maximal increase of intensity is not under passage (through the luminous tap water) of the oxygen-containing air, but under passage of the argon. Sparging the water by pure nitrogen also increases the chemiluminescence intensity to be intermediate between the air and argon.

The mechanism of this phenomenon is still not clear and its research is continued. Accumulation of data on the effect of various gases on water (in particular, the inert ones) is of interest not only for identification of this phenomenon mechanism, but, also, for the comparative analysis of water properties.

Thus, the water samples were studied in the following modes:

- Measuring the water own chemiluminescence
- Measuring the water chemiluminescence in the presence of the luminol
- Measuring the luminol-dependent chemiluminescence of water after nitrogen purge
- Measuring the luminol-dependent chemiluminescence of water after purging by argon

The water chemiluminescence in a liquid was measured by the radioactivity scintillation counters. These counters have photomultipliers with a maximum of spectral sensitivity at 450–500 nm registering photons with wavelengths from 340 to 600 nm.

Water was filled into standard vials of 20 ml and 25 mm in diameter. For registration of the luminol-dependent chemiluminescence, the luminol was added in into the water with concentration of 25 μM.

To registrate how gases effect on the chemiluminescence of water, the luminol is added, and its initial chemiluminescence intensity is measured. Further, the water is bubbled for 3 min by the gas and, after that, the chemiluminescence intensity is measured again.

Measurements of the WDN samples (from the same batch) were carried out. Figure 6.27 shows the results of representative experiment on measuring of own and luminol-dependent chemiluminescence of 20 ml sample 5.

It is seen that the own chemiluminescence is stable with 50 pulse/s. Whereas after adding the luminol into the water, the chemiluminescence intensity increases to more than 470 pulse/sec within 10 min.

Figures 6.28, 6.29, 6.30 and 6.31 present histograms of chemiluminescence intensities with their average values after reaching the steady-state radiation mode. Figure 6.28 shows that the lowest own radiation have samples 1 and 6, wherein the addition of luminol to both samples does not effect on the radiation intensity. The maximal radiation intensity has sample 5, and in presence of luminol, it is by several times higher than the luminol-dependent intensity of sample 3.

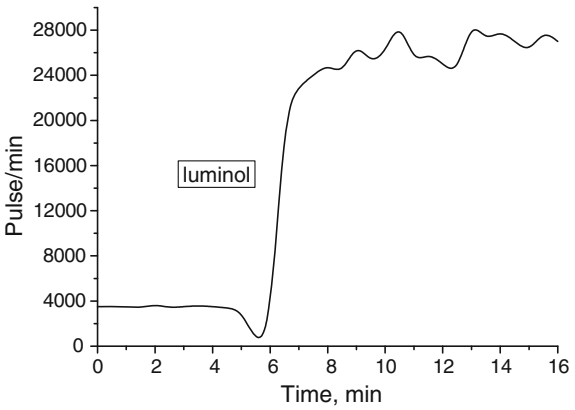

Fig. 6.27 Kinetics of own and luminol-dependent chemiluminescence of the sample 5

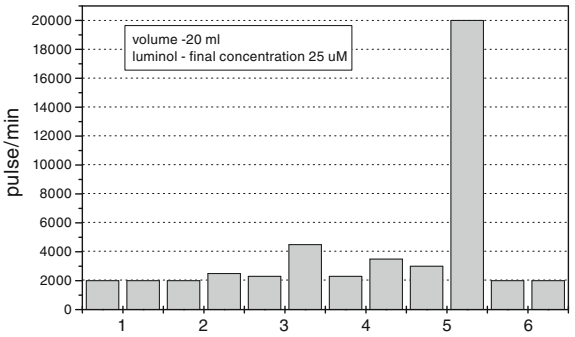

Fig. 6.28 Own and luminol-dependent chemiluminescence of the WDN samples

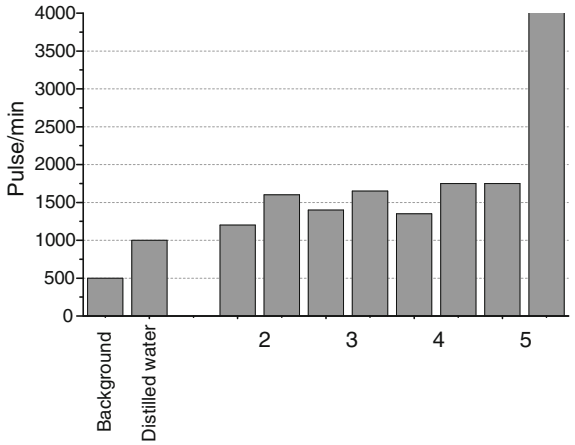

Fig. 6.29 Own and luminol-dependent chemiluminescence of the WDN samples after 6 days

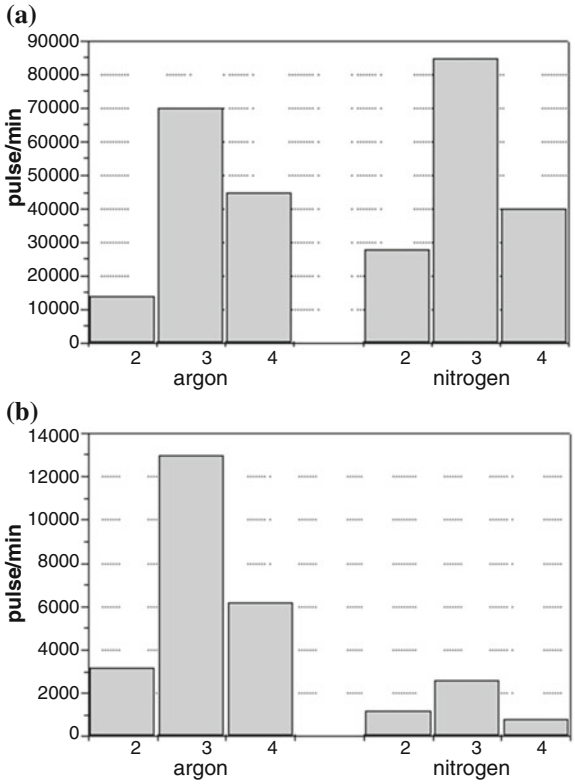

Fig. 6.30 Effect of sparging with argon and nitrogen on luminol-dependent chemiluminescence of the samples 2, 3, and 4. **a** on the day of treatment, **b** six days later

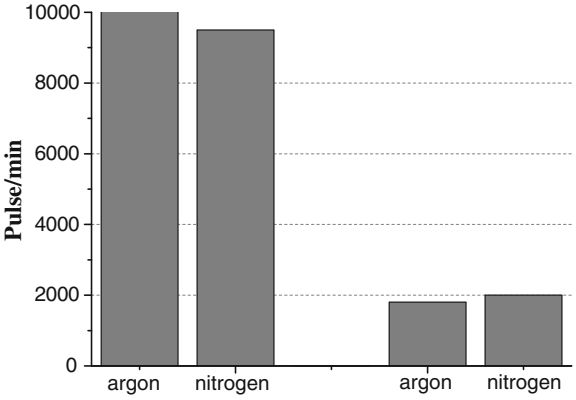

Fig. 6.31 Effect of sparging with argon and nitrogen on luminol-dependent chemiluminescence of sample 5 after 6 days of treatment by the PED

The chemiluminescence intensity measured after 6 days in the same samples decreased significantly, although the relative difference in their intensities has not changed (Fig. 6.29). In this graph, the dark current of the counter and the counting intensity are presented for comparison; here, the measuring chamber was a bottle with 20 ml of distilled water.

Interesting results were obtained for chemiluminescence of the water sparged with the nitrogen and argon. The argon stimulates emission in samples 2 and 3 that is weaker than by the nitrogen (Fig. 6.30), but in samples 4 and 5 (Fig. 6.31), the argon effect was somewhat stronger than that of the nitrogen.

Analysis of gases action showed that the argon effect in all samples was equal or higher than that of the nitrogen.

Under water treatment by the PED, the long-lived free radicals are formed in it, and their reactions are accompanied by the chemiluminescence.

Both the water own chemiluminescence intensity and its luminol-dependent one essentially depend on the experiment conditions (such as metal of the electrodes, inputted energy, etc.), under which the water is treated by the PED.

The decay time of these reactions is much larger than one of reactions accompanied by chemiluminescence in the tap water.

In measuring the chemiluminescence in water (sparged by the inert gases argon and nitrogen), the difference between the effects of these gases on different samples was seen. Moreover, after the treatment, the notable chemiluminescence changes were observed in the gases relative effect on water with different times of the decay.

These effects reveal some differences in the water properties resulting by different conditions of its treatment by the PED; also, differences in evolution of these properties during storage of various water samples were revealed.

Correlation between the chemiluminescent properties of water and its physical and chemical characteristics. In particular, we are interested in the redox potential pH. In the study, five samples of water of 40 ml were investigated. We used the single-photon detector based on the liquid scintillation spectrometer Mark II. By this unit, we measured the own samples radiation and one after addition of the luminol in the samples. Mainly peroxides and products of their transformations (that formed the active oxygen) were applied as indicators. Measurements were implemented in the water samples of 20 ml. Therefore, radiation of each sample was registered twice. Firstly, the water spontaneous emission was determined.

Then measuring was repeated after addition the luminol for the final concentration of 25 μM into the water. The ultrapure water Milli-Q was used as a check sample. The results of measurements are shown in Fig. 6.32, where 1 is check water, 2 is 10 J/ml, 3 is 8 J/ml, 4 is 6 J/ml, and 5 is 3 J/ml.

The data indicate that the sample 1 radiation is lowest and independent on the presence of the luminol. Sample 2 is characterized by the maximal radiation. The ratio of intensity of the luminol-dependent radiation to spontaneous one varies from sample to sample. In particular (omitting the background), it is maximal in samples 3 and 5 (3.1–3.2) and decreases significantly in samples 4 and 2 (1.9 and 2.5). In the second series, four water samples (1–4) were used. The results are shown in Fig. 6.33, where 1 is control water, 2 is 5 J/ml, 3 is 10 J/ml, 4 is 6 J/ml.

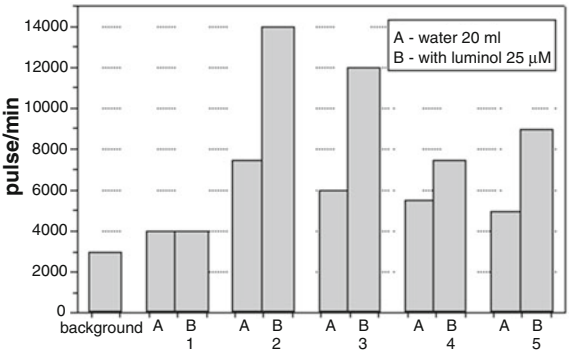

Fig. 6.32 Own emission of the samples 1–5

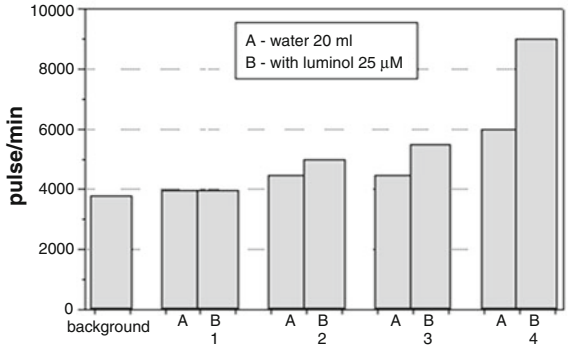

Fig. 6.33 Own emission of the samples 1–4

Here, the data indicate that the sample 1 radiation is lowest and independent on the presence of luminol. Sample 2 is characterized by the maximal radiation. The ratio of intensity of the luminol-dependent radiation to spontaneous one varies from sample to sample. In particular (omitting the background), it is maximal in samples 3 and 4.

Ratio of intensity of the luminol-dependent radiation to spontaneous one varies depending on the inputted energy.

6.9 Biological Properties of Nanoparticles

Previously it was shown that water treated by the PED has biological activity, i.e., ability to kill (for a long time) almost all known pathogenic microorganisms and fungi spores harmful to a human organism.

Experimental data on bactericidal effect of this water indicate that this property is stipulated by the charged nanoparticles of the electrodes metal.

To achieve reasonable, secure, and managed bactericidal effect, first of all, it is required to clarify in details this mechanism w.r.t. living beings.

The most interesting aspects of the PED action are:

- Its integral destroying impact onto a wide range of microorganisms
- Opportunities of the water disinfection

Therefore, more detailed statistics is necessary to accumulate on survival of microorganisms in the real conditions (in natural water, microbial community, pH of medium, etc.). Note that studies on microscopic fungi and cells are similar to ones on animals. Such investigations are very informative for understanding the mechanism of the PED action to avoid the toxic effects on humans.

In some our experiments, fungal organisms were used that have been cultured from spores. Note that investigations on fungal spores now become a convenient biological model in contrast to experiments on living organisms, animals, etc.

It was also necessary to perform carefully comparative analysis of physical characteristics of the water after its treatment in various modes in order to take into account the bactericidal components. Performed series of experiments and received data showed that bactericidity could be caused by many processes developing during and after treatment.

Our hypothesis was presumed and further studies implemented under the following assumptions:

- During the treatment, the shock waves and UV-irradiation effect onto the microorganisms in the water processed
- After the treatment, there are charged nanoparticles in the in water, and, interacting with the microorganisms, such particles damage them or cause their death
- After the treatment, the water is saturated with ions of the electrodes' metal, which are emitted by nanoparticles, and, under high concentration, the ions effect as toxic agents
- It is possible that there also exist other "after-effect" processes unknown till now

Physical properties of the treated water and its bactericidity vary in time. It is concerned both the inhibition processes (and possibly stimulation) of the microorganisms growth, the ionic composition, and other water properties, which may vary under the action of microorganisms, for example, due to interference of living and inorganic matters in the treated water.

Note that the metal ions under low concentrations are required for growth of microorganisms [27, 28]. In this connection, one cannot exclude the possibility of appearance of the "area of stimulation of the micromycetomas growth" under low concentrations of ions.

Obviously, that microorganisms, which have been effected by the PED and being in water after that, are at more negative effect in comparison with those placed in already treated water. In addition, the longer the bacteria are in the treated water, the more bactericidal effect. It was experimentally shown that microbes are longer in treated water, the stronger bactericidal effect.

On the other hand, by means of the secondary metabolism products (organic acids and enzymes), some microorganisms accelerate oxidation of the metal nanoparticles and transform them into ions, chelates, etc. [29, 30]. In the turn, they

affect onto bactericidal activity of the water. Under other equal conditions, the oxidation rate depends on ratio of the surface area to the nanoparticles number. Under decreasing the nanoparticles diameter, the ratio increases, and the ionization process is accelerated.

Even a glance over these circumstances shows that the effect of the water nanoparticles dispersions is a multivariate non-linear process. Therefore, to solve a problem of action of the water nanoparticles dispersions, it is necessary both to accumulate experimental data and to form the overall concept of biological activity of water nanoparticles dispersions.

Currently, approaches of nonequilibrium thermodynamics are used as the most general theoretical framework for study of dynamic properties of developing systems [31, 32].

Since the system "microorganisms ⇔ habitat" (under consideration) is open, it allows us to use the key concepts of the self-organization theory (synergetic), such as the dissipative structures, spontaneous symmetry breaking, instability, bifurcation, critical phenomena, nonlinearity, etc. Therefore, when discussing the process of death and survival of microorganisms in the water nanoparticles dispersions, we shall adhere to this point of view.

References

1. V.A. Kolikov, V.E. Kurochkin, L.K. Panina, Ph.G. Rutberg, Doklady Biol. Sci. **403**, 279 (2005)
2. Ph. Rutberg, V. Kolikov, V. Snetov, A. Stogov, A. Moshkin, M. Khalilov, J. Phys. Conf. Ser. **1**, 275 (2011)
3. Ph. Rutberg, V. Kolikov, V. Snetov, A. Stogov, L. Noskin, S. Landa, A. Arutunjan, in *IEEE Pulsed Power and Plasma Science Conference (PPPS-2007)* (Albuquerque, 2007)
4. G.A. Mesyats, J. Adv. Phys. Sci. **6**, 165 (1995)
5. Yu.D. Korolev, G.A. Mesyats, *Physics of Pulsed Breakdown in Gases* (URO-Press, Yekaterinburg, 1998)
6. F. Llewellyn-Jones, J. Platin. Met. Rev. **2**, 7 (1963)
7. K. Schoenbach, H. Fischer, J. Appl. Opt. **7**, 9 (1970)
8. V.L. Goryachev, A.A. Ufimtsev, A.M. Hodakovsky, J. Tech. Phys. Lett. **25**, 386 (1997)
9. V.L. Goryachev, Ph.G. Rutberg, V.N. Fedioukovitch, J. High. Temp. **5**, 34 (1996)
10. A.P. Il'in, J. Proc. Univ. Phys. **4**, 114 (1996)
11. V.Ya. Ushakov, O.B. Nazarenko, A.P. Il'in, et al., *Water and Wastewater Treatment*, (Tomsk, 1994) (in Russian)
12. B.M. Smirnov, J. Adv. Phys. Sci. **7**, 165 (1994)
13. B.G. Ershov, J. Rus. Chem. Jour. **XLV**(3), 20 (2001)
14. B.L.V. Prasad, S.I. Stoeva, C.M. Sorensen, K.J. Klabunde, J. Langmuir **18**, 7515 (2002)
15. Ph.G. Rutberg, V.L. Gorjachev, V.A. Kolikov, V.N. Snetov, A.Yu. Stogov, J. High Temp. Mater. Process. **1**, 14 (2010)
16. V.G. Levich, *Physicochemical Hydrodynamics* (Fizmatgiz, 1959) (in Russian)
17. O.V. Al'myasheva, B.A. Fedorov, A.V. Smirnov, V.V. Gusarov, J. Nanosystems: Phys. Chem. Math. **26**, 1 (2010)

18. F.G. Rutberg, V.V. Gusarov, V.A. Kolikov, I.P. Voskresenskaya, V.N. Snetov, A.Yu. Stogov, I.A. Cherepkova, J. Tech. Phys. **12**, 82 (2012)
19. A.Yu. Krutyakov, A.A. Kudrinskii, A.Yu. Olenin, G.V. Lisichkin, J. Uspechy Chem. **242**, 77 (2008)
20. A.I. Boronin, S.V. Koscheev, K.T. Murzakhmetov, J. Appl. Surf. Sci. **165**, 249 (2000)
21. A. Pyatenko, *Silver Nanoparticles: Collection of Articles*, ed. by Dr. D. Perez-Croatia (2010)
22. V.I. Avdeev, A.I. Boronin, G.M. Zhidomirov, J. Struct. Chem. **43**, 26 (2002)
23. S. Jadhav, S. Gaikwad, A. Rajbhoj, J. Cluster Sci. **22**, 121 (2011)
24. A.V. Korshunov, A.P. Il'in, Izv. Tomsk. Politekhn. Univ. **3**, 313 (2008)
25. V.A. Kotenev, N.P. Sokolova, A.M. Gorbunov, A.Yu. Tzivadze, J. Nanoscale Nanostruc. Mater. Coat. **6**, 43 (2007)
26. Ph.G. Rutberg, V.A. Kolikov, V.E. Kurochkin, L.K. Panina, A.Ph. Rutberg, J. IEEE Trans. Plasma Sci. **4**, 35 (2007)
27. O.Yu. Sentsova, V.N. Maksimov, J. Adv. Microbiol. **20**, 227 (1985)
28. G.M. Gadd, J. New Phytol. **124**, 25 (1993)
29. G.M. Gadd, A.J. Griffiths, Trans. British Mycol. Soc. **74**, 387 (1978)
30. G.M. Gadd, A.H. Brunton, J. Gen. Microbiol. **138**, 1561 (1992)
31. I. Prigogine, I. Stengers, *Order Out of Chaos* (Progress Publishers Moscow, Russian, 1986) (in Russian)
32. G. Haken, *Synergetics: The Hierarchy of Instabilities in Self-Organizing Systems and Devices* (Moskow, 1985) (in Russian)

Chapter 7
Impact of the WDN on Bacteria and Spores of Fungi

Abstract Bactericidity of the WDN depends on the inputted energy and properties of the electrodes' metal. Bactericidal effect was observed for both low (10^3 ml^{-1}) and high (up to 10^7 ml^{-1}) concentrations of bacteria. During 24 h (for most of bacteria within 4 h or less), almost all tested microorganisms and spores of microscopic fungi are killed. That fact indicates the effectiveness of using of water dispersions of metal nanoparticles as bactericidal agents. Potential applications of the method of water treatment by PED may be quite broad: disinfection of water and its long-term storage; usage of WDN for sanitary and antimoldy treatment of swimming pools, saunas, enclosed spaces, and treatment of seed, etc. At equal concentration of ions in two kinds of dispersions, the bactericidal action of dispersion, which contains both ions and nanoparticles, is higher than one containing only ions. Nanoparticles and clusters do not penetrate inside the bacteria but settle down on their cell walls and produce streams of toxic ions, which destroy the bacteria. Prolonged microbial resistance of water is the cooperative bactericidal action on bacteria of both oxide nanoparticles and positive ions emitting by them. The importance of this investigation is that the obtained results connect the PRMW with the parameters of PED and with properties of metal electrodes, moreover, the results give the opportunity to produce the dispersions with the required bactericidal properties, which can be considered as the bactericidal agents.

7.1 Impact of the WDN on Bacteria

Figure 7.1 shows bactericidity of the WDN of various metals of electrodes determined as $\log_{10}(N_f/N_i)$, where: N_i is initial concentration of bacteria, N_f is final concentration of viable bacteria after the PED treatment.

The plots confirm that the water treated by the silver electrodes has the highest bactericidal activity. These phenomena take place even for the higher concentration of the iron and copper nanoparticles (than that of the silver ones) under the same inputted energy (Fig. 7.2).

V. Kolikov and P. Rutberg, *Pulsed Electrical Discharges for Medicine and Biology*, Biological and Medical Physics, Biomedical Engineering,
DOI 10.1007/978-3-319-18129-5_7

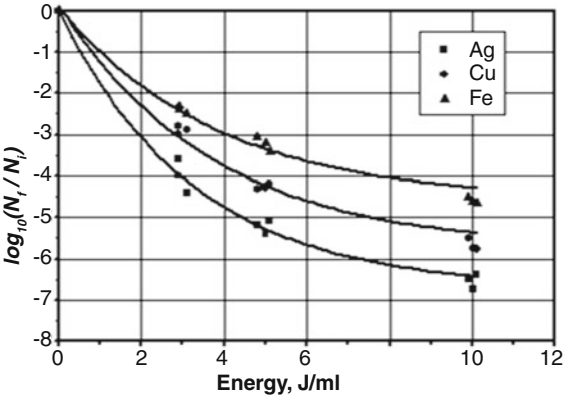

Fig. 7.1 Log_{10} (N_f/N_i) versus inputted energy (*E. coli*) [2]

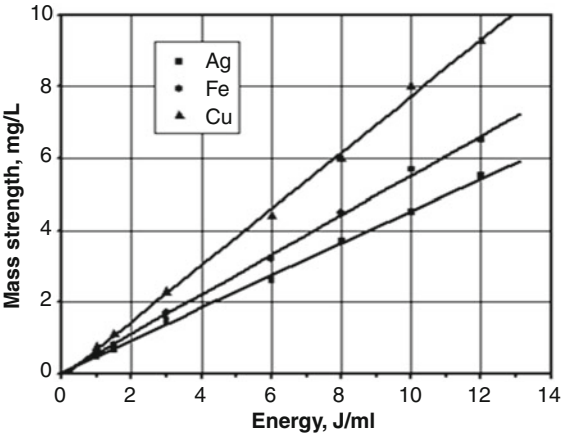

Fig. 7.2 Concentration of silver, copper, and iron nanoparticles in the WDN versus inputted energy [2]

This is because the silver ions have the highest toxicity against bacteria. According to their toxicity, ions of metals are ordered in the following order: Ag > Cu > Cd, Zn, and Pb > Mn, Fe > Mg, Ca [1].

Since both concentration of nanoparticles and bactericidity of the water dispersions are proportional to the inputted energy, some connection must exist between bactericidity and concentration of nanoparticles.

For example, the bactericidity of water dispersions is proportional to the total mass strength of the active nanoparticles.

Besides the *E.coli*, the treated water bactericidity has also been examined on *Klebsiella pneumonia*, *Staphylococcus aureus*, *Pseudomonas aeruginosa*, *Pseudomonas putida*, *Salmonella typhimurium*, *Serratia marcescens*, *Proteus vulgaris*, *Citrobacter freundii*, *Bacillus subtilis*, *Candida albicans*, and *Ulocladium chartarum.*

Distilled water treated by the PED saline was used for preparation of an isotonic saline and then was sterilized by a conventional method. For check, a sterile isotonic saline prepared in distilled water was used.

In tubes containing 9.0 ml of isotonic salines (with the WDN and check one), a 1.0 ml suspension of the test microorganisms strains was added that contained bacteria with concentration from 10^4 to 10^7 1/ml.

Immediately after adding and after 24 h of incubation at room temperature, the number of colonies was counted by the quantitative microbial method. If necessary, identification of the test strains and calculation of the colony forming units (CFU) per 1 ml of water were performed.

For various bacteria, the following culture media were used: *Klebsiella pneumonia*, *Pseudomonas aeruginosa*, *Salmonella typhimurium*, and *Bacillus subtilis* (on the ordinary nutrient agar), *Staphylococcus aureus* (on the yolk-salt agar), *Candida albicans* (on the Saburo medium).

Tables 7.1, 7.2, 7.3, 7.4, 7.5, 7.6 and Fig. 7.3 show some results of those tests with the WDN under inputted energy 5 J/ml.

Table 7.1 Concentration of the *Klebsiella pneumonia* after incubation

Bacterium	Saline	Concentration ml^{-1}			
		Initial	After 24 h	Initial	After 24 h
Klebsiella pneumonia	Test	5.2×10^3	0	2.2×10^3	0
Klebsiella pneumonia	Check	5.2×10^3	4.8×10^3	2.2×10^3	2.6×10^3
Klebsiella pneumonia	Test	5.2×10^4	0	2.2×10^4	0
Klebsiella pneumonia	Check	5.2×10^4	5.6×10^4	2.2×10^4	3.2×10^4
Klebsiella pneumonia	Test	5.2×10^5	0	2.2×10^5	0
Klebsiella pneumonia	Check	5.2×10^5	4.0×10^5	2.2×10^5	2.0×10^5
Klebsiella pneumonia	Test	5.2×10^6	8 CFU	2.2×10^6	3 CFU
Klebsiella pneumonia	Check	5.2×10^6	4.4×10^6	2.2×10^6	1.8×10^6

Table 7.2 Concentration of the *Klebsiella pneumonia* after incubation

Bacterium	Saline	Concentration ml^{-1}			
		Initial	After 24 h	Initial	After 24 h
Staphylococcus aureus	Test	4.0×10^3	0	4.2×10^3	0
Staphylococcus aureus	Check	4.0×10^3	4.2×10^3	4.2×10^3	4.0×10^3
Staphylococcus aureus	Test	4.0×10^4	0	4.2×10^4	0
Staphylococcus aureus	Check	4.0×10^4	4.4×10^4	4.2×10^4	3.6×10^4
Staphylococcus aureus	Test	4.0×10^5	0	4.2×10^5	0
Staphylococcus aureus	Check	4.0×10^5	3.8×10^5	4.2×10^5	4.5×10^5
Staphylococcus aureus	Test	4.0×10^6	60 CFU	4.2×10^6	12 CFU
Staphylococcus aureus	Check	4.0×10^6	4.9×10^6	4.2×10^6	3.9×10^6

Table 7.3 Concentration of the *Pseudomonas aeruginosa* after incubation

Bacterium	Saline	Concentration ml^{-1}			
		Initial	After 24 h	Initial	After 24 h
Pseudomonas aeruginosa	Test	6.1×10^3	0	4.2×10^3	0
Pseudomonas aeruginosa	Check	6.1×10^3	5.8×10^3	4.2×10^3	3.8×10^3
Pseudomonas aeruginosa	Test	6.1×10^4	0	4.2×10^4	0
Pseudomonas aeruginosa	Check	6.1×10^4	6.6×10^4	4.2×10^4	4.4×10^4
Pseudomonas aeruginosa	Test	6.1×10^5	0	4.2×10^5	0
Pseudomonas aeruginosa	Check	6.1×10^5	5.2×10^5	4.2×10^5	5.3×10^5
Pseudomonas aeruginosa	Test	6.1×10^6	3 CFU	4.2×10^6	5 CFU
Pseudomonas aeruginosa	Check	6.1×10^6	5.6×10^6	4.2×10^6	3.9×10^6

Table 7.4 Concentration of the *Candida albicans* after incubation

Bacterium	Saline	Concentration ml^{-1}			
		Initial	After 24 h	Initial	After 24 h
Candida albicans	Test	10^3	0	5.8×10^3	0
Candida albicans	Check	10^3	1.2×10^3	5.8×10^3	5.6×10^3
Candida albicans	Test	10^4	0	5.8×10^4	0
Candida albicans	Check	10^4	1.6×10^4	5.8×10^4	5.2×10^4
Candida albicans	Test	10^5	1 CFU	5.8×10^5	0
Candida albicans	Check	10^5	1.4×10^5	5.8×10^5	5.3×10^5
Candida albicans	Test	10^6	6 CFU	5.8×10^6	8 CFU
Candida albicans	Check	10^6	1.2×10^6	5.8×10^6	5.5×10^6

Table 7.5 Concentration of the *Salmonella typhimurium* after incubation

Bacterium	Saline	Concentration ml^{-1}	
		Initial	After 24 h
Salmonella typhimurium	Test	2.0×10^3	0
Salmonella typhimurium	Check	2.0×10^3	2.2×10^3
Salmonella typhimurium	Test	2.0×10^4	0
Salmonella typhimurium	Check	2.0×10^4	2.6×10^4
Salmonella typhimurium	Test	2.0×10^5	2 CFU
Salmonella typhimurium	Check	2.0×10^5	2.6×10^5
Salmonella typhimurium	Test	2.0×10^6	21 CFU
Salmonella typhimurium	Check	2.0×10^6	2.4×10^6

Figure 7.4 shows ratio of the final concentration N_f of the viable *E.coli* to their initial concentration N_i (10^6 ml^{-1}) as a function of the inputted energy. Here, the WDN were prepared on the apparatus equipped with one or four discharge chambers connected in series along the water flow.

Table 7.6 Concentration of the *Bacillus subtilis* after incubation

Bacterium	Saline	Concentration ml^{-1}	
		Initial	After 24 h
Bacillus subtilis	Test	6.0×10^3	0
Bacillus subtilis	Check	6.0×10^3	6.6×10^3
Bacillus subtilis	Test	6.0×10^4	0
Bacillus subtilis	Check	6.0×10^4	6.6×10^4
Bacillus subtilis	Test	6.0×10^5	0
Bacillus subtilis	Check	6.0×10^5	6.0×10^5
Bacillus subtilis	Test	6.0×10^6	0
Bacillus subtilis	Check	6.0×10^6	6.9×10^6

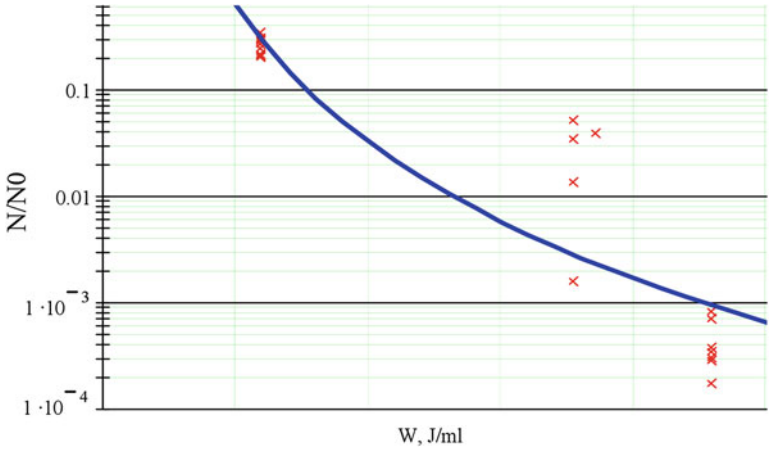

Fig. 7.3 Concentration of the viable bacteria under various inputted energies and electrode metals versus exposition time

It was found that, under the same inputted energy, the treatment implemented by means of several electrodischarge chambers (connected sequentially) is more effective than by one chamber. Comparison of the plots (Fig. 7.4) shows that the final concentration N_f of the viable *E.coli* to their initial concentration N_i (10^6 ml^{-1}) under the inputted energy of 2.5 J/ml is decreased from 3×10^{-3} ml^{-1} after one discharge chamber down to 10^{-4} ml^{-1} after four sequential chambers.

This decrease may be explained by multiple actions of the shock waves onto bacteria and mixing the treated water in the case of four chambers. Since the treated water can be considered as a bactericidal agent, it was of interest to determine its bactericidity versus ratio of dilution of the treated water by the initial one.

Figure 7.5 shows the final concentration of *E.coli* versus ratio of the dilution under the inputted energy of 10 J/ml for the initial concentration of these bacteria 7.9×10^3 ml^{-1} and after exposition of 24 h.

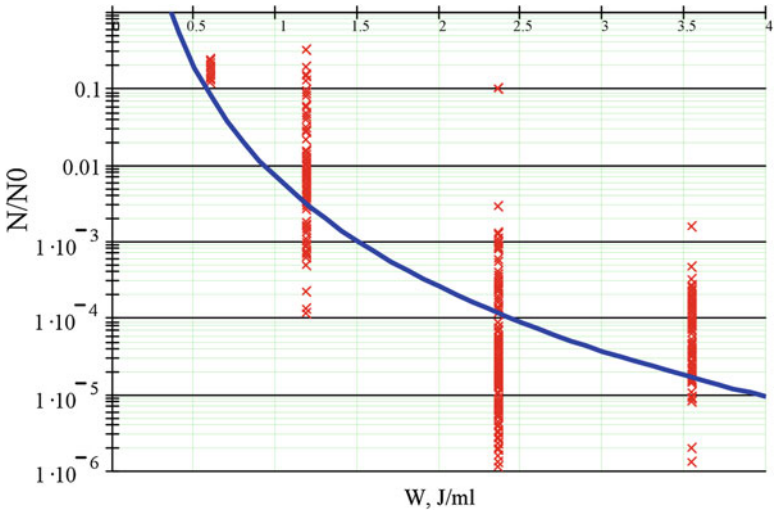

Fig. 7.4 Ratio of the final concentration N_f of the viable *E.coli* to their initial concentration N_i versus inputted energy [2]

Fig. 7.5 Final concentration of the *E coli* versus ratio of the dilution [2]

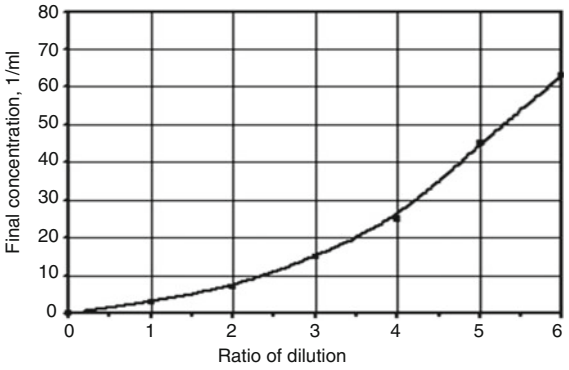

Rate of destruction of the *E.coli* in water treated by the PED with the Cu electrodes is presented in Fig. 7.6 [3]. Here, the electrodes made of the Ti, Fe, and Ag were used.

The dependencies have the exponential character; and all spores had been destroyed for the time from 15 min to 3 h.

Rate of destruction of *E.coli* in water treated by the PED at Cu electrodes, at inputted energy of 10 J/ml and initial concentration of bacteria 3.8×10^3 ml^{-1} and 5.1×10^6 ml^{-1} is presented in Fig. 7.7. Here, the inputted energy was of 10 J/ml and the initial concentrations of bacteria were 3.8×10^3 ml^{-1} and 5.1×10^6 ml^{-1}.

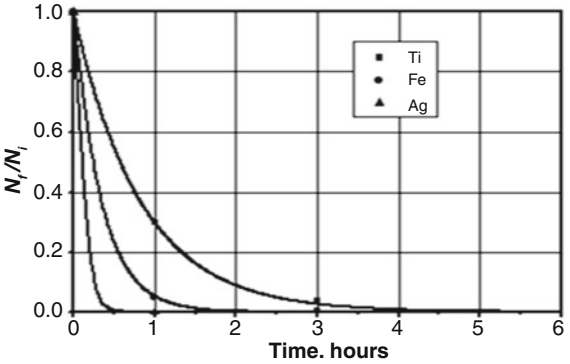

Fig. 7.6 Rate of destruction of the *U.chartarum* spores under the inputted energy of 10 J/ml [2]

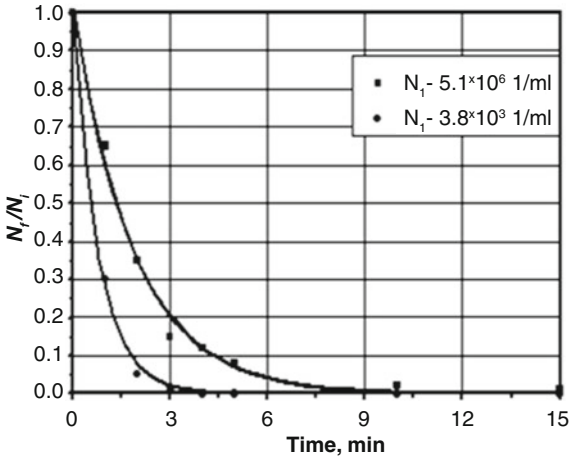

Fig. 7.7 Rate of destruction of the *E.coli* under the inputted energy of 10 J/ml [2]

The dependencies also have the exponential character; and, in dependence on the bacteria initial concentration, from 80 to 100 % of them had been destroyed for the time of 5 min.

The water nanoparticles dispersions have either bacteriostatic or bactericidal action against a wide range of bacteria depending on the metal of electrodes (degree of ion toxicity) and concentration of the nanoparticles (proportional to the inputted energy).

The bactericidal effect was observed for both low (10^3 ml^{-1}) and high (up to 10^7 ml^{-1}) concentrations of bacteria.

During 24 h (for most of bacteria within 4 h or less), almost all tested micro-organisms and spores of microscopic fungi are killed. This fact indicates effectiveness of using the water dispersions of metal nanoparticles as bactericidal agents.

7.2 Fungistatic Action of the WDN

Under treatment of water by the PED, processes leading to formation of the WDN occur in the water [4]. In this case, the WDN have antibacterial activity against a number of pathogenic bacteria and yeast spores. It is shown that the WDN bactericidity is retained for more than 1 year, but mechanism of the WDN action onto living organisms is not completely investigated. In practice, we obtain information about processes taking place in the WDN in presence of microorganisms. However, it is difficult to make the definitive conclusions about nature of these processes only based on studying its physical and chemical properties. So, such information can only help to formulate working hypothesis.

To clarify the mechanism of the WDN fungistatic/fungicidal action, it was necessary to perform tests of the WDN properties determination under various conditions and, further, to carry out analysis of results of comparative experiments.

Both the electrodes material and its chemical purity essentially determine the WDN properties. Thus, by changing the procession conditions, one can control the physic-chemical properties of the WDN (composition and concentration of nanostructures, etc.) and its biological activity.

In investigations, we used fungi from the pure cultures collection of the Laboratory of General Biophysics, St.-Petersburg State University. For study, melanin containing the fungal species *Ulocladium chartarum*, *Ulocladium consortiale*, *Phaeococcomyces sp*. were selected. These species are known for their high resistance to external influences such as UV-irradiation, high concentrations of heavy metals, oxidative stress, etc.

After treatment by the WDN (CFU/ml), the test results were evaluated morphologically (to identify possible disorders of normal development of spores) and by germination of the spores. The analysis was carried out by cultivation in Petri dishes on oatmeal agar at 23 °C and in the wells of microtiter plates in a liquid medium and in the WDN. Registration of the fungal growth in the wells was implemented on 96-channel photometer under discriminant mode by the procedure presented in paper [5]. Depending on the conditions of tests, we varied duration of exposure in the WDN, as well as duration of the subsequent cultivation of fungi.

In experiments, the electrodes of Ti, Ag, and Fe (and in various their combinations) were used. Deionized and tap waters treated by the PED were investigated under various inputted energies: 3, 5, and 10 J/ml. The WDN of various storage time from 3 h to 9 months at $t = 23$ °C.

Primarily, it was necessary to estimate the basic physical and chemical parameters of the WDN prepared under various modes. Study of the dispersed phase was performed by an inductively coupled plasma mass spectrometry, correlation spectroscopy, and capillary electrophoresis.

By the ICP-MS method, the elemental composition of WDN for three combinations of electrodes was investigated. Thus, for the Ti electrodes, concentration of Ti in the WDN was 748.97 μg/l; for combination of Ti and Ag, it was 391 μg/l of Ti

and 4,371 μg/l of Ag; for combination of the Ti and Fe, concentration was 291 μg/l of Ti and 320 μg/l of Fe.

Experiments have shown that decrease of the specific energy by 2 times directly leads to proportional decrease of Ag and Ti concentration in the WDN. For example, under specific energy of 10 J/ml, the Ag concentration in the WDN was 4.4 mg/l, but under the energy of 5 J/ml, it decreased to 2.4 mg/l. The Ti concentration was, respectively, 0.4 and 0.2 mg/l. Thus, for the same specific energy but with different electrodes, the biological properties of the WDN are different, since the WDN contains nanoparticles of different metals with significantly different concentrations.

By the dynamic light scattering and capillary electrophoresis, the nanoparticles sizes in the WDN were evaluated. It was found that the metal in the WDN is preferably in the form of clusters, which distributions in size are bimodal. Here, the main fraction is of ~ 10 nm and its part is of 90 %; additionally, there are fractions of other sizes.

To estimate the viability of spores after exposure in the WDN, the following experiments were performed. First, the deionized and tap waters were treated under the inputted energies of 3, 5, and 10 J/ml.

Then using the WDN of different storage periods from 3 h to 9.5 months, the suspensions of spores were prepared. Concentration of the suspensions corresponded to the control suspension. Then all samples were incubated at $t = 23$ °C. After exposure of 0, 3, 24, 48 h, and 7 days, the microprobes of each suspension were sown in 3 replicates on the agar medium for the control of survival and monitoring of colony morphology. Results of 10 series of tests are presented in Table 7.7.

Data in Table 7.7 show that the number of colonies after exposure in the control sample corresponds approximately to concentration of germinated spores in the initial suspension. However, in the WDN their concentration is decreased. Experiments have shown that staying of the *Ulocladium chartarum* spores in the WDN (deionized water) does not damage them, in spite of that such water can be considered as relatively adverse medium for development and germination of spores.

Another important factor is the number of spores in the initial suspension. Effect of the growth inhibition is clearly repeated only under the initial concentrations of spores not more than 10^3–10^4 ml^{-1}. It can be supposed that for the high concentrations of spores larger than 10^6 ml^{-1}, the main mass of reactive metal in the dispersion can certainly decrease below the threshold of sensitivity due to the adsorption of the nanoparticles on the fungi cell walls [6–8].

Fungicidal action under incubation of spores in the WDN over 2 days was noted. Such spores do not germinate in contact with the culture medium; but the mechanical damage of spores was not observed. For the Ti and Fe electrodes in some tests (Table 7.8), the effect of stimulating the spores' growth was observed. Obviously, it is associated with increasing (in the WDN) the concentration of microelements that are physiologically relevant for the fungi growth.

Monitoring the changes in the morphology of fungal colonies obtained under seeding the spores incubated in the WDN during 3 and 48 h was performed. It shows the following types of morphological abnormalities:

Table 7.7 Number of colonies of the *Ulocladium chartarum* after exposure in the WDN

Metal of electrodes	Energy J/ml	Number of fungi CFU/ml		
		Initial $\Delta t = 0$	After incubation $\Delta t = 3$ h	After incubation $\Delta t = 48$ h
WDN (*deionized water*)				
Ti Ag	Check	10^3	10^3	10^3
	5	10^3	10^3 stimulation	20–50 anomaly
	10	10^3	10^2 inhibition	10–20 anomaly, death after 2 weeks
Ti Ag	Check	10^3	–	(*) 3×10^2
	Saline	10^3	–	(*) 6×10^2
	5	10^3	–	(*) 0
	10	10^3	–	(*) 0
Ti Ag	Check	10^3	–	(*) 3×10^2
	Saline	10^3	–	(*) 1.5×10^2
	5	10^3	–	(*) 10^2
	10	10^3	–	(*) 0
Ti Ti	Check	2×10^2	1.5×10^2	10^2
	5	2×10^2	50	50 red pigment
	10	2×10^2	2×10^2	2×10^2 red pigment
Ti Ag	Check	10^3	10^3	10^3
	3	10^3	0	0
	5	10^3	0	0
	10	10^3	0	0
Ti Fe	5	10^3	100	100
	10	10^3	50	30
	Check	5×10^3	5×10^3	(**) 5×10^3
WDN (*tap water*)				
Ti Ag	5	5×10^3	–	(**) 0
	5 (dilution 1:2)	5×10^3	–	(**) 20–50
	5 (dilution 1:4)	5×10^3	–	(**) 2.5×10^3
	5 (dilution 1:8)	5×10^3	–	(**) 5×10^3
	10	5×10^3	–	(**) 0
	10 (dilution 1:2)	5×10^3	–	(**) 10–20
	10 (dilution 1:4)	5×10^3	–	(**) 100
	10 (dilution 1:8)	5×10^3	–	(**) 5×10^3

Notes (*)—time of incubation 24 h, (**)—time of incubation 7 days

- Emergence of colorless colonies of the *Ulocladium chartarum* with limited in growth rate; pigmentation is delayed for 4–5 days; for the Ti and Ag electrodes, the growth rate of colonies bounces after 11–12 days of seeding (spores were incubated during 48 h in the WDN with the inputted energies of 5 and 10 J/ml)

Table 7.8 Fungicidal effect on spores under incubation in the WDN

Metal Fungi	Energy (J/ml)	Number of fungi CFU/ml		
		Initial $\Delta t = 0$	After incubation $\Delta t = 3$ h	After incubation $\Delta t = 48$ h
Ti Ag *Ulocladium chartarum*	Check	10^3	10^3	10^3
	5	10^3	10^2	0
	10	10^3	10^2	0
Ti *Ulocladium chartarum*	Check	2×10^2	1.5×10^2	10^2
	5	2×10^2	5×10^2	5×10^2
	10	2×10^2	2×10^2	2×10^2
Ti Ag *Ulocladium chartarum*	Check	5×10^5	10^3	10^3
	3	5×10^5	0	0
	5	5×10^5	0	0
	10	5×10^5	0	0
Ti Ag *Phaeococcomyces sp.*	Check	10^5	10^3	10^3
	3	10^5	0	0
	5	10^5	0	0
	10	10^5	0	0
Ti *Ulocladium chartarum*	Check 1	10^4	10^3	0
	2.3	10^4	10^3	0
	5	10^4	2×10^2	0
	10	10^4	6×10^2	0
	Check 2	10^5	0	0
	3	10^5	2×10^3	0
	5	10^5	2×10^3	0
	10	10^5	3.5×10^3	0
	Check 3	10^6	10^5	0
	1.5	10^6	2×10^4	0
	5	10^6	3.5×10^3	0
	10	10^6	3×10^3	0
Ti Ag *Ulocladium chartarum*	Check 1	2.5×10^3	10^3	0
	5	2.5×10^3	0–100	0
	10	2.5×10^3	0	0
	Check 2	2.5×10^4	5×10^3	0
	5	2.5×10^4	10^3	0
	10	2.5×10^4	0–100	0
	Check 3	2.5×10^5	2×10^4	0
	5	2.5×10^5	$10^{3-}10^4$	0
	10	2.5×10^5	$50–10^3$	0
Ti Ag *Ulocladium chartarum*	Check	2.5×10^4	10^4	0
	5	2.5×10^4	5.5×10^3	0
	10	2.5×10^4	5×10^2	0

- Emergence of the *Ulocladium chartarum* colonies with significant brick-red pigment λ_{abs} = 410 nm (that is absolutely not typical for this fungi); here, the colonies were grown from spores incubated during 48 h in the WDN with the inputted energy of 5, 10 J/ml and the Ti electrodes; during growth of such colonies (after 2 weeks), the normal pigmentation is restored

Apparently, changes in pigmentation are caused by blocking the melanin synthesis inside the fungi cell walls on various stages of the process; but this blocking is stipulated by the WDN. Probably, the brick-red pigment is the oxyjuglone as a precursor of the melanin [9].

Under development of the fungi on a nutrient medium, normalization of the morphological parameters over time shows the reversibility of changes caused by the WDN action. We think that such changes do not affect onto genetic apparatus of fungal cells.

Under the same inputted energies, fungicidal action of the WDN with the Ag electrodes was higher than one with the Ti electrodes. This result can be explained as follows: firstly, by the higher metal Ag concentration in water and, secondly, by the significantly higher toxicity of the Ag ions than ones of the Ti and Fe [1]. Therefore, based on these data, it is impossible to make an unambiguous conclusion about the primary mechanism of the WDN fungistatic on micromycetomas: is it the fungistatic interaction of charged metal nanoparticles with the dipoles of microorganisms or is it the toxic effect of metal ions?

In this connection, it was of interest to compare the WDN fungicidal activity with the action of the $AgNO_3$ solutions under the equal concentration of Ag. Concentrations of these salt solutions were calculated using data of elemental analysis. Corresponding tests were carried out in the microtiter plates on three kinds of fungi. Since during culturing in all samples without growth medium the fungi do not develop, volumes of the of broth oat (from 10 to 200 μl of water solution) were added.

Experimental data show that the $AgNO_3$ ion solutions are more effective in inhibiting the fungi growth in comparison with the WDN effect. Thus, in solution of the $AgNO_3$ with the Ag^+ concentration of 1.5 mg/l (this corresponds to concentration of the Ag nanoparticles in the WDN under the inputted energy of 3 J/ml), the growth was not observed; but in the WDN itself, the growth took place.

This result can be explained by the fact that, although the metal concentrations in both cases are identical, the Ag is in different states: it has the ionic form in $AgNO_3$, but in the WDN, it has the form of nanoparticles. It is known that, in different states, heavy metals have different toxicity against microorganisms, and it is maximal for ions [1].

These results are consistent with the fact that increasing the exposure time of spores in the WDN increases a fungicidal action (Table 7.8). Moreover, it explains the prolonged antimicrobial properties of the WDN. Namely, in such systems the nanoparticles act as the Ag reservoirs that later can transform from the clusters to more toxic form, i.e., the ionic one. In the turn, this continuously replenishes the medium with the silver ions. It was found that for the *U.chartarum*, *U.consortiale*, and *Phaeococcomyces sp.*, the minimum inhibitory concentration (MIC) of silver

ion solution is of 1.25–1.5 mg/l, but in the WDN with the Ag nanoparticles, the MIC is 3–4 mg/l. Therefore, these MIC levels differ by 2.5–3 times.

These results in accordance with the fact that increasing of exposure of spores in the WDN increases the fungicidal action (Table 7.8) as well as explains the prolonged antimicrobial action of the WDN, since in such systems nanoparticles are reservoirs of Ag, which over time can transform from cluster form to more toxic—ionic form replenishing continuously water by the Ag ions. Minimal inhibitory concentrations for *U.chartarum*, *U.consortiale*, and *Phaeococcomyces sp.* (strain Ch. 49) of Ag ion solution is 1.25–1.5 mg/l and of the WDN is 3–4 mg/l, i.e. they are differed by 2.5–3 times.

Although these investigations are now continued, obtained results on the WDN biological activity (in various modes of their producing) provide a basis for development of disperse systems with required properties.

Therefore, the WDN can be considered as a kind of a liquid-phase nanomaterial with the "intellectual" dynamic properties. From this point of view, the results of our study are consistent with the data on antimicrobial activity obtained for planar and three-dimensional solid-state nanomaterials [10, 11]. These nanocomposite materials are constructed of a biologically-inert matrix doped by metals with the oligodynamic properties. In such composites, initially "locked" in the matrix heavy metal clusters can be released into the environment gradually causing necessary effect onto the microorganisms' metabolites. Thus, the nanomaterials provide interaction between the microorganism and the toxic agent in the feedback mode.

Potential applications of the method of water treatment by the PED may be quite broad: disinfection of water and its long-term storage; the WDN usage for sanitary and antimoldy treatment of swimming pools, saunas, enclosed spaces, treatment of seed, etc.

7.3 Prolonged Microbial Resistance of Water Treated by the PED

There are some electric methods for water and air purification:

- Pulsed electric fields
- Glow discharges
- Streamer/corona discharges
- Gliding discharges
- Barrier discharges
- Pulsed spark discharges (the PED here)

All these methods are approximately equal by efficiency since in all them, the acting factors are almost the same: UV-irradiation, OH radicals, H_2O_2, O_3, etc.

However, method of the pulsed electric discharges in water has essential advantages in comparison with other ones:

- Intensive shock waves
- Prolonged microbial resistance of water (PMRW)

Remind that the PMRW is the property of water (after treatment by the PED) to destroy a wide set of pathogenic bacteria for a long time (up to several months). Due to this property, water treated by the PED is the bactericidal agent.

Although investigations of these methods of water disinfection were carried out for a long time, unresolved problems still exist in this area; particularly, it is the PRMW genesis. It has been shown above that two groups of factors cause the bactericidal action of the PED in water:

- UV-irradiation and shock waves are factors of current action
- Hydrated electrons, OH radicals, H_2O_2, nanoparticles, and positive ions of the metal electrodes are the post action factors

Note that hydrated electrons exist approximately 0.5 ms and the OH radicals and H_2O_2 are present not more than several days. Therefore, it is evident that they cannot be considered as the PMRW factors. Thus, only the nanoparticles and positive ions of metal, which are produced by electrodes erosion, are responsible for the PMRW.

To reveal the role of nanoparticles in the PMRW, special experiments were carried out on inhibition of growth of the *U.chartarum* fungi spores in two modifications of the same treated water:

- Containing both ions and nanoparticles
- Containing only ions (after the removal of nanoparticles)

Water was treated by the PED with the Ag, Cu, and Fe electrodes under the specific inputted energy of 1.5, 3, 6, 8, and 12 J/ml.

Figure 7.8 shows the differences of final concentrations of *U.chartarum* viable spores as a function of inputted energy, where: N_i is final concentration of spores in water containing after removal of nanoparticles only ions; N_{in} is final concentration of spores in water containing both ions and nanoparticles.

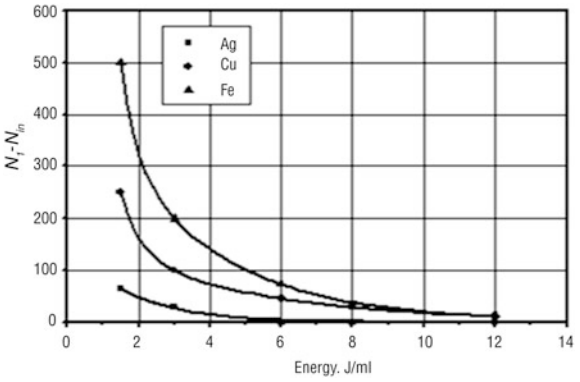

Fig. 7.8 Differences of the final concentrations of viable spores in two kinds of the WDN as a function of inputted energy [2]

The plots of differences between the final concentration N_i and the initial one N_{in} with the initial concentration of spores 10^3 ml^{-1} after 10 days incubation are shown in Fig. 7.8. It is seen that the fungicide effect is higher when both ions and nanoparticles are in the water.

The differences are maximal when the electrodes material is iron, which is a metal with the lowest toxicity of ions. In this case, the bactericidal effect of nanoparticles themselves is highest, whereas for the higher toxicity of ions, this difference is lower. Besides, these differences decrease under the inputted energy increase; i.e., under increase of the ions and nanoparticles concentration. Thus, nanoparticles in water increase its bactericidal action. This may be explained by the following two reasons:

- During incubation, the nanoparticles maintain concentration of ions at same level
- By means of their surface electric charge, the nanoparticles themselves participate in killing the spores

The most probable mechanisms of bactericidal action of the nanoparticles on bacteria are the following: penetration of nanoparticles inside bacteria [12], cooperative action of toxic ions emitted by nanoparticles, and surface electric charge of nanoparticles [13].

By electronic microscopy, it was detected that single nanoparticles and their clusters settle down on the bacteria walls (Fig. 7.9).

In contrast to the data presented in paper [12] (Fig. 7.9) shows, that nanoparticles do not penetrate inside the bacteria. When a bacterium adsorbs the ions, this removes concentration balance between the ions and nanoparticles. In the turn, this causes additional emission of ions from the nanoparticles. Due to this phenomenon, when nanoparticles approach close to a bacteria, directed streams of the toxic ions appear, which produce the mentioned bactericidal effect.

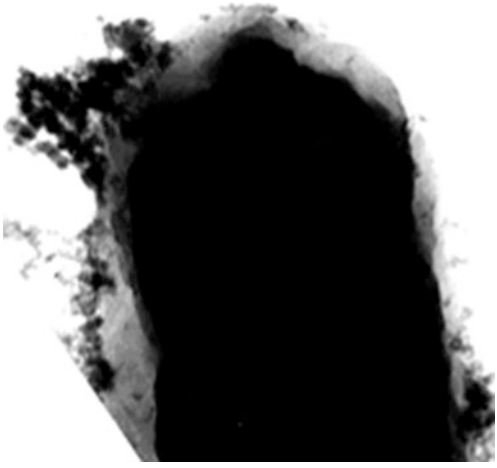

Fig. 7.9 Nanoparticles of Cu on the wall of the *E.coli* ($\times 10^5$) [2]

Water treated by the PED is the WDN containing both nanoparticles of the metal electrodes and positive ions, which are in the dynamic concentration equilibrium for several months.

Under equal concentration of ions in two kinds of dispersions, the bactericidal action of dispersion, which contains both ions and nanoparticles, is higher than one containing only ions.

The nanoparticles and clusters do not penetrate inside the bacteria but settle down on their cell walls and produce streams of the toxic ions, which destroy the bacteria.

The PRMW is the cooperative bactericidal action onto bacteria of both oxide nanoparticles and positive ions emitting by them.

The importance of this investigation is that the obtained results connect the PRMW with the PED parameters and with properties of the metal electrodes. Moreover, the results give an opportunity to produce the dispersions with the required bactericidal properties, which can be considered as the bactericidal agents.

7.4 Simulations of Microbes' Death in the WDN

Regularities founded in experiments are a basis of mathematical models describing the dynamics of death of microbes:

- Existence of a threshold initial bacterial concentration, at which there is no significant damaging effect of the WDN under low concentration of nanoparticles
- Connection of the initial threshold concentration of bacteria with concentration of nanoparticles in the WDN
- Dependence of the bacteria number decreasing in time on the ratio of the initial microbes' concentrations and particles

Model 1 Consider the system of equations:

$$\begin{aligned} \frac{dn}{dt} &= -\alpha \cdot nN \\ \frac{dN}{dt} &= k_s \frac{dn}{dt} \end{aligned} \tag{7.1}$$

where n is concentration of *E.coli* (m^{-3}); N is concentration of nanoparticles (m^{-3}); k_s is coefficient of sticking; $\alpha = \sigma v$ is reaction rate constant; σ is cross section (m^2); v is velocity (m/s).

Integrating the second equation of this system (4.14) and using the initial conditions

$$N - k_s n = C = N_0 - k_s n_0 \tag{7.2}$$

then first equation

$$\frac{dn}{dt} = -\alpha \cdot n(C + k_s n) \tag{7.3}$$

after integration leads to dependence

$$\frac{n}{n_0} = \frac{N_0 - k_s n_0}{N_0 e^{\alpha C t} - k_s n_0} \tag{7.4}$$

where $\alpha\ C = \sigma\ v\ (N_0 - k_s n_0)$.

If $C = 0$, we have the degenerate case ($k_s n_0/N_0 = 1$)

$$\frac{n}{n_0} = \frac{1}{1 + \alpha \cdot N_0 t} \tag{7.5}$$

where $\alpha\ N_0 = \sigma\ v\ N_0 \sim 1/\tau$ (the inverse relaxation time) at low $k_s \sim 0$, (rather $k_s n_0/N_0 = 1$)

$$\frac{n}{n_0} = e^{-\frac{t}{\tau}} \text{ is second degenerated case.}$$

Therefore, in the problem under considering, we define the following two parameters

$$\beta = 1 - (k_s n_0/N_0),\ 1/t = \sigma v N_0 (\text{parameter } \beta \text{ is depended on } k_s \text{ and } n_0/N_0)$$

At last, the decision has the form $\frac{n}{n_0} = \frac{\beta}{e^{\beta \cdot t/\tau} - 1 + \beta}$, $0 \le \beta \le 1$ (case $\beta < 0$ not regarded as then at $t/\tau \to \infty$, $n/n_0 \to const$).

This formula defines a family of similar solutions by parameter β

$n/n_0 = f(t/\tau,\beta)$, lying between two degenerate cases

$$\frac{n}{n_0} = e^{-\frac{t}{\tau}} \text{ and } \frac{n}{n_0} = \frac{1}{1 + t/\tau}. \tag{7.6}$$

At $\beta \approx 1$ ($k_s n_0/N_0 = 1$) sticking particles does not occur $N/N_0 \approx 1$, and the rate of decay of bacteria is relatively high.

At $\beta = 1$ ($k_s n_0/N_0 \approx 1$) is highest sticking, but the rate of decay of bacteria lowest and $N/N_0 \approx n/n_0$; strictly speaking, the parameter β can be changed by changing k_s and n_0/N_0 so that their product does not exceed 16.

Model 2 The model is more physically grounded. Here, the velocity of sticking "particles-killers" is controlled by the parameter τ_0 (characteristic time of sticking). Then the equations

$$\frac{dN}{dt} = -\frac{N}{\tau_0} \rightarrow \frac{N}{N_0} = e^{-t/\tau_0} \tag{7.7}$$

where N_0 is initial concentration.

If $\tau_0 >> t_e$, where (t_e is time of extinction), so $N/N_0 \approx 1 - (t/\tau_0)$. This limit asymptotic law is corresponded to $\beta \sim 1$ ($k_s\ n_0/N_0 = 1$) at first model for it $\frac{N}{N_0} \approx 1 - \frac{k_s n_0 t}{N_0 \tau}$, which shows that $\frac{\tau}{\tau_0} \sim \frac{k_s n_0}{N_0}$.

At $t_e/\tau_0 \rightarrow 0$, $N/N_0 \rightarrow 1$, i.e. no entrainment of nanoparticles.

Here, the first equation describes kinetics of interaction between the nanoparticles and *E.coli* bacteria. The equation is modified by introduction of the Arrhenius factor

$$\frac{dn}{dt} = -\sigma v n N \exp(-E_a n/N) \tag{7.8}$$

where E_a is relative activation energy (than E_a more, the smaller share of "particles-killers" can effect the living cells). The ratio N/n characterizes the "biochemical temperature" (the N/n higher, the more effectively the Arrhenius scheme works).

In this equation, the pre-exponential factor has the same form as in the first model. If we introduce the dimensionless variables $\xi = t/\tau$ and $x = n/n_0$, then the basic kinetic equation

$$\frac{dx}{d\xi} = -x \exp(-a\xi - E_s \frac{n_0}{N_0} x e^{a\xi}). \tag{7.9}$$

However, this equation has no an analytical solutions. Here, as in the Model 1, there are two defining parameter of the problem: the ratio $a = \tau/\tau_0$ of the kinetic characteristic of periods, where $\tau = 1/(\sigma\ v\ N_0)$; and E_a that can be interpreted as the coefficient of sticking k_s in Model 1. Increasing the coefficient k_s (under constant n_0/N_0) is equivalent to increasing the number of nanoparticles sticking to one bacterium (to destroy it) that leads to slowing the total process of extinction.

References

1. H. Siegel, *Metal Ions in Biological Systems. Concepts on Metal Ion Toxicity*, vol. 20 (Marcel Dekker Inc., Basel, 1986)
2. Ph.G. Rutberg, V.A. Kolikov, V.E. Kurochkin, L.K. Panina, A.Ph. Rutberg, J.I.E.E.E. Trans, Plasma Sci. **4**, 35 (2007)

3. E.V. Bogomolova, V.L. Gorjachev, V.A. Kolikov, A.I. Kulishevich, V.E. Kurochkin, L.K. Panina, Ph.G. Rutberg, Ph.G. Julaev, J. Mycol. and Phytopath. **5**, 37 (2003). (in Russian)
4. V.L. Goryachev, Ph.G. Rutberg, V.N. Fedioukovitch, J. High. Temp. **5**, 34 (1996)
5. V.E. Kurochkin, L.K. Panina, G.A. Paramonov, J. Mycol. Phytopath. **25** (1991) (in Russian)
6. O.Y. Sentsova, V.N. Maksimov, J. Adv. Microbiol. 20 (1985) (in Russian)
7. G.M. Gadd, J. New Phytol. **124**, 25–60 (1993)
8. G.M. Gadd, A.J. Griffiths, J. Microbial Ecol. **4**, 303-317 (1978)
9. N.N. Zhdanova, A.I. Vasilevskaya, *Melanin Fungi in Extreme Conditions* (Naukova Dumka Kiev, 1988) (in Russian)
10. V.I. Ivanov-Omskii, L.K. Panina, S.G. Yastrebov, J. Carbon. **4**, 38 (2000)
11. L.K. Panina, V.P. Petranovskii, N.E. Bogdanchikova, *2ndo Congreso Mexicano de Zeolitas Naturales* (Puebla, 2001)
12. I. Sondi, B. Salopek-Sondi, J. Colloid Interface Sci. **1**, 275 (2004)
13. V.A. Kolikov, V.E. Kurochkin, L.K. Panina, Ph.G. Rutberg, Doklady Biol. Sci. **403** (2005)

Chapter 8
Interaction of the WDN with Biological Objects

Abstract There are many reasons to suppose that the interest to the nanoparticles will have remain for a long time, and the first one is that the nanoparticles have unique properties due to their intermediate state between atom-molecular and condensed matter. Object of investigation was the interaction of nanostructures water dispersions and biological objects—standard human blood serum and chicken egg white lysozyme. Measurements of nanostructures (from here and then monomers are smallest oxide nanoparticles, clusters are nanoparticles aggregations, supramolecular complexes are aggregations of nanostructures, albumins, and lipoproteins) sizes by means of the laser correlation spectrometer of quasi-elastic light scattering were carried out. Except laser correlation spectrometer at investigation, transmissive electronic microscopy, and atomic force microscopy were used. Interactions of nanostructure of all investigated metals with blood serum are of same type and have differed only quantitatively. These distinctions are connected with sizes of nanostructures aggregates. Correlation between patient state and blood properties allows us to suppose potential diagnostic significance of new integral characteristics of patient state, characteristic radii of nanoparticles-serum components complex formed. Obtained results and data available from publications, lead us to possibility of using such nanostructures for diagnosis of some conformational diseases.

8.1 Interaction of the WDN with Blood Serum

Measurements of these nanostructures sizes were carried out by means of the laser correlation spectrometer of quasi-elastic light-scattering. Additionally to this unit, the transmissive electronic microscopy and atomic force microscopy were used.

Samples of the blood serum were exposed for 30 min under room temperature. The blood clots were separated by centrifugation at 3,500 g within 15 min. After that, the serum samples were diluted 20 times by a standard isotonic phosphatic buffer with ionic force corresponding to the solution of 150 mM NaCl.

Chicken egg white lysozyme (CEWL) solution was prepared in 25 mM by the TrisHCl buffer (pH 7.0) with the final CEWL concentration 1 mg/ml. This solution was used for incubation with nanoparticles dispersions (that was diluted 2 times).

V. Kolikov and P. Rutberg, *Pulsed Electrical Discharges for Medicine and Biology*, Biological and Medical Physics, Biomedical Engineering,
DOI 10.1007/978-3-319-18129-5_8

Protein + nanostructures mixtures were incubated for 1 h at room temperature with gentle stirring.

During the investigation, the main attention was paid to Ag, Pt, and Cu nanostructures. AFM examination of the smallest Ag nanoparticles shows that some of them are clusters (Fig. 8.1).

As well as Ag, Pt also forms clusters of various sizes. However, adhesion of the Pt nanoparticles is weaker than of the Ag ones.

Figure 8.2 shows that the Pt "monomers" are almost absent and the clusters size is not larger than 10 nm.

The Cu clusters are largest and steadiest ones among the investigated nanostructures. Nanoparticles in the Cu clusters are gathered as a "bunch of grapes" and their size achieves up to 600–1,000 nm (Fig. 8.3).

Distributions of nanostructures in size are polydispersity and have from three to five characteristic peaks: ~10, 30–100, 100–200, 400–1000 nm; and in the region larger than 1,000 nm (Fig. 8.4).

As well as many other tissue liquids, the blood serum is a solution with high concentration of macromolecules, basically, proteins. In such solutions, formation of macromolecular complexes of various sizes and various degree of stability takes place. These complexes can be formed since of both relatively weak noncovalent interactions and of strong specific interactions, for example, such as the antigen-antibody interactions resulting in formation of the immune complexes.

Such immune complexes can have either normal physiological character, or can be basis for appearance of pathological conditions. For example, it happens in the case of superfluous formation of the immune complexes [1] or beta-amyloid oligomers under the Alzheimer disease [2]. Registration of such complexes formed in biological systems can be a model for study of nanostructures effect on biological systems. It can give useful information on many normal and pathological processes in a human organism.

Figure 8.5a shows that in distributions of particles in a standard blood serum, there were mainly components with three hydrodynamics radius (R_h): 9–10, 30–40, and 130–160 nm. In Fig. 8.5a is distribution of particles in standard blood serum, (b) is distribution of serum with nanostructures of Ag, (c) is distribution of serum with nanostructures of Cu, and (d) is distribution of serum with nanostructures of Pt.

The first peak corresponds, basically, to the albumin and antibodies, second one to the low-density lipoproteins, and third one to the immune complexes.

Registration of such complexes formed in biological systems can be a model for study of nanostructures effect on biological systems. It can give useful information on many normal and pathological processes in a human organism.

After adding the nanostructures dispersions into a standard blood serum, two groups of particles with large R_h have appeared; in the first group, R_h was ~500 nm, and in the second one R_h is larger than 1,000 nm (Fig. 8.5b–d). Forming of supramolecular complexes of serum components and nanostructures lasts up to 40th min.

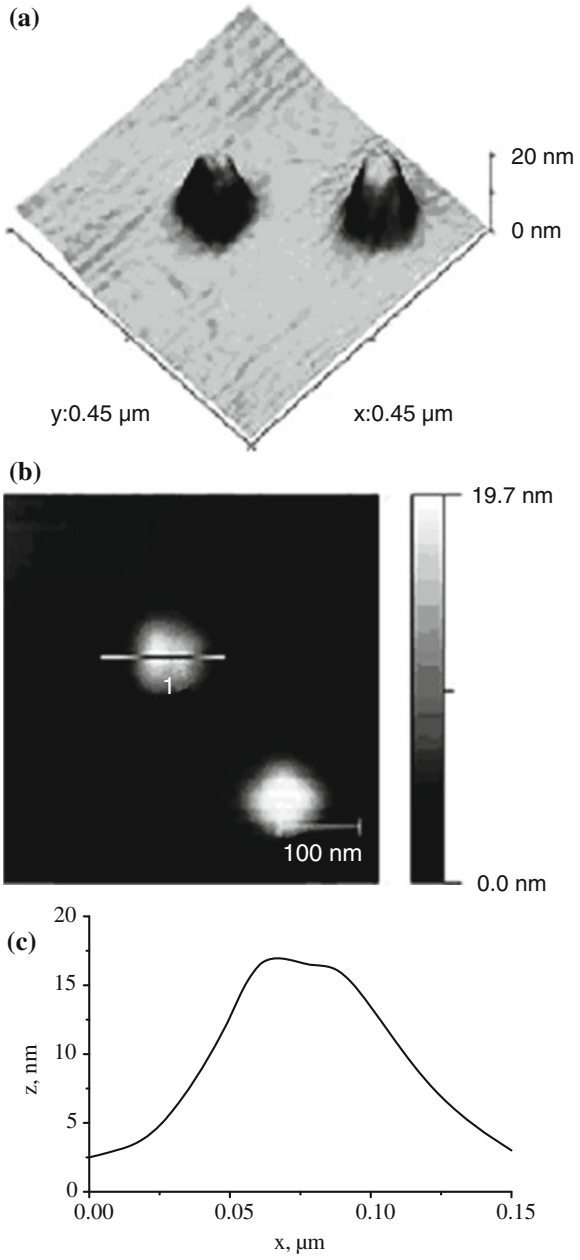

Fig. 8.1 3D image (**a**), 2D image (**b**) and profiles (**c**) of Ag clusters [24]

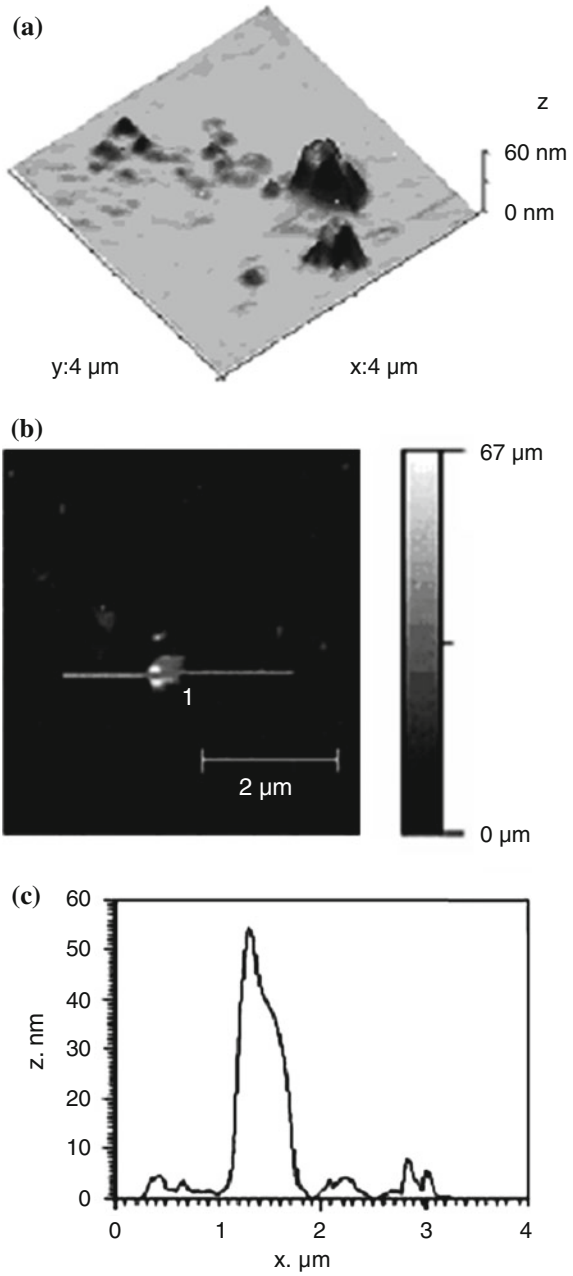

Fig. 8.2 3D image (**a**), 2D image (**b**), and profiles of Pt clusters (**c**) [24]

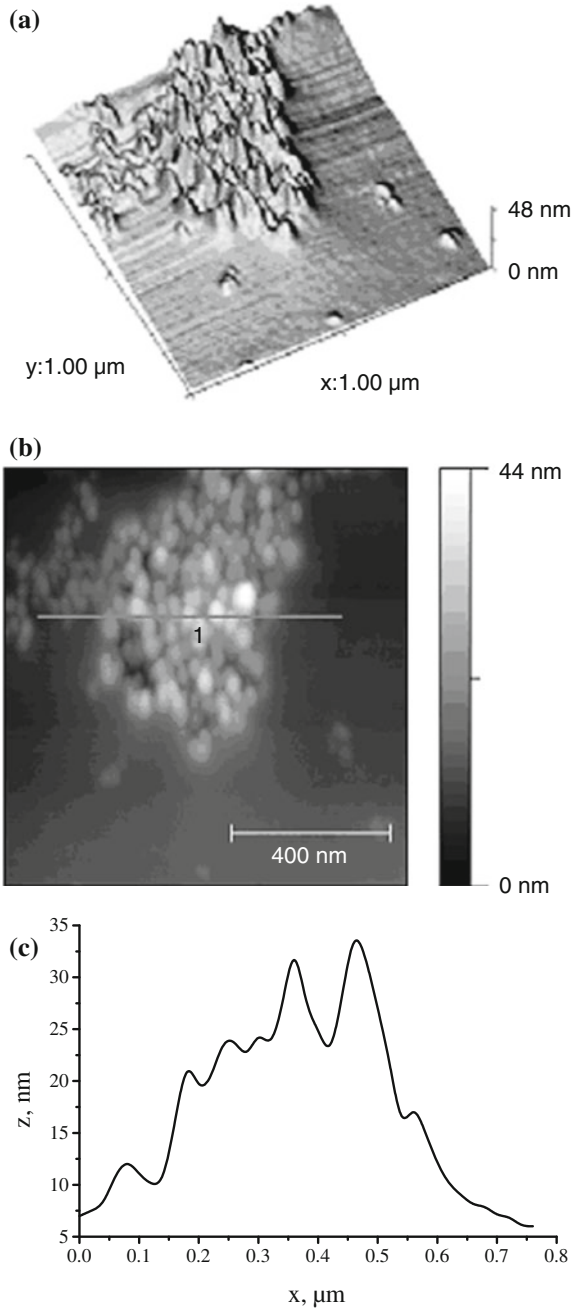

Fig. 8.3 3D image (**a**), 2D image (**b**) and profiles (**c**) of "bunch of grapes" type Cu cluster [24]

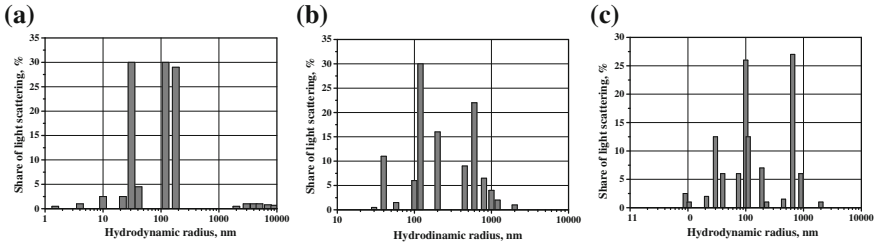

Fig. 8.4 Distribution of Ag (**a**), Cu (**b**), and Pt (**c**) nanostructures [24]

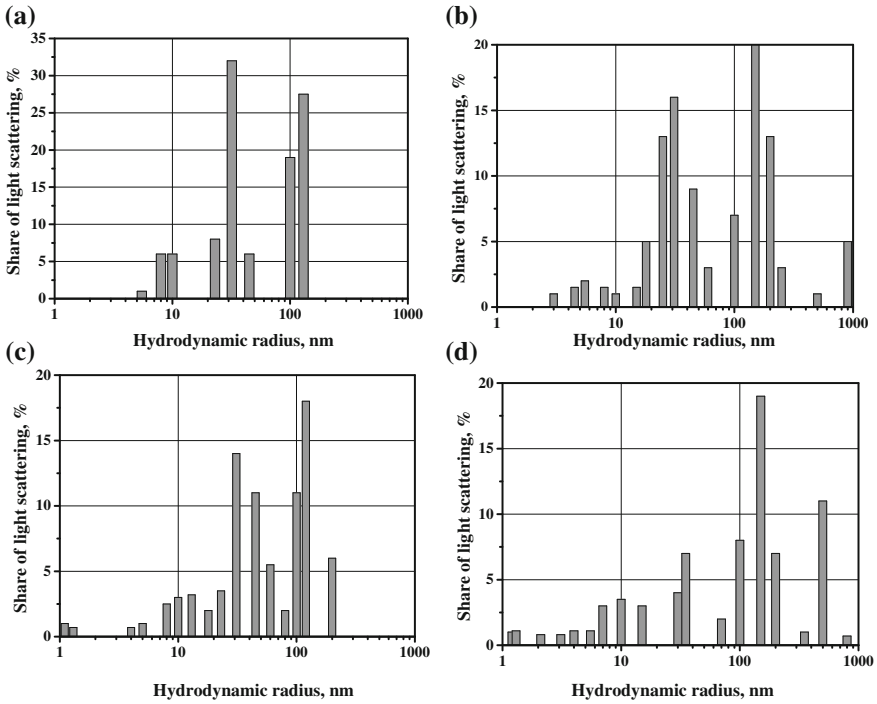

Fig. 8.5 Nanoparticles interaction with the human blood serum [24]

8.2 Interaction of the WDN with Lysozyme

Previously, special conditions were found, under which the lysozyme in water solution is in the form of a monomer of single particle with the $R_h \sim 2$ nm. Then to determine peculiarities of the protein—nanostructures interaction, we used the lysozyme solution (in distilled water as a control sample) and mixtures of the lysozyme and nanostructures dispersions of the Ag, Cu, and Pt.

Series of experiments were performed 4–9 times. There was significant difference in the hydrodynamic radii spectra of all nanoparticles after incubation with lysozyme. The most indicative difference was observed in the mixture "Ag nanoparticles—lysozyme". Average R_h values and root-mean-square deviations for this mixture are presented in Table 8.1.

Figure 8.6 shows the distributions of lysozyme (a), Ag nanoparticles used for this experiment (b), and supramolecular complexes of Ag in mixture (c).

Figure 8.7 shows the TEM-images of the Ag, Cu, and Pt nanostructures (Fig. 8.7a, d, g) and their supramolecular complexes. In Fig. 8.7a–c are nanostructures and supramolecular complexes of Ag, (d–f) are nanostructures and supramolecular complexes of Cu, and (g, h, i) are nanostructures and supramolecular complexes of Pt. (a, d, g) are nanostructures themselves; (b, e, h) are supramolecular complexes, (c, f, i) are supramolecular complexes after negative contrasting by SPM. Horizontal lines of 50 nm.

The TEM-images (Fig. 8.7b, e, h) show blurred outline of the oxide nanostructures, which is a protein layer on the nanostructures surface.

After negative staining, white aureoles around nanostructures have appeared, the aureoles are opaque for electron beam (Fig. 8.7c, f, i).

Interactions of nanostructures of all investigated metals with blood serum are of same type and differ only quantitatively. These distinctions are connected with sizes of the nanostructures aggregates.

Correlation between patient state and blood properties allows us to imply potential diagnostic significance of new integral characteristics of the patient state

Table 8.1 Average R_h and root-mean-square deviations for the mixture "Ag nanoparticles—lysozyme"

Substances	R_h, nm				
Peak number	1	2	3	4	5
Lysozyme	2.0 ± 0.07	–	–	–	–
Ag	–	5.1 ± 0.20	16.1 ± 1.18	71.2 ± 4.19	428.0 ± 4.29
Lysozyme + Ag	2.0 ± 0.05	6.6 ± 0.13	26.6 ± 1.5	109.2 ± 5.61	521.9 ± 7.3

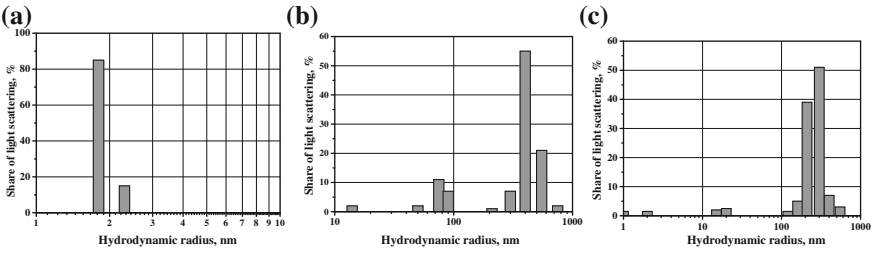

Fig. 8.6 Interaction of the Ag nanoparticles with the lysozyme [25]

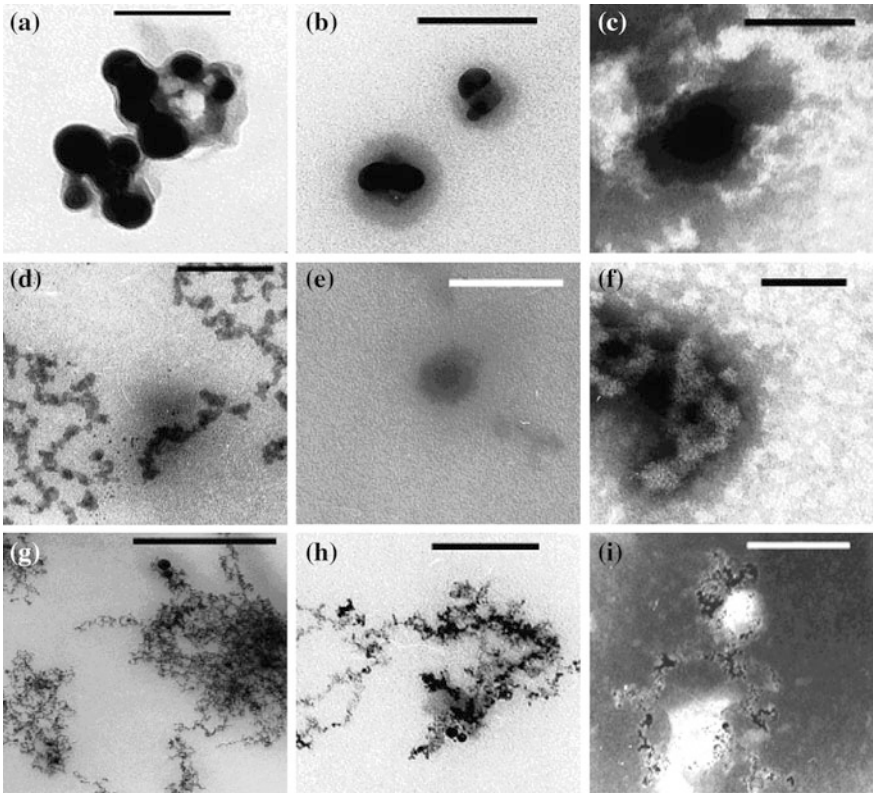

Fig. 8.7 TEM-images of the nanostructures and supramolecular complexes [25]

and characteristic radii of nanoparticles-serum components in their formed complex.

Obtained results and data available from publications give us possibility of using such nanostructures for diagnosis of some conformational diseases.

8.3 Interaction of the Magnetic Nanoparticles and Yeasts' Cells

Investigations show that water dispersions with the Fe nanoparticles are not only bactericidal medium, but also, the magnetoactive agents for modifying the micro-organisms' cells for their further transportation or concentration [3].

New directions in medicine and biotechnology can be provided due to recent advances in nanotechnology and bioengineering, in particular, by adsorption of nanoparticles by living cells [4–6].

A special place in these directions is occupied by the nanoparticles, which are sensitive to both magnetic and electromagnetic fields. In medical and biological researches in addition to quantum dots, application of the magnetic nanoparticles are most promising in terms of versatility and easiness of implementation in visualization of the cellular and sub cellular sites.

Nowadays, the magnemite and magnetite nanoparticles (encapsulated into a chemically inert matrix, for example, into a silicate one) are used for hyperthermia treatment of tumors, namely, by means of their heating with the eddy currents [7]. The magnetic nanoparticles are also used in polymer shells sewn in or adsorbed by chemical agents. Thus, if the agents use specific antibodies, then the magnetic nanoparticles carriers play the role of labels and can be visualized by the light or electron microscopy [8].

On the other hand, if a chemical agent is used as a drug component, then the hyperthermia can induce its release from the polymer matrix as a result of the phase transition. The property of magnetic nanoparticles to move under the effect of magnetic field can be used for directed transportation, deposition, and concentration in a given area [9, 10].

Regardless of a method used for producing nanoparticles, it is necessary to prevent them from sticking to each other and to the environment. For this purpose, the magnetic nanoparticles are coated with various materials such as precious metals or silica [11, 12].

For the coating, the following polymers are preferred: polyethylene glycol, polyvinylethanol, polyvinylpyrrolidone, fatty acids, and others. Using them, you can, firstly, modify the surface chemical groups to attach a variety of agents and, secondly, to ensure their biocompatibility [13].

It is shown that the binding of these particles with proteins or nucleotides stabilizes the particles and protects them from action of the proteases and nucleases [14, 15].

In our studies of non-selective capture and concentration of microorganisms, we used the paramagnetic nanoparticles (without envelopes) consisting of Fe_2O_3 and Fe_3O_4. The magnetic nanoparticles are adsorbed onto the surface of yeast *Saccharomyces cerevisiae*, form macroaggregates (Fig. 8.8), and are transported along the magnetic field lines into the desired area (Fig. 8.9). In Fig. 8.9a, b are macroscopic distribution and microscopy image of yeast cells at T = 0; (c, d) are the same at T = 10 min.

Mathematic simulation. There are a number of problems in study of cells modified by the magnetic nanoparticles modified cells and subcellular structures, as well as, of their directed transportation in a magnetic field. Note the following problems:

- what a minimal magnetic moment must a single nanoparticle have?
- what concentration of the magnetic nanoparticles per unit biostructures or what the total magnetic moment of entire biostructure is necessary for their motion in the magnetic field?
- what depth of the "capturing" layer of magnetic nanoparticles must be? etc.

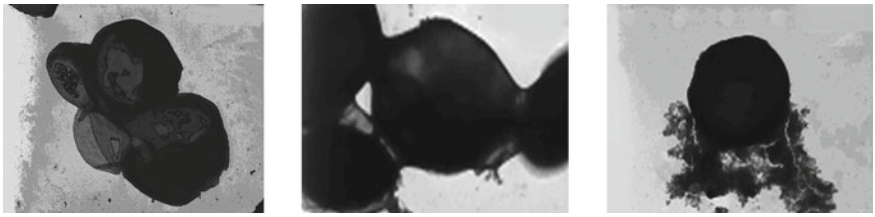

Initial cells. | Cells with nanoparticles. Initial stage of aggregation. | Cells with macroaggregates. Large aggregates.

Fig. 8.8 Cells of *Saccharomyces cerevisiae* yeast with positive contrast (×50,000) [3]

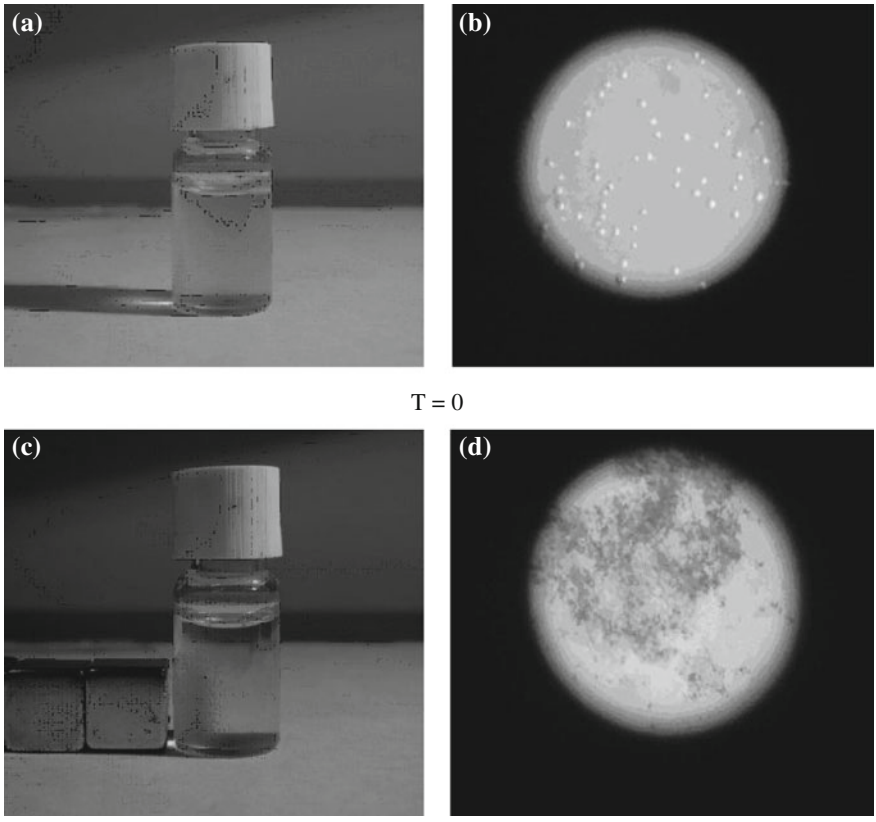

Fig. 8.9 Concentration of the *Saccharomyces cerevisiae* yeast cells modified by the magnetic nanoparticles under the action of magnetic field [3]

Existing models use the magnetohydrodynamic theory describing the behavior of conductive liquids and gases [16, 17]. In our case, it is necessary to develop a model describing the motion of a single magnetic nanoparticle and molecular—cellular objects with the magnetic nanoparticles attached to them. Moreover, it is necessary to study the most common variants of the model that allow one to describe the processes occurring at the same time during sedimentation and magnetic trapping.

The main assumption in such a model is continuity of the medium defined by the Knudsen number much smaller than one.

To describe the water nanoparticles dispersion behavior under the effect of a magnetic field, the following equations are required:

- One equation of continuity for fluids and particles
- Continuity equation for the whole dispersion
- Navier-Stokes equations for fluid
- Equation of the particles motion
- Equation of the diffusion flux
- Heat equation

In the case of application of a magnetic field, it is necessary to take into account (in the Navier-Stokes equations) the volumetric mass forces acting onto the fluid that are stipulated by the particles and magnetic field. Further, it is necessary to add equations describing the conduction currents in the fluid and changes that they cause in the magnetic field. At last, equation of the particles' motion should include the following volumetric forces: inertia, added mass, Basset-Boussinesq viscous friction, buoyancy, gravity, and magnetic ones [18–20].

Note that the nanoparticles (that are smaller than 50 nm and consisting of a ferromagnetic material) interact strongly with the magnetic field like a paramagnetic ion with an unusually large spin and without possessing the hysteresis. Changes in the temperature cause fluctuations of the magnetic moment of a particle and are described by the Langevin function. Magnetization of the nanoparticles can be more than of one domain, but the magnetic nanoparticles carrying only a single-domain are also described by the Langevin function subjected to its spherical shape and uniform filling of the volume [21]. Such particles of the iron oxides were used to modify the surface of cells and to communicate with biomolecules as specific magnetic labels and carriers for targeted drug delivery. Distribution of the particles concentration corresponds to the usual equation systems for diffusion—convection that have quasi-periodic solutions.

The magnetic moment of an ensemble of such particles

$$\vec{M} = \frac{4}{3} N_n \pi r_n^3 M_s L\left(\frac{4\pi r_n^3 M_s B}{3kT}\right)\frac{\vec{B}}{B} \tag{8.1}$$

where N_n is number of nanoparticles in the ensemble, r_n is radius of nanoparticles, M_s is scalar value of the magnetic saturation of material is a single-domain particles,

k is Boltzmann constant, T is absolute temperature, $\overrightarrow{B}$ is magnetic field, B is strength of magnetic field, $L(\xi) = cth(\xi) - \frac{1}{\xi}$ is Langevin function.

When the water is pure, the magnetic field can be considered as irrotational. Under this assumption, the magnetic field has no effect onto the fluid and the expression for its interaction with the magnetic nanoparticles

$$\vec{F}_M = \nabla_B(\vec{M} \cdot \vec{B}) \tag{8.2}$$

The diffusion flux is expressed based on the Fick's first law and the ratio of the Einstein-Stokes equation [22, 23]

$$\vec{j} = \frac{kT}{6\pi r\eta} gradn \tag{8.3}$$

where n is concentration of microparticles, r is radius of particle, η is dynamic viscosity coefficient of pure liquid.

In practice, a model is of interest that describes the stationary motion of nanoparticles in a steady, irrotational magnetic field in a stationary fluid under the absence of a temperature gradient.

This physical model can be reduced to a mathematical description of the flow with only one phase of the particles. But such a model needs two equations of continuity, which includes: the diffusion flow and the flow under the influence of directed forces and the particles motion under the effect of viscous friction, buoyancy, gravity, and magnetic force.

In this case, the continuity equation has the form

$$\frac{\partial n}{\partial t} = \frac{kT}{6\pi r\eta} \nabla^2 n - n \cdot div\vec{v} - \vec{v} \cdot gradn \tag{8.4}$$

The expression for the correct translation of the density "cluster" is

$$\rho = \rho_m \left(1 + N_n \left(\frac{r_n}{r_m}\right)^3 \left(\frac{\rho_n}{\rho_m} - 1\right)\right) \tag{8.5}$$

where ρ is recalculated density of cluster, ρ_m is cluster density of material, r_m is radius of the cluster, ρ_n is material density of nanoparticle, r_n is nanoparticle radius, N_n is number of nanoparticles in same cluster.

When flow of the free single-domain nanoparticles is calculated, we suppose that $\rho_m = \rho_n$.

Then the equation of motion

$$\vec{v} = \frac{2r_m^2}{9\eta} \left(\frac{r_n^3 N_n M_s L(\xi) gradB}{r_m^3} + \vec{g}(\rho - \rho_0)\right) + \vec{v}_0 \tag{8.6}$$

where g is acceleration of gravity, ρ_0 is density of pure liquid, $\vec{v}_0$ is velocity field of a stationary flow.

From (8.1)–(8.6), we have obtained the equations system describing the nanoparticles motion in water dispersion in a steady, irrotational magnetic field in a stationary fluid under the absence of a temperature gradient:

$$\begin{cases} \dfrac{\partial n}{\partial t} = \dfrac{kT}{6\pi r_m \eta} \nabla^2 n - n \cdot div\vec{v} - \vec{v} \cdot gradn \\ \vec{v} = \dfrac{2r_m^2}{9\eta} \left(\dfrac{r_n^3 N_n M_s L(\xi) gradB}{r_m^3} + \vec{g}(\rho - \rho_0) \right) + \vec{v}_0 \\ \xi = \dfrac{4\pi r_n^3 M_s B}{3kT} \\ \rho = \rho_m \left(1 + N_n \left(\dfrac{r_n}{r_m} \right)^3 \left(\dfrac{\rho_n}{\rho_m} - 1 \right) \right) \end{cases} \tag{8.7}$$

To solve the obtained equations system, it must be supplemented by an equation that specifies the field B if that field is not specified explicitly $B = 3119 \cdot 0.0729^d$, where d is distance from the point magnet (cm).

To solve the equations system (8.7) with the partial differential equation, boundary value problem with boundary conditions of the second kind was posed, where the particle flux across the boundary is zero.

The particles adhesion to the area boundary is assumed to be neglected. The computational area is a hollow vertical cylinder with end and sidewalls thickness of 0.2 cm, height of 10 cm, and diameter of 4 cm.

The boundary value problem is defined by boundaries of this computational area. The magnet is represented as a point source at the center of the cylinder sidewall. Its conditional image in the plane $x = 0$ in the form of the surface values of induction, as well as, the induction profile on the chosen gap are shown in Fig. 8.10, where black point on side surface is the location of a magnet.

We simulated motion of the magnetic single-domain nanoparticles of 30 nm in diameter with the uniform initial volume concentration of 10^9 m^{-3} in the fixed pure water at the temperature of 20 °C. The gravity was taken into account.

Figures 8.11 and 8.12 show the calculated concentration distributions of the single-domain nanoparticles and microbial cells, the modified magnetic nanoparticles at the instants of 1 and 10 min in the form of the surface values in the plane x = 0 and the profile of (A).

In addition, these figures show that some of nanoparticles and cells of microorganisms (that were modified by the nanoparticles) are concentrated at the place of the magnet location.

During investigation, the paramagnetic iron oxides nanoparticles (without membranes) were used for nonselective capturing and concentrating of the microorganisms. The magnetoactive nanoparticles were adsorbed on surface of the

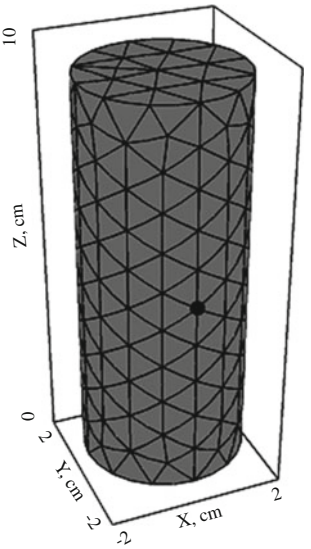

Fig. 8.10 Area under calculation [3]

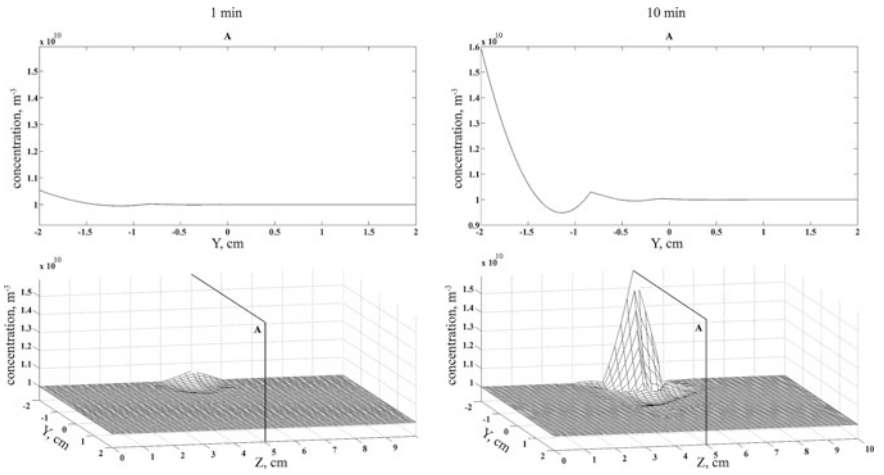

Fig. 8.11 Distribution of concentration of the single-domain particles in 1 and 10 min as a surface of values in a plane x = 0 and a structure (*A*) [3]

Saccharomyces cerevisiae yeast; they formed macroaggregates (Fig. 8.8), and were transported to the required point under effect of the magnetic field (Fig. 8.9).

In our previous simulations, only the magnetohydrodynamic theory was used that describes the behavior of conducting liquids and gases. We had simulated motion both of the single magnetic nanoparticles and of molecule-cellular objects (with the magnetic nanoparticles attached to them).

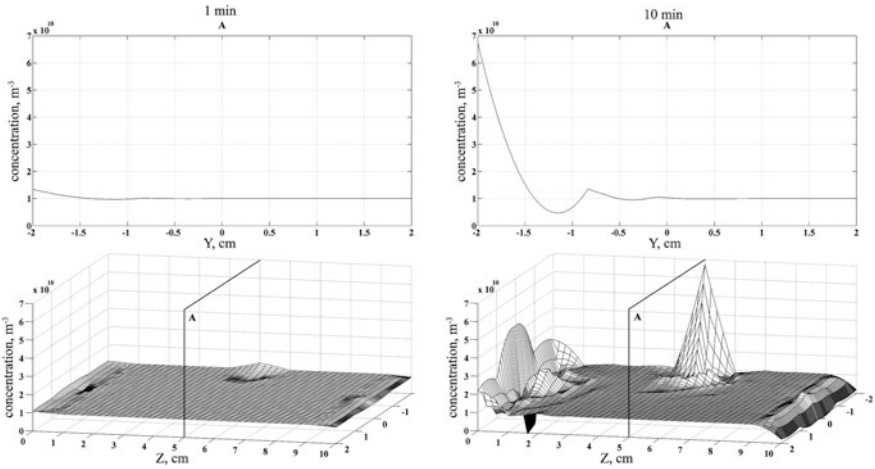

Fig. 8.12 Distribution of concentration of the microorganisms modified by the magnetite nanoparticles in 1 and 10 min as a surface of values in a plane x = 0 and a structure (*A*) [3]

As the basic assumption in this simulation, the continuity of the media (determined by the Knudsen number much less than 1) was adopted. For description of motion of a mixture (of a liquid and nanoparticles) under effect of external forces, the system of equations had been established that describes the stationary motion of the nanoparticles dispersion in the time-constant and magnetic field (without vortices) in the fixed liquid and under absence of the temperature gradient.

References

1. V. Wiwanitkit, J. Ren. Fail. **28**(2), 185 (2006)
2. P. Taboada, S. Barbosa, E. Castro, V. Mosquera, J. Phys. Chem. B Condens. Matter Mater. Surf. Interfaces Biophys. **26**, (2006)
3. F.G. Rutberg, V.A. Kolikov, V.N. Snetov, A.Yu. Stogov, E.G. Abramov, E.V. Bogomolova, L.K. Panina, J. Tech. Phys. **12**, 82 (2012)
4. Q.A. Pankhurst, J. Connolly, S.K. Jones, J. Dobson, J. Phys. D: Appl. Phys. **36**, 167 (2003)
5. O.V. Salata, *Applications of nanoparticles in biology and medicine*. J. Nanobiotechnol. **2** (2004)
6. H. Gu, K. Xu, C. Xu, et al., J. Am. Chem. Soc. Chem. Commun. (2006)
7. D. Weller, A. Moser, J. IEEE. Trans. Magn. **35**(6), 4423 (1999)
8. C. Berry, A. Curtis, J. Phys. D: Appl. Phys. **36**, 182 (2003)
9. A.-H. Lu, E.L. Salabas, F. Schuth, *Magnetic nanoparticles: synthesis, protection, functionalization, and application*. Angew, Chem. Int. Ed. **46**(8), 1222–1244 (2007)
10. C. Lang, D. Schüler, J. Phys. Condens. Matter. **18**, 2815 (2006)
11. J. Hong, P. Gong, D. Xu et al., J. Biotechnol. **128**, 597 (2007)
12. W. Tan, K. Wang, X. He et al., J. Med. Res. Rev. **5**, 24 (2004)
13. V.I. Shubayev, T.R. Pisanic II, J. Sungho, J. Adv. Drug Delivery Rev. **6**, 61 (2009)
14. X.X. He, K. Wang, W. Tan et al., J. Am. Chem. Soc. **125**, 7168 (2003)

15. M.-H. Liao, D.-H. Chen, J. Biotech. Lett. **23**, 1723 (2001)
16. I.M. Kirko, G.E. Kirko, *Magnetohydrodynamics. Modern Vision Problems*, (Moscow-Izhevsk, 2009)
17. S.I. Syrovatsky, J. Physics-Uspekhi 3, LXII (1957) (in Russian)
18. L.D. Landau, E.M. Lifshitz, *Theoretical Physics, vol. VI, Hydrodynamics*, (FIZMATLIT, Moskow, 2001) (in Russian)
19. Y.A. Nevsky, A.N. Osiptsov, J. Tech. Phys. Lett. **7**, 35 (2009) (in Russian)
20. L.I. Sedov, *Continuum Mechanics* (Nauka, Moscow, 1976) (in Russian)
21. M.I. Shliomis, J. Physics-Uspekhi, 112 (1974) (in Russian)
22. J.K. Betchelor, *Introduction to Fluid Dynamics*, (SIC "Regular and Chaotic Dynamics", 2004)
23. L.D. Landau, E.M. Lifshitz, *Theoretical Physics* (PHYSMATLIT, Moscow, 2001)
24. P. Rutberg, V. Kolikov, V. Snetov, A. Stogov, L. Noskin, S. Landa, A. Arutjuman, V. Egorov, A. Sirotkin, J. High Temp. Mater. Proc. **3**, 13 (2009)
25. F.G. Rutberg, V.A. Kolikov, V.N. Snetov, A.Y. Stogov, E.G. Abramov, E.V. Bogomolova, L. K. Panina, J. Tech. Phys. **12**, 57 (2012)

Chapter 9
WDN and Living Beings

Abstract This chapter describes results of study of the impact (of the WDN produced by the PED) onto living organisms Goryachev et al. (Electro Med 99, First International Symposium on Nonthermal Medical/Biological Treatments Using Electromagnetic, 1999). In order to clarify and justify possibility of using the WDN as a portable water and medical agent, investigations on the experimental animals have been performed in the following areas:

- Impact of the WDN on biochemical systems and internal organs
- Impact of the WDN on antioxidant protection
- Impact of the WDN on endocrine system and intestinal microflora
- Impact of the WDN on immune system
- Estimation of genotoxicity and mutagenicity of the WDN

Aim of study was to investigate impact of WDN on biochemical systems and internal organs of rats at short (4-times day after day) intravenous and long-term (up to 3 months) use as the sole source of drinking and comprehensive study of state of basic physiological and biochemical systems by the activity of serum blood enzymes, by the content in serum blood of metabolites, and according to the morphological studies in long-term use by animals of WDN as the sole source of drinking and at its short-term intravenous injection. Study in accordance with available publications and methodic guidelines was performed.

9.1 Impact of the WDN on Biochemical Systems and Internal Organs

The aim of study was to investigate the WDN impact onto biochemical systems and internal organs of rats. The WDN was used as follows: by short (4-times per day after day) intravenous injections and by long-term (up to 3 months) drinking as the only source [1].

V. Kolikov and P. Rutberg, *Pulsed Electrical Discharges for Medicine and Biology*, Biological and Medical Physics, Biomedical Engineering,
DOI 10.1007/978-3-319-18129-5_9

Comprehensive study of state of the basic physiological and biochemical systems was implemented. Here, we estimated the following morphological parameters: activity of the serum blood enzymes, the content of metabolites in the serum blood.

This study was performed in accordance with available publications and methodic guidelines.

The study was performed on male rats of initial weight of 160–180 g; the animals were housed in standard vivarium conditions. Experiments were performed on 3 groups of rats. Animals of the first group were injected intravenously through a day 4-times day. The saline solution of 0.9 % with a dose of 0.5 ml was applied that was prepared by using the WDN. The check animals were injected intravenously by the same dose of the saline solution prepared with the distilled water. Animals of the second and third groups used the WDN as the only source of drinking without limitation for 4 and 12 weeks, respectively.

During the experiment, the following indices were estimated: general conditions of the rats, their behavior in the herd, the attitude to food and water, condition of the coats, visible mucous membranes, and dynamics of the body weight.

After completion of the WDN delivery, the animals were placed for 24 h in the metabolic cages for selection of daily urine. Measurement of daily diuresis and microscopy of sediment were implemented. Then the rats were decapitated and the blood smears were prepared for counting of the blood cell.

The resulting serum was investigated by means of the standard spectrophotometry methods using the analyzer "Spectrum".

The activity of the following indices was determined: the alanine aminotransferase, aspartate aminotransferase, alkaline phosphatase, lactate dehydrogenase, creatine kinase, cholinesterase, lipase, trypsin and trypsin inhibitor, the content of triglycerides, creatinine, total protein, and the urea nitrogen.

Basing on concentration of malondialdehyde, the content (in serum) of products reacting with thiobarbituric acid was estimated by the M. Uchiuama and M. Michara method. The content of reduced glutathione was measured by the J. Seldak and R.M. Linday method.

The parametric Student *t*-test was applied to determination of differences value between the compared indicators. Differences in the compared groups of animals were considered as reliable under 95 % level of significance ($p < 0.05$).

After the slaughter of animals, autopsy was carried out for macroscopic analysis of their internal organs. For histological examination, samples of the liver and small intestine were fixed by the 10 % formalin solution and than filled with paraffin. The paraffin sections were stained with the hematoxylin-eosin. Moreover, the frozen liver sections were stained to determine fatty inclusions by the Sudan IV unit.

Table 9.1 presents the data on impact of the short-term intravenous injection of the WDN onto the biochemical indices of the rats' blood in Group 1.

As it is seen from the table, the short-term intravenous injections of the WDN are not accompanied by changes in the enzymes activity. These data provide a conclusion of absence of any express damaging impacts of the WDN onto the structure of the parenchymal organs: liver, myocardium, pancreas, skeletal muscle, and brain. The normal state of the protein-synthesizing activity of the liver shows no changes

Table 9.1 Data on impact of the short-term intravenous injection of the WDN onto the biochemical indices of the rats' blood

Indices	Check	Test
Triglycerides (mmol/l)	1.06 ± 0.18	1.6 ± 0.43
Creatinine (mmol/l)	68.1 ± 2.5	64.6 ± 4.2
Total protein (g/l)	64.5 ± 1.4	68.6 ± 1.4
Alanine aminotransferase (U/l)	70.6 ± 6.4	80.4 ± 14.5
Aspartate aminotransferase (U/l)	230.8 ± 16.5	247 ± 9.6
Alkaline phosphatase (U/l)	372 ± 52	396 ± 93
Lactate dehydrogenase (U/l)	2,269 ± 213	2,170 ± 155
Creatine kinase (U/l)	5,194 ± 384	4,922.6 ± 911
Urea (mmol)/(g × l)	3.4 ± 0.6	3.5 ± 0.5
Trypsin (mmol)/(g × l)	0.48 ± 0.1	0.64 ± 0.14
Trypsin inhibitor (mmol)/(g × l)	32.4 ± 1.1	31.9 ± 1.6
Lipase (%)	8.4 ± 2.5	10.0 ± 2.6
Cholinesterase (mmol)/(g × l)	0.22 ± 0.17	0.73 ± 0.21
Malondialdehyde (μmol/l)	4.2 ± 0.29	5.48 ± 0.34[a]
Reduced glutathione (mmol/l)	26.95 ± 2.55	18.96 ± 1.74[a]

Note [a]reliable difference from control (at $p < 0.05$)

in the serum protein content. Moreover, the normal levels of creatinine in the serum and urea lead to conclusion that there is no disorder in the detoxifying function of the liver and in the renal excretory function.

It is interesting to note that intravenous injection of the WDN was accompanied by increase in the blood serum of content of final product of the lipid peroxidation and malondialdehyde by 30 % above the average value. Apparently, the increase in this index represents that the WDN under the intravenous injection has, in particular, pro-oxidant activity, which leads to initiation of the free radical reactions. In addition, this is evidenced by decrease in the serum of the reduced glutathione concentration by 40 %.

The data on analysis of the rats' daily urine of this group are shown in Table 9.2.

These data indicate that intravenous injection of the WDN changes the alkaline urine reaction to the acidic one and reduces content of the protein, leukocytes, and erythrocytes. Presence of the triplephosphats in urine after intravenous injection of the WDN had not been detected. Thus, under intravenous injection of the WDN, the "purifying" effect is manifested.

The data on elements of the rats' blood of Group 1 are shown in Table 9.3.

The data indicate that intravenous injection of the WDN does not change the blood. From autopsy of rats of the experimental and check groups, any differences in macroscopic picture of the internal organs have not been detected. The rats' lungs of the experimental group were airy and pale pink. The heart size did not differ from the normal one. The heart muscles were moderately dense and of the brownish color. The liver capsules were thin and transparent. The liver surfaces were smooth and of the dark brown color. Consistency of the liver parenchyma was moderately

Table 9.2 Data on the rats' daily urine

Indices	Check	Test
Protein (g/l)	0.16	0.099
White blood cells in field of view	35–40	3–5–7
Erythrocytes in field of view	3–5–8	3–5–8
Salts	Tripelphosphates	–
Reaction	Alkaline	Acidic

Table 9.3 Data on elements of the rats' blood

Indices	Check	Test
Stab white blood cells (%)	0.5 ± 0.5	0
Segmented leukocytes (%)	30.5 ± 5.5	39 ± 12
Eosinophils (%)	1	0.5 ± 0.5
Monocytes (%)	7 ± 1	4.5 ± 0.5
Lymphocytes (%)	60.5 ± 6.5	56 ± 11

dense. The kidney capsules were easily removed, thin, and transparent. The kidney surfaces were smooth and had the grayish-brown color. In sections of the kidney body, the cortex and medulla stood out distinctly. The stomachs were of the normal size. The mucous membranes of the stomach body were folded, shiny, and of the pale pink color.

Under histological examination of the liver sections stained by the Sudan IV unit, there were no signs of fatty degeneration. When viewing the paraffin sections of liver stained by the hematoxylin-eosin, the degenerative changes were not found. Cytoplasm of the hepatocytes is oxyphylic one. Nuclei of these cells were clear with sufficient content of chromatin. Signs of degeneration of the nuclear structures were not detected.

Microimage of structure of small intestine of the rats in Group 1 is presented in Fig. 9.1.

Microimage of the rats liver structure in Group 1 is represented in Fig. 9.2. In the histological examination of sections of small intestine of the rats injected intravenously by the WDN, any epithelium defect is not detected. The enterocytes nuclei were clear. The hyperemia or inflammatory infiltration were absent. Structure of the small intestinal mucosa of rats in the experimental group did not differ from the control one.

In observation of state of the rats injected intravenously by the WDN, any abnormalities are not detected. The rats' attitude to food and water did not change. State of the visible mucous membranes and coat was without peculiarities. Any abnormal behavioral responses were absent.

Thus, according to performed studies, one can conclude that the short intravenous injections of the WDN do not lead to appearance of any pathological reactions in the rats organisms. However, it should be noted that the treatment of the PED water leads to its moderately expressed pro-oxidant properties.

The data on biochemical indices of the blood serum of rats used the WDN as the only source of drinking for 1 month (Group 2) are shown in Table 9.4.

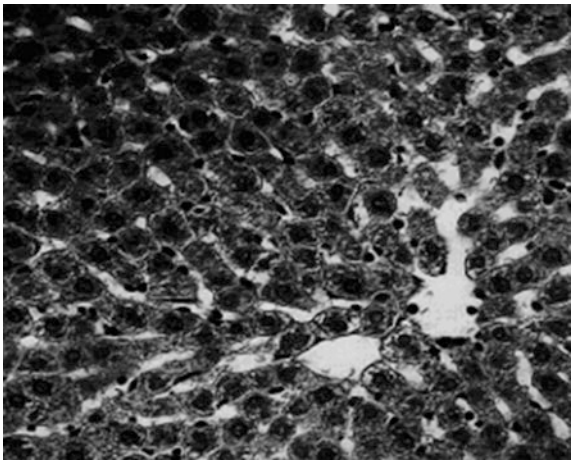

Fig. 9.1 Structure of the rats' liver in Group 1 (×140)

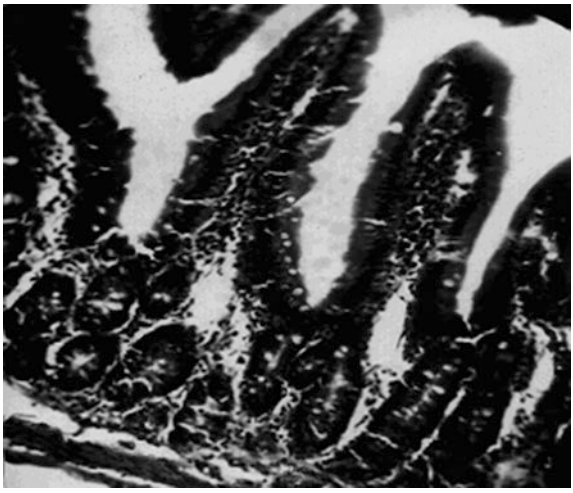

Fig. 9.2 Structure of small intestine of the rats in Group 1 (×280)

These results indicate that there is no effect of the long consumption of the WDN onto the enzymes activity and onto the metabolites content in the serum. This reflects absence of the WDN damaging effect onto the basic physiological systems of the rats' organisms.

From the data presented in Tables 9.5 and 9.6, it is seen that consumption of the WDN by rats for 1 month had not noticeable effect on the results of clinical analysis of the urine and blood cell composition.

During the observation period, the body weight gain of animals in the experimental group was almost same as that of rats in the check group (18 and 14 %, respectively, Table 9.7).

Table 9.4 Data on biochemical indices of the blood serum of rats used the WDN as the only source of drinking water for 1 month

Indices	Check	Test
Triglycerides (mmol)/l	0.5 ± 0.1	0.8 ± 0.2
Creatinine (mmol)/l	51.3 ± 4.4	45.3 ± 5.4
Total protein (g/l)	74.5 ± 1.4	72.3 ± 2.7
Alanine aminotransferase (U/l)	78.4 ± 9.2	83.6 ± 13.7
Aspartate aminotransferase (U/l)	231.6 ± 17.4	258.4 ± 19.1
Alkaline phosphatase (U/l)	421 ± 36	508 ± 103
Lactate dehydrogenase (U/l)	2,175 ± 111	2,061 ± 244
Creatine kinase (U/l)	4,586 ± 263	3,862 ± 452
Urea (mmol)/(g × l)	3.22 ± 0.16	3.12 ± 0.29
Trypsin (mmol)/(g × l)	0.21 ± 0.05	0.35 ± 0.05
Trypsin inhibitor (mmol)/(g × l)	22.8 ± 2.1	20.8 ± 2.0
Lipase (%)	22 ± 2	17.4 ± 0.6
Cholinesterase (mmol)/(g × l)	0.55 ± 0.19	0.39 ± 0.2
Malondialdehyde (μmol)/l	5.26 ± 0.25	5.24 ± 0.45
Reduced glutathione (mmol)/l	21.5 ± 5.8	17.5 ± 5.3

Table 9.5 Effect on the urine and blood cell composition

Indices	Check	Test
Protein (g/l)	0.06	0.099
White blood cells in field of view	3−4−5	5−8−10
Erythrocytes in field of view	–	1
Salts	Tripelphosphates	Tripelphosphates
Reaction	Alkaline	Acidic

Table 9.6 Effect on the urine and blood cell composition

Indices	Check	Test
Stab white blood cells (%)	2 ± 0	0[a]
Segmented leukocytes (%)	28.5 ± 4.5	26.5 ± 2.5
Eosinophils (%)	3 ± 3	2.5 ± 2.5
Monocytes (%)	6.5 ± 1.5	3.5 ± 1.5
Lymphocytes (%)	60 ± 6	67.5 ± 1.5

Note [a]reliable difference from control (at $p < 0.05$)

Table 9.7 The body weight gain of animals in the experimental group

Weight indices	Check	Test
Before test (g)	182.5 ± 2.7	166.2 ± 5.5
After 1 month (g)	207 ± 4.5	196 ± 8.2
Weight gain (%)	14	18

The WDN application for 1 month had no effect on the macroscopic picture of internal organs and did not lead to changes in structure of the hepatic parenchyma and walls of small intestine. Because of absence of the histological changes in the liver and small intestine, their micro images are identical to ones shown in Figs. 9.1 and 9.2.

During observation of the animals' condition through all the period of the WDN use, no abnormalities were detected in visible condition of the mucous membranes and coat, attitude to food and water, and behavior of animals in the herd.

Data on the blood biochemical parameters in animals, which used the WDN as the only source of drinking for 3 months (Group 3) are presented in Table 9.8. The data show that long use of the WDN does not result in the norm deviation of the most investigated parameters. This indicates absence of the harmful effects in the important biochemical systems of the rats' organisms and in state of the cellular structures.

The exception was observed in the lipase activity, which was reduced on the average by 30 % in the rat experimental group. Assumption of potential harmful effects of the WDN onto the pancreas secretory function, which could be done basing on this fact, is not confirmed by absence of changes in activity of the trypsin and trypsin inhibitor.

Question is still open on the causes and mechanisms of some decreasing in the lipase activity. The reasons are still unclear of the malondialdehyde decrease (by 18 %) in serum. Note that the malondialdehyde is one of the final products of lipid peroxidation. This fact is not consistent with the trend of reducing the glutathione concentration in serum (with not reaching, however, the level of measuring accuracy).

Table 9.8 Data on the blood biochemical parameters in animals, which used the WDN as the the only source of drinking

Indices	Check	Test
Triglycerides (mmol/l)	1.1 ± 0.1	0.8 ± 0.1
Creatinine (mmol/l)	48.6 ± 5.7	57.2 ± 4.4
Total protein (g/l)	70.3 ± 4.1	79.5 ± 2.3
Alanine aminotransferase (U/l)	135.5 ± 13.9	97.4 ± 10.0
Aspartate aminotransferase (U/l)	203.5 ± 17.6	204 ± 17.3
Lactate dehydrogenase (U/l)	1,235 ± 386	1,824 ± 437
Creatine kinase (U/l)	4,487 ± 287	4,413 ± 366
Trypsin mmol/(g × l)	0.42 ± 0.03	0.33 ± 0.05
Trypsin inhibitor (mmol)/(g × l)	19.1 ± 1.7	19.1 ± 0.7
Lipase (%)	28 ± 2	18 ± 1[a]
Cholinesterase (mmol)/(g × l)	0.59 ± 0.27	1.25 ± 0.35
Malondialdehyde (μmol/l)	4.64 ± 0.2	3.8 ± 0.29[a]
Reduced glutathione (mmol/l)	18.51 ± 5.08	14.78 ± 3.39

Note [a]reliable difference from check (at $p < 0.05$)

However, it should be noted that such a reduction of the glutathione is a reflection of stimulation of the free radical reactions; here, the stimulation leads to the lipid peroxidation and, eventually, to the malondialdehyde accumulation.

These observed changes (mentioned above) in the content of the malondialdehyde and reduced glutathione are not explained until now. However, it should be noted that the changes of malondialdehyde content detected in experimental animals are insignificant in their value, and the changes of reduced glutathione content formally are not reliable.

Analysis of the daily urine and animal blood cells is shown in Tables 9.9 and 9.10.

Data in these tables indicate that use of the WDN for 3 months leads to increase of the protein excretion in urine.

However, the absence of other deviations of the urine indicators and normal level of the creatinine in blood (Table 9.11) show that use of the WDN for 3 months does not damage kidneys and their function state.

Results of analysis of the blood cells show the absence of changes in hematopoiesis during long use of the WDN.

Use of the WDN for 3 months does not effect onto dynamics of the rats body weight, which increase in the rats experimental and check groups was about 50 %.

In macroscopic and histological examination of the internal organs of animals, any abnormalities have not been detected.

At the end of experiment, other indices were also normal; those are general condition of rats, state of visible mucous membranes and hair coat, behavior in the herd, and attitude to food and water.

Data on the biochemical indices of the blood of animals used the WDN as the only source of drinking for 3 months are shown in Table 9.11.

Table 9.9 Data on the daily urine and animal blood cells

Indices	Check	Test
Protein (g/l)	0.066	0.099
White blood cells in field of view	3−4	4–2–5
Erythrocytes in field of view	–	1–2
Salts	Tripelphosphates	Tripelphosphates
Reaction	Alkaline	Acidic

Table 9.10 Data on the daily urine and animal blood cells

Indices	Check	Test
Stab white blood cells (%)	1 ± 1	0
Segmented leukocytes (%)	37.5 ± 10.5	32.5 ± 2.5
Eosinophils (%)	5.5 ± 3.5	5 ± 2
Monocytes (%)	49.5 ± 3.5	55.5 ± 2.5
Lymphocytes (%)	38.5 ± 11.5	32.5 ± 2.5

Table 9.11 Data on the biochemical indices of the blood of animals used the WDN as the only source of drinking

Indices	Check	Test
Triglycerides (mmol/l)	0.9 ± 0.1	0.8 ± 0.1
Creatinine (mmol/l)	47.6 ± 1.7	48 ± 1.3
Total protein (g/l)	81.15 ± 3.11	84.22 ± 3.66
Alanine aminotransferase (U/l)	47.4 ± 2.2	62.2 ± 3.0[a]
Aspartate aminotransferase (U/l)	94.5 ± 12.3	101.8 ± 14.6
Alkaline phosphatase (U/l)	372 ± 52	396 ± 93
Lactate dehydrogenase (U/l)	1,408 ± 369	1,174 ± 393
Creatine kinase (U/l)	5,148 ± 502	4,549 ± 832
Trypsin mmol/(g × l)	0.56 ± 0.07	0.64 ± 0.14
Trypsin inhibitor (mmol)/(g × l)	23.6 ± 2.1	26.1 ± 1.8
Amylase (%)	2795 ± 123	2754 ± 201
Cholinesterase (mmol)/(g × l)	0.68 ± 0,19	0.59 ± 0,11
Malondialdehyde (μmol/l)	4.64 ± 0.2	3.8 ± 0.29[a]
Reduced glutathione (mmol/l)	18.51 ± 5.08	14.78 ± 3.39

Note [a]reliable difference from control (at $p < 0.05$)

These data show that long using the WDN by experimental animals of, as the only source of drinking did not cause any violations in the majority of investigated parameters.

Exception was the alanine activity, which is higher by 30 % than the corresponding index in the check group.

According to the formal criteria, this may indicate of slightly expressed disorder of the liver parenchyma state.

However, no changes in activity of the cholinesterase and total protein were observed, and it allows us to suppose that long use of the WDN has any hepatotoxic effect.

Results of analysis of the blood cells animals are given in Table 9.12.

Data presented in Table 9.12 show no effect of long use of the WDN onto the state of the hematopoietic system of experimental animals.

Results of analysis of the experimental animals' daily urine are presented in Table 9.13.

Here, the data indicate that use of the WDN for 3 months did not cause any violations of the urine indices. Combination of the biochemical data and obtained results shows that there is no damaging effect of the WDN onto the renal function and urinary tracts.

During the use of the WDN by rats, there were no any abnormal behavioral responses in the herd. The normal relationship to food and water was maintained through all the experiment.

In the macroscopic and histological examination of the internal organs and brain, no visible changes were revealed. In addition, such phenomena as the edema, congestive hyperemia, and petechial hemorrhages were not detected. Presence of the exudate in the

Table 9.12 Data on the animals' blood cells at long use of the WDN

Indices	Check	Test
Stab white blood cells (%)	2 ± 1	1 ± 1
Segmented leukocytes (%)	41.4 ± 6.5	39.0 ± 2.5
Eosinophils (%)	6.5 ± 1.5	5.9 ± 2
Monocytes (%)	52.5 ± 3.1	54.4 ± 3.1
Lymphocytes (%)	36.5 ± 8.6	32.8 ± 6.1

Table 9.13 Data on the experimental animals' daily urine

Indices	Check	Test
Protein (g/l)	0.099	0.16
White blood cells in field of view	9–13	10–15
Erythrocytes in field of view	3–5	4–7

pericardial, pleural, and peritoneal cavities were not revealed. The mucous membrane of stomach and small and large intestines had not any macroscopic changes.

Short intravenous injection of the WDN and long (up to 3 months) use of the WDN as the only source of drinking do not have any damaging effect onto parenchyma of the internal organs and state of the main metabolic systems.

Long intravenous injection of the WDN has no damaging effects onto the hematopoietic system.

Short intravenous injection of the WDN is characterized by a moderate, pro-oxidant effect that manifested in increasing the malondialdehyde concentration in the serum of the experimental animals and in reducing the glutathione concentration.

Long use of the WDN has no toxic effects on the animals' organisms.

9.2 Impact of the WDN on Anti-oxidant Protection

Purpose of the research is in study of impact of the WDN (used in the experiment as the only source of drinking) onto generation of the reactive oxygen species and onto state of the anti-oxidant protection system. Investigations were performed in accordance with the references and guidelines. Research results show that use by experimental animals of the WDN for 3 months (as the only source of drinking) did not intensify the free radical oxidation and generation of the reactive oxygen species, and does not effect onto the anti-oxidant protection system. This confirms absence of any pro-oxidant properties of the WDN.

Nowadays, the process of free radical oxidation is widely recognized as a universal mechanism for development of any kind of the pathological state [2–5]. Imbalance of the organism pro- and anti-oxidant systems causes the development of oxidative stress that complicates the disease course. Under these circumstances, mobilization of the anti-oxidant system plays an important role, since it reduces accumulation of the reactive oxygen species and prevents beginning the oxidative stress.

When the anti-oxidant protection is insufficient, the balance of the pro-and anti-oxidant systems is shifted toward the pro-ones. As a result, conditions appear for intensifying the biological macromolecules (nucleic acids, lipids, and proteins), the degradation, damage of cell membranes, and beginning the structurally integrated and functional disorders.

In this connection, the purpose of this investigation was an experimental study of presence of the WDN pro-oxidant capacity (under its use by experimental animals as the only source of drinking) and research of the anti-oxidant protection system.

The study was performed on male rats with the initial weight of ~170 g. The animals were housed in the standard vivarium conditions. The rats used the WDN as the only source of drinking water for 12 weeks without limitation. Animals of the check group used the tap water. Water consumption by rats of the experimental and check groups was recorded daily.

After the experiment completion, the animals were decapitated; and serum (in some cases, plasma) of their blood was obtained and used for analysis.

To identify possible stimulating effect of the WDN onto the processes of the free radical oxidation, the following components in the serum were measured: the protein thiol groups, concentration of the reduced glutathione, and the malondialdehyde content (as one of the final products of the lipid peroxidation).

9.2.1 Determination of Protein Thiol Groups by Amperometric Titration

Reagents

1.	Sodium citrate	3.8 % solution
2.	Sodium chloride	0.9 % solution
3.	Potassium chloride	30 % solution
4.	Silver nitrate	0.001 n. solution
5.	Ammonia buffer	0.2 M, pH 7.4
6.	Electrolyte	4.2 g potassium iodide and 1.3 g doubleiodine mercury in 100 ml of the potassium chloride solution
7.	Gel	3 g of agar in 100 ml of the potassium chloride solution

The test run. The 0.5 ml of serum was introduced into the titration vessel with a magnetic stirrer containing 25 ml of ammonia buffer; the electrode was immersed into the salt solution and titration was started by the silver nitrate solution. Content of the thiol groups in the test solution is equivalent to volume of the silver nitrate spent for the titration and is expressed in μmol/ml of serum.

9.2.2 Determination of Malondialdehyde

Reagents

1.	Tris-HCl buffer	0.025 n., pH 7.4
2.	Trichloroacetic acid	17 % solution
3.	2-thiobarbituric acid	0.8 % solution

The test run. The 3 ml of the buffer was added into 0.5–1.0 ml of serum; and the mixture was shaken for 30 min. Then the protein was precipitated by adding the 1 ml of trichloroacetic acid. The mixture was thermo stated at room temperature for 10 min and then centrifuged under 2,000 rev/min for 10 min. Into 2 ml of supernatant, 1 ml of the 2-thiobarbituric acid was added and the samples were placed into the boiling water bath for 10 min. After cooling the samples to the room temperature, they were photo measured at the wavelength of 532 nm against the check samples.

The malondialdehyde volume was determined (in μmol/l) by the formula: $C = E\ k_e\ V_p/V_s$, where E is optical density of the sample, k_e is molar extinction coefficient (1.56×10^{-5} M cm), V_p is volume of paintable sample, V_s is volume of serum.

9.2.3 Determination of Reduced Glutathione

Reagents

1.	Sulfosalicylic acid	20 % solution
2.	Tris-HCl buffer	0.1 M with 5 mM EDTA, pH 8.5
3.	5.5 = dithiobis-2-2 nitrobenzoic acid	(4 mg/ml of ethanol)

The test run. Into the test-tube, the 0.4 ml of sulfosalicylic acid was added to 0.8 ml of serum; then the mixture was stirred and centrifuged for 10 min under 3,000 rev/min. Into 0.53 ml of supernatant, 0.22 ml Tris-HCl buffer and 24 ml of 5.5 = dithiobis-2-2 nitrobenzoic acid were added. The mixture was stirred and photo measured at wavelength of 412 nm against the check sample. Concentration of the reduced glutathione (in mmol/l) was determined by the calibration curve.

To assess the state of antioxidant system of the rats that for a long time used drinking the WDN, the following parameters of the animals blood plasma were determined and evaluated: the total anti-oxidant activity, activity of superoxide dismutase, the dismutation of superoxide anion-radical O_2 with forming of hydroperoxide H_2O_2, the plasma ability of the subsequent splitting the H_2O_2.

9.2.4 Chemiluminescent Determination of Total Antioxidant Activity

The test run. To estimate the total anti-oxidant activity, we used the riboflavin chemiluminescent reaction with hydroperoxide under presence of the cupric ions. The reaction mixture contained 720 μl of 100 mM phosphate buffer with pH 9, 40 μl of 2.7 mM solution of $CuSO_4 \times 5H_2O$, 40 μl of 53 mM solution of riboflavin, 100 μl of 100 mM H_20_2 solution, and 100 μl of the water bidistillate. An experimental sample contained 100 μl of the blood plasma instead of water. Measuring the lightsum was performed for 1 min at 37 °C. The TAA was expressed in conventional units per 1 mg of protein and was calculated by the following formula: $TAA = (1–L_{ts}/L_{cs})/A_p$, where: L_{ts} is lightsum of test sample, L_{cs} is lightsum of control sample, A_p is protein content in the reaction mixture.

9.2.5 Determination of Activity of Superoxide Dismutase (ASOD) with Quercetin Autooxidation Reaction

Reagents

1. EDTA 5×10^{-4} M
2. Tetramethylethylenediamine (TMED) 0.05 M. Before examining 0.28 ml of 0.05 M TMED was poured into 40 ml EDTA, and the resulting mixture used for analysis—solution number 1
3. Phosphate buffer 0.1 M, pH 7.8
4. Quercetin 1.5 mg dissolved in 10 ml of dimethylsulfoxide

The test run. The incubation medium contains 0.5 ml of the solution number 1, 0.5 ml of phosphate buffer, and 0.1 ml of the quercetin. Into the experimental sample, the material containing SOD (0.02–0.05 ml of plasma) was added. The final volume 3.5 ml of the test and check samples were adjusted by the water bidistillate. The absorbance of the check and test samples at the wavelength of 406 nm was recorded. The quercetin auto-oxidation reaction is carried out for 20 min at the room temperature. After the incubation period, the absorbance was re-recorded and the difference between its initial E_i and final E_f values was calculated. The standard units of ASOD were calculated using the formula: $E_f/E_i–1$.

Standard unit of plasma antioxidant ability of O_2 dismutation is 50 % of the quercetin oxidation inhibition.

9.2.6 Determination of Plasma Ability to the H_2O_2 Splitting

Reagents

1.	Tris-HCl	0.05 M, pH 7.4
2.	H_2O_2	0.01 M
3.	Sodium azide	0.02 M

The test run. For simultaneous analysis, two check and two test samples were prepared. Each test sample is compared with the corresponding check one. The first check incubation medium of 1 ml contained 0.1 of 0.05 M Tris-HCl pH 7.4 and 0.02 ml of the native plasma. The final volume of 2.5 ml was adjusted by the water bidistillate. The experimental sample 1 of 0.1 ml contained 0.05 M Tris-HCl, 0.02 ml of the native plasma, and required volume of water. The reaction was run by adding (only into the test samples) the 1.8 ml of 0.1 M H_2O_2. After incubation for 10 min in the water bath at 37 °C, the absorbance was immediately measured in the check and test samples at the wave length of 230 nm. By comparison of extinction of the check and test samples, the extinction was evaluated that is caused by presence of the hydroperoxide remaining after destruction. For evaluation, the coefficient of the molar extinction 0.071 was used.

The results reflect the total ability of plasma to splitting the H_2O_2. The incubation medium of the check sample 2 and test sample 2 were of 0.1 ml and, in addition, contained 0.05 M Tris-HCl, 0.02 ml of plasma, and 0.4 ml of 0.2 M sodium azide as inhibitor of the enzymes capability to split the hydroperoxide (catalase). The final volume of 2.5 ml was adjusted by the water bidistillate. The reaction was run in the test sample by adding the 1.8 ml of 0.1 M H_2O_2. The samples were incubated in the water bath at 37 °C for 10 min and then their absorbance was immediately measured at the wavelength of 230 nm. The indices obtained were in accordance with non-enzymatic ability of the plasma to split the hydroperoxide. Difference between the results of tests 1 and 2 reflected the plasma enzyme ability to the splitting. The enzymatic ability of plasma was assessed by loss of the hydroperoxide for 1 min and expressed in the international units: mM $H_2O_2 \times 10^4$ per 1 mg of protein.

In the tables presented below in text, the average values of studied parameters and the average square errors are shown.

Determination of the difference values between the compared samples of indicators was performed using the parametric Student *t*-test. Differences in two compared groups were considered as correct at 95 % of significance level ($p < 0.05$).

Three month period of observation shown that daily use of the WDN by animals did not differ significantly from use of the tap water (Table 9.14).

Monthly water used by animals of both groups could probably be explained by seasonal changes. It is interesting to note also the tendency of reducing the daily use of the WDN during the 3rd month of the experiment.

Table 9.14 Data in 3-month period of daily use of the WDN

Group of animals	Daily use of water ml		
	1st month	2nd month	3rd month
Check	15.8	17.8	22.7
Test	15.8	17.1	19.9

Table 9.15 Data on dynamics of the animals' body weight

Period	Before test	1st month	2nd month	3rd month	Gain (%)
Check	174 ± 6.5	227 ± 9.8	247 ± 10.3	270 ± 11.6	55.2
Test	169 ± 6.9	223 ± 10	237 ± 11.1	269 ± 12.2	59.2

Data on dynamics of the animals' body weight during the period of observation are shown in Table 9.15.

These data show no difference in dynamics of the rats' body weight that used the tap water or WDN for a long time.

Date of the protein (SH) and disulfide (SS) groups' content in the blood serum of the rats after 3 months from the beginning of the WDN use are shown in Table 9.16.

As it follows from the data of Table 9.16, long use of the WDN had no effect onto content of the thiol and disulfide groups in blood. This indicates to absence of development of the oxidative stress in animals using the WDN. Also, these are the evidenced data of the reduced content of the glutathione in the animal serum and malon dialdehyde as it is presented in Table 9.17.

Data in Table 9.17 show the absence of intensification of the free radical oxidation and lipid peroxidation processes under long use of the WDN.

Table 9.18 shows data on level of the total antioxidant activity (TAA) of the blood plasma.

Data in Table 9.18 allow one to conclude that use of the WDN (as the only source of drinking for 3 months) did not have significant impact onto the level of total antioxidant plasma. Note that in some limits, this index can be a generalized indicator of effectiveness of the antioxidant systems and leads to conclusion about absence of the WDN pro-oxidant effect.

Table 9.16 Date of the protein (SH) and disulfide (SS) groups' content in the blood serum of the rats

Group of animals	Content of SH-groups (μM)	Content of SS-groups (μM)
Check	342 ± 31	144 ± 12
Test	329 ± 28	151 ± 16

Table 9.17 Content of the glutathione and malon dialdehyde in the animal serum

Group of animals	Malon dialdehyde (μM)	Reduced glutathione (μM)
Check	3.97 ± 0.15	3.01 ± 0.25
Test	4.03 ± 0.17	3.2 ± 0.31

Table 9.18 Data on level of the total antioxidant activity (TAA) of the blood plasma

Animal group	Level of TAA standard units
Check	0.17 ± 0.03
Test	0.13 ± 0.02

Table 9.19 Activity of the superoxide dismutase (SOD) of the blood plasma

Group of animals	SOD activity standard units/min/ml
Check	0.79 ± 0.13
Test	0.99 ± 0.16

Table 9.20 The animals' plasma ability to split H_2O_2

Group of animals	Total activity	Non-enzymatic activity	Enzyme activity
Check	0.36 ± 0.06	0.042 ± 0.005	0.268 ± 0.055
Test	0.31 ± 0.03	0.036 ± 0.008	0.248 ± 0.036

Of effectiveness of antioxidant systems saving under use of the WDN can be considered on activity of the superoxide dismutase (SOD) of the blood plasma (Table 9.19). Superoxide dismutase is one of the most functionally relevant components of the antioxidant protection system of organism. Superoxide dismutase provides the dismutation of superoxide-anion O_{2-} with forming of hydrogen peroxide undergoing by subsequent splitting.

Table 9.20 shows the results of experimental determination of the animals' plasma ability to split H_2O_2. Both the total activity of animals' plasma and its enzymatic and nonenzymatic components were evaluated.

Here, the data show absence of change of the of plasma ability to the splitting the H_2O_2 in animals after long use of the WDN.

The WDN use during 3 months (as the only source of drinking) does not affect drinking regimen of animals, does not cause change of the daily water use, and does not intensify processes of the free radical oxidation and generation of reactive oxygen species. This reflects absence of the WDN pro-oxidant properties.

9.3 Impact of the WDN on Endocrine System and Intestinal Microflora

The aim of investigation was to study the effect of the long WDN use by experimental animals onto functional state of the endocrine system and intestinal microflora. It was shown that the WDN use for 3 months did not cause any changes of content in the blood serum of the following indices: thyroxin, thyrotropin hormone, somatropin hormone, and cortisone. In some rats, the WDN use has led to emergence of moderate imbalance of the intestinal microflora.

Experiments were carried out on the male rats weighing 180–210 g. The animals were kept under the standard vivarium conditions in compliance with the GLP

requirements. The test group rats used the WDN as the only source of drinking without limitation for 12 weeks. The check group of rats used the tap water. On the next day after completion of the experiment period, the rats were decapitated and their blood serum was taken to determine the content of the thyrotropin hormone (TSH), somatropin hormone (HGH), thyroxine, and cortisol.

Determination of TSH was carried out by the "ELISA" method using the "Thyroid IFA TSH" kit. The main components of the kit are the following: eight dimple strips with monoclonal antibodies on the inner surface of the wells immobilized against the TSH, calibration samples based on the serum containing some amount of the TSH, concentrate of the conjugated anti-TSH-peroxidase and tetramethylbenzidine solution.

The kit operation mode was the following. In the wells during incubation, the investigated serum was added, and the binding of the TSH and monoclonal antibodies was immobilized on the inner surface of wells by the beta-subunit of hormone. During the second incubation, the conjugate of the monoclonal antibodies to the alpha-subunit of hormone was bound (by means of the peroxidase) with the TSH that was immobilized during the first incubation.

In the subsequent incubation with a solution of tetramethylbenzidine (peroxidase substrate), the solution coloring takes place in the wells during the enzymatic reaction. The coloring degree is proportional to the TSH content in the sample. After measuring the solution optical density in the wells by the spectrophotometer of vertical scanning at the wavelength of 450 nm (with basing on the calibration curve), the TSH concentration in the serum samples is determined.

For determination of thyroxine and HGH hormone in the blood serum, the kits "Steroid ELISA cortisol" were used for the determination of the cortisol content. For determination of the HGH content in the blood serum by the "ELISA" method, the test system "Eurogenetic" and analyzer "Uniplan" were used. In all cases, the methodology of analysis was basically the same.

The tables presented below in the text show the average values of parameters and the average square errors. Determination of differences between the compared samples was performed by using the parametric Student *t*-test. Differences in the two groups were considered as significant at 95 % level ($p < 0.05$). Before decapitation, the animals were placed in the metabolic cages for 4–5 h to obtain a stool for bacteriological analysis of the intestinal microflora.

Data on content of the studied hormone in the blood serum of the test and control groups of animals are shown in Table 9.21.

As it follows from the data shown in Table 9.22, the long WDN use (as the the only source of the rats drinking) did not cause changes in the major indicators characterizing the state of endocrine system.

For determination of the intestinal microflora of animals before the WDN use, some differences in microflora state were found. These differences allowed us to divide animals into two groups (Table 9.22).

As it follows from the data of Table 9.22, the long WDN use caused the bacterial imbalance of more then half of animals (Group 1). This manifested the failure of the *Escherichia coli* and *Enterococcus faecalis*. In Group 2 of animals (40 %), the

Table 9.21 Data on content of the studied hormone in the blood serum

Group of animals	Name of hormone			
	Thyroxine	TSH	HGH	Cortisone
Check	24.5 ± 4.3	0.08 ± 0.01	1.48 ± 0.08	7.7 ± 1.4
Test	26.2 ± 5.2	0.07 ± 0.02	1.42 ± 0.1	8 ± 1.6

Table 9.22 Data on the intestinal microflora of animals before and after the WDN use

Group of animals	Intestinal microflora
Group 1 (60 % of rats) before the use of the WDN	*Staphylococcus saprophyticus, Enterococcus faecalis, Proteus vulgaris, Escherichia coli*
Group 1 after the use of the WDN	*Proteus vulgaris, Staphylococcus saprophyticus*
Group 2 before the use of the WDN	*Proteus vulgaris, Escherichia coli, Staphylococcus saprophyticus*
Group 2 after the use of the WDN	*Proteus vulgaris, Escherichia coli, Staphylococcus saprophyticus*

Enterococcus faecalis was absent in the intestinal microflora before the WDN use. Its use by these animals did not cause any changes in the intestinal microflora.

Moreover, it should be noted that in all the examined animals before and after the long WDN use, the *Staphylococcus aureus* and yeast-like fungi *Candida* were absent in the intestinal microflora.

The long WDN use (as the the only source of the rats drinking) does not cause any disorders of endocrine system in terms of levels: the thyroxine, thyroid-stimulating hormone, growth hormone, and cortisone in the blood serum.

The long WDN use resulted in the imbalance of intestinal microflora in more than half of animals. This manifested the failure of the *Escherichia coli* and *Enterococcus faecalis*. At the same time, before the WDN use in rats with absence of the *Enterococcus faecalis*, the emergence of the imbalance was not detected.

The short WDN use by animals does not cause any imbalance of the intestinal microflora.

9.4 Impact of the WDN on Immune System

The aim of this part of investigations was studying the immunotoxic properties of the WDN in comparison with the portable water.

The experiments were performed on 30 rats, weighing 180–200 g. Cages with the animals were placed in separate rooms. The light regime was 12 h in the light and 12 h in the dark. The temperature was of 18–20 °C. The relative humidity was of 50–70 %. The temperature and relative humidity were recorded daily. The airing and air sterilization using a quartz lamp were also carried out daily.

During the study, each animal was examined daily. The examination included assessment of the animal overall behavior and state. During injection of the WDN, the inspection was carried out immediately after two hours and in the next day after the injection. By palpation, the visually detected abnormal formations were inspected. The inspection results were recorded in the laboratory cards.

To evaluate the WDN immunotoxic properties, state of the non-specific and specific humoral and cellular immunity was investigated under the unlimited the WDN use by animals for 30 days.

Animals were divided in two groups:

- Group 1—males, the check (C) ones with ordinary drinking water
- Group 2—males, with the WDN injection

Determination of phagocyte activity of peritoneal cells. Evaluation of the WDN impact onto the natural resistance of organism was carried out according to the guidelines of Pharmacological Committee. The phagocyte activity of macrophages was determined in the test group (that used the WDN daily for 30 days) and the check one (that used ordinary drinking water) of animals.

To study the phagocyte activity, the rats were euthanized by chloroform and their abdomen was washed by introducing of 3 ml of the RPMI 1640 medium. The liquid obtained was kept in the silicone tubes on ice and was recovered and then centrifuged under 1,000 rev/min for 10 min. The precipitate was resuspended in the RPMI 1640 medium, the number of cells was counted in the Goryaev chamber and adjusted to the concentration of 5×10^6 ml^{-1}.

The equal volume of the dead *Staphylococcus aureus* suspension was added to the cells in the ratio of 1:10. Further, the mixture was incubated at 37 °C for 30 min. The *Staphylococcus aureus* was pre-opsonized by the rats fresh pool serum by means of incubation of the bacteria with whole serum for 10 min at 37 °C and, further, the three-fold laundering was implemented. After the incubation of the peritoneal exudate with opsonized *Staphylococcus aureus*, the smears were prepared from the suspension onto the glass slides. The smears were dried, fixed by methanol for 10 min, and stained by the Romanowsky-Giemsa for 45 min.

The smears were viewed by a microscope with the 650 zoom. Here, calculation was performed of the total number of cells, number of cells containing phagocytes *Staphylococcus aureus*, and number of the *Staphylococcus aureus* inside of each phagocytizing neutrophil.

Basing on these data, the following parameters were calculated:

- Phagocyte index, i.e., the percentage of the phagocyte cells to the total number of cells in the smear
- Phagocyte number, i.e., the average number of the bacteria absorbed by one phagocyte

Determination of hemagglutinin titer in the serum. To determine the WDN effect on the humoral immune response, estimation of the antibody titer to erythrocytes of sheep (ES) in the test and check rats groups was used.

The rats after injection were immunized intraperitoneally by 0.2 ml of 10 % ES in the physiological saline. On the seventh day, the blood serum was obtained, and then it was heated under 56 °C for 30 min to inactivate the complement components.

To determine the titer of hemagglutinin, the microupdatings hemagglutinin reaction was used by means of the Takachi microtiter. By means of the microtiter dropper, 25 μl of serum were added into the first and second wells under dilution of 1:5. There, as in all subsequent wells (from 2 to 12) of each row of microplate 25 μl of l% of normal rabbit serum were introduced in 0.15 M NaCl.

Further, by means of a dilution device, 25 μl of serum was mixed into the 25 μl of microtiter. Then the mixture was transferred to the second well of this row, and so on, until the 11th well inclusively. The 12th well was as the check one where there was only 1 % normal rabbit serum. After dilution of the serum, set of the two-fold dilutions, from 1:5, 1:10, etc., was obtained.

Then, into all wells, the 25 μl of 0.5 % ES suspension was injected into 1 % normal rabbit serum. Then the plates were shaken and allowed to stand at room temperature for 1 h. During this time, the reaction finished, and in the check sample with 1 % rabbit serum, the precipitate was formed that indicates the negative reaction in this well. In the test wells, the titer of antibodies was determined, i.e., the highest dilution of serum was evaluated, which there is a clear agglutination of the erythrocytes. The serum titer was expressed as the reciprocal of the titer value or as the logarithm to the base 2 (lg).

To determine the isotype of antibodies, the 25 μl of 0.2 M solution of 2-mercaptoethanol (2-ME) was added to the 25 μl of a five-fold diluted immune serum, and this mixture was incubated at 37 °C for 30 min. Other reaction steps (serum dilution, entering the erythrocytes) were performed by the method described above. Evaluation of the immunoglobulin class of antibodies to ES was implemented as follows. The total antibody titer (without 2-ME) is the sum of interactions of the l gM and l gG of antibodies with the ES, and the antibodies l gG is the titer of reaction in presence of the 2-ME. It is so since the l gM is the antibodies titer that are sensitive to the 2-ME.

Determination of significance of slow-type reaction of hypersensitivity. Sensitization of the rats by 10^7 ES of 0.1 ml subcutaneously was performed. In the 5th day after the injection, as the permissive dose, the 2×10^8 ES of 20 μl was injected under the aponeurotic plate of one limb. In the contralateral paw, the saline of the same volume was also injected.

After 24 h, the significance of local reaction was assessed by the ratio of foot edema of the test and check paws. Size of the foot was measured by means of calipers. The reaction index (*IR*) was calculated by

$$IR = [(h_t - h_c / h_t)] \times 100\,\%$$

where h_t and h_c are test and control sizes of foot, respectively.

The experimental results were processed by the variational statistics methods using the Student *t*-test.

Determination of phagocytic activity of peritoneal cells. Results of evaluation of the phagocytic index and specific phagocytic activity of the individual phagocytes are given in Table 9.23.

These data show that the phagocytic index (i.e., percentage of the peritoneal cells absorbing the *Staphylococcus aureus*) in rats of the test group did not differ from that in the check group of rats. At the same time, in the case of the WDN use, the phagocytic number (i.e., number of the absorbed microbes per one phagocyte) is almost by 3 times higher than that of animals in the check group.

This allows one to conclude that the WDN impact stimulates the phagocytosis rate.

Study of the humoral immune response to ES. To identify changes of the specific humoral immune response, definition of the hemagglutinin titer in the test and check groups of rats immunized by the ES was used. In the 7th day after immunization, the antibodies titer in the serum to the ES and the l gG-antibodies titer to the antigen were determined. The results are shown in Table 9.24.

Analysis of these data shows that the WDN application does not effect onto the antibodies biosynthesis of the sheep erythrocytes.

Study of significance of the slow-type hypersensitivity. To study the WDN effects onto the specific cellular immunity, the significance of the slow-type hypersensitivity reactions was estimated in the test and check groups of rats. The data are presented in Table 9.25.

Analysis of these data shows that there are no essential changes in significance of the slow-type hypersensitivity reactions in the test group in comparison with that in the check one.

Table 9.23 Data on evaluation of the phagocytic index and specific phagocytic activity of the individual phagocytes

Group of animals	Number of measurements	Phagocytic index	Phagocytic number
Check	10	5.54 ± 1.42	6.80 ± 0.56
Test	10	6.00 ± 1.11	24.35 ± 1.38[a]

Note [a]P < 0.05 versus check

Table 9.24 Antibodies titer in the serum to the ES and the l gG-antibodies titer to the antigen

Group of animals	Total titer	l gG-antibody titer
Check	7.43 ± 0.23	6.83 ± 0.22
Test	7.93 ± 0.33	7.23 ± 0.29

Note—the antibodies titer is presented in log 2

Table 9.25 The WDN effect onto the specific cellular immunity

Group of animals	Reaction index	Reliability P
Check	181.1 ± 5.1	–
Test	179.3 ± 4.5	> 0.05

Notes n—number of animals

The WDN stimulates the phagocytosis rate and does not affect onto the antibodies biosynthesis of the sheep erythrocytes and onto significance of the slow-type hypersensitivity reactions.

The WDN has no immunotoxic properties, and the revealed changes of phagocytosis are stipulated by increasing the non-specific immunity.

9.5 WDN and Genotoxicity

The WDN genotoxic effects in vivo were studied. Tests were performed on animals (rats) as indicators. The index of the DNA leukocyte was used and calculated as the ratio of the DNA concentration measured fluorimetrically to the number of leucocytes in 1 ml of blood. Test of the WDN effect on mutagenic activity was performed in vitro, with peripheral blood lymphocytes of a donor and using a cytogenetic test. The WDN used by male and female rats as the drinking water for 1 month; and in this test any expressed gematotoxic and genotoxic effects were not observed. Application of the WDN in the cytogenetic testing has not detected mutagenic effect; here, the test was carried out on a human blood lymphocyte culture.

To evaluate the genotoxic effects in vivo basing on changes of the leukocytes' DNA, the method of genotoxicity diagnostics with low doses of radiation and chemical effects was used. To evaluate the WDN genotoxicity in vitro, the standard cytogenetic test for determination of mutagenic activity on peripheral blood lymphocyte culture of donor was applied.

In the tests, in vivo, male and female rats of weight 180–240 g were used. Animals of each sex were divided into 3 groups:

- Intact check, 10 rats
- Check animals using drinking water with $PbCl_2$ under concentration of 100 mg/l and irradiated by dose of 25 cGy, 10 rats
- Animals using the WDN instead of drinking water, 20 rats

Determination of hematological and biochemical parameters was performed by analysis of the blood samples from the tail vein of animals two times:

- 1 day after (to study early effects)
- 30 days after (to assess of recovery efficiency)

Total number of the leukocytes was determined by the conventional chamber-melange method.

In genotoxicity testing on animals as indicator, the DNA index (ID) of leukocytes was determined. This index was calculated as the ratio of the DNA concentration (mg/ml) to the number of leucocytes in 1 ml of the blood measured fluorimetrically without flow cytometer. The DNA content in the samples was determined using the fluorescent dye, i.e., the 4.6-diamidino-2-phenylindole

(DAPI) ("Serva", Germany) with the final concentration of 0.1 μg/ml after lysis of the blood samples under obtaining nucleoid conditions.

As a standard sample, the sonicated DNA of calf thymus was used. The ID of peripheral blood leukocytes of the intact rats was taken as appropriate to the diploid (2c) DNA content of white blood cells.

If the ID value was less than 2c, this meant that the number of cells in the sample having DNA amount less than diploid is increased by the apoptotic dying cells. All measurements of fluorescence were performed on the fluorescence spectrophotometer "Model-850". For DAPI, the values λ_{exc} = 350 nm and λ_{em} = 450 nm were chosen, and for ethidium of bromide, ones were λ_{exc} = 510 nm, λ_{em} = 590 nm.

Testing the WDN effect onto the mutagenic activity and peripheral lymphocytes was implemented on the donor blood cultured in vitro by the conventional method.

The WDN samples of 0.3 ml were injected into two penicillin vials with incubation medium (5 ml) under sterile conditions. In the other two vials (for check), the sterile saline of 0.3 ml was injected with the same incubation medium.

After, the blood incubation was performed for 71 h in thermostat at 37 °C. The cytogenetic samples with metaphase plates were prepared to study chromosomes. The routine-stained chromosomes were analyzed. In each variant of the test, 500 cells were analyzed. Statistical procession of the experimental data was performed using the Student *t*-test.

Early genotoxic effects in vivo. At early stages (24 h after the WDN injection into the rat blood), no significant changes in the total number of leukocytes were detected in comparison with the check animals (Table 9.26). Therefore, the WDN has not any gematotoxic effect.

The Measurements of biochemical parameters showed no significant changes in the DNA leukocyte index in blood of the experimental rats comparing with that of the intact check group in the early period after the WDN injection, whereas in the check group, the value of this parameter was significantly different from that in the intact check group. Thus, the WDN injection does not lead to significant early genotoxic affects in organisms both male and female rats (Table 9.27).

Results of recovery. The WDN injection *ad libidum* did not cause the death of animals (either males or females) for 30 days.

At 1 month after the WDN injection, there were no any changes in the total leukocytes number of rats in comparison with that in the intact check animals (Table 9.28).

Table 9.26 Effect of the WDN injection into the rat blood on the total number of leukocytes

Group of animals	Males	Females
Intact check	12.4 ± 2 (n = 10)	12.5 ± 1.1 (n = 10)
Genotoxicity check	8.4 ± 1.1 (n = 10)	13.8 ± 1 (n = 10)
Injection of the WDN	9.9 ± 0.6 (n = 20)	14.2 ± 1.5 (n = 20)

Table 9.27 Effect of the WDN injection on early genotoxic affects in organisms both male and female rats

Group of animals	Index DNA of leukocytes in the blood of males (n-number of animals)	Index DNA of leukocytes in the blood of females (n-number of animals)
Intact check	8.4 ± 0.61 (n = 10)	9.7 ± 0.5 (n = 10)
Genotoxicity check	4.92 ± 0.95 (n = 10)	4.91 ± 1.05 (n = 10)
Injection of the WDN	8.72 ± 0.7 (n = 20)	10.22 ± 0.8 (n = 20)

Notes n—number of animals

Table 9.28 Effect of the WDN injection on the total leukocytes number of rats

Group of animals	Males	Females
Intact check	10 ± 0.7 (n = 10)	11.7 ± 0.9 (n = 10)
Injection of the WDN	9.6 ± 0.6 (n = 20)	11.9 ± 0.9 (n = 20)

Notes n—number of animals

Determination of the DNA content in leukocytes at 1 month after the injection does not also detect any significant differences in the blood parameter of experimental rats in comparison with that of the intact check group of animals (Table 9.29). Considering this, there is a reason to believe that the WDN injection does not have any genotoxic effects onto the whole organism.

Results of studies in vitro. In preparation of the lymphocyte culture for the tests, a series of the 1.9 % polyploid cells was compounded (for injection of the physiological saline). In the samples obtained from the cell culture by introducing the WDN, there were no additional cytogenetic abnormalities as well as in the samples of the check group. Thus, the investigated solutions with the WDN have not any mutagenic effect.

Under the WDN injection into the drinking water for male and female rats, no noticeable gematotoxic and genotoxic effects were observed for 1 month after the injection.

In the cytogenetic test with the WDN in cultured human blood lymphocytes, no mutagenic effect has been observed.

Table 9.29 Data on the DNA content in leukocytes at 1 month after the injection of the WDN

Group of animals	Index DNA of leukocytes in the blood of males (n-number of animals)	Index DNA of leukocytes in the blood of females (n-number of animals)
Intact check	8.4 ± 0.6 (n = 10)	9.3 ± 0.4 (n = 10)
Injection of the WDN	7.6 ± 0.3 (n = 10)	9.6 ± 0.6 (n = 10)

Notes n—number of animals

9.6 Impact of the WDN on Crayfishes

The WDN antimicrobial properties can have negative effects on human beings. To assess the toxicity of aquatic medium, a variety of methods are used with application of the enzymatic test kits, algae, ciliates, and aquatic organisms; and corresponding information is obtained about their under the standard conditions and about deviation of the behavior investigated parameters under stress.

It seemed convenient and reliable to use the decapod crayfishes as bio-indicators and to assess the quantitative parameters of the functional state of crayfishes by the reactions of their cardiovascular system. For noninvasive registration of cardiac activity of crayfishes, the optical fiber sensor was used. The principle of this method is in distinguishing and measuring the fluctuation component of the scattered and reflected back infrared range radiation of a low-power semiconductor laser.

For study the adult crayfish *Astacus astacus L.* (TL = 96.4–98.5 mm; CL = 48.5–46.2 mm), an appropriate aquarium and desiccator of 1.7 liters were used. State of the animal was assessed by its cardiac activity. At the initial stage of test, the animal is placed into ordinary settled tap water from the aquarium where it was before and then its cardiac activity was recorded.

The change in heart rate (HR) under rest and during experimental stress was investigated. The stress was caused by raising the animal up the bottom of the aquarium. According to the experimental data, in such state, the decapod crayfishes showed a clear change in the heart rate proportionally to the degree of water pollution. Then, the animal was placed into the desiccator in the same suspended state in the testing water, and changes in the cardiac activity were recorded.

Having been placed into the WDN with high concentration of the Ag and Ti (with the inputted energy of 5 J/ml), the crayfish showed decrease in the heart rate (the bradycardia effect) in comparison with that in the ordinary water (Fig. 9.3a, b), where a is initial state of animal (20 min) and then under stress at these conditions (20–50 min), b is in WDN of energy 5 J/ml (1 h).

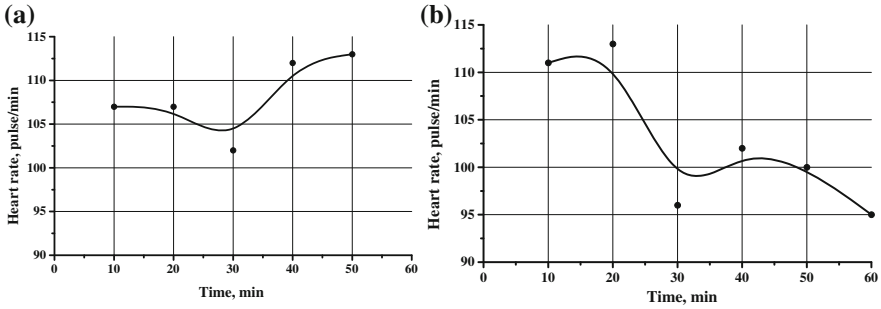

Fig. 9.3 Change in HR of the *Astacus astacus* crayfish in ordinary water

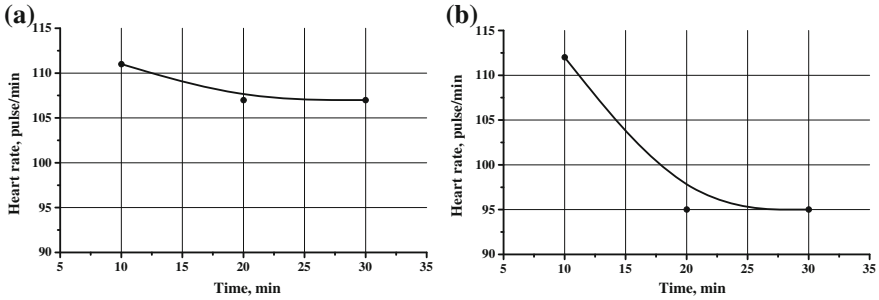

Fig. 9.4 Change in HR of the *Astacus astacus* crayfish in the WDN

The cardiac bradycardia appeared also under placing the animals in water with the higher concentrations of these metals and with the inputted energy 8 and 12 J/ml (Fig. 9.4a, b), where a is 8 J/ml for 30 min., b is 12 J/ml for 30 min.

Under standing the *Cambarus diogenes diogenes* crayfishes in the WDN with concentration of Ag 8.41 ± 0.17 mg/l, the animals showed a change in the metabolic processes associated with the excretion of metabolic products, and changes in the Na ion fluxes. This decrease in excretion of the Na ions can be explained by the inhibition of Na/K—ATPhase in the terminals of crayfishes' gills in the WDN with high Ag content. The results obtained in the experiments allow one to suppose that, been placed into the WDN, the animals rebuild their respiratory function due to changes in the permeability of the gill membranes. Under this, the cardiac activity rhythm becomes slower and the bradycardia is observed.

In the short tests, it was found that under placing the crayfishes into the WDN for 1.5–2.0 h, a decrease in the heart rate (bradycardia) takes place.

References

1. V.L. Goryachev, A.I. Kulishevich, Ph.G. Rutberg, V.B. Dolgosaburov, in *Electro Med 99, First International Symposium on Nonthermal Medical/Biological Treatments Using Electromagnetic. Fields and Ionized Gases* (Norfolk, 1999)
2. B.A. Freeman, J.D. Grappo, J. Lab. Invest. **47**, 412–426 (1982)
3. B.P. Yu, J. Physiol. Rev. **74**, 139–163 (1994)
4. M. Martinez-Cayvela, J. Arch. Pharm. **1**, 39 (1998)
5. E. Cadenas, J. Annu. Rev. Biochem. **51**, (1989)

Chapter 10
Application of the PED and WDN

Abstract The resulting experimental data of performed investigations on both the PED, and WDN of metal electrodes allow us to consider the possibility of using those and others in various fields of scientific research. These areas are primarily biology, medicine, and ecology. Solvents play important role in formation of three-dimensional structure and functioning of biological macromolecules. At the same time, most common methods of analysis, such as atomic force microscopy and transmission electron microscopy, are often require at sample preparation of applying it to surface, which can significantly effects on sample properties. It should be noted that single-component solutions of biomacromolecules are extremely rare in vivo, while many methods of investigation require of one-component solutions of macromolecules after chromatographic purification, i.e. at such experiments considerable part of information about the behavior of molecules functioning in their natural environment is lost. Using of the WDN in medicine based on their properties to kill a wide range of pathogenic microorganisms and spores of opportunistic to human fungal cultures. In addition, in oncology can be used the property of WDN to retard the growth of malignant tumors. The possible use of PED themselves in virology based on the impact of shock waves generated during discharges in water on the shell of viruses that can allow to prepare anti-virus vaccines. Cytostatic effect was confirmed by a significant growth suppression, cytodystrophic changes, and fibrosis of transplanted Pliss lymphosarcoma in the rats that received regular intravenous injections of WDN. The role of silver atoms in the stabilization of molecular structure of DNA, inhibition of tumor growth and/or reversion of the malignant phenotype requires further studying at tissue, cellular, and molecular levels.

10.1 Biology

Solvents play important role in formation of three-dimensional structures and function of the biological macromolecules. At the same time, the most common methods of analysis, such as the atomic force microscopy and transmission electron

V. Kolikov and P. Rutberg, *Pulsed Electrical Discharges for Medicine and Biology*, Biological and Medical Physics, Biomedical Engineering,
DOI 10.1007/978-3-319-18129-5_10

microscopy, are often require to implement some actions over the sample surface during its preparation. However, such actions can significantly effect onto the sample properties.

It should be noted that the single-component solutions of are extremely rare in vivo. However, as a rule, many methods of investigation require namely the one-component solutions of macromolecules after the chromatographic purification. As a result, in such experiments, a considerable part of information is lost, especially, on the molecules behavior and their functioning in the natural environment.

It is important that study of one-component systems can provide much more information about the structure of individual molecules in comparison with methods for study of the ensemble average parameters. As an example, denote analysis of the spectra of quasielastic light scattering in the chicken egg lysozyme solution (with the molecular weight of 14.4 kDa and hydrodynamic radius of about 1.75 nm).

By chromatographical and electrophoretical methods, the pure protein was dissolved in the phosphate buffered saline (PBS) under concentration of 1 mg/ml. Then it was filtered through a column for centrifugation with a pore size corresponding to the molecular weight of 30 kDa.

Figure 10.1 shows that, according to the QLS data, the lysozyme with the concentration of 1 mg/ml is present in the solution as monomers only at the first minutes of the test, where on X-axis twice hydrodynamic radius of the scattering particles [1].

Then the weak interactions lead to forming the aggregates. This process is determinant at the initial stages of forming the amyloid fibrils. At the same time, creation of such aggregates was not detected in experiments with the gel electrophoresis or chromatography.

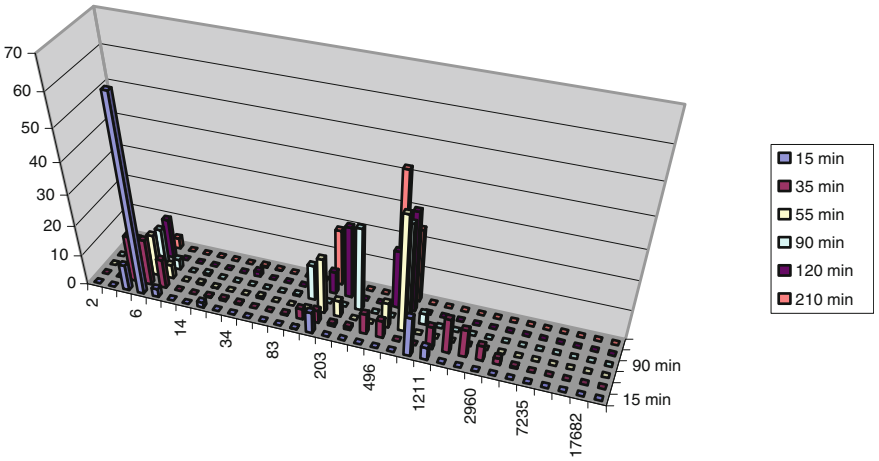

Fig. 10.1 Aggregation of the lysozyme [1]

Another example of the QLS successful application to study of the biological macromolecules in solution is investigation of changes in the DNA conformation in dependence on the solution ionic strength.

As was mentioned above, a considerable part of information on the behavior of samples in solution can be lost during preparation of samples for the AFM and TEM.

At the same time, the QLS gives information about the fine structure of the particles under study. As an example of application of combination of the QLS and TEM microscopy, study of the Pt nanoparticles can be noted. Such a combination allows one to describe the system most accurately.

Figure 10.2 shows the results of the QLS and TEM tests of the Pt nanoparticles, where length of black line is 50 nm.

The TEM image shows the branched structure of ~100 nm size and more. The AFM images of the same samples show the smaller nanoparticles (Fig. 10.3).

Basing on the QLS data, one can assume that some of these nanostructures were formed by drying the sample. It could be supposed since according to the QLS, there are nanoparticles in the solution that are not observed in the AFM image. However, the nanoparticles of such a size are components of the observed

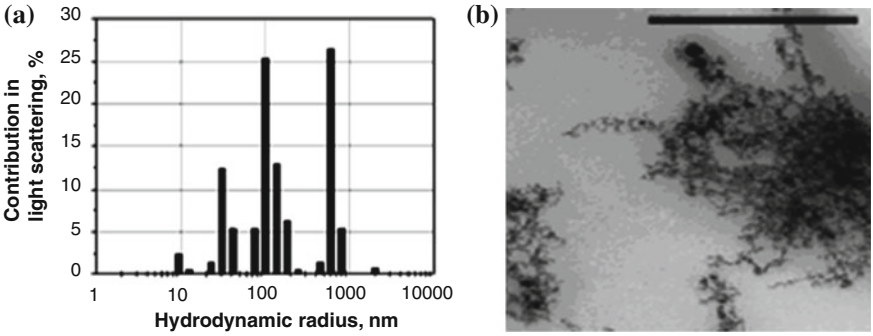

Fig. 10.2 QLS spectrum (**a**) and TEM image (**b**) of the Pt nanoparticles [1]

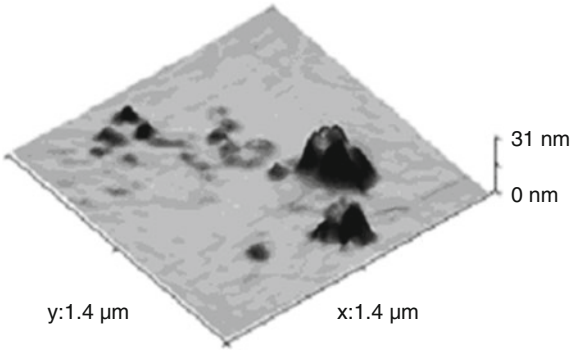

Fig. 10.3 AFM image of the Pt nanoparticles and clusters [1]

aggregates. Apparently, the sample drying leads to increase of the local concentration and to the nanoparticles aggregation. Thus, combination of the mentioned methods allows one to obtain information about the structure of nanoparticles and their behavior in solution.

Application of the QLS to diagnosis is also promising. It is so since preparation of samples of the biological liquids (such as the blood or urine) requires a minimal processing.

Figure 10.4a shows the QLS spectrum of human serum of a healthy donor, where (a) is healthy donor, (b) is patient with Myasthenia, (c) is Myasthenia patient blood serum after protein A adding. There are three distinct distribution peaks those correspond to the albumin, immune complexes, and lipoproteins.

Figure 10.4a presents the QLS spectrum of blood serum of a patient with the Myasthenia disease. There are additional peaks that correspond to particles with the larger hydrodynamic radius. Note that such particles disappear after deposition of the immune complexes (by means of the A protein) that were immobilized on the micro-spheres (Fig. 10.4c).

Thus, this test can be used for clarification of the Myasthenia disease diagnosis.

Similar principles can be used for diagnosis of other diseases, such as predisposition to the urolithiasis. One of the important factors affecting onto forming the kidney stones is disorder in the system that controls the oxalate crystal growth. The Tamm-Horsfall protein (THP) is the major urinary mammals' protein that is capable to prevent the oxalate crystals growth. Defects in glycosylation of the THP lead to disorder of its function. These defects can be detected by a change in the THP aggregation ability under presence of the sodium chloride.

Figure 10.5 demonstrates that formation of such irreversible complexes can be eliminated from the normal THP complexes by the QLS technique. Thus, the QLS can be used in diagnostics of at least two diseases.

Another possible the QLS application is in the area of nanoparticles study. The data from such application show that the QLS allows us to make a simple test of the nanoparticles interaction with the blood serum.

Resent investigations confirmed that nanoparticles can be used as the cargo for drug delivery or as an adjuvant for vaccines. Both applications demand injection of the nanoparticles solution into the blood flow. During experiments with using the QLS technique, it was shown that effects of various nanoparticles onto the blood components are significantly different. There are distributions corresponding to the Ti oxide and Zn oxide effects onto the human blood serum (Fig. 10.6).

It is seen that addition of the Zn oxide leads to aggregation of the blood components. However, the Ti oxide nanoparticles have a significantly lower effect of aggregation.

Combination of the QLS, AFM, and TEM methods is appropriate technique for study of the macromolecules basic properties in their biological solutions with nanoparticles.

Results of study of the nanoparticles mixtures and biological liquids can be used in diagnostics of a number of diseases and, at the first stage, to investigation of nanoparticles biosafety in medical applications.

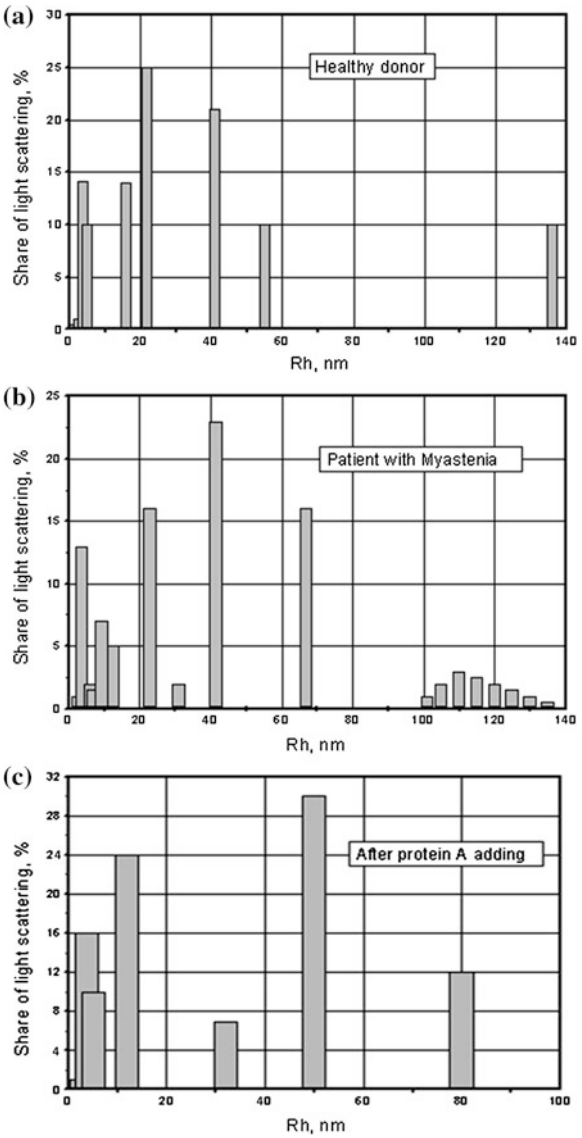

Fig. 10.4 Hydrodynamic radius of the blood components at the Myasthenia disease [1]

10.2 Surgery

The WDN applications to medicine are based on the WDN properties to kill a wide range of pathogenic microorganisms and spores that are opportunistic to human fungal cultures. In addition, the WDN property to retard the growth of malignant tumors can be used in oncology. Possible application to virology of the PED themselves is based on the shock waves impact onto the shell of viruses under the

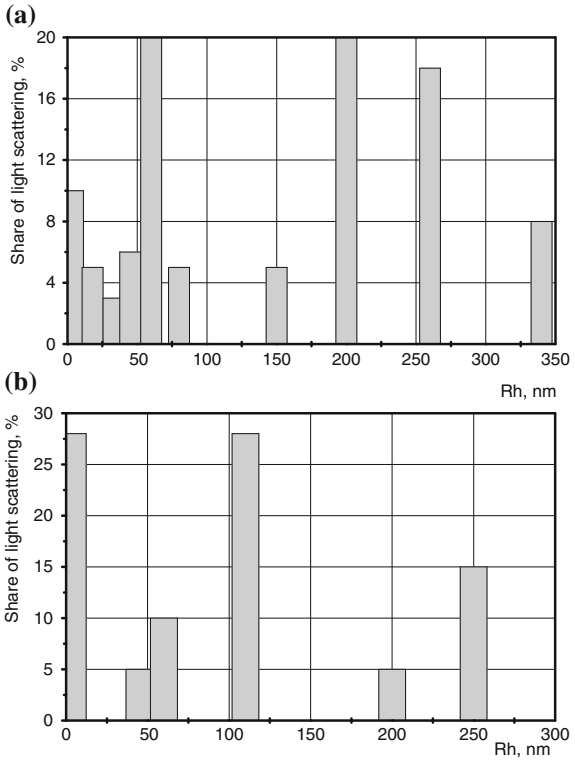

Fig. 10.5 Difference in aggregation of the THP in control (**a**) and disease (**b**) [1]

waves generation during discharges in water. This phenomenon can allow one to prepare the anti-virus vaccines.

The WDN bactericidal properties can be used in surgery for treatment of the flesh upper purulent wounds with chronic components. Patients with such wounds are of a large number and they differ by etiology of the diseases; but their general feature is long treatment without any positive changes [2]. In these cases, long application of antibiotics leads to abnormality of the immune processes and to decreasing the antibacterial resistance against the microbial flora [3]. Moreover, local antiseptics are frequently toxic and can oppress processes of reparation in the wound [4].

Our investigations are addressed to finding out methods of the WDN application to treatment of purulent wounds with chronic components and comparison of these methods efficiency with that of treatment by the sodium hypochlorite [5].

It was found that the WDN of Ag usage during the first 5 days is characterized by the high active reparative processes with their maximum on the third—4 days and further subsequent moderate healing. Under the local WDN application, there were no cellular atypia and preternatural emergences of the inflammatory reactions. It is possible to assume that, in future, the WDN usage will allow one to correct the practice of outpatient therapy of the chronic and slow pyoinflammatory diseases.

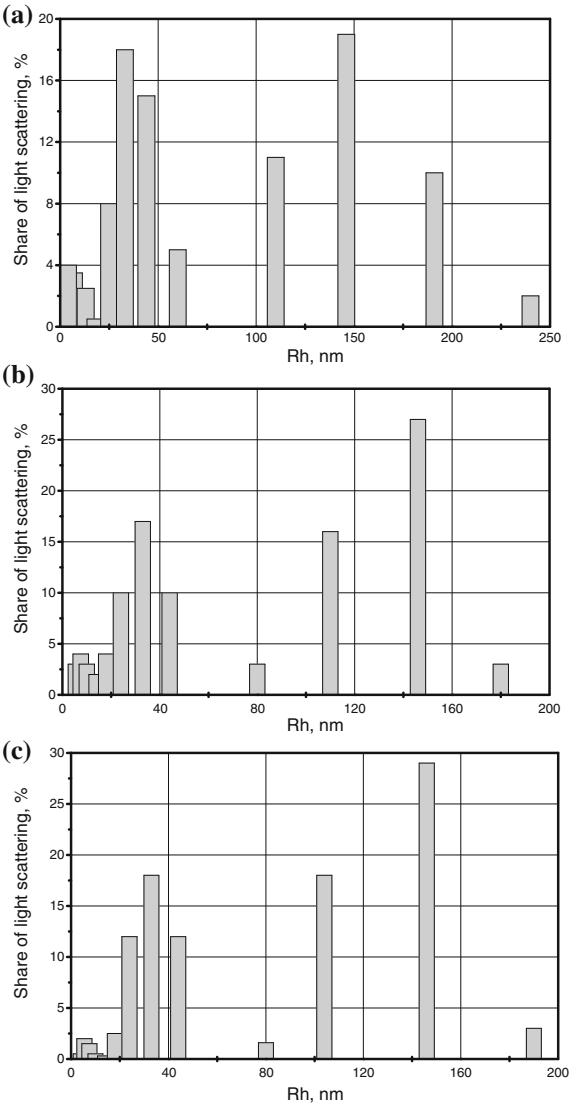

Fig. 10.6 Human blood serum components (**a**) and its aggregation with Zn oxide nanoparticles (**b**), and Ti oxide nanoparticles (**c**) [1]

For determination of the WDN parameters, we used the techniques of dynamic quasi-elastic scattering and high effective ionic capillary electrophoresis.

The following WDN characteristics had been determined: distribution of a share of the "small" nanostructures subfractions and a surface electric charge of nanostructures in dependence on the pulse duration. These characteristics were estimated by the laser correlation spectrometer and by the unit for capillary electrophoresis (Fig. 10.7).

For the clinical researches, the WDN were formed with maximal share of the "small" nanostructures and maximal surface electric charge. Such nanostructures were created under the pulse duration of 5–10 μs.

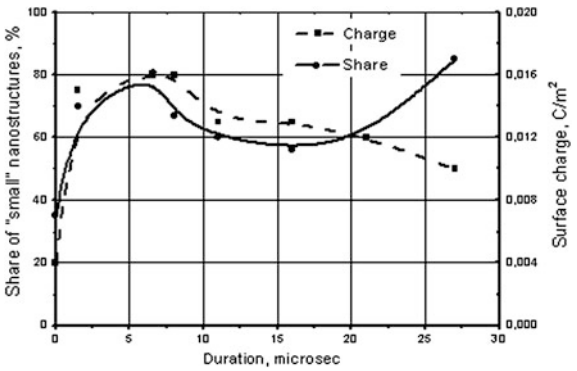

Fig. 10.7 Share and charge of "small" (<100 nm) nanostructures [5]

Clinical research was carried out on 133 rats of the "VISTAR" line of both sexes with weight of 170 ± 30 g. The animals were divided in three groups: one check group of 31 animals and two test groups of 51 animals each.

For treatment of wounds, we used the Ag WDN (of 2 months after its preparation) and, for comparison, the solution of sodium hypochlorite of 600 mg/l.

Purulent wounds of the initial area of 150 ± 50 mm^2 were made by means of seeding (into the inter shoulder-blade areas) the gauze napkin impregnated with a solution of low viral strain of the *Staphylococcus aureus*. Lancing and surgical sanitation of the abscess were carried out on the seventh day after infecting. The treatment procedures were performed in the test groups of animals by the WDN of 4.5 mg/l concentration and, for comparison, by the solution of sodium hypochlorite of the 600 mg/l concentration once per day during 14 days.

For comprehensive assessment of wound healing process, the methods of planimetric, bacteriological, and histological examination of the wounds were used. The examinations were carried out on the 3rd, 5th, 7th, 10th, and 14th days.

The bacteriological investigation of the purulent wounds included a study of the qualitative composition of microbial pathogens and quantitative counting the microorganisms.

Estimation results of the quantitative composition of microflora in the wounds (per 1 g of the tissue) are shown in Table 10.1.

It is seen that application of the sodium hypochlorite solution and the WDN make the effective elimination of the pathogens in the wounds. However, this phenomenon was not observed in the check group of animals.

The morphodynamic changes in the wound healing process under application of the WDN and sodium hypochlorite are presented in Table 10.2 in comparison with that in the check group.

Analysis of data in the table revealed decrease of the wound healing time in the experiments, in which the sodium hypochlorite and the WDN were applied to treatment of the purulent wounds.

Table 10.1 Quantitative composition of microflora in the wounds

Groups of animals	1st day CFU	3rd day CFU	5th day CFU	7th day CFU
Check	$(3.5 \pm 1.6) \times 10^7$	$(3.9 \pm 1.9) \times 10^7$	$(3.8 \pm 1.4) \times 10^7$	$(3.7 \pm 1.4) \times 10^7$
Sodium hypochlorite	$(3.9 \pm 1.7) \times 10^7$	$(5.3 \pm 1.6) \times 10^5$	$(3.8 \pm 0.5) \times 10^4$	No growth
WDN	$(3.7 \pm 1.5) \times 10^7$	$(6.5 \pm 1.1) \times 10^5$	$(3.9 \pm 0.6) \times 10^4$	No growth

Table 10.2 The morphodynamic changes in the wound healing process under application of the WDN and sodium hypochlorite

Clinical signs	Groups of animals		
	Check (days)	Sodium hypochlorite (days)	WDN (days)
Period of wound cleansing	9.1 ± 0.1	4.5 ± 0.2	4.3 ± 0.2
Period of appearance of granulations	8.3 ± 0.2	4.3 ± 0.2	4.2 ± 0.2
Period of wound granulations filling	13 ± 0.3	6 ± 0.1	5.9 ± 0.2
Beginning of edge epithelization	10.6 ± 0.2	6.3 ± 0.2	6.3 ± 0.1

Application of the sodium hypochlorite and the WDN to the purulent wound treatment led to changes in the wounds areas of experimental animals. The data are presented in Table 10.3.

It should be noted that there is the diurnal decrease of the wound areas in experimental animals due to daily application of the sodium hypochlorite and the WDN. The data are given in Table 10.4.

Analysis of the data on the daily decrease in the wound areas shows a positive impact of the sodium hypochlorite and the WDN onto the purulent wounds. It should be noted that the WDN have the more effective impact onto the wound healing. In the check group of animals, the dynamics of decreasing the surface area of wounds was significantly slower. The total reduction of the wounds areas on the 14th day is presented in Table 10.5.

Data of in this table show that, after 14 days, the greatest common factor of decreasing the wound areas was stated in the test group that used the WDN. Changes of the wounds areas in mm/day during the treatment are given in Table 10.6.

Here, the data demonstrate that the shortest time of healing was observed with the WDN application; and the healing period was slightly shorter than that in the case of application of the sodium hypochlorite solution.

Analysis of the planimetric data and the healing time shows the high activity of wound healing under the WDN using, which exceeds that of the sodium hypochlorite solution.

Table 10.3 Changes in the wounds areas of experimental animals mm^2

Days	Groups of animals		
	Check (mm^2)	Sodium hypochlorite (mm^2)	WDN (mm^2)
1	40.2 ± 5.1	400.1 ± 3.1	400.2 ± 6.2
3	390.1 ± 1.9	355.2 ± 2.5	333.5 ± 5.1
5	366.4 ± 0.7	238.5 ± 6.3	219.4 ± 4.7
7	355.7 ± 8	182.3 ± 13.5	165.7 ± 9.1
10	334.2 ± 1.1	154.4 ± 10.4	138.9 ± 11.3
14	275.8 ± 0.6	70 ± 5.3	52.3 ± 2.3

Table 10.4 Changes in the wounds areas of experimental animals (%)

Days	Groups of animals		
	Check (%)	Sodium hypochlorite (%)	WDN (%)
3	2.5 ± 0.1	11.2 ± 0.2	16.6 ± 0.2
5	6 ± 0.1	32.9 ± 0.1	34.2 ± 0.1
7	2.9 ± 0.1	23.4 ± 0.1	24.4 ± 0.1
10	6 ± 0.2	15.3 ± 0.1	16.1 ± 0.1
14	17.4 ± 0.3	54.6 ± 0.1	62.3 ± 0.1

Table 10.5 The total reduction of the wounds areas on the 14th day

Groups of animals		
Check (%)	Sodium hypochlorite (%)	WDN (%)
31.08 ± 0.2	82.5 ± 0.1	86.9 ± 0.1

Table 10.6 Changes of the wounds areas in mm/day during the treatment

Days	Groups of animals		
	Check (mm^2/day)	Sodium hypochlorite (mm^2/day)	WDN (mm^2/day)
3	10.1 ± 1.2	44.9 ± 3.5	66.7 ± 2.5
5	23.7 ± 2.7	117 ± 5.6	114.1 ± 5.2
7	10.7 ± 1.1	55.9 ± 6.7	53.7 ± 5.4
10	21.5 ± 1.2	27.9 ± 4.5	26.8 ± 3.7
14	58.4 ± 5.7	84.4 ± 6.5	86.6 ± 4.9

Thus, results of our investigation of wound healing in animals with the purulent wounds confirmed the WDN high effectiveness; this is equal or larger than that in using the sodium hypochlorite solution.

Our study has shown that the WDN with local application to treatment of the purulent wounds has the antiseptic properties. So, it can be recommended as a means of comprehensive prevention and healing of the wound infections.

Often, the chronic purulent wounds are complicated by the damaged tissue metabolism and local pathomorphism, and there is no reason to hope on their quick healing. Therefore, the aim of treatment by the WDN is to prevent possible complications.

Note there is a well-known phenomenon of the reactivation of existing microflora that may adapt to antibiotics and to access additional associations of pathogens into the nutrient medium of wounds. It results in considerable adverse effects. Nowadays, the antibiotic resistance becomes more and more pressing problem. Under this, the traditionally used antiseptics can inhibit the regeneration processes in the wound. Moreover, under long-term use of antibiotics in large-affected areas, they lead sometimes to the total patient intoxication.

Our investigation showed that the WDN have not the systemic toxicity. This may open new possibilities to cure a large number of patients. Note other important the WDN features: the relative easiness and cheapness of their manufacturing, their storage does not require special conditions, and they retain their antibacterial properties for a long time.

In the investigations, we used the WDN that have the maximal share of the "small" nanostructures with the largest surface electric charges. Such nanostructures are formed under the PED duration of 5–10 μs.

It was founded that the bacterial contamination of purulent wounds disappears on the seventh day under the WDN local use.

The following phenomena were observed: acceleration of the wound cleansing and positive healing morphodynamics with the earlier boundary epithelization.

As a result, the WDN local application enhances the appearance of early signs of the purulent wounds healing in comparison with using the sodium hypochlorite solution.

Under the local WDN application, there were no cellular atypia and preternatural emergences of the inflammatory reactions.

Positive results of our investigations on the local WDN application allow us to recommend this method for use in the clinical practice.

10.3 Oncology

The goal of this study was to investigate the antitumor properties of the silver WDN in experiments with the Pliss lymphosarcoma. This was the first study, which demonstrated that the WDN reliably inhibited the tumor growth in vivo. In some cases, a long-term systemic injection of the WDN led to regression of the tumor growth that was confirmed by the results of the histomorphological analysis [6].

In contemporary investigations in experimental and clinical oncology, the progress is mainly determined by the intensive introduction of achievements of the fundamental physics and chemistry [7, 8]. Nanoparticles, nanotubes, nanocapsules, dendrimers, and nanoconductors compose an incomplete list of the high-tech developments. All they are used for study of the targeted delivery of the anticancer

drugs and radioactive labels to cancer cells. Moreover, they are used for designing new methods of precise detection of the transformed cells, proteins, DNA, and individual genes [9, 10].

In particular, promising nanotechnological approaches in oncological studies are based on the nanoparticles with new physicochemical and biological properties [11]. It is known that the Ag nanoparticles and ions have an intrinsic cytotoxic activity [12, 13] and have a prolonged antimicrobial effect when applied on the silicon structures [14]. Results of the microbiological studies indicate that the interaction of the Ag ions with molecules of the extracellular lipoprotein matrix. This increases the permeability of the plasma membrane of the microbial cells and eventually causes their death [15]. However, as far as we know, this effect has not been used for studying the antitumor effects.

The WDN antitumor activity was studied with the maximal mass fraction of small nanoparticles under their concentration of 4.0 ± 0.5 mg/l. Experiments were performed on the 19 male inbred albino rats weighing 250–300 g. The rats were divided into two groups: experimental (n = 9) and check (n = 10). The Pliss lymphosarcoma cell line was used.

The tumors were transplanted to animals under aseptic conditions by injecting the tumor tissue suspension of 0.2 ml into the subcutaneous tissue of the right hind limb. The WDN was injected through a plastic catheter of 0.7 mm in diameter. The catheter was transplanted into the jugular vein and subcutaneously fixed in the occipital region of the animal head. Immediately after the tumor transplantation, the experimental rats daily (twice per day) received the WDN injections of 1 ml of saline. The check animals were injected with saline. The tumors sizes were assessed as the average value of two transverse diameters of the tumor node. All died animals were necropsied and, further, studied histologically. The results were statistically processes using the unpaired Student t-test. Such procession is the standard method used in medico-biological studies.

The growth of Pliss lymphosarcoma was observed in all animals starting from the third day after the tumor transplantation (Fig. 10.8), where PS is injection of saline, WDN is injection of the WDN, n is number of survived animals in group, * differences are trustworthy at $p < 0.05$.

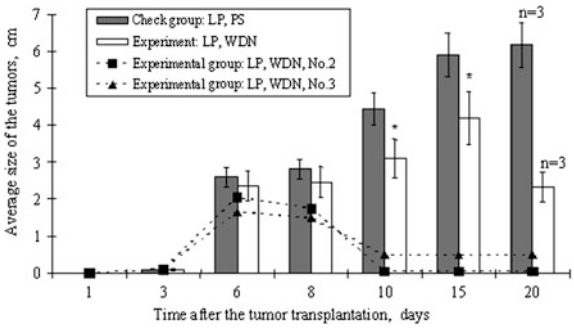

Fig. 10.8 Growth of the Plyss lymphosarcoma (LP) [6]

In the check group, the average size of tumors increased from 0.7 ± 0.1 cm (4th day) to 6.3 ± 0.7 cm (19th day). The size of tumors in the experimental group (measured on the 10th day after the tumor transplantation) was significantly smaller of that in the check group. It was 3.1 ± 0.5 cm in the experimental group versus 4.4 ± 0.3 cm in the check one ($p < 0.05$). The average lifespan of animal in both groups did not differ: 19.6 ± 1.5 days in the experimental group and 19.3 ± 1.5 days in the check one ($p > 0.05$). In two animals of the experimental group, the tumor regress was observed starting from the eighth day of the experiment. Morphological analysis of the tumor tissue in the check group revealed uniform fields of the malignant lymphoma (Fig. 10.9a), where a is check group, b, c are experimental groups.

In the experimental group, the malignant tumor was characterized by the higher content of detritus, predomination of dystrophically changed atypical cells (Fig. 10.9b), and marked fibrosis (Fig. 10.9c).

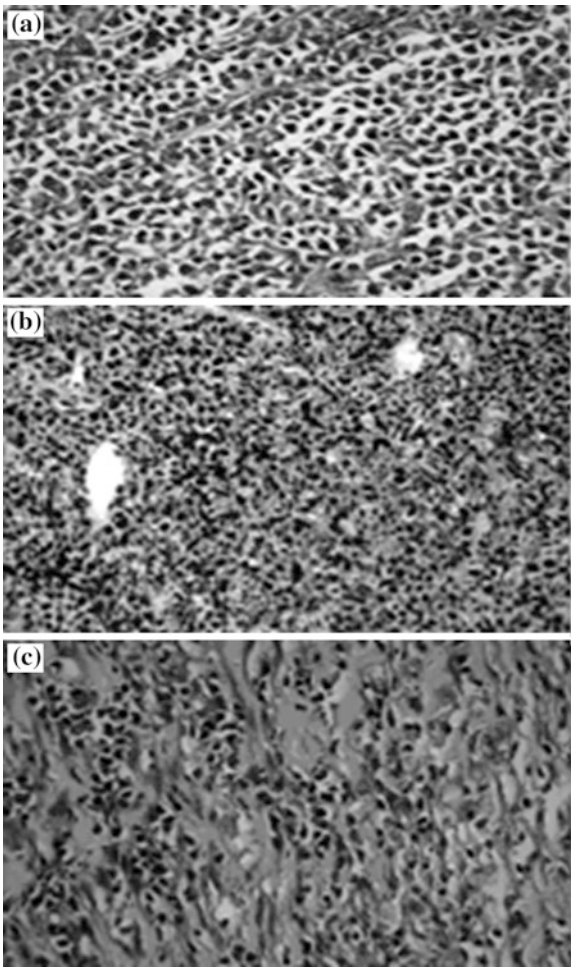

Fig. 10.9 Morphological pattern of the tumor tissue [6]

Determination of the Ag, Fe, Zn, Cr, Sb, Hg, and Co content in the DNA samples was implemented. The estimation was performed on samples obtained from the benign (fibroadenoma) and malignant (adenocarcinoma) human breast tumors. The decreased silver content was revealed in the DNA of the malignant cells.

It was supposed that the cytostatic effect of the silver is the result of active physicochemical interaction of the silver atoms with the functional groups of intracellular proteins, as well as, with the DNA nitrogen bases and phosphate groups [16].

In our experiments, the WDN long-term injections apparently restored the concentration of silver atoms and led to physicochemical stabilization of the DNA molecular structure in tumor cells.

Further studies of the mechanism of the discovered biological effect have to be implemented. Their results may become the basis for development of preparations based on nanoparticles and aimed to treating the malignant neoplasm in the clinical practice.

10.4 Stomatology

Generalized periodontitis is the systemic disease characterized by a progressive course, early manifestations at a young age, and a high incidence reaching the 98 % of patients of the age 35–44 years. These data are confirmed by conclusions of the WHO Expert Committee.

Initial signs of the periodontal disease are bleeding gums and gingivitis, which are considered as a damage of the tissue structures. The late diagnosis triggers development of the pathological process in the periodontitis. As a result, this leads to increase of the teeth mobility, destruction of the tooth holding tissue, and, ultimately, to their loss.

The generalized periodontitis leads not only to destruction of the structures holding the tooth, but, also, to more serious multi-factorial and multi-level pathological processes in the maxillofacial part. In addition, the relationship of generalized periodontitis was revealed with the systemic osteoporosis, kidney and gastrointestinal tract, urogenital, cardiovascular, and endocrine systems. The close relationship of periodontitis with the genetically determined and hereditary factors was also found.

The patients periodontal status was assessed by the depth of periodontal pockets, mobility of the teeth, presence of retraction and gingival bleeding index, state of strands, bridles, lips, tongue, width of the attached gingiva, and the depth of the mouth vestibule.

Hemodynamic evaluation was carried out by a computer periodontal biomicroscopy and reography of periodontal. In identifying the indications for depulping of the teeth, study of the microflora composition and morph-functional state of the

pulp and root canals was performed in comparison with those in the periodontal pockets.

Progression and aggravation of processes in the periodontal lead to infection and severe morphological changes in the patients' pulp teeth and cause generalized severe periodontitis. In the root canals of a single-rooted tooth, the facultative and obligate anaerobes were identified. The gram-negative flora dominates over the gram-positive one by 1.5–3.0 times. In histological, histochemical, and morphometric studies, the inflammatory infiltrates had been found in the dental pulp in 41.3 % of cases. Of these, 5.9 % are macrofocal, and 53.1 % are smallfocal.

It was established that such infections as urogenital chlamydia and stomach ulcer recur due to persistence of the *Hlamidia Trochomatis* and *Helicobacter pillory* in the plaques.

Under mild periodontitis, the occupational health was primarily used, and selection of the personal care products was performed. Important part of these investigations was devoted to normalization of the occlusal factors. We chose the following methods: the orthodontic treatment, selective polishing, and functional therapy with using various medical devices. In addition, surgical treatment and curettage were carried out in some cases.

Under moderate periodontitis, the flap operations are the main methods for treatment along with the above-mentioned ones. The osteotropic materials and membranes are injected into the bone pockets. In this group, the orthodontic treatment is carried out only after the surgery.

Under severe generalized periodontitis, it is necessary to use the combined treatment and depulping the teeth. After depulping the teeth, the splinting by fiberglass or temporary bridges of plastic are required. Surgical treatment by means of the flap operations is carried out with application of osteotrophic materials, biomodifiers, and membranes.

The aim of the investigation was impact of the Ag WDN (under concentration of 40 mg/l) onto the periodontal pockets microflora.

This method was applied to 121 patients of ages from 30 to 40 years with a diagnosis of the generalized periodontitis of moderate severity. The patients had the periodontal pockets depth of 5–6 mm and the bone tissue resorption of the alveolar outgrowth to half-length of the roots. These states of the disease were confirmed by standard methods of clinical studies of periodontal, by orthopantomographic tests, and parallel radiography. From all patients, samples of the periodontal pathogens were taken out the periodontal pockets. It was performed by the sterile paper points. Further, the samples were placed into the sterile Eppendorf tubes with a preservative (RT-PCR).

Separately, to detect pathogenic microorganisms, the smears from the mucous transitional fold, floor of the mouth, and the gingival margin were taken and placed into the test tube filled with a nutrient medium.

This approach indicated the anaerobic and conditionally pathogenic flora in the periodontal pockets and revealed the flora sensitivity to antibiotics. The study was carried out at the initial examination and after 3 weeks of therapy.

The following procedures were implemented:

- Removal of dental plaque and selection of the personal care products
- Instead of the recommended antibiotics, the periodontal pockets were washed by the WDN from the syringe
- It was followed by imposition of the medical hardening VOCO-PACK bandage
- Treatment was performed during 2 weeks in 1 day with the interval of 2–3 days between
- Whole coarse was of 4–5 visits

After 3 weeks, the re-sampling of microflora was carried out. After the treatment, the observations showed that the gums inflammation had disappeared, the periodontal pocket depth decreased by 1.5–2.0 mm. The results were confirmed by the RT-PCR and UPF tests.

Preliminary results of study of the periodontal pathogens were also obtained by the laser spectroscopy. Tests at the initial visit and ones after the 3 weeks treatment were carried out.

Results of treatment with the WDN application are illustrated by the following examples.

Example 1 Patient P., 39 years old. Diagnosis: generalized periodontitis of moderate severity. The periodontal pockets depth is up to 5–6 mm, the exudate is seropurulent. The teeth mobility is of the first—second degrees. The ortopantomogramma illustrates such degrees of the periodontitis severity (Fig. 10.10). Radiographic changes in the alveolar bone only after 6–12 months are possible. At the initial examination, analysis of composition of the microflora content from the periodontal pockets was carried out. The initial RT-PCR data of the periodontal pockets microflora before the treatment are shown in Table 10.7.

The composition of conditionally pathogenic microflora and sensitivity to antibiotics at the initial examination are presented in Table 10.8.

The WDN application resulted in the total disappearance of the above pathogenic bacteria (Table 10.9).

Example 2 Patient B., 32 years old. Diagnosis: generalized periodontitis of moderate severity. The periodontal pockets depth is up to 4–5 mm; the exudate is

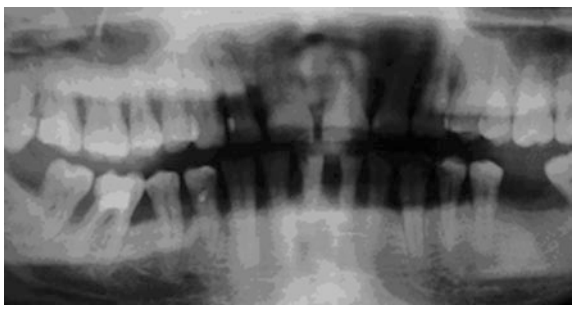

Fig. 10.10 Ortopantomogramma of the patient P

Table 10.7 Initial data of the periodontal pockets microflora before the treatment

No.	Bacteria	Norm (ml^{-1})	Result (ml^{-1})
1	*Actinobacillus actinomycetemcomitans*	–	10^3
2	*Porhpiromonas gingivalis*	–	–
3	*Prevotella intermedia*	–	10^3
4	*Tannerella forcythensis*	–	10^7
5	*Treponema denticola*	–	10^6

Table 10.8 Composition of pathogenic microflora and sensitivity to antibiotics at the initial examination

No.	Bacteria	Norm (ml^{-1})	Result (ml^{-1})	Sensitivity to antibiotics	
1	Seeding on UPF	–	10^5	Antibiotics	Reaction
2	*Enterococcus faecalis*	–	10^5	Amoxiclav	Sensitive
				Ampicillin	Sensitive
				Vancomycin	Sensitive
				Doxycycline	Stable
				Clindamycin	Stable
				Chloramphenicol	Stable
				Norfloxacin	Sensitive
				Erythromycin	Stable

seropurulent. The teeth mobility is the first degree. The ortopantomogramma illustrates such degree of the periodontitis severity (Fig. 10.11 and Table 10.10).

At the initial examination, analysis of composition of the microflora content from the periodontal pockets was carried out.

Pathogenic and conditionally pathogenic microorganisms of the diagnostically-significant amount are not detected (Table 10.11).

Application of the WDN treatment during 4 months resulted in decrease of the *Tanerella forcythensis* from 10^7 to 2×10^4 ml^{-1}, and the total disappearance of the *Porphiromonas gingivalis, Prevotella intermedia,* and *Treponema denticola* (Table 10.12).

The results of examination and treatment of patients with generalized periodontitis of moderate severity indicated that the reproducible therapeutic effect in 121 patients was observed after 1–4 months. In all cases, the acute inflammation process was not revealed in periodontal.

The WDN therapeutic effect is characterized by decreasing the bleeding gums, exudation of periodontal pockets, and pain. These phenomena were confirmed by results of the microbiological studies and data of the laser spectroscopy.

So, there are reasonable prospects of the WDN application to the treatment of patients with generalized periodontitis.

Table 10.9 The WDN' effect on the pathogenic bacteria

No.	Bacteria	Norm (ml^{-1})	Result (ml^{-1})
1	*Actinobacillus actinomycetemcomitans*	–	–
2	*Porhpiromonas gingivalis*	–	–
3	*Prevotella intermedia*	–	–
4	*Tannerella forcythensis*	–	–
5	*Treponema denticola*	–	–

Table 10.10 Initial data on the periodontal pockets microflora before the treatment

No.	Bacteria	Norm (ml^{-1})	Result (ml^{-1})
1	*Actinobacillus actinomycetemcomitans*	–	–
2	*Porhpiromonas gingivalis*	–	10^7
3	*Prevotella intermedia*	–	10^7
4	*Tannerella forcythensis*	–	10^7
5	*Treponema denticola*	–	10^7

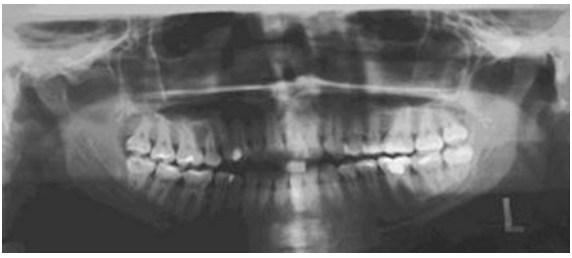

Fig. 10.11 Ortopantomogramma of the patient B

Table 10.11 Data on the pathogenic and conditionally pathogenic microorganisms

No.	Bacteria	Norm (ml^{-1})	Result (ml^{-1})
1	Seeding on UPF	–	–

Table 10.12 Data on application of the WDN during 4 months

No.	Bacteria	Norm (ml^{-1})	Result (ml^{-1})
1	*Actinobacillus actinomycetemcomitans*	–	–
2	*Porhpiromonas gingivalis*	–	–
3	*Prevotella intermedia*	–	–
4	*Tannerella forcythensis*	–	2×10^4
5	*Treponema denticola*	–	–

10.5 Virology

The study is aimed to investigation of possibility of a gentle disintegration of the shell and core of viruses under the impact of the shock waves generated during the PED in water in order to prepare a material for the anti-virus vaccines. As a prototype of viruses, the yeast *Saccharomyces cerevisiae* was used in these experiments.

The gentle disintegration of yeast viruses is an important task in biotechnology. It is known that the PED in water destroys the microorganisms by the shock waves, UV-irradiation, and by other factors. These actions affect simultaneously and, as a result, produce complete destroying the microorganism and denaturizing the proteins that include the target protein. The main goal of this investigation was to develop a method for generation of shock waves for destroying yeast cells. Yeast cells frequently use in biotechnology.

For investigation of shock waves effect on yeast, the leak-proof flexible plastic UV-opaque cuvettes were used. Applications of various modes of the PED and optimal conditions were investigated to gentle disintegration of the *Saccharomyces cerevisiae* yeast cells by shock waves.

Shock waves are formed in flowing water at the initial stage (ignition) of the PED occurred between the electrodes (3, 4) in the discharge chamber (2). High voltage pulses from the generator (1) were supplied (Fig. 10.12).

The electrodes of the discharge chamber were "wire to wire" with the inter-electrode gap of 5–10 mm and the water flow channel with diameter of ~15 mm. The PED parameters were the following: duration 0.2–27 μs, inputted energy smaller than J/pulse, current rise rate 10^6–10^9 A/s, pulses frequency 50–100 Hz.

Figure 10.13 shows the typical waveforms of the discharge current and voltage, where current is 20 A/div, voltage is 10 kV/div, time is 5.0 μs/div.

The 60 μl of tested yeast *Saccharomyces cerevisiae* suspension was used. It was cultivated in the standard media: 1 % yeast extract, 2 % peptone, 2 % sucrose during 12 h at 42 °C. The suspension was located into the UV-opaque plastic cuvette, which was tightly stuck by an elastic thin film.

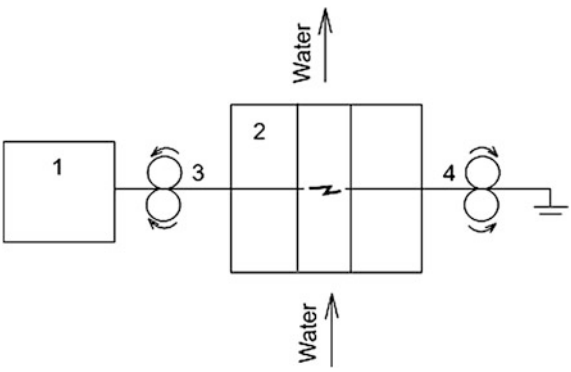

Fig. 10.12 Schematic circuit of the electrodischarge apparatus

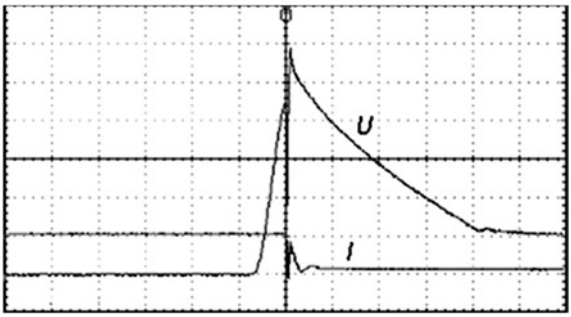

Fig. 10.13 Waveforms of the discharge current (*I*) and voltage (*U*)

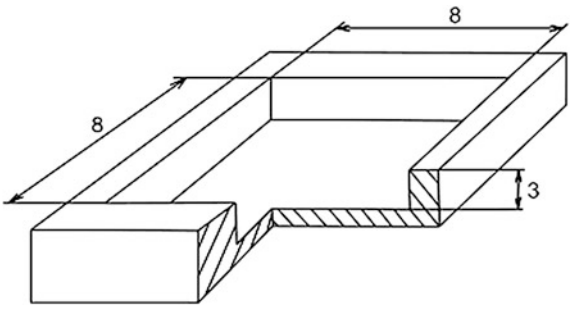

Fig. 10.14 Design of the cuvette

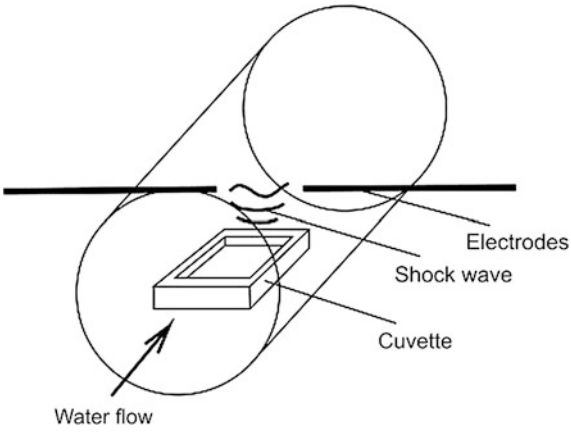

Fig. 10.15 Location of the cuvette in the electrodischarge chamber

The cuvette 8 × 8 × 3 mm (Fig. 10.14) with cells suspension was placed on the electrodischarge chamber bottom in parallel to the PED axes at the distance of 3 mm from it (Fig. 10.15). Impact of the shock waves onto the yeast was implemented by 25–500 pulses.

After treatment, the cuvette content had been investigated by microscopy after staining the sample by the vital "methylene blue" stain. In (Fig. 10.16) damaged cells are black, intact cells are white.

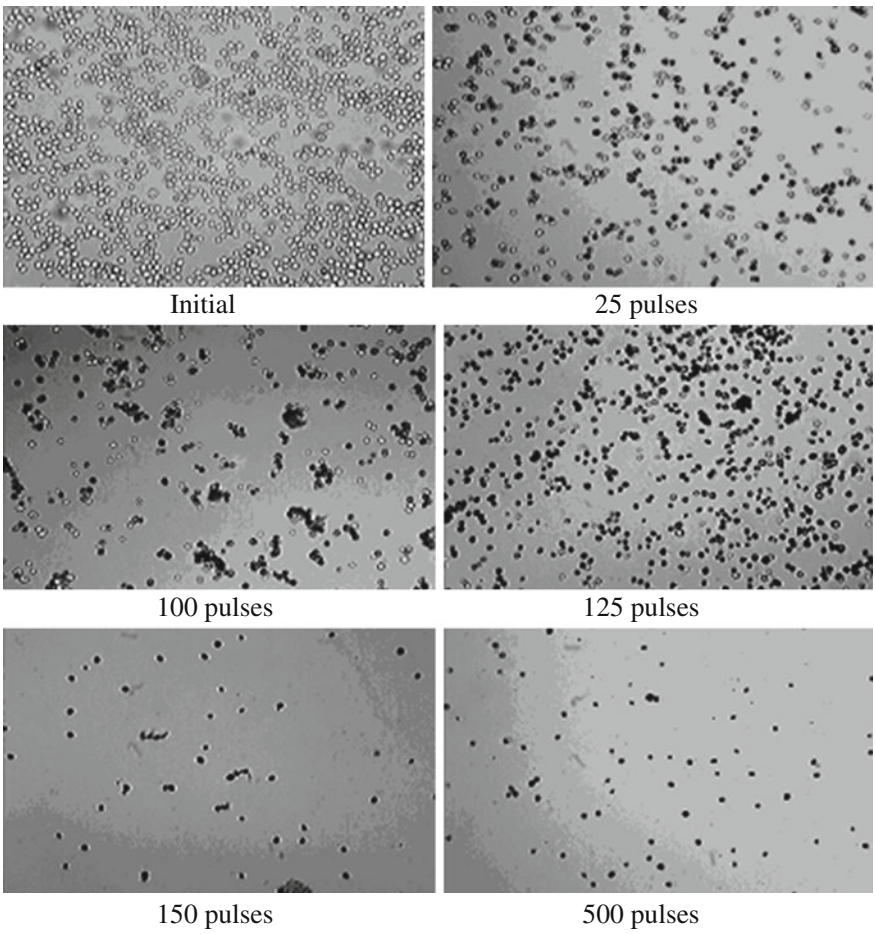

Fig. 10.16 Cells before and after treatment

Results of the microscopy tests are presented in Fig. 10.16.

Figure 10.17 shows that the cells walls were damaged totally after impact of the 150 shock waves. However, the yeast cells morphology remained intact even up to 500 pulses; only such action is enough to disrupt the cells walls of more than 99 % yeast cells.

This confirms that the shock waves generated by the PED in water effectively impact also onto the structure of the viruses and this leads to a drastic change in their morphology. So, this approach can be used in the pharmaceutical preparation of vaccines (Fig. 10.18).

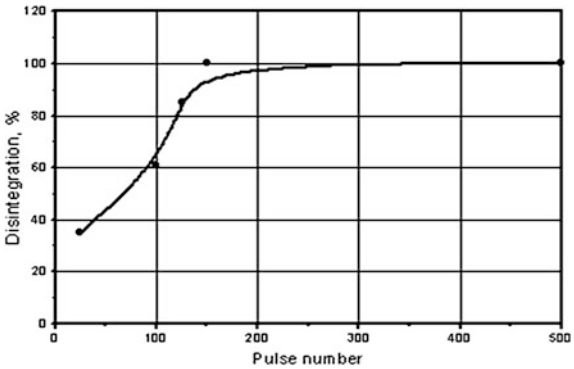

Fig. 10.17 Disintegration of the cells versus number of the pulses

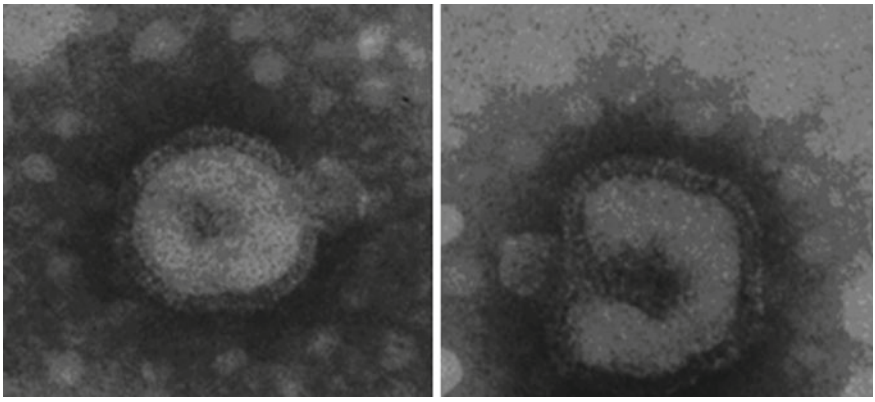

Fig. 10.18 Structure of a virus

Impact of the shock wave leads to various damage rates of the yeast cells during the time of their exposition in the discharge chamber. Under the pulse number exceeding 150, there is complete disintegration of cells.

Thus, the investigated way of decomposition of the yeast cells can be a basis for development of industrial process manufacture of the recombinant proteins that present in the yeast cells.

This method can be used in the pharmaceutical preparation of vaccines.

10.6 Ecology

In previous experiments on the water disinfection and increasing its microbicidal properties, the tap water or distilled water was treated by the PED. Then samples of the isotonic solutions were prepared and used. In these experiments, the bacteria concentration in the check samples remained virtually unchanged after a day pause. It was seen that, in the processed medium, the bacteria do not reproduce. This evidenced the oppressive conditions for the microorganisms.

However, conditions in these experiments are not always sufficient for reliable conclusions. For example, the officially adopted methodologies do not recommend to studying the effects of drugs onto the depressed cultures and under adverse conditions. Therefore, we undertook experiments to study the PED effect onto survival of microorganisms living in the natural conditions, namely, in water of the Neva River (St.-Petersburg, Russia).

The first series of experiments was developed and carried out in cooperation with the Laboratory for microbiology (LFM) of the Center for the study and control of water, St.-Petersburg, Russia.

According to the experiments program, the survival of microorganisms is determined by the change in the number of sanitary-indicative microorganisms in the Neva water without the PED treatment and after it.

By standard methods, the number of viable sanitary-indicative microorganisms was estimated in the Neva River untreated water (check samples) and in the Neva River water after treating by the PED with the inputted energies of 5 and 10 J/ml. Were measured:

- Total bacterial count (TBC)
- General and thermotolerant coliform bacteria
- Spores of the sulphite-reducing clostridia and coliphages

Determination of the microorganisms number in the water was performed after $\Delta t_1 = 6$ h and $\Delta t_2 = 24$ h after the water treatment.

10.6.1 Test Run

Day 1. Three sterile 0.5 l containers with the Neva River water were selected. All containers were placed and stored in refrigerators at (1–6) °C. One container was stored in the LFM, the other two ones were in IEE RAS at the same temperature.

Day 2. Containers were removed from the refrigerators at 9:00 am. At 11:00 am in the LFM, the seeding of water from container 1 was performed to determine the number of viable sanitary-indicative microorganisms. These data were taken as the initial ones at the instant $\Delta t_0 = 0$. After seeding, container 1 was maintained under the temperature of (20–25) °C.

At 11:00 am in the IEE RAS, treatment of the water of containers 2 and 3 was implemented by the PED with the inputted energy of 5 and 10 J/ml.

Further, the treated water was delivered to the LFM.

Through 6 h after the treatment, simultaneous seeding of water was carried out in containers 1, 2, and 3.

Day 3. All containers with water were maintained at the temperature of (20–25) °C. Procedure of the water seeding in the check and test containers was repeated through 24 h after the treatment.

Results of the sanitary and microbiological analyzes are shown in Tables 10.13, 10.14, 10.15, 10.16 and 10.17.

Table 10.13 Number of saprophytic microorganisms after the incubation

Container	Sample	Number of saprophytic microorganisms (TBC)			Note
		Initial $\Delta t_0 = 0$	After incubation $\Delta t_1 = 6$ h	After incubation $\Delta t_2 = 24$ h	
1	Check	1,698	4,943	33,400	Colonies of spore forms is increased
2	5 J/ml	–	139	131	
3	10 J/ml	–	105	50	

Table 10.14 Number of coliform bacteria after the incubation

Container	Sample	Number of coliform bacteria CFU/100 ml			Note
		Initial $\Delta t_0 = 0$	After incubation $\Delta t_1 = 6$ h	After incubation $\Delta t_2 = 24$ h	
1	Check	9,250	10,900	16,000	
2	5 J/ml	–	515	400	
3	10 J/ml	–	242	250	

Table 10.15 Number of thermotolerant coliform bacteria after the incubation

Container	Sample	Number of thermotolerant coliform bacteria CFU/100 ml			Note
		Initial $\Delta t_0 = 0$	After incubation $\Delta t_1 = 6$ h	After incubation $\Delta t_2 = 24$ h	
1	Check	4,270	5,670	5,270	
2	5 J/ml	–	339	247	
3	10 J/ml	–	176	85	

Table 10.16 Number of spores of the sulphite-reducing clostridia after the incubation

Container	Sample	Number of spores of the sulphite-reducing clostridia CFU/20 ml			Note
		Initial $\Delta t_0 = 0$	After incubation $\Delta t_1 = 6$ h	After incubation $\Delta t_2 = 24$ h	
1	Check	4	32	17	
2	5 J/ml	–	12	8	
3	10 J/ml	–	11	6	

Table 10.17 Number of the coliphages after the incubation

Container	Sample	Number of the coliphages CFU/100 ml			Note
		Initial $\Delta t_0 = 0$	After incubation $\Delta t_1 = 6$ h	After incubation $\Delta t_2 = 24$ h	
1	Check	20–33	20–33	–	
2	5 J/ml	–	3.6	Not determined	
3	10 J/ml	–	9.3	Not determined	

These tables show that the number of bacteria in the check experiments is increased versus time, whereas in the treated water their concentration is decreased. Moreover, the morphological structure of bacterial colonies shifted to spore forms that are more resistant to adverse conditions.

The next three sets of experiments were implemented under the same procedures. However, here, only the number of saprophytic microorganisms (as the most representative indicator) was considered.

The various initial numbers of microorganisms (from 5×10^3 up to $>10^6$ ml^{-1}) were obtained the water exposure for various times under 8 and 25 °C.

Under this, the preliminary rearing or growth inhibition of microorganisms was performed. The treatments by the PED were carried out both under various inputted energies and with various electrodes metals. In addition, the "cyclical" treatment mode (i.e., two times with the inputted energy of 5 J/ml) was investigated.

During culturing on the nutrient agar, the number of colonies was counted (Fig. 10.19). Growth of microorganisms only in check (a) was observed.

Results on survival of the Neva River water microorganisms after the PED treatment are presented in Table 10.18.

Water treated by the PED inhibits the growth of microorganisms. The stable bactericidal effect was observed under the initial microorganisms' concentrations of 10^3 CFU/ml. In all experiments, the total bactericidal effect had not been achieved under the initial microorganisms' concentrations larger than 10^6 CFU/ml. Application of the silver electrodes enhances the bactericidal effect.

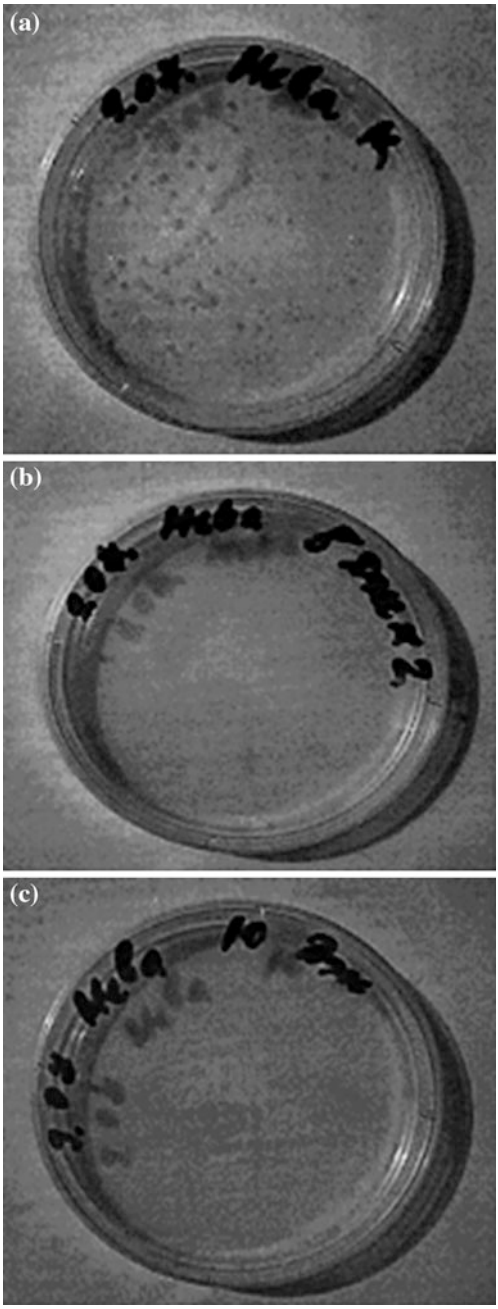

Fig. 10.19 Survival of the Neva River water bacteria in check (**a**), after treatment under energies 5 J/ml (**b**), and 10 J/ml (**c**)

Table 10.18 Data on survival of the Neva River water microorganisms after the incubation

Set	Mode of treatment		Number of microorganisms TBC CFU/ml		
	Metal	Energy J/ml	Initial $\Delta t = 0$	After incubation $\Delta t = 3$ h	After incubation $\Delta t = 24$ h
1	Check	–	2.5×10^4	$(4–5) \times 10^4$	6.5×10^5
	Ti Ag	3	2.5×10^4	10^4	10^2
	Ti Ag	10	2.5×10^4	0	0
	Ti	6	2.5×10^4	1.5×10^4	3.5×10^3
	Ti	10	2.5×10^4	0	0
2	Check	–	$>2.5 \times 10^6$	$>2.5 \times 10^6$	10^7
	Ti Ag	3	$>2.5 \times 10^6$	10^6	10^6
	Ti Ag	5	$>2.5 \times 10^6$	10^5	10^3
	Ti Ag	10	$>2.5 \times 10^6$	10^3	100–500
3	Check	–	5×10^3	7.5×10^3	1.5×10^5
	Ti Ag	5	5×10^3	50	0
	Ti Ag	5 + 5	5×10^3	0	0
	Ti Ag	10	5×10^3	0	0

References

1. E. Cadenas, J. Annu. Rev. Biochem. **51**, (1989)
2. D.N. Fedorov, A.N. Ivashkin, V.V. Shinin, A.V. Vasiliev, A.A. Ivanov, J. Arch. Pathol. **1**, 64 (2002). (in Russian)
3. A.V. Volenko, A.A. Menshikov, G.P. Titova, S.V. Kuprikov, J. Surg. **10**, (2004) (in Russian)
4. A.N. Lyapunov, B.M. Datsenko, N.A. Mohert et al., J. Probl. Drug Therapy (1995) (in Russian)
5. M.E. Pinchuk, V.A. Kolikov, Ph.G. Rutberg, A.G. Leks, R.V. Dolinovskaya, V.N. Snetov, A. Yu. Stogov, J. Phys.: Conf. Ser. **406** (2012)
6. Ph.G. Rutberg, M.V. Dubina, V.A. Kolikov, F.V. Moiseenko, E.V. Ignat'eva, N.M. Volkov, V.N. Snetov, A.Yu. Stogov, Doklady Biochem. Biophys. **421,** 191–193 (2008)
7. M.C. Roco, S. Williams, P. Alivisatos (World Technology Division, Loyola College, 1999)
8. D. Hanahan, R.A. Weinberg, Cell **1**, 100 (2000)
9. K.Y. Kim, Nanomedicine **2**, 3 (2007)
10. A.G. Cuenca, H. Jiang, S.N. Hochwald, M. Delano, W.G. Cance, S.R. Grobmyer, Cancer **3**, 107 (2006)
11. M. Ferrari, Nat. Rev. Cancer **3**, 5 (2005)
12. J.S. Kim, E. Kuk, K.N. Yu, J.H. Kim, S.J. Park, H.J. Lee, S.H. Kim, Y.K. Park, Y.H. Park, C. Y. Hwang, Y.K. Kim, Y.S. Lee, D.H. Jeong, M.H. Cho, Nanomedicine **1**, 3 (2007)
13. C. Baker, A. Pradhan, L. Pakstis, D.J. Pochan, S.I. Shah, J. Nanosci. Nanotech. **2**, 5 (2005)
14. F. Furno, K.S. Morley, B. Wong, B.L. Sharp, P.L. Arnold, S.M. Howdle, R. Bayston, P.D. Brown, P.D. Winship, H.J. Reid, J. Antimicrob. Chemotherapy **6**, 54 (2004)
15. I. Sondi, B. Salopek-Sondi, J. Colloid Interf. Sci. **1**, 275 (2004)
16. E.L. Andronikashvili, J. Biophysics **5**, (1987) (in Russian)

Index

V. Kolikov and P. Rutberg, *Pulsed Electrical Discharges for Medicine and Biology*, Biological and Medical Physics, Biomedical Engineering,
DOI 10.1007/978-3-319-18129-5